On-loom Fabric Defect Detection - State-of-the-Art and Beyond

Prozessintegrierte Qualitätssicherung gewebter Textilien - Stand der Technik und neue Entwicklungen

Von der Fakultät für Elektrotechnik und Informationstechnik der Rheinisch-Westfälischen Technischen Hochschule Aachen zur Erlangung des akademischen Grades eines Doktors der Ingenieurwissenschaften genehmigte Dissertation

vorgelegt von

Dipl.-Ing, M.Sc.
Dorian Schneider
aus Berlin

Berichter:

Univ.-Prof. Dr.-Ing. Dorit Merhof
Univ.-Prof. Dr.-Ing. Peter Vary

Tag der mündlichen Prüfung: 16.07.2015

Abstract

Weaving is one of mankind's oldest crafts. The process of interlacing two sets of yarns in an orthogonal way according a predefined pattern is a technology which is as old as human civilization. Over the centuries, the textile industry evolved into a high-tech industry, characterized by highly sophisticated production machines which operate mostly autonomously and are uncoupled from any human interaction. Built into safety relevant products like airbags, safety belts, fire resistant clothing, bullet-proof cloth or artificial vascular grafts, technical woven fabrics impose highest production quality standards. Reliable and fast quality assurance is thus crucial. The industrial standard approach for quality assurance is still based on human, manual inspection. In order to augment the production throughput, to achieve lower labor costs and to guarantee stable product quality, the development of reliable methods for fully automatic fabric quality control has become a vital topic for research around the world. Within this thesis, the development of a novel, loom-integrated automated visual inspection system for high resolution woven fabric defect detection is described. Accordingly, this work is divided into three major parts.

Part I investigates a set of 14 selected state-of-the-art fabric defect detection algorithms to assess the current detection performance of existing methods. The study is conducted with unified fabric image databases and assessment metrics and therefore represents the first fabric defect detection benchmark of this kind published in literature.

Motivated by the benchmark results, Part II discusses the design of a novel, high-resolution traversing camera inspection system for locating and classifying potential defects in woven fabrics. The implemented prototype can track single yarns in real-time during production and measures fabrics with regards to geometry, extent, orientation and shape for the first time. This is a major improvement compared to hitherto approaches that treat fabrics as near regular texture and apply pattern analysis algorithms to detect defects. The detailed description of the image processing pipeline is complemented by a comprehensive on-line evaluation and in-depth discussions about mechanical system integration, vibration damping, imaging strategies and product costs.

The proposed image processing framework is finally extended in Part III by two additional algorithmic features. First, a method is discussed that allows an automatic classification of fabric weave patterns without any prior knowledge about the investigated material. Furthermore, an algorithm for adaptive measurement of changing yarn densities is presented. Again, both extensions were extensively evaluated and the results are directly compared to state-of-the-art performance measures.

Zusammenfassung

Die Weberei ist eines der ältesten Handwerke der Menschheit. Die Webtechnik verknüpft vertikal und horizontal verlaufende Fäden gemäß eines vorgegebenen Musters. Über die Jahrhunderte hinweg hat sich die Textilindustrie zu einer Hightechindustrie entwickelt, mit vollautomatisierten Webmaschinen, die Gewebe in enormen Durchsatzraten produzieren. Folglich ist eine robuste und schnelle Qualitätskontrolle von großer Bedeutung. Der heutige Standardansatz zur Qualitätssicherung von Textilien basiert jedoch immer noch auf menschlicher Sichtkontrolle, was langsame Bearbeitungszeiten und geringe Fehlererkennungsraten bedingt. Die Entwicklung automatischer Verfahren für die Qualitätskontrolle von Textilien ist demnach ein sehr relevantes Forschungsgebiet. Die vorliegende Arbeit stellt ein neu entwickeltes, hochauflösendes Machine Vision System vor, das in die Webmaschine integriert ist. Das System wertet Kamerabilder aus, um Fehler in gewobenen Textilien automatisch zu erkennen.

Um eine Aussage über den aktuellen Stand der Technik treffen zu können, führt Teil I eine umfassende Leistungsanalyse bereits publizierter Verfahren zur Fehlerkontrolle (bildbasiert) von Textilien durch. Eine Auswahl von 14 Algorithmen wird erstmalig mit einheitlichen Datenbanken und einheitlichen Bewertungsmaßen auf ihre Leistungsfähigkeit hin untersucht.

Teil II beschreibt das Design eines hochauflösenden Kamerasystems, das beweglich in die Webmaschine integriert ist und so Fehler im Material frühzeitig erkennt und klassifiziert. Der entwickelte Prototyp ist in der Lage, einzelne Fäden im Gewebe in Echtzeit zu lokalisieren und erstmalig mit Bezug auf die Fadenform, -lage und -erscheinung zu vermessen. Dies ist ein wesentlicher Fortschritt im Vergleich zu bisherigen Methoden, die Gewebe als reine Texturen interpretieren und Musteranalyseverfahren einsetzen, um Fehler zu erkennen. Neben der detaillierten Beschreibung der Algorithmen beinhaltet Teil II auch eine umfassende Leistungsanalyse des entwickelten Systems. Zudem werden die mechanischen Komponenten, einschließlich der Schwingungsdämpfung und der Bildaufnahme, ausgiebig beschrieben.

Der dritte Teil führt zwei zusätzliche Erweiterungen ein. Zuerst wird ein Verfahren vorgestellt, das die Bindung eines unbekannten Gewebes ohne Vorwissen automatisch bestimmt. Zudem wird ein Algorithmus präsentiert, der es ermöglicht die Dichte eines Gewebes kontinuierlich zu vermessen, auch wenn sie diese im zeitlichen Verlauf ändert. Beide Methoden werden, wie in den vorhergehenden Abschnitten auch, umfangreich evaluiert und mit dem Stand der Technik verglichen.

Contents

Abstract (English/Deutsch) **i**

List of figures **ix**

List of tables **xi**

Acknowledgements **1**

I Background and overview **3**

1 Introduction **5**
1.1 Motivation & Objectives 7
1.2 Scientific contributions 8
1.3 Research consortium 9
1.4 Outline 10

2 Background on weaving **13**
2.1 Historical context 14
2.2 The weaving machine 15
2.2.1 Terminology and weaving basics 16
2.2.2 Modern weaving machines 17
2.3 Fundamental weave pattern 20
2.4 Fabric defects 22

3 Fabric image databases **29**
3.1 FIDB-A: TILDA Database 29
3.2 FIDB-B: Synthetic database 31
3.3 FIDB-C: High resolution, off-loom 32
3.4 FIDB-D: Low resolution, off-loom 33
3.5 FIDB-E: High resolution, on-loom 33
3.6 FIDB-F: High resolution, synthetic blur, off-loom 34
3.7 FIDB-G: High resolution, motion blur, on-loom 35

3.8 FIDB-H: High resolution, no defects, rotation, off-loom 36
3.9 FIDB-I: High resolution, no defects, off-loom 37

II State-of-the-art 41

4 Benchmarking the state-of-the-art 43
4.1 Automated Visual Inspection - Overview 43
4.1.1 Objectives & advantages 44
4.1.2 Literature overview 45
4.2 Fabric defect detection - State-of-the-art 46
4.2.1 Literature survey 47
4.2.2 Available algorithms 48
4.2.2.1 Wavelet based methods 51
4.2.2.2 Gabor Filter based methods 55
4.2.2.3 Statistical methods 57
4.2.2.4 Filtering based methods 61
4.2.3 Evaluation 65
4.2.3.1 Datasets 65
4.2.3.2 Assessment criteria 66
4.2.3.3 Parameter selection 69
4.2.4 Results 70
4.2.5 Discussion 72
4.2.6 Conclusion 74

III On-Loom Imaging 79

5 On-loom visual inspection 81
5.1 Introduction 81
5.1.1 Loom mounted detection systems 83
5.2 Mechanical integration 84
5.2.1 Camera mount 84
5.2.2 Illumination 88
5.2.3 Image acquisition 92
5.3 Image processing algorithms 92
5.3.1 Main challenges 93
5.3.2 Pre-processing 93
5.3.2.1 Deconvolution 95
5.3.2.2 Histogram Equalization 100
5.3.3 Feature extraction 103

5.3.4 Yarn tracking . . . 108
5.3.4.1 The grid matrix . . . 110
5.3.4.2 The yarn matrix . . . 112
5.3.4.3 Trajectory interpolation . . . 115
5.3.5 Defect detection . . . 116
5.3.5.1 Grid control . . . 116
5.3.5.2 Yarn spacing and curvature measurement . . . 117
5.3.5.3 Block partitioning . . . 118
5.4 Evaluation . . . 121
5.4.1 Datasets . . . 122
5.4.2 Assessment criteria . . . 122
5.5 Results . . . 123
5.5.1 Computing time . . . 123
5.6 Economic feasibility . . . 126
5.7 Discussion . . . 127
5.8 Conclusion . . . 130

IV Extensions 133

6 Blind weave detection 135
6.1 Introduction . . . 135
6.2 Methodology . . . 137
6.2.1 Rotation detection and correction . . . 138
6.2.2 Yarn density estimation . . . 141
6.2.3 Blind feature point extraction . . . 142
6.2.4 Grid vector pair estimation . . . 142
6.2.5 Feedback loop for candidate selection . . . 144
6.2.6 Weave detection . . . 145
6.3 Evaluation . . . 146
6.4 Results . . . 147
6.5 Discussion . . . 148
6.5.1 Parameter sensitivity . . . 150
6.5.2 Limitations . . . 151

7 Adaptive density measurement 153
7.1 Introduction . . . 153
7.2 Methodology . . . 155
7.2.1 Adaptions to the yarn tracking algorithm . . . 156
7.3 Evaluation . . . 158
7.3.1 Fourier analysis . . . 158

7.3.2 X-ray measurement 160
7.3.3 Generalization capabilities 161
7.3.4 Precision and measurement uncertainty 161
7.4 Results 162
7.5 Discussion 163

V Conclusion **169**

8 Summary **171**

9 Outlook **175**

Appendices **179**
A Surface inspection literature by domain 181
B Derivation of the optimized form of the ZNCC 186
C Matlab pseudo code for the grid map build algorithm 188
D Examples of the yarn tracker output 190
E Detailed blind weave detection results 192

Bibliography **195**

About the author **213**

List of Figures

2.1 Illustration of a loom, side view 16
2.2 Illustration of the four basic steps in weaving 18
2.3 Illustration of a plain weave fabric 20
2.4 Illustration of a twill fabric weave 21
2.5 Illustration of a satin fabric weave 22
2.6 Illustrations of common fabric defects in warp direction 25
2.7 Illustrations of common fabric defects in weft direction 26
2.8 Illustrations of the two most common spot shaped defects 27

3.1 Fabric samples and ground truth from database FIDB-A 30
3.2 Fabric samples and ground truth from database FIDB-B 31
3.3 Fabric samples and ground truth from database FIDB-C 32
3.4 Fabric samples and ground truth from database FIDB-E 34
3.5 Fabric samples and ground truth data from database FIDB-F 35
3.6 Images and ground truth data from image database FIDB-G 36
3.7 Overview of the blind weave database FIDB-H 37
3.8 Overview of the density measurement database FIDB-I 38

4.1 Scheme of a different Wavelet decomposition strategies 52
4.2 Defect detection results for varying hit and fault rates 70

5.1 Spectra of two machine vibration measurements 85
5.2 Scheme and CAD model of a camera vibration damper 86
5.3 Camera motion in dependence of the loom frequency 88
5.4 CAD model of the traversing illumination system 89
5.5 Difference between top-light and back-light 89
5.6 Scheme of the image acquisition strategy 91
5.7 Block diagram of the On-Loom image processing framework 94
5.8 Overview of different deconvolution performances 99
5.9 Illustration of the CLAHE interpolation concept 102
5.10 Illustration of wefts, warps and float-points 106
5.11 Illustration of the feature extraction pipeline 109

5.12 Illustration of a satin weave fabric and its grid matrix 110
5.13 Examples for grid and yarn vector selections 111
5.14 Illustration of a satin weave fabric and its yarn matrix 112
5.15 Sample of a 3-1 polyester twill fabric 114
5.16 The concept of yarn tracking by interpolation 115
5.17 Illustration of bin compressing process 119
5.18 Block partitioning for yarn texture analysis 120
5.19 Image of the On-Loom prototype mounted to a loom 121
5.20 On-Loom defect detection examples on database FIDB-C 122
5.21 On-Loom defect detection examples on database FIDB-G 125
5.22 Cost forecast for the On-Loom defect detection system 127

6.1 Block diagram of the blind weave detection framework 139
6.2 Rotated fabric images and corresponding Fourier spectra 140
6.3 Clustered float-point features 144
6.4 Approximated weft and warp trajectories 146
6.5 Results of the parameter variation experiment 150

7.1 Scheme of a loom with MV system and X-ray sensor 160
7.2 On-loom density measurement during 360 seconds 164
7.3 On-loom density measurement for 60 seconds 165
7.4 Row and column scan-line profiles of a sample fabric 167
7.5 Results of the all-in experiment for density measurement 168

1 Fabric samples with super-imposed yarn trajectories 1/4 190
2 Fabric samples with super-imposed yarn trajectories 2/4 190
3 Fabric samples with super-imposed yarn trajectories 3/4 191
4 Fabric samples with super-imposed yarn trajectories 4/4 191

List of Tables

3.1 Overview Table of the fabric evaluation databases 39

4.1 Overview of fabric defect detection algorithms implemented in Part I . 50
4.2 Results table of the algorithmic benchmark, 1/2 77
4.3 Results table of the algorithmic benchmark, 2/2 78

5.1 The three most dominant frequencies occurring during loom operation 85
5.2 List of investigated non-blind deconvolution algorithms 96
5.3 Running times and FOD values for several deconvolution algorithms . 98
5.4 Correlation metric evaluation results 105
5.5 On-Loom evaluation results 124
5.6 Costs overview of the On-Loom prototype 128
5.7 Basic conditions for the economic efficiency calculation 129

6.1 Optimal parameter settings for blind weave detection 148
6.2 Blind weave detection evaluation results 149

7.1 Evaluation results for adaptive weft density measurement, 1/2 164
7.2 Evaluation results for adaptive weft density measurement, 2/2 166

1 Evaluation results for the blind weave detection framework, 1/2 193
3 Evaluation results for the blind weave detection framework, 2/2 194

Acknowledgements

To begin with, I would like to thank Prof. Til Aach for giving me the opportunity of working at the LfB and for expressing his confidence in me to work on this intriguing research topic. I am sincerely grateful to my supervisor Prof. Dorit Merhof for guiding me through the overall process of creating this thesis. Her numerous hints, her advice and valuable suggestions for improvement are part of every page of this work. I also thank her for a great collaboration at the LfB, under her direction I never felt like a simple employee but as an equitable research colleague. Thank you.

I would like to thank Timm Holtermann for a very productive collaboration within this project, Timm is a great colleague and friend. Without him, the achievements of this thesis would not have been possible. The findings in Section 5.2 are partly the results of his work and are summarized in this work with his approval. I extensively thank Martin Staas who made important contributions to the overall success of the On-Loom project within the scope of his student assistant work at the LfB. Moreover, within the context of their Diploma theses, I express my gratitude to Björn Schiefen for his contributions to the yarn tracking algorithm in Section 5.3.4 and to Tilo van Ekeris for his contributions to the deconvolution module in Section 5.3.2.1.

Dorian Schneider

PART I

BACKGROUND AND OVERVIEW

1 Introduction

The textile industry is one of the oldest and (from a global point of view) one of the most connotative manufacturing industries. In fact, besides nutrition and shelter, clothing is one of the three basic human needs [1]. This also explains why the fabrication of textile manufacture is with high certainty as old as human civilization. Congruently, fabrics have a major impact on everyday life, not only because they form the basis of most apparel, but also of many household and industry related products.

Since the beginning of the industrial revolution in the late 18th century, the textile production turned into a high-tech industry, characterized by highly sophisticated production machines which operate mostly autonomous and uncoupled from any human interaction. The production pipelines are highly optimized to allow for a maximum of produced material at a minimum of costs and time. The quality and thus the price of these fabrics depends to a great extent on the amount and the occurrence of flaws within the material. The human eye is very sensitive and can detect deviations in patterns as fine as 20 µm. Reliable and fast quality assurance is thus crucial for modern textile companies and motivates extensive efforts to identify automated solutions.

The industrial standard approach for quality assurance is still based on production machine separated cloth inspection assemblies, operated off-line by trained human inspectors. In such a setup, the produced fabric is loaded into a separate machinery which consists of a large back-light illuminated area over which the fabric is unrolled once again. Up to three highly trained human inspectors control every meter of the material and manually mend occurring flaws when necessary. Obviously, the efficiency of this approach is limited by low inspection speeds, a short attentiveness period and low defect detection rates of human inspectors (about half an hour and 70%, respectively [2]).

In order to augment the production throughput, to lower labor costs, and to guarantee stable product quality, the development of reliable methods for fully automatic fabric quality control has become a vital topic for research around the world. State-of-the-art inspection systems generally operate with digital cameras combined with complex machine vision algorithms to locate and assess material defects automatically. System designs can roughly be classified into two separate concepts. The first category is given by off-line systems that monitor produced materials apart from the loom on a separate cloth inspection table, as a conventional human inspector would do. They are straight forward to set up and benefit from steady operation conditions. As adverse characteristic, the control and production process are decoupled, excluding the possibility to immediately stop the loom in case of severe and repetitive defects. On-line systems on the other hand are directly mounted onto the loom and monitor the material on-line during manufacturing. They allow immediate intervention in case of defects and can hence minimize losses.

Woven fabric products form the major branch of the textile manufacturing industry, besides the production of knitted fabric and non-woven fabric [3]. Correspondingly, this work is entirely dedicated to the research area of on-line (on the loom: on-loom), vision based quality control of woven fabrics. The major challenges in the construction of visual inspection systems that operate on-line are identified by

- strict limitations for costs,
- vast inspected areas,
- fast production speeds, and
- machine induced vibrations.

Consequently, machine vision algorithms face the problems of

- a large variability of possible textiles for inspection,
- highly varying fabric defects (that are unknown prior their occurrence),
- strict requirements for robustness,
- large data volumes, and
- tight constraints with respect to computational needs.

To this day, most of the aforementioned problems could not be solved in a satisfactory manner. For this reason, human inspection still defines the status quo in quality control for woven fabrics.

Within this scope, the first part of this work thoroughly investigates how current algorithms for automated fabric defect detection generally perform. Consistent databases,

standardized benchmark frameworks, and clearly defined assessment criteria allow to analyze the weaknesses and strengths of different classes of inspection algorithms in a unified matter. Based on the obtained insights, Part III of this work goes beyond the state-of-the-art and proposes new algorithmic methodologies to overcome most of the existing shortcomings. Even though the scope of the second part clearly prioritizes algorithmic aspects, also hardware related topics such as image acquisition and mechanical integration are covered. The findings allow to further provide solutions statements for related topics of automatic fabric weave detection and low latency fabric density measurement.

1.1 Motivation & Objectives

More than 500 scientific publications published in the last 20 years address the topic of automated fabric defect detection. The algorithmic variety employed in these papers stretches over the entire methodological bandwidth of the pattern recognition area (see Part II of this work). Although each publication claims good to excellent detection performances, reported results exhibit in fact a severe lack of standardization. None of the authors provide image databases or ground truth data for competitive benchmarks, there are no standard metrics for assessment (often metrics are not provided at all), computing times rarely discussed, spatial image resolutions vary drastically (most often they are not mentioned at all), and the quality of the technical writing deviates significantly. Own implementations of some selected methods demonstrated that the defect detection performance, when tested with real-world image data, is not able to meet the requirements for practical application.

In summary, due to a lack of standardized, quantitative and transferable evaluation results, no information can be inferred from the great amount of topic related resources that can enlighten the general accomplishments or deficiencies of the research area of automated fabric defect detection in the last two decades. This insight motivates the conduction of a standardized benchmark of selected algorithms in Part II of this work. The objectives here are to

1. compare and assess the detection performance of existing methods,
2. highlight their weaknesses with regards to real-world application,
3. make a distinction between working and non-functional techniques,
4. use standardized codes, metrics and databases for evaluation.

The deflating results of the benchmark motivate the main contribution of this work. Accordingly, Part III introduces a novel, loom-integrated automated visual inspection (AVI) system for high precision woven fabric defect detection. As state-of-the-art detection algorithms apply texture analysis methods to investigate lowly resolved image data, a new design concept is proposed which allows to track and measure single yarns in fabric images. The new approach turns the classic pattern analysis task of fabric defect detection into a measurement procedure. The main objectives during the system design are to

1. overcome current drawbacks in terms of detection precision,
2. flexibly handle any woven material,
3. measure single yarns instead of analyzing patterned structures,
4. allow for real-time, in-process quality control,
5. design hardware that can be integrated into any loom,
6. reduce costs for practical application.

The required solutions to the above challenges let two additional problem statements emerge. Since woven fabrics consist of two distinct and orthogonal yarn sets which are interlaced according to a predefined pattern, one may ask if it is possible

- to find the braiding pattern without prior knowledge? and
- how the yarn density can be measured in a robust way?

Finding answers to these questions is the objective of Part IV of this work.

1.2 Scientific contributions

The main contributions of this work are defined by the design of new image processing techniques for non-destructive, visual measurement of woven fabrics. The research results of this work were published in several international and peer-reviewed proceedings and journal papers. The approval to partially re-use the published content within this thesis was requested for each paper individually and was given by all corresponding editors. In detail, innovative solutions were found for the problems of

1. Real-time image deconvolution to improve the quality image data that has been degraded by motion blur [4] (Section 5.3.2.1).

2. Real-time image enhancement to compensate for image degradations caused by the optical path and the illumination setup [5, 6] (Section 5.3.2.2).
3. Algorithms for precise yarn segmentation to measure the thickness of single yarns in woven fabrics with pixel precision [7] (Section 5.3.4).
4. In-process camera vibration damping to reduce the impact of image degradation caused by the vibrations of the operating loom [8] (Section 5.2.1).

The above list of achievements defines the foundation for the On-Loom yarn tracking framework, which comprises the main contribution of this work:

5. An overall On-loom system design including hard- and software such as detailed on-loom defect detection results [9] (Chapter 5).

On top of this, two extensions were developed, which comprises:

6. An innovative solution for blind weave detection [10] (Section 6.1).
7. Algorithms for high precision yarn density measurements [11, 12] (Section 7).

All Matlab and C++ source codes of the proposed methods are publicly accessible throughout the On-Loom imaging project website [13].

1.3 Research consortium

The findings of this work are part of a public domain project entitled On-Loom Imaging, which was funded by the *Arbeitsgemeinschaft industrieller Forschungsvereinigungen* (AiF)[1] with a budget of approximately half a million Euro for a period of 30 months. The intention was to design a loom-integrated visual inspection system for woven fabrics which provides the possibility of a direct feedback loop to the loom in order to adjust and modify machine parameters on-line during production. The project was accompanied by a committee of 16 midsize companies from the weaving and surface inspection sector. Three institutes of RWTH Aachen University were involved in the realization of the project: from the department of mechanical engineering, the

[1] http://www.aif.de/en

Werkzeugmaschinen Labor (WZL)[2] and the *Institut für Textiltechnik* (ITA)[3] worked on mechanical and hardware related problems. Both institutes contributed one research assistant and one student assistant to the project. From the department of electrical engineering, the *Institute of Imaging & Computer Vision* (LfB)[4] was responsible for the algorithmic pipeline, including image acquisition and processing, controlling and information storage. Besides the author, one student assistant was assigned to the On-loom Imaging project by the LfB.

1.4 Outline

This thesis is divided into five parts and is structured as follows.

- Part I (Chapters 1, 2 and 3) provides a general introduction into the field of on-loom fabric defect detection. In Chapter 2, essential information regarding the special field of weaving is provided. The theoretical background on woven fabrics is explained and put within its historical context, the fundamental nomenclature is clarified, and current technologies for weaving are outlined. Several fabric image databases were created to assess the performance of the algorithms designed in this work. As these databases are referenced and used throughout this entire theses, Chapter 3 concentrates and bundles the information by giving a brief overview of all database characteristics.
- Part II (Chapter 4) provides an overview of the state-of-the-art in textile inspection. Section 4.1 first discusses the state-of-the-art of automated visual inspection in general, including a thorough overview of related literature and commercially available systems. Section 4.2 then focuses on the domain of automated visual inspection for woven fabrics. Here, a qualitative benchmark is conducted on a representative selection of 14 earlier published algorithms for fabric defect detection. Using uniform assessment criteria and a standardized image database, the algorithms are evaluated with regard to their real-world applicability.
- Part III (Chapter 5) introduces a novel traversing AVI system for high precision fabric defect detection. Mechanical integration, image acquisition, vibration damping and complete material coverage are discussed in this context. The core

[2] http://www.wzl.rwth-aachen.de/en
[3] http://www.ita.rwth-aachen.de/andere_ sprachen/englisch/
[4] http://www.lfb.rwth-aachen.de/?lang=en

of the chapter describes an innovative algorithmic framework which treats fabrics as a composition of single yarns instead of a repeating texture. This allows to overcome many of the shortcomings encountered by previous methods as the pattern analyses problem is shifted towards a measurement task, which allows for straight forward defect classification and significantly improved detection results. The proposed system is realized as a prototype on a real-world loom and is validated with extensive test runs and subsequent ground truth enabled evaluations. The chapter closes with detailed cost analysis for the prototype system which is further extended by an economic efficiency calculation for a potential commercial distribution of the system.

- Part IV (Chapter 6) addresses the problem of blind weave detection and robust density measurement. First, the results of previous sections are extended in Section 6.1 to design an iterative framework which is able to automatically detect weave (yarn interlacing) patterns without any prior knowledge. The proposed method is able to analyze woven fabrics of any rotation, material or binding. Moreover, Section 7 presents a method for highly precise on-line measurements of fabric yarn densities with a very short time delay between production and measurement. The measurements are done locally as opposed to previous methods and allow for an on-line controlling of the fabric grammage.
- Finally, Part V (Chapters 8 and 9) concludes the work with a summary, outlook and recommendations for future work.

2 Background on weaving

With approximately 1200 small to mid-size businesses, more than 120,000 employees and almost 29 billion Euro of sales in 2011, the textile and apparel industry is the second biggest consumer goods industry in Germany (after the food industry). Mostly as component supplier to the apparel, agriculture, transportation, logistic, construction, chemistry, automotive, health, metal and electronics industry, more than 40 % of the German volume of sales is generated abroad. It must be distinguished between the apparel and the textile industry. The latter has a share of 54% of the total turnover and can be sub-categorized into several finer industry sectors, whereas weavers and producers of technical textiles are the most prominent. Built into tire cords, airbags, filtration devices, safety belts, fire resistant clothing, bullet-proof cloth, image conductor cables, plasma screens, helmets, artificial vascular grafts and countless more products, technical woven fabrics define the main target for the propositions of this thesis, as they must fulfill highest standards in quality and consistency.

This chapter provides the reader with a general overview of the production process of woven fabrics. After presenting a brief historical outline of the craft of weaving, the operating mode of modern weaving machines is discussed. The topic of raw materials and fabric design is covered, and a compact discussion of common fabric defects concludes this section. The intention here is to provide the reader with all technical terms and weaving relevant information in order to make subsequent chapters coherent and understandable.

2.1 Historical context

Weaving is one of mankind's oldest crafts. In fact, recent research activities revealed that Stone Age hunters, some 30,000 years ago, were already able to handle wild flex fibers to weave fabrics for baskets and tools [14]. Accordingly, the process of interlacing two sets of yarns in an orthogonal way according a predefined pattern is a technology which is as old as human civilization. Mostly used as the basic material to create cloth, woven fabrics ever since provided protection against the elements, emphasized social hierarchies, and facilitated human actions in all imaginable situations.

Until the middle age, weaving was carried out as a cottage industry. Weavers worked from home, whereas the main production technology was the vertically operated, warp-weighted loom in combination with woolen and linen fibers. For centuries, technologies didn't change. Only in the 16th century, the vertically operated loom frame was replaced by a horizontal design which allowed higher production rates and pioneered the invention of the mechanic loom. Only in 1733, John Kay made a significant contribution which revolutionized the domain of weaving and initiated the full automation of the process: the flying shuttle. Operated manually, it allowed to produce much more material in less time and with less labor. The augmented productivity in weaving caused a significant shortage of threat which lead to other important inventions like the spinning mule.

The first mechanical loom was invented by Edmund Cartwright in 1785. It's invention was shuttle operated and steam powered and could be controlled from a single operating position. However, the machine turned out to be nonviable due to significant weaknesses during operation. In 1805, Joseph-Marie Jacquard added the functionality to weave arbitrary fabric patterns at large scales by shedding each warp end individually. However, only two decades after Jacquards invention power looming enforced itself in the industry since other technologies in related areas as spinning, sizing and powering had to be developed first. In the early 1830s, approximately 100,000 power looms were already installed in England [15]. The amount of weave machines raised exponentially with the introduction of the semi-automatic Lancashire Loom invented by Kenworthy and Bulloughs in 1842. The first electrical powered loom was introduced by Werner von Siemens in 1879 in Berlin. Until the middle of the 19th century, the operating principle of using a shuttle loom didn't change considerably. Major improvements were, however, achieved in the areas of winding and warping, such as the feeding mechanisms of yarns.

To this date, natural fibers as wool, linen, cotton, silk, jute, hemp etc. were used as raw material for the weaving process. The advent of synthetic fibers such as Polyester, Nylon or Carbon in the first half of the 20th century completely revolutionized the industry. The man-made fibers had material properties that allowed the creation of products with non-imaginable properties like extreme heat durability, water repellency or filtering characteristics. Accordingly, new looms had to be engineered in order to face the requirements that were imposed by the new physical properties of the fibers.

In 1953, the first commercial projectile weaving machine was sold and started to replace the shuttle as major yarn insertion system. The new system used multiple bullet shaped projectiles to carry the yarn across the loom. In 1972, the production of the first rapier loom started and three years later, in 1975, the first commercial air jet weaving machine became available. The yarn insertion rates raised drastically with these inventions. Technical details about the injection systems of these modern weaving machines will be briefly covered in the subsequent section.

Even though the basic principle of weaving didn't change for millenniums, the new technologies allowed for significant higher production rates, resulting in lower product and labor costs. With continuing advances in logistics and machinery, there was a reduced need for trained man power. Moreover, rising salaries in industrial countries and a quick globalization of the textile business let the historical centers of fabric production (i.e. England, central Europe, Japan and the U.S.) move to Asian countries as India, China, and Bangladesh. At the end of the 1980s, technical fabrics replaced apparel fabrics as the largest market [16] for woven products.

2.2 The weaving machine

With 5 billion Euro turnover, the German textile machinery industry was by far the biggest global player in 2012 [17] before Japan and China. With approximately 20,000 employees, 121 small to middle sized companies and 16 related research institutions [18], it has a major impact on the global textile market. Next to the most important sectors of spinning and finishing machinery, the weaving branch takes an important role within the industry. The following sections guide the reader through technical details of the weaving process. Before the operating principles of today's weaving machines are briefly discussed, the basic steps of the craft of weaving are presented. Since it is of great importance for later chapters, the basic design pattern

of woven fabrics are introduced and within this context, common fabric defect types are highlighted.

2.2.1 Terminology and weaving basics

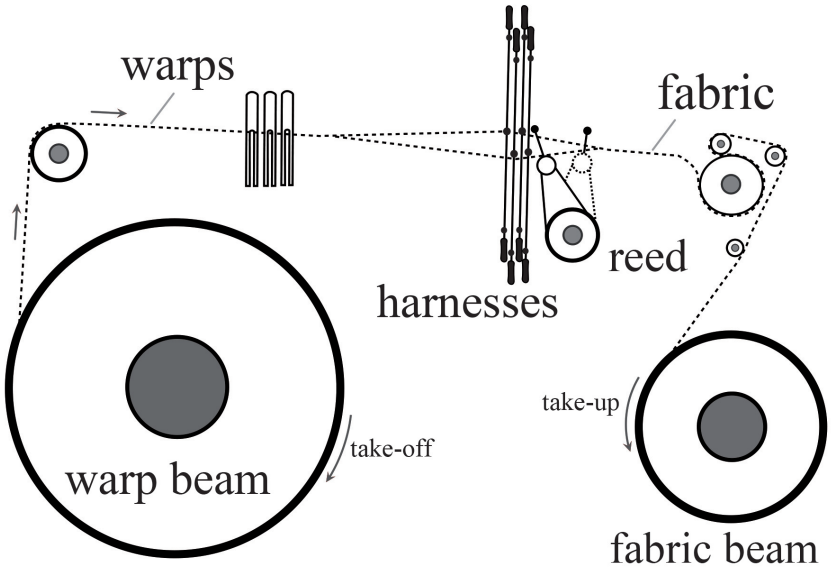

Figure 2.1: Illustration of a loom, side view. Shown are the warp beam, harnesses, reed, and the fabric beam.

Woven fabrics consist of two yarn sets which are denoted as *warps* and *wefts*, respectively. Both yarn types pass above and below each other at right angles according to a given pattern to create the fabric. With respect to the production direction, the term *warp* identifies yarns that pass longitudinal along the weaving machine whereas *wefts* are inserted across warp yarns in a transversal fashion. The pattern formed by the two sets is called the fabric's *weave*. In this work, the term *float-point* denotes the intersection points between wefts and warps, whereupon it is distinguished between *weft-floats* (weft is on top) and *warp-floats* (warp is on top). Figure 2.3 illustrates the interplay of wefts and warps for a basic fabric weave.

All weaving machines have five major components in common. The *warp beam* is the feeding device for warps which is located at the back of the loom. The *fabric beam* collects the readily produced fabric. The *harness* is a frame which is located between the two beams, to raise or lower single warps according to the predefined weave. To do so, each yarn is passed through multiple *heddles* which are attached to a harness

each. Finally, the *reed* functions like a comb to align (respectively beat) inserted wefts close to the produced fabric. Figure 2.1 illustrates the very basic components of a weaving machine.

The process of weaving can be decomposed into the five basic motions of shedding, picking, beat-up, letting of, and take up.

- *Shedding* is a synchronized up- and downwards motion of single harnesses to form a tunnel between the warps of the weaving machine. The tunnel is denoted as *shed*. Since a warp is conducted through at least two heddles (and is hence linked to the motion of at least two harnesses), the way single harnesses move up or down with respect to each other defines the final fabric weave.
- *Picking* denotes the action of inserting a weft through the opened shed of the fabric. An inserted weft is denoted as *pick*. While weft insertion using a shuttle was the main picking technique for centuries, today's weaving machines use either projectiles, air, water, or rapiers to transport the pick across the loom. The speed of picking determines the production throughput of the weaving machine and is hence of great importance for machine and textile producers.
- *Beating-up* is the action of the reed aligning the new inserted pick with the already produced fabric in a comb like fashion. The strength of the beat-up motion co-determines the density of the final fabric.
- *Letting of* and *Take-up* are the two motions of rolling off the warps from the warp beam and rolling up the directly produced fabric on the fabric beam.

All five actions are synchronized to each other to allow for a smooth weaving process without mutual disruption. Figure 2.3 depicts the actions of shedding, picking and beating in a sequence of illustrations.

2.2.2 Modern weaving machines

As mentioned in earlier sections, the flying shuttle was the global standard for automatic weaving for centuries. In fact, at the end of the 1990s more than 80 % of the 3.2 million weaving machines in worldwide use were still shuttle looms [15]. But due to their limited production speed of a maximum of 500 m of weft filling per minute and an extraordinary high noise level, they are now quickly replaced by modern, shuttleless weaving machines with more efficient weft insertion mechanisms. Shuttleless

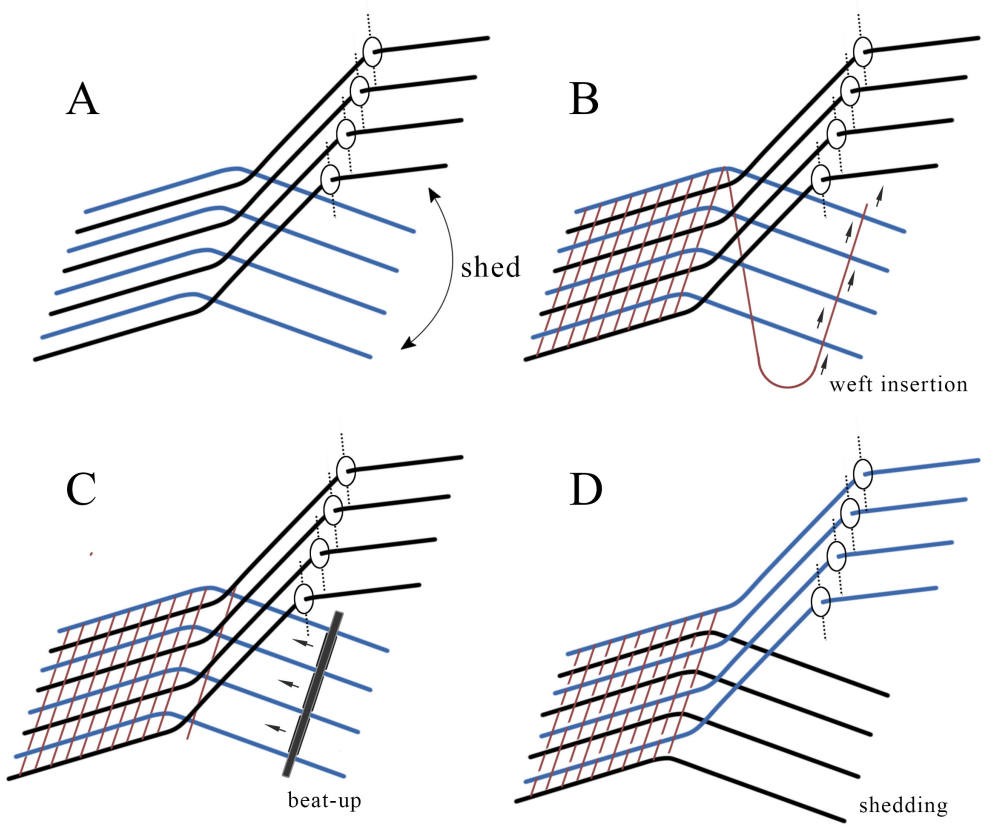

Figure 2.2: Illustration of the four basic steps in weaving. A) During the shedding step, a tunnel (shed) is formed between groups of warps. B) A weft is inserted through the shed. C) The loosely aligned weft is beat-up and pushed against the fabric. D) Shedding is repeated with different groups of warps.

weaving machines can be categorized into four weft insertion methodologies using either projectiles, rapiers, water, or air.

- *Projectile weaving machines.* While the weft supply in a shuttle loom is directly built into the shuttle, projectile weaving machines employ a small, hook-like carrier that is shot (usually using springs) across the loom to place the weft inside the opened shed. The carrier is often denoted as *gripper*. Here, the thread supply comes from a reel on the side of the loom and thus, only a small portion of yarn must be transported during each pick. The smaller size of the gripper and its lowered weight allow projectile weaving machines to operate much larger fabric width and reach higher insertion rates than shuttle looms. Two kinds of gripper machines exist. The first model is unidirectional as the

gripper travels only from left to right. A conveyor transports the projectile back and hence multiple projectiles are used simultaneously. The second model is bidirectional and uses only one gripper but two yarn supply reels on each side of the weaving machine. Once the projectile is shot across the loom, it is attached to the second weft reel and is shot back to the other side. The typical insertion rate of modern projectile weaving machines is about 1200 m of weft filling per minute.

- *Rapiers weaving machines.* Rapier looms use a grabber to pinch the weft and carry it through the shed. The grapper (or rapier) can either be a telescoping rod or a flexible steel tape. At the end of the shed, the yarn is released and the rapier is pulled back to pick up another weft. More advanced systems use two rapiers instead of one. Here, each rapier moves only half the length of the loom. While the first grapper carries the weft to the middle, the second takes over and finishes the movement. This way, only half the distance needs to be covered by each rapier. Common insertion rates of modern rapier weaving machines range at 1300 m of weft filling per minute.

- *Water jet machines.* The most economically efficient weaving machines are based on the principle of water jetting. Here, a small jet of water is shot across the loom transporting a weft with it. Since only a small portion of water needs to be used during each insertion, these machines are very cost saving while allowing for very high production speeds. Since the material wets during production, only a limited set of yarns can be processed with this method as standard yarn sizings are water soluble and warps may lose their strength when getting in contact with water. Common insertion rates of water jet systems range at 2000 m filling per minute.

- *Air jet weaving machines.* Similar to water jetting, air jet weaving machines use compressed air provided by a nozzle to project the weft through the shed. They employ electronically controlled support nozzles to carry the yarn all along the entire width of the fabric. Air jet weaving machines are the fastest but also most expensive weaving machines among the shuttleless models. They play a major role within this work, as all automatic fabric defect detection innovations proposed in this thesis have been realized using an air jet weaving machine. Air jet machines reach an insertion throughput of up to 2200 m weft filling per minute and thus form the fastest technology in weaving.

2.3 Fundamental weave pattern

The weave is a fundamental property of the fabric and co-determines the look and feel as well as physical properties of the material. Several weave pattern classes exist, the three fundamental weave pattern being the *plain*, the *twill*, and the *satin* weave. All other weave pattern can somehow be derived from this basic set. The algorithms proposed in this thesis were designed to invest fabrics composed by either one of these three weave pattern. More complex pattern like the *Jacquard* pattern are not treated as they only represent a minor branch within the woven fabric sector and have practically no relevance for technical fabrics. In fact, during the research work on the *On-Loom Imaging* project (see Section 1.3), a poll has been carried out among the project committee to conclude for the most important yarn and material characteristics these companies face during daily production [19]. The evaluation clearly showed that only plain, twill and fabric weaves are relevant for this work.

- *Plain weave*. The plain weave is the simplest and most common of all weaves. Within the pattern, weft and warps are alternately lifted and lowered during the weaving process so that a regular criss-cross pattern is created which looks alike from the back and front of the fabric. A major part of the technical fabrics invested in this work consist of a plain weave. Figure 2.3 illustrates the structural concept of a plain weave and depicts two corresponding real-world samples.

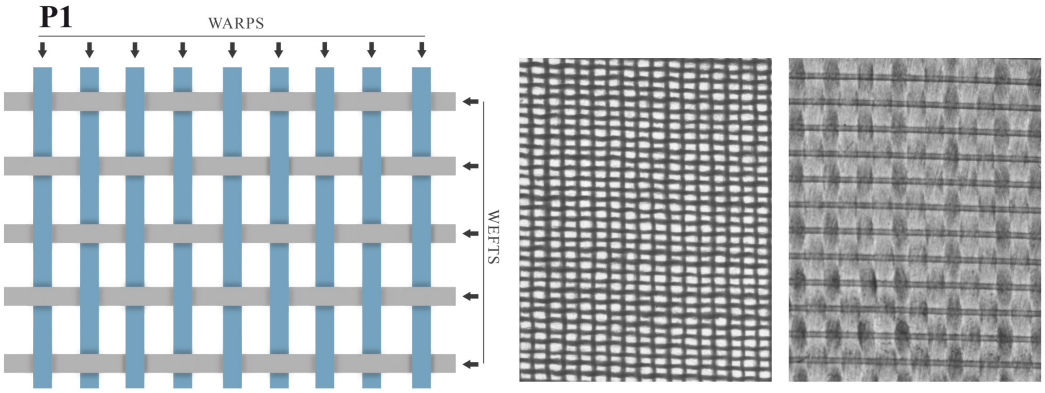

Figure 2.3: Illustration of a plain weave fabric (left) and corresponding real-word samples (right).

- *Twill weave.* Twill fabrics can be easily identified by a diagonal lined pattern which is characteristically for these materials. Twill fabrics are produced by passing a weft over at least one warp and subsequently under at least two warps. The pattern repeats for the next weft but is shifted to the right (or left) by one. The shift between two filling yarns is denoted as *step*. The visually appearing, diagonal patterns of these fabrics are denoted as *wales*. Unlike plain fabrics, the back and front side of twill fabrics look differently. Twill weaves are often described using a fraction notation like 3/1, where the nominator indicates the number of warps that are lowered followed by the numbers of warps in the denominator that are lifted when the filling yarn is inserted. Because they are constituted by fewer yarn intersection, twill fabrics can be produced in a very dense fashion which makes them very durable. Figure 2.3 illustrates the structural concept of a 3/1 twill weave and depicts two corresponding real-world samples.

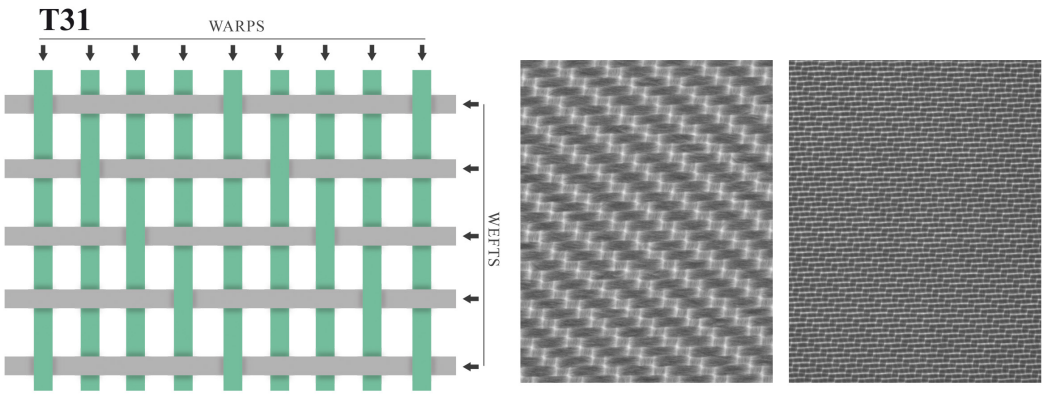

Figure 2.4: Illustration of a twill fabric weave (left) and corresponding real-word samples (right).

- *The satin weave.* Satin weave fabrics do not show any characteristical diagonal lines since interlacings are placed so that no regular progression is created. In satin weaves, at least two weft-floats are followed by one warp-float. The next weft shifts this pattern by at least two steps. This way, the front side of the material is dominated by wefts which gives the material a shiny and highly decorative look. As for twill weaves, a fractional notation can be used to characterize satin materials. Here, the nominator denotes the number of subsequent weft-floats and the denominator denotes the step amount. Figure 2.5 illustrates the structural concept of a 4/2 satin weave and depicts two corresponding real-world samples.

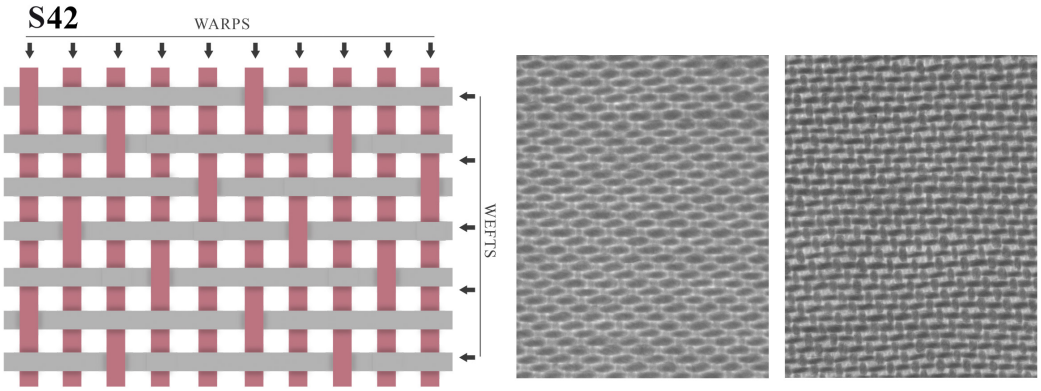

Figure 2.5: Illustration of a satin fabric weave (left) and corresponding real-word samples (right).

2.4 Fabric defects

Fabric defects occur with a broad diversity in shape, form, size, and contrast. Due the mechanics of the weaving machine, some defect types are more likely to occur than others, while the typical size of single defects in fabric images ranges from a few millimeters (1-2 mm^2) to several centimeters (1-2 cm^2). One major problem for automated visual inspection systems is the handling of the large variety in yarn materials which makes no fabric and no defect look like another. This section intends to give the reader an overview of the main characteristics of common defects as they constitute the major issue addressed in this work. Defects are here categorized into three coarse domains, namely defects that occur in weft direction, defects that occur in warp direction, and spot-like defects. If possible, a scheme is given to illustrate the nature of the defect and if available, a fabric sample with the corresponding defect is additionally shown. This section limits itself to defects that are relevant for the understanding of subsequent chapters. A more comprehensive register of weaving defects can be found in [20].

Common defects in warp direction:

1. *Warp Stripes.* Warp stripes can be caused by an overstretching of several warps, corded warps or the processing of warp yarns that differ slightly. A wrong spacing between adjacent warps can be the reason for Warp Stripes too. Figure 2.6a

illustrates the visual appearing of Warp Stripes.

2. *Broken Ends*. If exposed to too much mechanical stress or friction, it can happen that warps break during the weaving process. If not noticed, this results in bright stripes in warp direction and usually the endings of the warp get woven into the fabric creating a defect that looks similar to the *Loop* defect. Figure 2.6b illustrates a Broken End defect.
3. *Double End*. If two or more warps are woven as one yarn, a thick bar in production direction characterizes the look of the fabric. Figure 2.6f depicts a scheme of a plain weave with a Double End
4. *Misfeeds*. A common defect is created if single warps are threaded through the wrong harnesses within the shed. This continuous weave defect can be difficult to see with the naked eye. Figure 2.6c depicts a twill fabric sample with a Misfeed defect and a corresponding scheme.
5. *Capillary Breaks*. When the sizing of single warps is abraded or rough or the raw warp material is defective so that filaments stick out the yarn, one speaks of Capillary Breaks. Figure 2.6d shows a scheme of a plain weave with Capillary Breaks in warp direction.
6. *Reed Marks*. If too many warps are threaded trough a single reed dent, or single reed dents are damaged or defective, horizontally passing white bars may be visible in the material as shown in Figure 2.6e.

Common defects in weft direction:

1. *Stop Marks*. During the starting and stopping process of a loom, the yarn material is stressed and loosened which causes local deviations in the weft density. These deviations manifest themselves as thick horizontal bars across the entire length of the material (see Figure 2.7). Stop Marks are a very common defect type and are of great importance for this work.
2. *Thick/Thin Weft*. When the raw material for filling yarns has quality issues, single yarns can be inserted into the fabric that are thicker or thinner than the rest of the material (see Figure 2.7b).
3. *Double Pick*. As for the defect type *Double End*, a Double Pick is created when two wefts are accidentally inserted at the same time into the shed. It has a similar appearance as the *Thick Weft* defect as shown in Figure 2.7c.
4. *Missing Pick*. When the weaving machine fails to insert one or multiple wefts at a specific location, a larger gab is created that is denoted as Missing Pick defect. Figure 2.7d illustrates a Missing Pick on the example of a plain weave fabric.
5. *Loose Pick*. If a weft is looser (i.e. it sticks out more and is not as tight) as the other yarns, experts talk about a Loose Pick. Figure 2.7e shows a fabric image and a corresponding scheme of a Loose Pick defect.

6. *Loops*. Using air jet weaving machines, a common defect occurs when a weft is not properly carried across the loom by the air jet and gets coiled up so that yarn loops are created within the material. An example of a Loop defect is depicted in Figure 2.7f.

Most of the above mentioned defects can also occur as local defects without any specific orientation. Additionally, two more common spot-like defects occur frequently in woven fabrics:

1. *Knots*. Knots in fabrics may be caused by external objects that are woven into the material, entanglings, small local loops or dirt. Figure 2.8a shows some Knot defects in fabric images.
2. *Slubs*. Slubs are local areas of a yarn, that have less or no twist and hence spread wider than the rest of the yarns. Examples of Slubs are shown in Figure 2.8b.

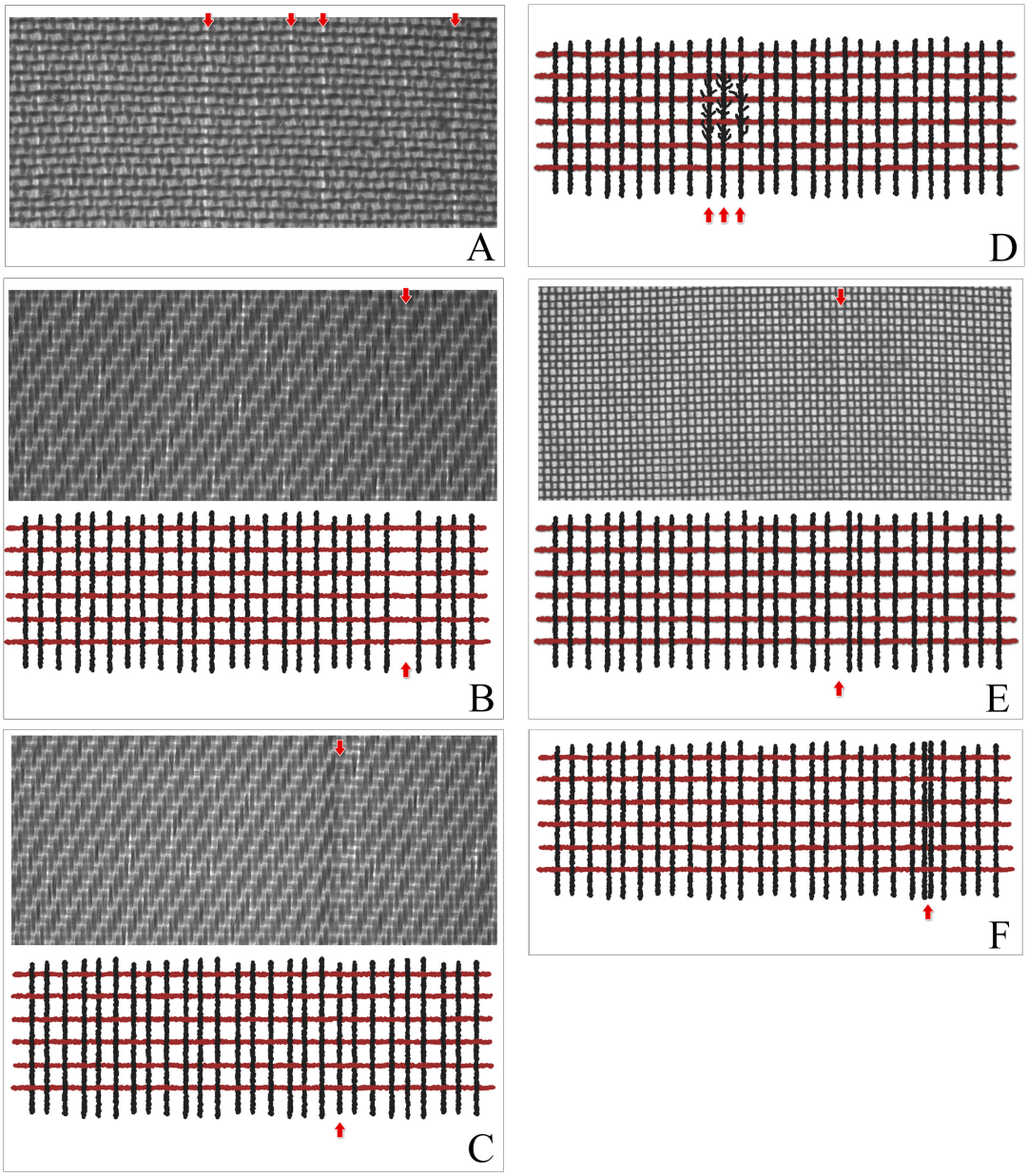

Figure 2.6: Illustrations of common fabric defects in warp direction. Shown are a) Warp Stripes, b) Broken Ends, c) Double Ends, d) Misfeeds, e) Capillary Breaks, and f) Reed Marks.

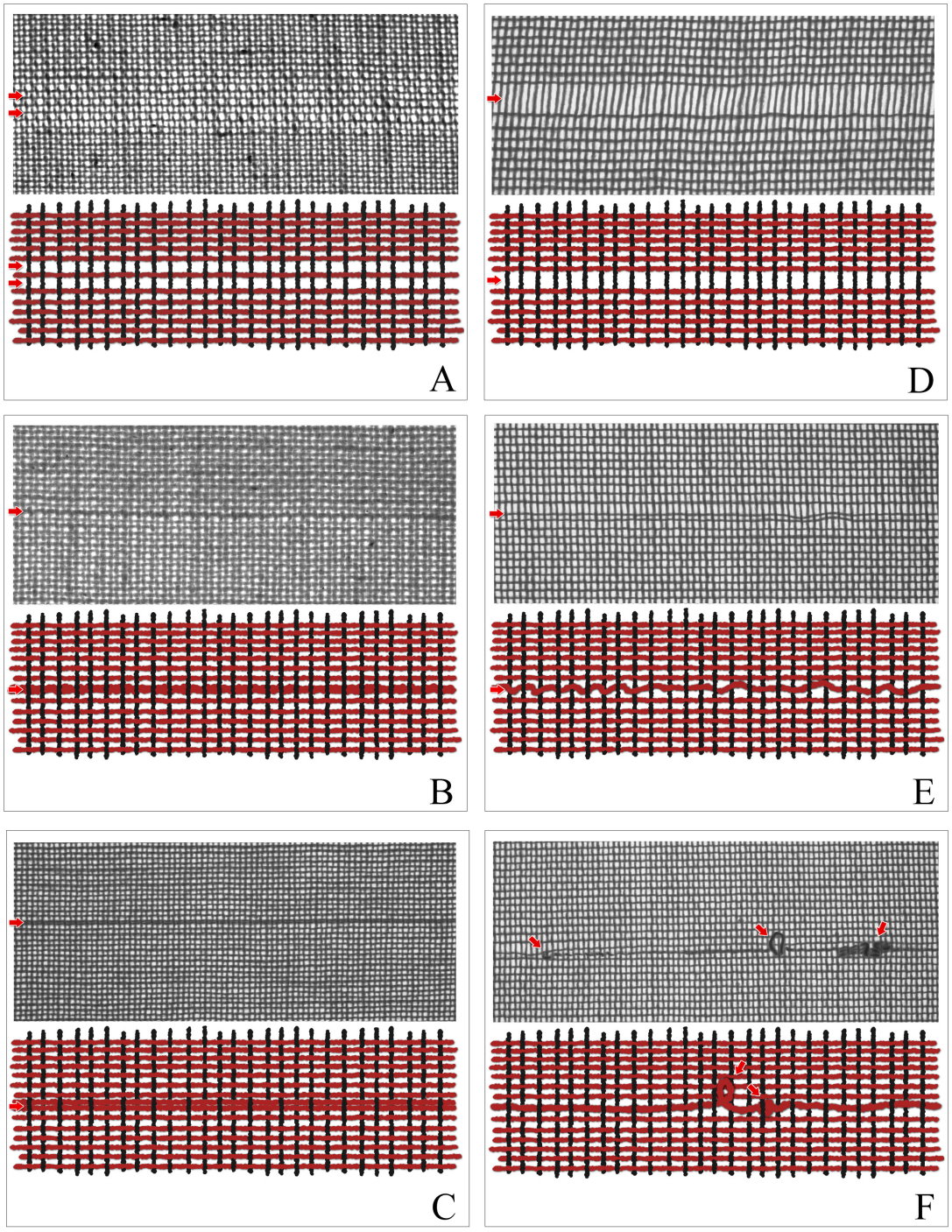

Figure 2.7: Illustrations of common fabric defects in weft direction. Shown are A) a Stop Mark with creating a local density drop, B) Thick Yarn, C) Double Pick, D) Missing Pick, E) Loose Pick, and F) a Loop.

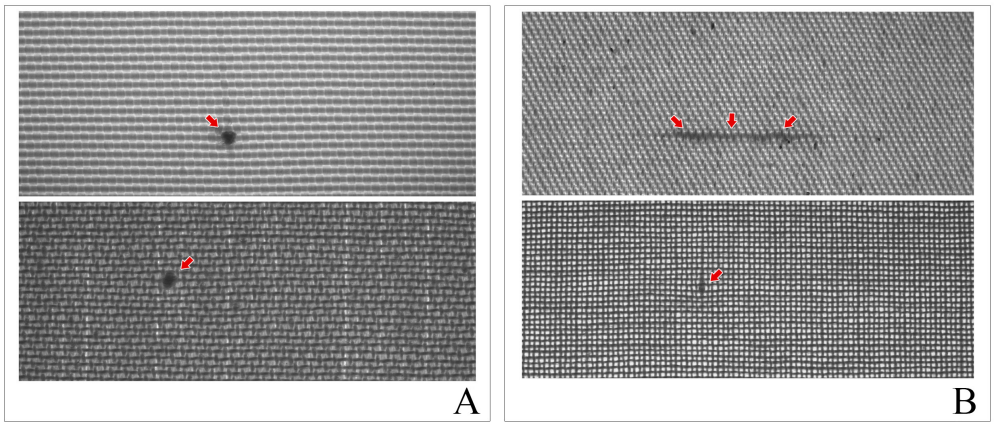

Figure 2.8: Illustrations of the two most common spot shaped defects A) Knot and B) Slub.

3 Fabric image databases

Nine Fabric Image Data Bases FIDB-{A-I} were constructed to assess the performance of the algorithms developed in this work. The following section lists the technical details and parameters of each database. The first five sets FIDB-{A-E} are used to assess the defect detection capabilities of current state-of-the-art algorithms (see Section 4.2). Database FIDB-F was composed to select a suitable deconvolution algorithm (see Section 5.3.2.1), FIDB-G was created to assess the performance of the On-Loom defect detector (5.5), FIDB-H is the foundation for the evaluation of the blind weave detection extension (see Section 6.1), and FIDB-I finally serves as evaluation platform for the assessment of the adaptive density measurement extension (see Section 7). All databases that were acquired with the matrix camera discussed in Section 5.2, are composed by images with 8 bit/pixel, a discrete resolution of 2456×2058 pixels and a spatial resolution of 415 pixels/cm. In the following, these images are denoted as images with *standard resolution*. Considerable manual effort was put into labeling to annotate all images with precise ground truth labels for fabric defects, float-points and yarn densities. The terms *on-* and *off-loom* here denote images that were acquired by a camera mounted onto the loom or images acquired in the laboratory, respectively. Table 3.1 summarizes the properties of all databases employed in this work.

3.1 FIDB-A: TILDA Database

The first image database FIDB-A consists of 540 fabric images selected from the TILDA database [21]. TILDA is the only publicly available fabric defect image database. The database is purchasable from the Institute of Computer Vision and Pattern Recogni-

tion, University of Freiburg[1]. Here, six non-patterned classes were chosen, namely the classes C1R1, C1R3, C2R2, C2R3, C3R1, and C3R3. From each class, 15 defect-free and 75 defective samples were selected. The defects are medium to big sized with respect to the image dimensions and are all easily perceivable with the eye. Each image is discretely resolved with 768×512 pixels, however, the spatial resolution is unknown. Also, the illumination technique to acquire the images is unknown. No blur or vignette effects degrade the signals. The images are, however, rotated in an arbitrary way, i.e. wefts and warps are not necessarily parallel to the image borders. For each image, a ground truth with pixel precision has been manually generated. A corresponding binary image indicates the presence of a defect with pixel values different to zero. Figure 3.1 depicts an sample of each class with corresponding ground truth labels.

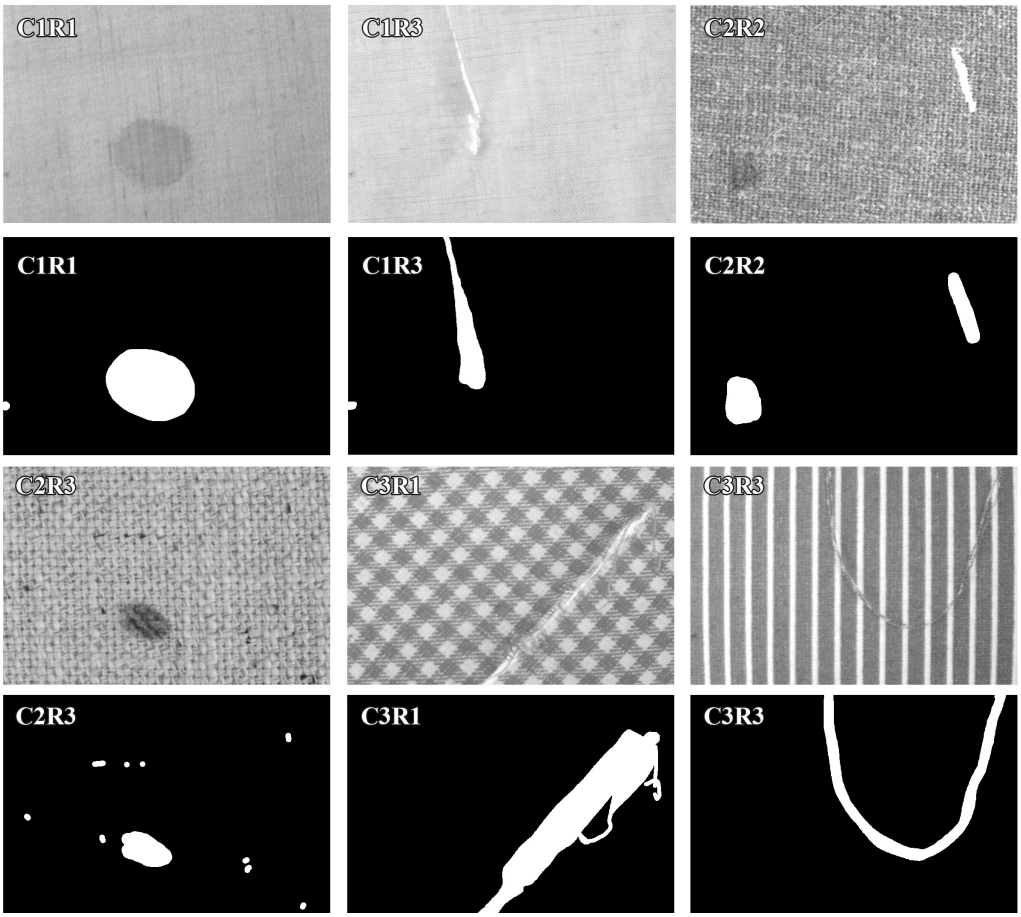

Figure 3.1: Defective fabric samples and corresponding ground truth labels from the image database **FIDB-A**. The database is composed of images from six classes (indicated with text on each image) of the TILDA fabric defect database [21].

[1] http://lmb.informatik.uni-freiburg.de

3.2 FIDB-B: Synthetic database

The second database FIDB-B is a synthetic database that was manually designed in this work using a photo processing software. In sum, 40 images were included with medium to large sized defects of any kind. Each image is composed by a near regular netting of wefts and warps with varying densities. While drawing, randomness and noise has been added to each yarn to simulate natural shape irregularities. Though, the fabric structures of the synthetic images are relatively regular and all included defects show distinctive edges and shapes. Each image has a discrete resolution of 640×640 pixels. Blur or vignette distortions were not simulated. Wefts and warps run perfectly parallel to the image borders. Ground truth data with pixel precision has been generated for each image. Figure 3.2 shows several examples of synthetic fabric images within the database FIDB-B and corresponding ground truth labels.

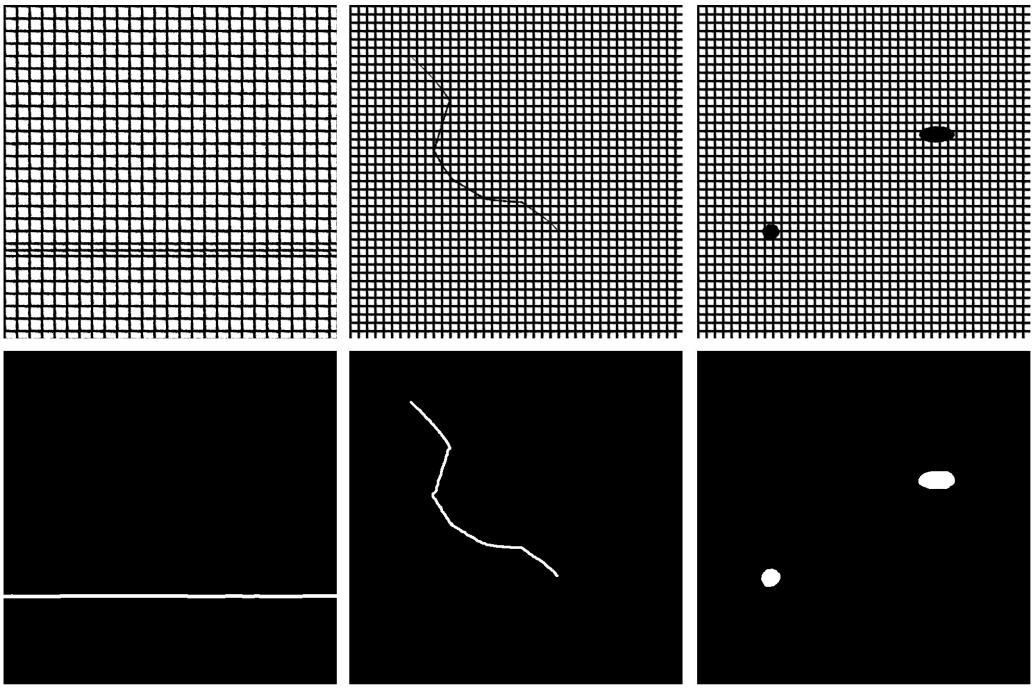

Figure 3.2: Defective fabric samples and corresponding ground truth labels from the synthetic image database FIDB-B. The database is composed by 40 manually designed images. Slight shape randomness and noise has been added to simulate the behavior of real-fabrics.

3.3 FIDB-C: High resolution, off-loom

The third database FIDB-C contains 54 real-world fabric images acquired at the laboratory with the standard resolution and back-light illumination. The images were acquired from various fabric types with either cotton or polyester material and are based on plain, twill, or satin weaves. Single yarns can be distinguished within the images. The weft densities of the samples range between 8-30 wefts/cm. For each fabric sample, 1-3 defective images and 1 defect-free reference image were acquired. The images show vignette degradations towards the borders. Contained defects range from very small defects (1-2 mm^2, i.e. ≈ 0.08 % of the total number pixels in one image) to large defects (1-2 cm^2, i.e. ≈ 8.00 % of the total number of pixels in one image). All common defect types are represented: thick wefts, double wefts, loops, wrong spacing, stop marks, yarn curvature, and more. Ground truth data with pixel accuracy has been generated for each defective sample. Figure 3.3 illustrates three samples from the fabric image database FIDB-C and corresponding ground truth labels.

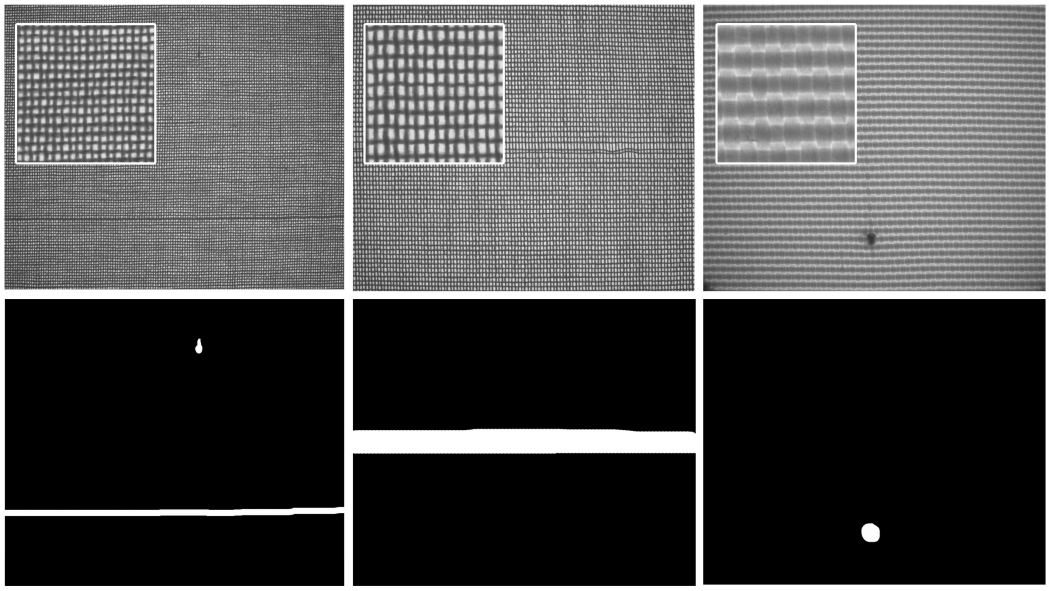

Figure 3.3: Defective fabric samples and corresponding ground truth labels from the image database FIDB-C. The database is composed by 54 real-world fabric images acquired in the laboratory using back-light illumination. Various materials, weaves, densities, and defects are covered. The database is highly resolved with 415 pixels/cm.

3.4 FIDB-D: Low resolution, off-loom

Database FIDB-D is a down-scaled version of FIDB-C. Here, the spatial image resolution of the 54 fabric images were reduced to 80 pixels/cm by down-scaling. This results in a discrete resolution of 490×411 pixels for each image. The motivation here is to create an extended real-world database with a spatial resolution that corresponds to the resolutions of fabric images commonly used by other authors for their evaluation of proposed defect detection algorithms. All other characteristics of the database correspond to FIDB-C.

3.5 FIDB-E: High resolution, on-loom

Database FIDB-E is composed by 4000 fabric images directly taken from the operating loom with a static camera. Just as for database FIDB-C, images were acquired with the standard resolution and back-lighting. Material and weave were selected to be polyester and twill, respectively. Artificial defects were forced into the material (while the loom was operating) by deliberately leaving single wefts out, inserting blob like defects with a pointed tool, drawing on the material with a pen, changing the pickage over time, leaving single warps out, changing the binding during production, and provocating stopmarks and loops. Again, defect sizes range from 1 mm^2 to 2 cm^2. A large amount of small defects is present in FIDB-E (≈ 400). The images show vignette degradations in the border regions but are free of motion blur. The camera was not moved with respect to the loom. The majority (+70 %) of the images is defect-free; for the remaining 30 % ($\approx$ 1200 images), ground truth labels were created manually by dividing each image into a grid of 8×8 non-overlapping blocks. Each block covering at least 20 % of a defect was labeled as defective. This method allows a much faster generation of the ground truth data since entire blocks can be classified as defective as opposed to selecting single pixels. Figure 3.4 depicts two images of FIDB-E and the corresponding block-based ground truth labels.

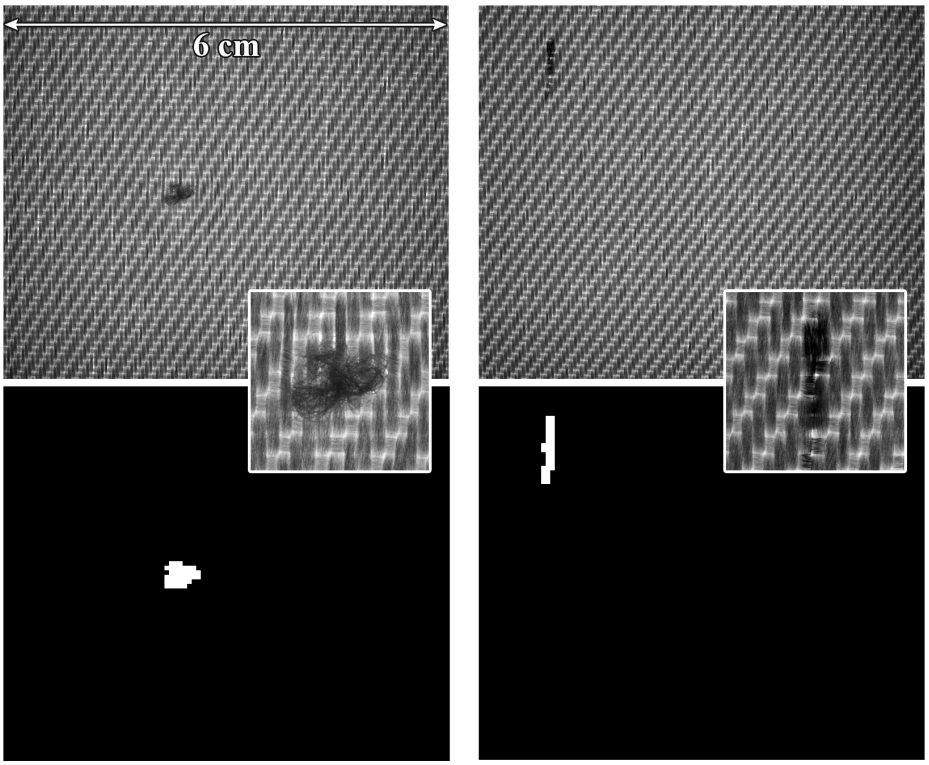

Figure 3.4: Two samples of the on-loom database FIDB-E with indicated scale and two spot defects highlighted at full resolution. Vignette degradation can be observed within the border regions. The database contains 4000 images, where +70 % are defect-free. Ground truth labels were created for more than 1200 defective samples at block resolution. Many small defects are contained in the database.

3.6 FIDB-F: High resolution, synthetic blur, off-loom

Database FIDB-F was composed to assess the output quality of the deconvolution algorithms discussed in Section 5.3.2.1. Accordingly, a set of 48 images was composed, categorized in 4 fabric types and 12 images for each type. The images where acquired with standard resolution and back-light. The blur was simulated according to the computations made in Equation 5.3.2.1, i.e. a box filter with 27 filter coefficients was used as convolution kernel. For each synthetically blurred image, the original sharp input image was kept as ground truth reference. Later experiments revealed that float-point labeling is necessary to evaluate the performance of the feature detector and the deconvolution algorithms (see Section 5.3.3). For this purpose, all warp and

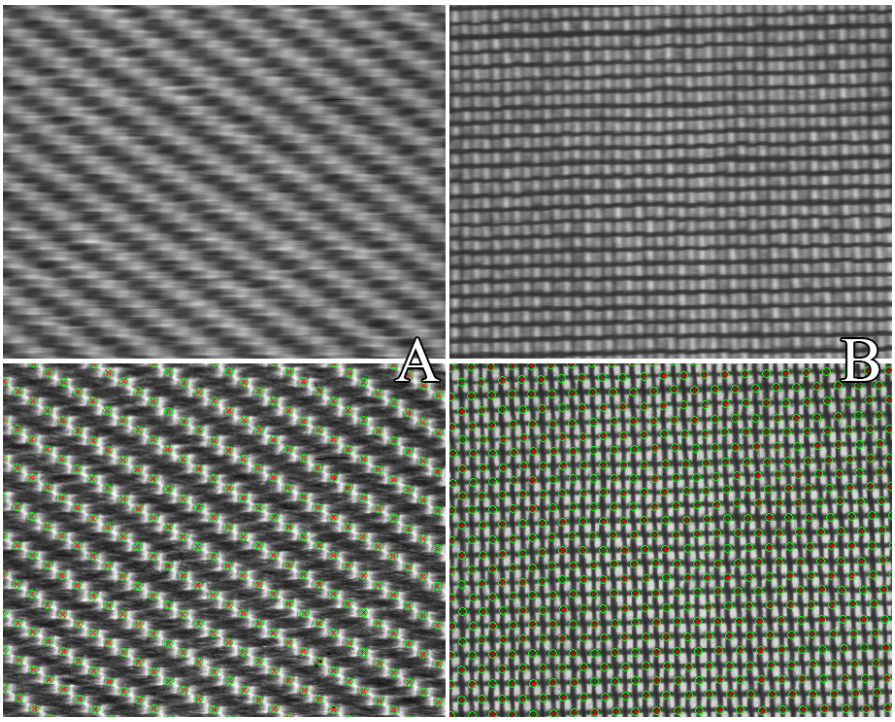

Figure 3.5: Two samples of the database FIDB-F with synthetically blurred images (top) and corresponding sharp ground truth images with labeled weft-floats.

weft crossing points in the sharp FIDB-F reference images were manually labeled. In total, 72,818 float-point labels are contained in the database. Figure 3.5 shows two sample images from FIDB-F with their float-point labels.

3.7 FIDB-G: High resolution, motion blur, on-loom

The additional on-loom database FIDB-G was acquired with the same properties as FIDB-E, but the images are degraded by motion blur as they were directly acquired from the traversing On-Loom prototype system (see Section 5). FIDB-G is composed by 4000 fabric images with standard resolution. The database contains only one material, i.e. a polyester fabric with twill weave. As for FIDB-E, all kinds of artificial defects were forced into the material, with similar sizes and appearance rates of small defects. The images show vignette degradations in the border regions and additional motion blur as the camera was placed on a moving traverse during the acquisition.

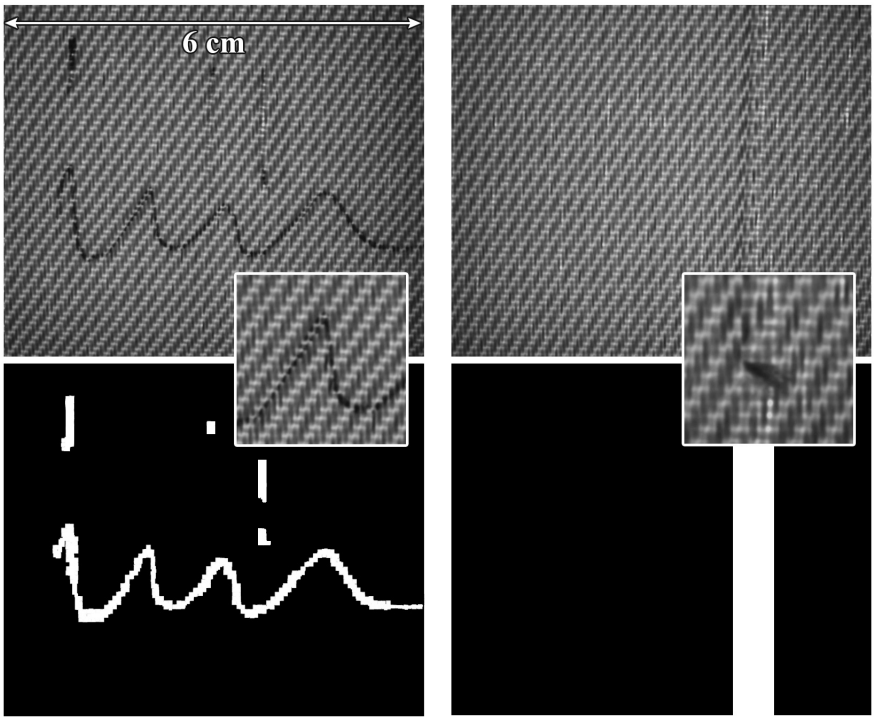

Figure 3.6: Two samples of the image database FIDB-G. All parameters correspond to the database FIDB-E but additional motion blur is present in the images as they were acquired by a traversing camera as described in Section 5.2.3.

The same procedure for creating the ground truth labels as in FIDB-E was applied. Images were divided into a grid of 8×8 non-overlapping blocks. Each block covering at least 20 % of a defect was labeled as defective. Figure 3.6 depicts two images of FIDB-G and the corresponding block-based ground truth labels.

3.8 FIDB-H: High resolution, no defects, rotation, off-loom

The database FIDB-H was created to evaluate the blind weave detection algorithm introduced in Chapter 6. It comprises 140 gray-scale off-loom images of 14 different industrial fabric materials. All images were acquired with a matrix camera and back-light, front-light and mixed illumination (depending on the fabric material) at a resolution of 2456×2058 pixels, while the spatial resolution was set to approximately $460 px/cm$. Contained samples are either of cotton, polyester, viscose, or carbon

material. Plain, twill, as well as satin weaves are covered in the database and fabric densities reside in a range of 2-64 yarns/cm. No defects are contained in the image data. All images have only mono-colored wefts/ warps and do not show any prints or colored pattern. Letters A to N are assigned to each fabric class to facilitate the identification in the evaluation. Ten images were acquired of each sample whereas single samples were subsequently rotated from 0° to 180° in steps of 20°. Manually generated ground truth data for the fabric weaves and the yarn densities was created for each sample in the database. Figure 3.7 depicts examples of all fabrics within the database.

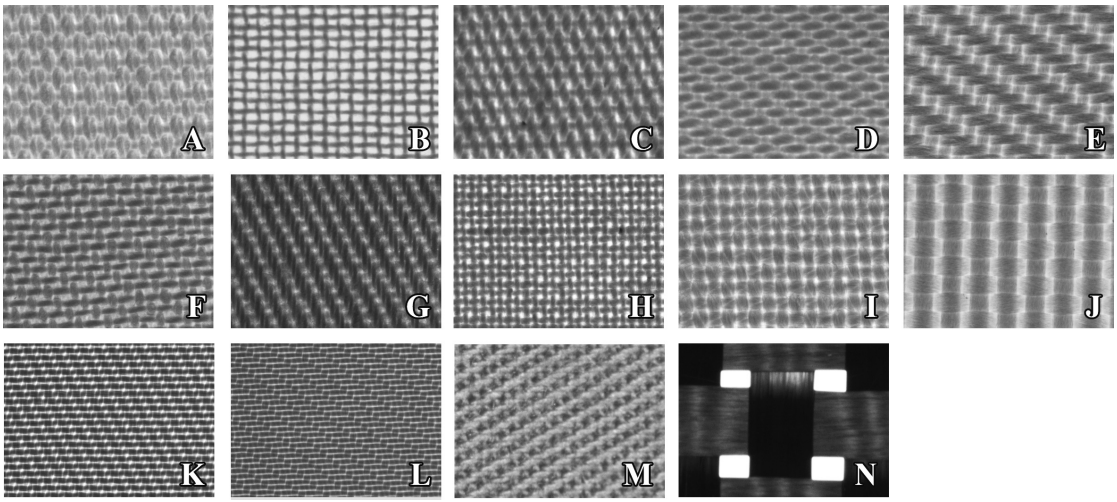

Figure 3.7: Overview of the blind weave detection evaluation database FIDB-H. Extracts (approximately 3% of original size) of 14 fabric samples contained in the provided image database. Images are annotated with corresponding identification letters A-N.

3.9 FIDB-I: High resolution, no defects, off-loom

In order to evaluate the generalization capabilities of the adaptive fabric density measurement algorithm introduced in Section 7, an off-loom database FIDB-I was finally created. Database FIDB-Is is a set of 50 fabric images, acquired using back-light, front-light and mixed illumination at a resolution of 2456 × 2058 pixels. As before, the spatial resolution was set to 460 px/cm. All images are defect-free and are not degraded by motion blur. The database contains 10 fabric types consisting of either cotton, polyester or viscose material. Plain, twill, as well as satin are covered. For

each fabric type and for each sample, the weft and warp densities in yarns/cm were manually measured and stored as ground truth for later evaluations. Letters A to J were assigned to each fabric class for identification. Figure 3.8 depicts examples of all fabrics within the database FIDB-H.

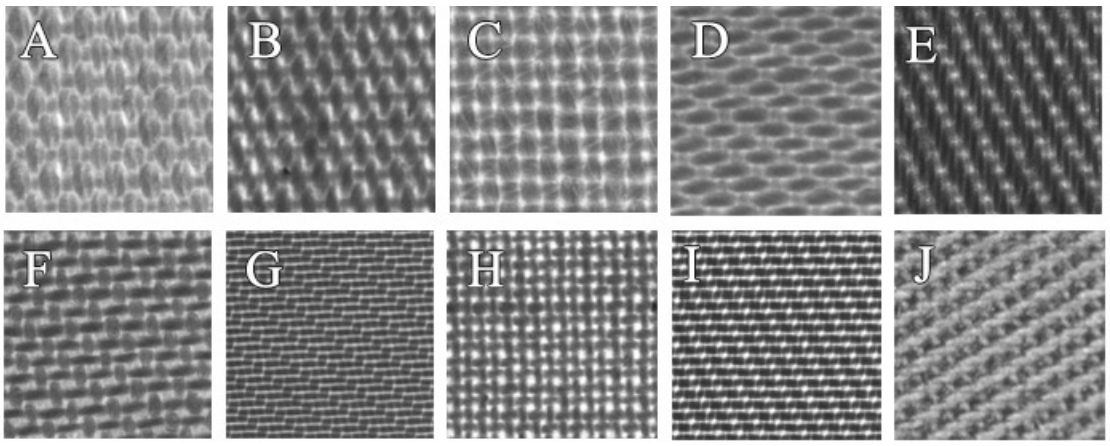

Figure 3.8: Overview of the adaptive density measurement evaluation database FIDB-I. Image sections (approximately 3% of the original image) of 10 fabric samples contained in the provided image database. The images are annotated with corresponding identification letters A-J.

Table 3.1: Overview Table of the fabric image databases used in this thesis for evaluation purposes. Indicated are the type of each database, i.e. if the database was acquired on-loom, off-loom, if it is synthetic, the number of images in it, and the resolution (image and spatial). It is additionally indicated if the database contains defective, blurred or rotated images. The last column indicates the type of ground truth labels of the database.

	type	images	image/spatial resolution	defects	blur	rotation	ground truth
FIDB-A	off-loom	90	768 × 512 unknown	✓	✗	✗	defect labels pixel precision
FIDB-B	synthetic	40	640 × 640 -	✓	✗	✗	defect labels pixel precision
FIDB-C	off-loom	54	2456 × 2058 415 px/cm	✓	✗	✗	defect labels pixel precision
FIDB-D	off-loom	54	490 × 411 80 px/cm	✓	✗	✗	defect labels pixel precision
FIDB-E	on-loom	4000	2456 × 2058 415 px/cm	✓	✗	✗	defect labels block precision
FIDB-F	off-loom	48	2456 × 2058 415 px/cm	✗	✓	✗	sharp reference images
FIDB-G	on-loom	4000	2456 × 2058 415 px/cm	✓	✓	✗	defect labels block precision
FIDB-H	off-loom	140	2456 × 2058 460 px/cm	✗	✗	✓	weaves yarn densities
FIDB-I	off-loom	50	2456 × 2058 460 px/cm	✗	✗	✗	yarn densities

PART II

STATE-OF-THE-ART

4 Benchmarking the state-of-the-art

4.1 Automated Visual Inspection - Overview

Quality control is a major component in modern production lines. Most products, independently of their area of application, have somehow passed through a quality control procedure. Whereas the realization of these quality control mechanisms among different product domains varies extensively, they share in common that recent technological advances allowed to increase their degree of automation significantly. In fact, 20 years ago human visual inspection was still the standard in quality control for almost every industrial sector. However, today's production lines most often employ highly automated systems to control product quality and standard compliance by reducing any human intervention to a minimum. Visual inspection is a sub-domain in the area of quality control. Here, camera systems and machine vision algorithms are used to acquire and analyze images of products in a contact-less manner. As opposed to functional testing, where the product is altered (compressed, stretched, flexed, heated, etc.) in some way to see if it shows specific characteristics, visual inspection does not alter or modify the product in any way. This section first discusses the topic of automated visual inspection (AVI) in a general way to provide a smooth introduction to the topic. Detached from its specific application in the area of fabric defect detection (which is covered with great detail later in Section 4.2), it is first discussed how AVI systems might be employed in other environments than the textile industry, as for example in the paper, wood or metal sectors.

4.1.1 Objectives & advantages

The advantages of automating the process of human visual inspection are manifold. To begin with, costs can be reduced as human inspectors are replaced by steadily operating machines. The same way, as machine malfunctions can be found and fixed quicker, the exclusion rates for defective products can be lowered. Significantly faster throughput can be achieved as the inspection task can be accomplished within fractions of a second. Moreover, tailor-made inspection systems can provide higher accuracy and reliability than human inspectors as they are not prone to fatigue or distraction. Finally, industrial environments are often adverse to human operators as they are either too loud, hot, humid or since dangerous materials are processed. Automated inspection systems bypass this problematic and reduce concerns for safety measures.

The objectives of visual inspection tasks can be categorized into three classes. 1) In *dimensional verification*, the product is measured with regards to its geometry, extent, orientation or shape, and it is controlled if these properties range within predefined limits. This area of application requires precise measurements and is most often based on line and edge detection algorithms such as feature detection and matching mechanisms. 2) Within the context of *completeness inspection*, it is controlled if products have all necessary parts, if their parts are placed at the right locations or if too many parts were placed. Again, edge detection and feature matching mechanisms are frequently used in these applications. Precise measurements are not mandatory in these applications as binary decisions (yes/no, all parts are present) are often sufficient. 3) Finally, the area of *surface inspection* (SI) detects cracks, scratches, texture irregularities and possible abrasions in products. In contrast to dimensional verification and completeness inspection, SI generally deploys pattern analysis methods like fuzzy logic, statistical filters, spectral methods and machine learning algorithms. It is the most active research area within the context of automated visual inspection. In fact, practically all publications in the field of visual fabric inspection can be associated with the class of surface inspection, see Section 4.2.1. As it will be shown later in Section 4.2.5, classical SI approaches generally imply a certain degree of uncertainty in terms of the reliability of their detection results. Accordingly, the major contribution that has been achieved in this work is that for the first time, a framework could be developed that shifts the task of fabric defect detection from a surface inspection problem to a dimensional verification task. This way, the uncertainty factor can be reduced to a minimum as discussed in Section 5.7.

The major drawbacks of most AVI systems are defined by their lack of flexibility and their tailor-made design process. Each individual inspection task requires different algorithmic methodologies and hardware components. Illumination, image acquisition and computing hardware must be selected and configured during each setup and often considerable research must be done to develop new algorithms that can handle a specific investigation problem. Sometimes even the production pipeline needs to be adopted in order to integrate a new AVI system. Once the system is up and running, its robust performance is generally bonded to a specific investigation job and can hardly be transferred to other problem statements. Its single-unit production and inflexible character often makes the installation of a new AVI system an expensive and time-consuming task. This is the reason why most companies that commercialize automated visual inspection systems are specialized in the quality control of a specific product, as for example the inspection of bottles, screws or paper only.

4.1.2 Literature overview

The most recent survey about the topic of automatic visual inspection was conducted in 2003 by Malamas et al. [22]. The authors reviewed 94 AVI related papers and discussed potential hardware and software components for inspection systems. Eight years earlier, in 1995, Newman et al. [23] published a survey paper that covers 272 inspection related publications within the years 1988 to 1993. As one of a few, the paper includes a feasibility study for AVI systems. Also in 1995, Thomas et al. [24] focus on the aspect of real-time inspection. The authors discuss 82 papers that deal with algorithms that are computationally efficient enough to be used in industrial real-time environments. Bayro-Corrochano et al. [25, 26] provide a broad review of AVIs that is divided into two parts. First, they cover conventional methods like classic image processing techniques and secondly discuss more advanced topics like the use of fuzzy systems or neural networks. Finally, Chin et al. published the oldest but also most comprehensive survey on the topic [27–29]. Even though cited papers do not correspond to the state-of-the-art anymore, the massive amount of 660 listed publications provides an over-complete abstract of all components that are related to AVI, including topics like X-ray inspection, imaging hardware and other system components. Most recently, Xie et al. [30] reviewed 155 papers related to the subcategory of industrial surface inspection. Here, inspection algorithms for the analysis of stone, steel, textile, wood and ceramic materials are highlighted. The majority of these methodologies belongs to the class of texture analysis algorithms. This

publication is very relevant to this thesis as many of the listed algorithms (or parts of them) are both quantitatively and qualitatively benchmarked in Section 4.2. In Annex A, the reader is provided with a detailed list of papers that treat specific problems in the area of surface inspection other than fabric inspection. The mentioned papers are not yet referenced in any of the above listed survey papers.

4.2 Fabric defect detection - State-of-the-art

It can be stated with confidence that nearly all fabric defect detection systems that have either been published in literature or that are commercially available, are based on a machine vision setup in some way. This implies the need for sophisticated digital image processing algorithms to analyze the content of the acquired camera images and distinguish potential abnormalities within it. As has been mentioned earlier, the amount of published algorithms for detecting defects in fabrics is vast. In fact, more than 500 scientific papers have been published during the last two decades, each of them discussing different methods and strategies to effectively detect defects in fabric images. The great effort spent to find solutions to the problem statement emphasizes the importance of the topic for industrial applications. In sharp contrast, as it will be discussed with more detail in Chapter 5, very few defect detection systems are commercially available. Also the fact that new publications and hence new methods for fabric defect detection appear on a monthly basis suggests that the question of how to robustly detect fabric defects on-line could not yet be answered in a satisfactory manner.

As vast as the number of publications, as manifold are the methods the authors use to evaluate their results. Almost every paper is based on custom-built fabric image databases. This implies a lack of uniform image resolutions; different fabric types, materials, weaves and differently appearing fabrics are processed in each presented work. Many papers do not even illustrate their reference images but simply present the detection results. With regards to quantitative evaluations, basically every author introduces custom assessment criteria. Frequently the assessment criteria are not even detailed but only percentages of correctly detected defects are given. Moreover, the characteristics of detected defects, i.e. their size, shape, textural appearance, etc. are also very seldom discussed. The topic of real-time, i.e. how computationally consuming is the proposed method is, again, barely touched. To sum up, the research area of automated fabric defect detection shows severe lacks of standardization which

makes it impossible to compare different methods. But, at a first glance, all methods seem to have achieved a very high degree of detection precision. In fact, none of the papers that has been studied in this work reports detection accuracies below 90%.

The next sections intend to clarify how well or poor today's state-of-the-art algorithms for fabric defect detection perform. To this end, 14 publications for fabric defect detection were selected according specific selection criteria. These criteria include the coverage of the most common approaches within the research area, the quality and comprehensibility of the technical writing, a complete and reproducible description of the processing framework, and more. Section 4.2.2 lists these criteria and describes the detailed technical processing pipelines for each algorithm. If applied, modifications are explained that were added to the original algorithm to improve its results. During the evaluation, four well defined assessment criteria were applied to evaluate all algorithms on five fabric image databases. Section 4.2.3 precisely describes the evaluation setup and gives technical details about the images. The results of the competitive benchmark are presented and discussed in Sections 4.2.4 and 4.2.5. To begin with, an overview of available literature in the research area of fabric defect detection is provided.

4.2.1 Literature survey

Three recent survey papers summarize the state-of-the-art in visual fabric defect detection. 1) In 2008, Kumar [31] reviewed 162 publications for fabric inspection. This work is considered as the most detailed and influential paper in the research area with +250 citations. 2) Mahajan et al. [32] followed one year later by covering 122 topic related publications. 3) In 2011, Ngang et al. [33] published the most up-to-date fabric inspection survey with 139 cited papers. Also in 2011, Kumar published a book chapter about computer vision based fabric defect analysis which lists several highly topical publications within the research area [34, 35]. None of the cited surveys could provide either a quantitative nor a qualitative assessment of the reviewed papers since, as the authors state by themselves, important information for such a comparison is withhold by most authors. A direct benchmark among different algorithms for fabric flaw detection was first (and last) conducted by Bodmarova et al. [36], who compared algorithms based on the ideas of co-occurence matrices, normalized cross-correlation, blob detection and spectral analysis. All algorithms were manually implemented by the authors. They conclude that the approach based on cross-correlation computations seems to be the most accurate but also most computational expensive method.

The vast majority of all published papers have in common that they consider fabric as a near regular texture that may be degraded by abnormalities (defects) of a repetitive background pattern (fabric). The task of discovering these abnormalities is generally tackled using pattern and texture recognition methods such as Gabor filter banks, Wavelet based sub-band decomposition, texture descriptors, or statistical approaches. Within this scope, Randen and Husoy [37] published an extensive survey in the research area of texture classification in 1999 which had a high impact on the research community.

4.2.2 Available algorithms

This section highlights specific methodologies and applications for fabric flaw detection. An overview is provided in Table 4.1. The methodological spectrum of all published papers stretches over the entire toolbox of the pattern and texture analysis research area. Hence, scientists tried to categorize existing methods for fabric defect detection according to their basic procedures. Kumar [31] classified all existing methods into three categories: *Statistical* approaches, *spectral* approaches and *model based* approaches. The main category here is the statistical class were he subsumes very common methods such as morphological filtering, neural network based approaches, correlation and co-occurrence matrix based approaches. The proposed division is, however, unsuitable for this work as it is too coarse and does not correctly acknowledge the impact of specific algorithm classes. Ngang et al. [33] propose a more detailed classification which consists of six classes for statistical, spectral, model based, learning based, structural and hybrid approaches. The spectral class here subsumes methods such as Gabor and Wavelet filtering whereas the hybrid class summarizes methods like Local Binary Pattern and co-occurrence based methods. Again, it is believed that the proposed categorization does not optimally reflect the occurrence of available algorithms for fabric defect detection. By direct investigation of the state-of-the-art, this work proposes a slightly different classification. It is here believed that algorithms based on the concept of Gabor filter banks are by far the most popular approach to handle the problem of defect detection in textiles. They are assigned to a discrete class in this work due to their prominence in literature. Also Wavelet based approaches are very common in the area, even though their usage seems to decrease slowly, since they are more and more used for pre-processing purposes only. Again, due to their prominence, a discrete class is here assigned to Wavelet based approaches. Texture descriptor based approaches like Local Binary Pattern and corresponding derivatives

are based on the statistical analysis of image pattern and can be placed in the same category as co-occurrence based approaches or statistics driven methods. Under the term *filtering based* methods, we here subsume all approaches that use filters (in exception of Gabor and Wavelet filters which have their own class each) of any kind, including morphological filters, optimized filters, singular value decomposition and correlation based approaches. The class of model based approaches as represented by methods such as Markov Random Fields [38, 39], Autoregressive models [40] or Poisson models [41, 42] is fairly unrepresented in literature. In fact, no corresponding paper has been published in the last 10 years. The class is hence not considered in this categorization. Since almost every paper somehow combines a basic method with several other advanced techniques, all papers can be considered as hybrid approaches which is the reason why a hybrid class is not separately considered in this work. The above considerations result in a categorization for fabric defect detection methods into four classes:

- Gabor filter based approaches
- Wavelet based approaches
- Statistics based approaches
- Filtering based approaches

In order to perform a benchmark among common methods within the different classes, 14 representative papers have been selected and were implemented directly in Matlab in order to be tested on standardized evaluation databases. The selection criteria for each paper were:

1. Clear and correct writing. Numerous spelling and grammar mistakes were considered as indicators for a lack of quality.
2. Thorough and comprehensible description of the method. If the framework was not described inchoately, the method was not considered.
3. Representative character for one of the above listed classes.
4. Uniqueness. If the basic method was too similar to an already implemented method, it was not considered.
5. A general applicability to fabrics. Methods that can only be applied to one material or one specific task were not considered.
6. Topicality. The paper should not be older than 10 years. Exceptions were only made for papers with a promising algorithmic pipeline.
7. Reviewed publication. Papers that were not peer-reviewed were not considered. Journal papers were preferred to proceeding papers.

Table 4.1: Overview of the publications that were implemented to be assessed in a qualitative benchmark for state-of-the-art fabric defect detection algorithms. For each publication, its class, identification code (used in later sections), the author (for clarity the co authors were not listed), the paper title and the corresponding reference are listed.

Class	ID	Authors	Title	Ref.
Wavelets	W1	Kim	"Texture classification and segmentation using wavelet packet frame and Gaussian Mixture Model"	[43]
	W2	Yang	"Discriminative fabric defect detection using adaptive wavelets"	[44]
	W3	Sari-Sarraf	"Vision system for on-loom fabric inspection"	[45]
Gabor	G1	Kumar	"Fabric defect segmentation using multichannel blob detectors"	[46]
	G2	Bodnarova	"Optimal Gabor filters for textile flaw detection"	[44]
Statistics	S1	Tajeripour	"Fabric defect detection using modified local binary patterns"	[47]
	S2	Raheja	"Real time fabric defect detection system on an embedded DSP platform"	[48]
	S3	Latif-Amet	"An efficient method for texture defect detection: sub-band domain co-occurrence matrices"	[49]
	S4	Ngan	"Regularity Analysis for Patterned Texture Inspection"	[50]
	S5	Chetverikov	"Finding defects in texture using regularity and local orientation (1. algorithm)"	[51]
Filtering	F1	Mak	"Fabric defect detection using morpholfilters filters"	[52]
	F2	Kumar	"Defect detection in textured materials using optimized filters"	[53]
	F3	Chetverikov	"Finding defects in texture using regularity and local orientation (2. algorithm)"	[51]
	F4	Abouelela	"Automated vision system for localizing structural defects in textile fabrics"	[54]

The subsequent sections now introduce the selected algorithms and give technical outlines on the proposed methodologies. An overview of all implemented algorithms with corresponding references is given in Table 4.1. Regarding the nomenclature, the operator $(\times)$ will henceforth be used to indicate algebraic dimensions, for instance the dimension of a matrix or a vector. On the other hand, the operator $(\cdot)$ denotes a point-wise multiplication, respectively a matrix multiplication when indicated.

4.2.2.1 Wavelet based methods

Several recent Wavelet based papers for fabric defect detection were considered as candidates for a direct Matlab implementation. For a detailed mathematical background on digital Wavelet theory and history, it is here referred to Mallat's standard book [55] and to a more comprehensive book for non-mathematicians written by Fugal [56]. With regards to the selection criteria listed above, papers by Kim et al. [57], Ngang et al. [58], Serdaroglu et al. [59, 60], and Yang et al. [61] all employ Wavelet decomposition to detect defects in fabrics but were rejected, because they were either lacking technical details, the method was too similar to a method that has been implemented already or they were too restrictive about the kind of material that can be processed. The papers by A) Kim et al. [43], B) Yang et al. [44] and C) Sari-Sarraf [45] meet the selection requirements, give a good representation of available Wavelet based methods and are hence outlined in this section. After giving a brief summary about the concepts behind each method, reported performances, necessary parameters and potential modifications applied during the implementations are discussed for each method.

The classical Wavelet Packet Decomposition (WPD) is a multi-scale analysis of a given signal that decomposes the discrete-time input into several frequency bands (also called coefficient channels) by means of a pair of complementary high- and low-pass quadrature mirror filters (QMF). Given a discrete 1D input signal, the WPD first decomposes the signal into a high frequency detail coefficient channel and a low frequency approximation coefficient channel. Since the spectral bandwidth of both channels is reduced by half after each filter operation, both channels are subsequently down-sampled by a factor of two. The process repeats for each new detail and approximation coefficient channel so that a binary decomposition tree is created. Several other decomposition schemes are known and established, among others The Wavelet Packet Frame Decomposition (WPFD) [62] and the Stationary or Undecimated Wavelet Decomposition (UWD). Figure 4.1 illustrates the concept of the

WPD, WPFD and UWD for the case of a 1D-Signal.

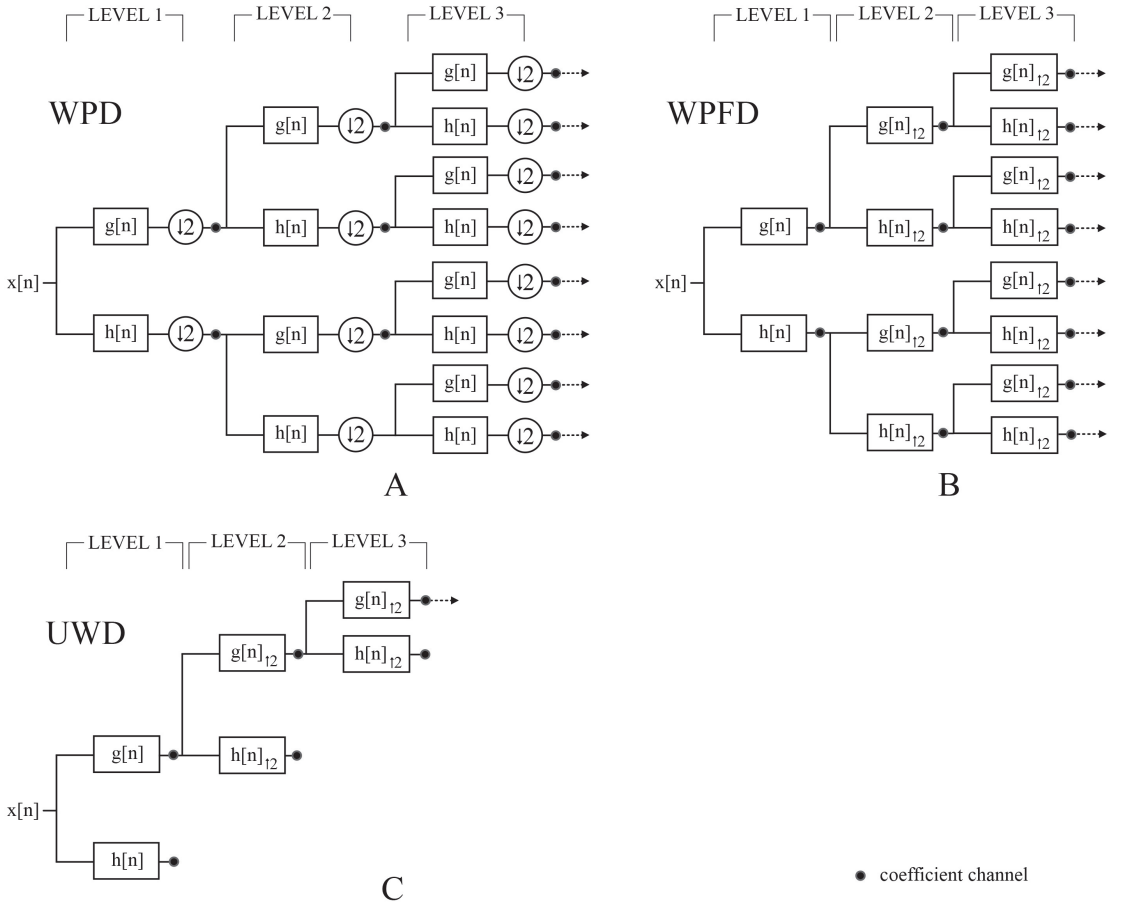

Figure 4.1: Scheme of a multi-scale A) Wavelet Packet Decomposition (WPD), B) Wavelet Packet Frame Decomposition (WPFD), and C) Undecimated Wavelet Decomposition(UWD) for three decomposition levels of a given 1D input signal $x[n]$. A) WPD: After each filter operation by one of the quadrature mirror filters $g[n]$ or $h[n]$, the corresponding output signal is down-sampled by a factor of two and the process is recursively repeated. B) WPFD: After each filter operation by one of the quadrature mirror filters, the corresponding filter is up-sampled by a factor of two and the process is recursively repeated. C) UWD: As for the WPFD approach, the filters are up-sampled but only the approximation channel is extended for further decomposition.

1.A: The method proposed in the paper entitled *"Texture classification and segmentation using Wavelet Packet Frame and Gaussian Mixture Model"* by Kim et al. [43] is an unsupervised method built on the concept of the Wavelet Packet Frame Decomposition (WPFD). The Daubechies-Wavelet based Packet Frame Decomposition is here combined with Gaussian Mixture Models [63] to approximate the distribution of non-defective feature vectors. The algorithm was originally designed for texture

classification, but was applied for fabric defect detection in the same paper, too.

Parameters and characteristics:

The method is unsupervised, detects defects at pixel level and doesn't require any reference data. Four major parameters must be configured which are 1) the dimension of the non-overlapping blocks which divide the image into sub-regions for a more efficient processing, 2) the dimension of the Gaussian Mixture Models, 3) a classification threshold, and 4) the maximum depth of the WPFD decomposition.

Reported performance:

The method was tested by the authors on selected images of the TILDA fabric image database [21]. The images were cropped to a size of 512×512 pixels, the spatial resolution is unknown. No quantitative evaluation has been conducted, instead six images from the database with corresponding detection results are shown. The detection results look precise and seem to be promising.

Modifications:

The original algorithm determines the classification threshold for the distinction of defective and non-defective blocks automatically. Our implementation uses a fixed threshold that is determined from defect-free fabric samples, since the originally proposed method turned out to be unstable at this point.

1.B: Yang et al. propose in their paper "*Discriminative fabric defect detection using adaptive wavelets*" to use a UWD decomposition for feature extraction. The distinctive characteristic in this method is the use of adaptive Wavelets which are optimized in a training phase based on labeled reference images. The supervised algorithm deploys an optimization step that adjusts the Wavelet parameters and the training vectors at the same time in the learning phase. Defect detection is performed in a detection phase using the pre-trained parameters.

Parameters and characteristics:

The method is block-based and doesn't allow for a defect detection at pixel level. The method is classified as supervised since a priori information of potential defects is necessary. The important parameters are 1) the dimension of the non-overlapping blocks that divide the input image into sub-regions, 2) the number of iterations for the cost-function optimizer in the off-line learning phase, 3) the tap size of the Wavelet filters, 4) a smoothness parameter of the cost-function, and 5) the maximum decomposition level of the UWD pyramid.

Reported performance:

The authors evaluated their method on a custom image database of 25 fabric images containing five of the most common fabric defects. The discrete resolution

of each fabric image was 256 × 256 pixels. Information about the spatial resolution was not given. The assessment metrics are defined by means of the error rate (number of all wrong classified blocks, i.e. false positives + false negatives, divided by the total number of blocks), the detection rate (true positives divided by the total number of blocks), and the false alarm rate (false negatives divided by the total number of blocks). The authors report an error rate (ER) of 1.6%, a detection rate (DR) of 97.5 % , and a false alarm rate (FR) of 0.625 % on their database. The results worsen to 4.5 % ER, 93.3 % DR, and 3.97 %, respectively, for tests on fabrics containing non a priori trained fabric defects.

Modifications:

The method has been implemented as described without modifications.

1.C: A straight forward method based on the principle of Wavelet based feature extraction is proposed by Sari-Sarraf [45] in his paper "*Vision system for on-loom fabric inspection*". The work is one of the few publications that discuss the overall machine vision system for fabric defect detection, including hardware, image acquisition and algorithms. Here, the image is decomposed into several Wavelet channels using UWD. The channels are subsequently fused by Bernoulli's rule of combination [64]. The authors use two statistic metrics and automatic thresholding according to Otsu's method [65] to detect anomalous regions in the fused image.

Parameters and characteristics:

The method is unsupervised and block-based. The main parameters are defined by 1) the maximum decomposition level of the UWD, 2) two thresholds for the inclusion/exclusion of single channels within the fusion process, and 3) the threshold for the general assessment of defective and non-defective images based on the global correlation coefficient variance.

Reported performance:

The evaluation has been conducted in several on-line experiments with more than 3700 acquired monochrome fabric images with a discrete resolution of 256 × 256 pixels. The spatial resolution has been reported to be 40 pixels/cm and 80 pixels/cm in two experiments, respectively. The assessment was conducted in terms of the metrics *detection rate* (not specified in the paper) and the false alarm rate (number of false-positively classified images divided by the total number of images). The detection rate was determined to be 89 % and the false alarm rate to be 2.5 %, in average. The authors report much better results for defects with clear and visible edges (up to 100 % detection accuracy) in comparison to defects with rather subtle intensity transitions (50 % detection accuracy).

Modifications:

Instead of using Otsu's method for the determination of the final defect detection

threshold, the parameter has been selected empirically in this work, based on the analysis of defect-free reference images.

4.2.2.2 Gabor Filter based methods

As a filter that can be scaled and shifted in an arbitrary way, Gabor filters (GF) define a sub-category of Wavelet filters. Due to their unique design on the basis of complex modulated sine functions, they can be used as kernel functions for the Short-Time Fourier transformation. Their effectiveness in dividing a given signal into distinct frequency bands for individual analysis, made the application of Gabor Filters by far the most popular technique for defect detection in woven fabric images. In the time domain, the impulse response of a Gabor filter is a Gaussian distribution which is modulated by a complex sinusoidal function. In the Fourier domain, the transfer function becomes a bandpass filter which can be tuned to arbitrary frequencies and bandwidths. Each Gabor filter is composed by a real and an imaginary part which can be used in combination or individually for feature extraction. Several authors propose to use GFs for feature extraction in combination with a wide variety of other techniques. Similar to a previously discussed method which was based on Daubechies-Wavelets, Zhang et al. [66] propose to use a Gabor filter bank and combine it with Gaussian Mixture Models for fabric defect detection. Srikaew et al. [67] present a strategy for the optimization of GFs in combination with Principal Component Analysis. Comprehensive experiments using a Gabor Filter bank and image fusion techniques were conducted by Kumar et al. [68] and Arivazhagan et al. [69]. Jain et al. [70] address the more general problem of texture segmentation using Gabor Filters. Benchmarks among different methodologies that deploy GF have been conducted by Raheja et al. [71] and Grigorescu et al. [72]. Two Gabor filter based methodologies have been selected for implementation in this work and are presented now.

2.A: Kumar and Pang propose to use a symmetric Gabor Filter bank with 16 filter kernels in their work "*Fabric defect segmentation using multichannel blob detectors*" [46]. The main characteristic of the proposed method is the usage of a channel comparison scheme which compares filter channels from an unknown image to corresponding channels from a defect free reference image using a differential method. Again, Bernoulli's rule of combination [64] in combination with first order statistics are used to fuse single channels into one image and to subsequently identify potentially defective pixels in the image.

Parameters and characteristics:

since the method requires defect-free reference images for the calibration of thresholds and for the channels comparison scheme, it is classified as semi-supervised. As the configuration parameters of the filter bank are considered to be fixed, the method has only two variable parameters: 1) A threshold for the creation of the difference channels (controls the sensitivity of the system), and 2) the dimension of the Gabor filter masks.

Reported performance:

Tested images were reported to have a resolution of 385 × 287 pixels each, and a spatial resolution of approximately 40 pixel/cm. The image database comprises 9 fabric images. As assessment metric the authors use the percentage of all defective pixels that were not classified as defective. The results show a very high variance across the database images. The values range from 2 % to 30 % miss-classification rate.

Modifications:

Instead of calculating the final threshold γ from a defect reference image, it has been determined empirically in this work.

2.B: Bodnarova et al. [73] propose to use a set of five Gabor filter pairs to detect defects in woven fabrics in their paper "*Optimal Gabor filters for textile flaw detection*". Each pair consists of a bandpass filter (background texture diminution) and a post-connected low-pass filter (noise removal). The filter kernels are optimized to the texture of a reference image during a learning phase using a cost function that minimizes a version of the popular Fisher criterion [74] for two-class separation problems.

Parameters and characteristics:

The method is semi-supervised as a defect-free image is required during the learning phase. As parameters, the method requires 1) a fine tuner that controls the sensitivity of a bi-level threshold used in the algorithm, 2) several parameters for the cost function optimizer (e.g. the convergence limit), 3) the filter mask dimension, and 4) a parameter that controls the spatial extension of the Gabor filter kernel pairs.

Reported performance:

The evaluation image database comprises 35 fabric images of size 150 × 150 pixels and a spatial resolution of 60 pixels/cm. Results were reported based on visual assessment and by means of the metrics *overall detection* (OD), *misdetection* (MD), and *false alarm* (FA) rates - none of which has been defined in the work. The

reported results state values of OD = 100 %, MD = 0 % and FA = 16 %. The illustrated detection results visually match to the defects present in the images.

Modifications:
The paper has been implemented without modifications.

4.2.2.3 Statistical methods

The term *statistical methods* for fabric defect detection here represents algorithms that are found on the ascertainment of statistical information about the texture of the fabric material. In most cases, a probability density function (PDF) is modeled for specific statistical occurrences that characterize the fabric texture. The test models are subsequently compared to reference models by means of a distance/similarity measure. Significant deviance suggests the presence of defects. Texture descriptors such as Local Binary Pattern (LBP) [75] and its variants [76, 77], Tamura features [78] and Haralick features [79] (i.e. co-occurrence statistics) are most commonly used in the context of statistical fabric defect detection. Applications for these texture descriptors as defect detectors are among others reported by Mäenpää et al. [80, 81], Livarinen [82], and Mingde et al. [83]. Bodmarova et al. [36] reported that the usage of auto-correlation statistics is a very suitable tool for detecting flaws in woven materials. Thus, five statistical methods for fabric defect detection have been selected in this work for implementation: A) The publication of Tajeripour et al. [47] discusses the usage of a modified LBP operator for fabric defect detection, B) Raheja et al. use co-occurrence statistics in a real-time system based on DSP hardware [48], C) Ngan and Pang introduce a method based on scan-line profile statistics [50], D) Latif-Amet [49] combine Wavelet filters and co-occurrence statistics, and finally F) Chetverikov and Hanbury [51] employ auto-correlation statistics for the measurement of regularity in textures.

3.A: In their paper "*Fabric Defect Detection Using Modified Local Binary Patterns*", Tajeripour et al. [47] [75] modify the popular LBP descriptor for detecting defects in fabric images. The standard LBP operator uses a circular sampling and transformation scheme to compute a descriptor for each pixel in image. The circular approach makes the method invariant to rotations but requires computational expensive interpolations. Since rotation invariance is generally not a requirement for defect detection tasks, Tajeripour et al. changed the circular neighborhood to a rectangular neighborhood. In combination with other modifications presented in the paper, the method is able to run in real-time.

Parameters and characteristics:

The algorithm is semi-supervised and block-based. It can be used as a multi-scale system since several LBP operators with different rectangular shapes can be easily combined into one operator. The adjustable parameters are: 1) The size of the rectangular neighborhood, 2) the dimensions of the detection blocks, and 3) the overlap factors of the blocks.

Reported performance:

The method was evaluated on an image database of 33 patterned and non-patterned images of dimension 256×256 pixels and a spatial resolution of 80 pixel/cm. The evaluation was conducted by means of the detection rate (DR) that has been defined by

$$DR := \frac{T_p + T_n}{N} \cdot 100,$$

where T_n is the number of defect-free blocks that have been classified as defect-free (true negative), T_p is the number of defective blocks that have been classified as defective (true positive) and N is the total number of blocks in each image. Reported results for a variety of different experiments show detection rates of 95 %, in average.

Modifications:

The paper has been implemented without modifications. All experiments reported in the paper were reproduced. Instead of the proposed log-likelihood ratio, several other similarity metrics for PDF comparison as discussed in [84] were tested.

3.B: In their recent work "*Real time fabric defect detection system on an embedded DSP platform*", Raheja et al. [48] outline the design of a detection system based on co-occurrence statistics and embedded hardware. The authors put special emphasis on the real-time implementation of the rather simple algorithmic framework on a digital signal processor.

A gray level co-occurrence matrix (GLCM) $\mathbf{C}$ for a given texture image $\mathbf{I}$ represents the distribution of conditional joint probabilities of its intensities. It is computed according to

$$\mathbf{C}_{\theta,d,k}(i,j) = \sum_{p=1}^{N} \sum_{q=1}^{M} \begin{cases} 1, & \text{if } \tilde{I}_k(p,q) = i \text{ and } \tilde{I}_k(p+\delta x, q+\delta y) = j \\ 0 & \text{otherwise} \end{cases}, \tag{4.1}$$

$$\text{where } \delta x = d \cdot \cos(\theta) \text{ and } \delta y = d \cdot \sin(\theta). \tag{4.2}$$

The values N and M represent the height and width of the image, respectively, $\tilde{I}_k$ is the texture image with k (reduced) gray-levels, $0 \leq i \leq k$ and $0 \leq j \leq k$ are discrete intensity values of $\tilde{I}_k$. The inter-pixel distance d, inter-pixel orientation θ and the binning factor k are three adjustable parameters for each GLCM. Within the scope of texture analysis, Haralick [79] proposed a set of scale- and shift-invariant features that can be easily computed from a GLCM. The most commonly used features are the Energy (ENG), the Contrast (CNT), the homogeneity (HOM), the Correlation (COR), and the Inverse Difference Moment (IDM).

Parameters and characteristics:

The method is unsupervised and block-based. Six parameters control the algorithm: 1) the GLCM inter-pixel orientation, 2) the GLCM inter-pixel distance, 3) the GLCM binning factor, 4) the block size, 5) the block overlap, and 6) the detection threshold.

Reported performance:

Since no quantitative evaluation results were reported, the performance is here summarized with respect to a related work the authors published simultaneously [71]. Here, the method was evaluated on a fabric database of 60 gray-scale images of size 512×515 each, no information about the spatial resolution was given. As assessment metric, the authors use the true detection rate (TD), the false detection rate (FD) and the misdetection rate (MD). No precise information about these metrics is given. Reported values are TD = 98.33 %, FD = 1.67 %, and MD = 0.00 %.

Modifications:

The method has been implemented without modification. Though, various combinations of the available parameters were tested other than the standard values recommended by the authors.

3.C: Latif-Ahmet et al. [49] use a combination of the Wavelet Packet Decomposition (see Section 4.2.2.1), Battle-Lemarie-Wavelets and co-occurrences statistics for feature extraction in their work "*An efficient method for texture defect detection: sub-band domain co-occurrence matrices*". Each step of the method is similar to methods that were discussed earlier in this chapter, but the way in which these methods were combined is new and promising.

Parameters and characteristics:

The method is semi-supervised and block-based. Six parameters control the algorithm: 1) The number of coefficients for the Wavelet filter kernels 2) the inter-pixel

distance in the GLCM (has been fixed to 1 in the paper), 3) the GLCM binning factor (fixed to 8), 4) the block size, 5) a rejection threshold for detecting low energy filter channels, and 6) the defect detection threshold.

Reported performance:

The method was evaluated on an image database of 36 images of discrete resolution 256×256 pixels. The spatial resolution was not detailed. The authors report a detection rate (DR, see Equation (4.1)) of 90 %. A comparison to other methods using Gabor features and Markov Random Field features has been conducted. According to the authors, these methods yield slightly better performances of DR = 92 % and DR = 91 %, respectively, at the expense of significant higher computational complexity.

Modifications:

The method has been implemented without modifications.

3.D: Ngan and Pang propose in their paper "*Regularity Analysis for Patterned Texture Inspection*" [50] an innovative method to measure the regularity of a (patterned) texture based on the processing of single rows and columns with moving average and standard deviation filters. Here, the authors define two features denoted as Light Regular Band (LRB) and Dark Regular Band (DRB). The features are computed row-wise and column-wise by means of a sliding window filter that uses first order statistics to locate intensity irregularities in the image.

Parameters and characteristics:

The method detects defects at pixel level and is semi-supervised. The tap size of the sliding filters is the only adjustable parameter.

Reported performance:

The evaluation was conducted on an image database of 106 patterned images of dimension 256×256, the spatial resolution was not discussed. Again, the detection rate, see Equation (4.1), is used as assessment metric but has been evaluated here on entire images rather than blocks. The total DR is given by 91.1 %, i.e. 105 of 106 images were correctly classified.

Modifications:

The method has been implemented without modification.

3.E: The final method that has been investigated in this work within the category of statistical fabric defect detection was proposed by Chetverikov and Hanbury [51] in 2002. In their work entitled "*Finding defects in texture using regularity and local orientation*", the authors discuss two methods to detect irregularities in (patterned)

textures. Whereas the second method is based on edge analysis and morphological filtering and will be discussed in the next section, the first algorithm describes a procedure to measure the regularity of an image auto-correlation function in order to detect abnormalities within it. The method was published earlier by the authors [85] in 1998, but was tested on fabric images in 2002 for the first time.

Parameters and characteristics:

The method is block-based and unsupervised. Three parameters control the process which are 1) the size of the blocks , 2) the block overlap, and finally 3) the detection threshold.

Reported performance:

The evaluation was conducted on the TILDA fabric image database [21]. In total, 150 images with a dimension of 768×512, were selected. The spatial resolution is unknown. The overall performance was assessed with regards to correctly and falsely classified images. Several of the investigated fabric images could not be analyzed by the algorithm (which is why the second algorithm was proposed). For the images that could be processed, the authors report 63 correctly classified images versus 7 falsely classified images.

Modifications:

A normalized (with regards the signal standard deviation) auto-correlation has been used in this implementation, because no details were given by the authors regarding this specific processing step.

4.2.2.4 Filtering based methods

Apart from Wavelet and Gabor filters, the category of filter based algorithms for fabric defect detection subsumes methods that somehow involve a filtering operation (other than low-pass filtering for noise removal). All kinds of filters belong to this class including Eigenfilters, optimized filters, binomial filters, rank order filters, morphological filters and more. A few examples of published methods within this class that were not cited in other literature overviews yet and which were not selected for implementation in this work either are listed for completeness. Shi et al. [86] deploy the concept of grayscale contrast deviation functions to detect potential defects in textile images. Furthermore, Mak and Tian [87] propose to use filters designed using the singular value decomposition (SVD) to detect flaws in fabric materials. Similarly, Kumar [88] and Castilho et al. [89] deploy a filter designed using the principal component analysis (PCA) to generate feature vectors and train a neural networks to classify defective and

non-defective fabric pixels. All above mentioned methods have algorithmic pipelines that seem to be promising. However, the papers are not detailed enough for a direct implementation as important parameters are not given. For example, the neural network approaches do not either mention important neural network training parameters nor the kind of neural network that was employed. As a result, four alternative methods were selected in this work for implementation. To begin with, A) Mak et al. [52] propose to use a framework of morphological filters to detect fabric defects. B) Kumar and Pang [53] describe the design of optimized filters, C) the edge and orientation analyzer proposed by Chetverkovs and Hanbury [51] is investigated and finally, D) Abouelela et al. [54] discuss a straight forward method based on median and variance filtering.

4.A: Mak et al. [52] discuss the use of a Gabor Wavelet Network (GWN) to determine optimal parameters for a structuring element. The structuring element is used to parametrize a set of morphological filters that are the key component for defect detection. In their work entitled "*Fabric defect detection using morphological filters*", the authors not only discuss the algorithmic framework but also cover its application within a real-time detection system. A detailed background on morphological filters can be found in [90].

Parameters and characteristics:

The method detects defects at pixel level, is semi-supervised and requires no parameters.

Reported performance:

The method was evaluated on 78 scanned fabric images with a dimension of 256×256 pixels. The spatial resolution is unknown. As assessment criterion, the authors visually and manually classify each processed image as either a 1) true detection (TD), i.e. white areas in the binary output image overlap only with defective areas, a 2) false alarm (FA), i.e. white areas in the binary image appear at locations where no defects are present, or as 3) missed detection (MD), i.e. no defects are detected at defective areas. The detection results are reported to be TD = 74, FA = 2, and MD = 2 the given dataset.

Modifications:

During the implementation, there have been experiments with differently shaped structure elements (other than a line) and it was tested if the returned parameters of the GWN could be replaced with Fourier analysis or empirically selected values, respectively.

4.B: In their paper "*Defect detection in textured materials using optimized filters*", Kumar and Pang [53] use the Fisher criterion [74] as object function to compute a

set of FIR filters that best separates defective from defect-free fabric images. The authors introduce a substantiated mathematical framework for the derivation of the filter coefficients which leads to a cost function in the form of the eigenvalue function. An optimum filter with maximum separation capability between a defective fabric sample and a defect-free sample can be found by computing a solution for the given function.

Parameters and characteristics:

The method is supervised and detects defects at pixel level. Four parameters control the process: 1) the number of generated optimal filters which depends on the amount of fabric training samples, 2) the kernel size of the optimized filters, 3) the kernel size and variance of a smoothing filter that is employed in the method and 4) the detection threshold.

Reported performance:

The method was tested on 16 plain and twill fabric images of size 256×256 pixels with a spatial resolution of 90 pixel/cm. As assessment criterion, the authors use the misclassification rate (MR), i.e. the ratio between the number of false positive pixels (defect-free pixels classified as defective) and the number of true positives (defective pixels classified as defective). For each fabric sample, the MR value is supported by the total number of true positives (t_p) and the total number of false positives(f_p). The authors tested several filter kernel sizes and different settings for the lowpass filter. Given an optimal filter kernel size, the MR is reported to be $0-2$ % for most tested images. The detection results shown in the paper look very promising.

Modifications:

The method has been implemented without modifications.

4.C: In Section 4.2.2.3, an outline of the texture regularity algorithm proposed by Chetverikov et al. [51] was given. Within the same paper, the authors discuss a second algorithm which measures dominant orientations and angular coherences within a texture image by analyzing edge information. Since the regularity algorithm showed deficiencies to process fabrics with no patterned content, the orientation approach was designed to overcome these shortcomings. Several morphological operations, including morphological closing/opening, reconstruction and connected components analysis are additionally used. It is referred to [90] for details on these operators.

Parameters and characteristics:

The method detects defects at pixel level and is completely unsupervised. 1) Five

thresholds need to be parameterized. The authors use constant, pre-defined values for the thresholds given any input image. Experiments, however, showed that the thresholds must be adapted individually to every fabric type in order to allow for meaningful detection results. Additional parameters are defined by 2) the block size which divides the image into smaller sub-regions, and 3) the block overlaps.

Reported performance:

The evaluation was conducted on the TILDA fabric image database [21]. 150 images with a dimension of 768 × 512 pixels, were selected from it. The spatial resolution is unknown. The overall performance was assessed with regards to correctly and falsely classified images. Several of the investigated fabric images could not be analyzed by the algorithm. For the images that could be processed, the authors report 60 correctly classified versus 3 falsely classified images.

Modifications:

The framework was implemented without any modifications of the core methods. Several listed constants (dimensions of structure elements, variance of the Gaussian lowpass filter, etc.) were, however, adjusted to improve the performance on the tested databases. The final merging of the binary detection images was added in this work, as the authors do not provide information on how these images are fused.

4.D: The final method implemented in this benchmark is presented by Abouelela et al. [54] in their work "*Automated vision system for localizing structural defects in textile fabrics*". It is the most straight forward defect detection framework investigated in this work as the image and pattern recognition methods employed here are very basic. The input image is simply low-pass filtered and up respectively downscaled four times in order to highlight potential defects. Yet, it is one of the few works that has been evaluated on a bulk image database with contains more than a couple dozens images. This way, the reported results are very meaningful and the algorithmic simplicity is a good contrast to the rather complex schemes discussed in earlier sections.

Parameters and characteristics:

The method works at pixel level and can be used as unsupervised algorithm. As for all other methods, the detection threshold can be learned from defect-free reference images which would make the method semi-supervised. The method requires the parameterization of three dimensions which characterize the dimension of sub-regions within the image and a value for the detection threshold.

Reported performance:

The method was evaluated on 500 images taken from an operating loom. Unfortunately, no information about the image resolution was given. The results were

assessed by means of a success rate (SR), false detection rate (FDR) and failure rate (FR). No details on these metrics were provided. The values for SD, FDR and FR are reported to be 91 %, 7 %, and 2 % respectively.

Modifications:
The method was implemented without modifications.

This closes the overview part of the algorithms that were implemented in this work. Table 4.1 summarizes the methods and assigns an identification code to each of them that will be used throughout the evaluation.

4.2.3 Evaluation

All discussed algorithms from Section 4.2.2 were manually implemented in Matlab. Consequently, the implementation followed strictly the algorithmic descriptions published in the corresponding papers. Since the scope of this chapter is to benchmark existing methods and not to propose improved algorithms, modifications were only applied when specific parts of the algorithmic pipelines showed obvious deficiencies that could be quickly handled with minor modifications. As an example, a common scenario for these adaptations is the manual selection of a threshold instead of learning it using reference data. For each algorithm, the applied modifications are documented in Section 4.2.2. Before the benchmark is conducted, the evaluation framework is first described.

4.2.3.1 Datasets

The fabric image databases FIDB-A to FIDB-E (see Sections 3.1-3.5) were used as evaluation platform to assess the performance of each algorithm. The databases cover a wide range of materials, weaves, resolutions and were acquired under various acquisition conditions. Each image is coupled to a ground truth file that marks potential defects that should be detected by an algorithm.

4.2.3.2 Assessment criteria

Two qualitative metrics, two quantitative metrics, and two additional assessment criteria were used in this work to evaluate the fabric defect detection performance of each algorithm.

Quantitative assessment. To begin with, an analyzed fabric image and the corresponding ground truth label are divided into a grid of non-overlapping blocks of size 8×8 pixels each. In this work, a block $\mathbf{B}_i$ is considered as defective if at least 20 % of its pixels are labeled as defective, it is defect-free otherwise. In a formalized notation, this can expressed as

$$\begin{aligned} &\forall\, i \in \{1, .., M\} : \\ &\mathbf{B}_i := \begin{cases} \text{defective}, & \text{if } p_i / P \geqslant 0.20 \\ \text{defect-free}, & \text{otherwise.} \end{cases} \end{aligned} \tag{4.3}$$

Here, M is the total number of blocks in an image, the value p_i represents the amount of pixels labeled as defective in a given block $\mathbf{B}_i$, and P being the total number of pixels in a block. The block size of 8×8 pixels represents a good balance between precision and effectiveness on the given databases. A block in the binary output image is classified as

- True Positive (TP) if $B_i \mapsto$ *defective* $\wedge$ $G_i \mapsto$ *defective*
- True Negative (TN) if $B_i \mapsto$ *defect-free* $\wedge$ $G_i \mapsto$ *defect-free*
- False Positive (FP) if $B_i \mapsto$ *defective* $\wedge$ $G_i \mapsto$ *defect-free*
- False negative (FN) if $B_i \mapsto$ *defect-free* $\wedge$ $G_i \mapsto$ *defective*.

Again, $\mathbf{B}_i$ denotes a block in the processed fabric image, $\mathbf{G}_i$ denotes the corresponding block in the ground truth image, and the operator $\wedge$ represents a boolean AND operation.

The *hit rate* (HR) of a given algorithm is now defined as the total number of correctly detected, defective blocks ($|TP|$), divided by the total number of defective blocks ($|TP| + |FN|$) in the ground truth,

$$HR = \frac{|TP|}{|TP| + |FN|} \cdot 100 \ \ [\%]. \tag{4.4}$$

The operator $(|\cdot|)$ denotes the cardinality of a set, i.e. the amount of corresponding blocks. The HR ranges in the interval $[0,100]$, whereas high values indicate very precise defect localization, which is why the *hit rate* is an indicator for the defect segmentation capability of a given system. The HR is given in percent (%) in this work. It is directly related to the metric *recall*, which is a very commonly used metric for assessing the performance of a given classifier. The difference is that the assessment in this work is conducted block-wise and not at pixel level. This modification makes the overall assessment more robust against noisy false classifications and allows for a much quicker generation of the ground truth data.

To get a measure for the system's false segmentation rate, the *fault rate* (FR) is introduced. Again, the assessment is conducted block-wise with 8×8, non-overlapping blocks. The FR is defined as the ratio of false-positive labeled blocks divided by the total number of defect-free blocks in the ground truth, i.e.

$$FR = \frac{|FP|}{|FP| + |TN|} \cdot 1000 \ \ [‰]. \tag{4.5}$$

The FR here ranges in the interval $[0,1000]$, whereas values above 5 already characterize very frequent false segmentations. The higher multiplication factor (1000 instead of 100) was chosen to facilitate the reading and interpretation of the values as they are generally rather small compared to the other metrics. The fault rate corresponds the *fallout* or *false positive rate* of a system. The combination of the *hit rate* and the *fault rate* defines the quantitative assessment criterion in this work. The two measurements were computed for each database individually on the set of all available blocks within the database.

Qualitative assessment. The practical usefulness of a visual inspection system is not necessarily well rated by its precision for defect segmentation, but rather by its general ability to indicate the presence of defects in an image. Moreover, fabric defects have a very low occurrence probability which means that the vast majority of the images acquired by the visual inspection system are expected to be defect-free. Thus, a good defect detection system should only alert if a defect is actually present in the image in order to save time and relieve a human operator from any interventions. To consider these observations, a coarse assessment was conducted on all five databases individually by means of the coarse hit rate (CHR) and the coarse fault rate (FR). In this context, the coarse hit rate is defined by

$$CHR = \frac{1}{Q} \sum_{i=1}^{D} h(\mathbf{I}_i) \cdot 100 \ \ [\%] \tag{4.6}$$

$$h(\mathbf{I}_i) = \begin{cases} 1, & |P_{Gi}| >= 1 \wedge HR_i \geq 15 \\ 0, & \text{otherwise.} \end{cases}$$

Here, the term $\mathbf{I}_i$ represents a fabric image within the database x, the value D represents the total number of images in it, and Q is the total number of defective images. The value HR_i is the achieved hit rate for the image $\mathbf{I}_i$, the value $|P_{Gi}|$ denotes the number of positive (defective) blocks in the corresponding ground truth of the image $\mathbf{I}_i$. In words, the CHR is the fraction of processed images in the database that are actually defective, and that were labeled with a HR of at least 15 %. The value of 15 % is large enough to indicate the presence of defects in an image, even if potential post-processing methods are employed (to decrease false alarms) that might spuriously remove some true positive segmentations. The CHR ranges in the interval $[0, 100]$.

Similarly, the coarse fault rate (CFR) is defined by

$$CFR = \frac{1}{O} \sum_{i=1}^{D} f(\mathbf{I}_i) \cdot 100 \ \ [\%] \tag{4.7}$$

$$f(\mathbf{I}_i) = \begin{cases} 1, & |P_{Gi}| = 0 \wedge FR_i \geq 2.0 \\ 0, & \text{otherwise.} \end{cases}$$

The value O is the total number of defect-free images in a given database x and the value FR_i is the fault rate for the image $\mathbf{I}_i$. The coarse fault rate represents the fraction of defect-free images in the database that were labeled with a fault rate of at least 2.0 ‰. An effective and practically usable AVI system should have a CHR that is 100 % and a CFR that is as close to zero as possible.

Real-time performance. Moreover, the real-time capability of each algorithm was assessed on a qualitative basis. Here, the computational complexity of each algorithm was estimated by measuring the computation time of its core functions, which were implemented in highly optimized and parallelized C++ code for this purpose. As an example, the Fourier Transform and its inverse for detection algorithms based on filtering was implemented in C++ (using optimized libraries) and its computation time was measured. The overall computational complexity of each algorithm was accordingly estimated and its real-time ability (binary *yes* or *no*) was rated with respect to a given image database and computational hardware consisting of an i7950 CPU, 8GB RAM and an NVIDIA GTX 580 GPU.

Small defect detection robustness. The ability of a given algorithm to robustly detect

small defects was additionally assessed, i.e. defects that cover ≤ 0.1 % of the total amount of pixels in an image. For this purpose, the total amount of small defects in a given database was computed. If at least 80 % of these defects could be detected (i.e. at least 50 % of its pixels were labeled as defective) the algorithm was attributed with the ability to robustly detect small defects (binary *yes* or *no*).

4.2.3.3 Parameter selection

The adjustable parameters of each algorithm are listed in Section 4.2.2. The optimum parameter sets reported by the original authors were always tested first in this evaluation. However, specific parameters needed to be adjusted in order give optimal detection results for the fabric images tested in this work. Within this scope, parameters were either empirically fine tuned, e.g. block sizes (if applicable) were adjusted to match the spatial resolution of the given database and thresholds were manually tuned to improve the performance. On the other hand, since most algorithms do not require many parameters to be adjusted, brute force optimization was performed to find optimal parameter settings by either maximizing the cost function

$$f := (1+\beta) \cdot \frac{HR \cdot (1-FR)}{\beta \cdot HR + (1-FR)} \tag{4.8}$$

for each database and algorithm. Equation (4.8) is a weighted version of the F1-score metric [91] that represents the harmonic mean of the two test accuracies HR and FR. The weighting factor β was chosen empirically to be $\beta = 10$ to reflect the fact that small changes of FR have a similar impact on the quality of the results as larger changes of HR. Also the fact that FR and HR have different units (percent vs. per mille) is partly compensated by the weighting factor β. The reverse value $1-FR$ was chosen to ensure that higher values represent better results. In general, it is difficult to define a cost function that considers HR and FR simultaneously, as both accuracies have different value ranges that cannot be easily normalized. The computational complexity was not considered in this evaluation on a quantitative basis which is why all parameters were optimized with respect to the defect detection performance rather than the computing time. All parameters were adjusted anew for each database.

4.2.4 Results

Tables 4.2 and 4.3 list the benchmark results for all five databases and all 14 algorithms. Values for HRs, CHRs and CFRs are rounded to the nearest integer and are given in percent (%). The values for FRs are given in permille (‰) without rounding. Check and cross marks represent *yes* and *no* statements. The abbreviations used to identify each algorithm are itemized in Table 4.1. Figure 4.2 illustrates some detection results with corresponding hit and fault rates, in order to give the reader an idea of the meaning of these values. Best results can be observed for the synthetic database FIDB-B. Here, hit rates of up to 96 % can be reported, which is an indicator for very high defect segmentation quality, whereas the fault rates achieve values far below 1.0 ‰. A maximum CHR of 99 % with no reported false alarm was achieved by Ngang's method (S4). Most algorithms are able to robustly detect small defects in FIDB-B and real-time processing can be achieved by all algorithms except S5.

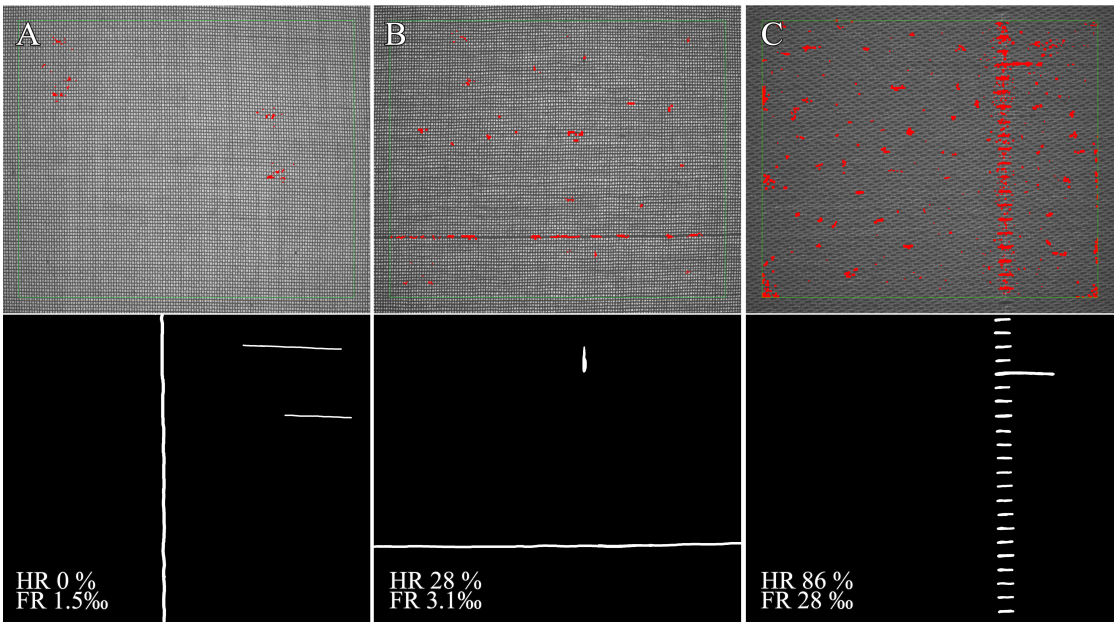

Figure 4.2: Three defective fabric samples with super imposed defect detection results (red). The green border marks the region of evaluation for images of the databases FIDB-C to E. The corresponding Hit (HR) and fault rates (FR) such as the ground truth labels are shown.

The results worsen on the TILDA database FIDB-A. The best performance values were achieved by the Gabor filter bank G1 (CHR 95 %), the LBP approach S1 (CHR 91%), the

regular band method S4 (CHR 86 %) and Chetverikov's regularity approach S5 (CHR of 93 %). These high detection rates are directly connected to significantly higher CFR values with respect to FIDB-B of up to 9%.. Only the aforementioned algorithms were capable to robustly detect small defects. The statistical and Gabor based methods perform better than filtering and Wavelet based methods.

The border regions of each image in the database FIDB-C were not analyzed because vignette degradations would spuriously worsen the results. Instead, a frame with 100 pixels distance to the image borders was drawn and all assessments were performed within it. Three of the tested algorithms were able to robustly detect small defects. The algorithms with the best detection results (G1 and S5) are computationally expensive so that a real-time performance is not possible on the database. The algorithms F2 and F4 show high detection results as the CHR reaches values of 93 %. The detection performance is linked to high CFRs of 44 % and 36 %, respectively. The best performance with real-time applicability on FIDB-C can be observed for algorithm S1, achieving a CHR of 91 % and a CFR of 9 %. The Wavelet based methods completely collapse on the database.

The results on FIDB-C improve on its down-scaled version FIDB-D. In detail, the Gabor filter bank (G1) achieved the best results among all methods as 98 % of the defective images were correctly labeled and only one of 11 (9 %) defect-free sample was spuriously marked as defective. The method G1 is able to process the input images in real-time. Small defects could only be robustly detected by the methods G1 and S1. The G1 defect segmentation performance is given by a HR of 77 % and a FR of 1.98 ‰– the best result among all non-synthetic databases.

Finally, the bulk evaluation on the extensive database FIDB-E was performed. As expected, the performance of all algorithms worsened with respect to their results on FIDB-C. The performance values of the Wavelet algorithms W1-W3, the filtering based methods F1-F3 and the Gabor approach G2 are very low. The detection results here appear to be more or less random. Four algorithms, however, achieved notable results. The methods S1 and S4 have CHRs of 89 % and 84 %, respectively. The detection results are accompanied by CFRs of 7 % and 12 %, respectively. Thus, more than 196 defect-free images out of 2800 were labeled as defective. The defect segmentation capability is mediocre as suggested by hit rates of 71 % and 74 %, respectively. Again, best performances can be reported for the algorithms G1 and S5. Here, a maximum of 91 % CHR and 71 % HR could be achieved. As for the others methods, G1 and S1 are

both sensitive to false alarms as shown by minimal values of CFR 6 % and FR 1.99 ‰. The algorithms G1 and S1 are computationally too demanding to process the images of FIDB-E in real-time. None of the tested algorithms was able to robustly detect small defects.

4.2.5 Discussion

Among the four defined classes of defect detection algorithms, the Wavelet based methods produced the weakest results. In fact, acceptable results could only be achieved on FIDB-B which is by definition the easiest database, as the synthetic fabric images show a very high regularity without local distortions and simulated defects have very sharp and distinct edges. On the other four databases, all three Wavelet based methods fail to robustly detect defects. Moreover, the detection mechanisms are so sensitive to false alarms that even correct detections are probably the result of random effects. A closer look into single Wavelet channels, as fundamental part of the multi-resolution decomposition, clearly showed that the Wavelet filters (of any kind) can only emphasize present defects in a fabric image if sharp and easy distinguishable edges of a noticeable size are present. Though, fabrics of this kind are the exception in real-world environments, subtle contrast and color differences and blurred edges are more commonly encountered. Low-contrast and small defects get simply filtered out within the decomposition pipeline and hence no information is left for subsequent feature extraction modules. As a conclusion, it can be stated that Wavelet decomposition might be a powerful tool in the world of pattern recognition, but it is not suitable for robust fabric flaw detection as the requirements here differ significantly. Also, the filtering based approaches could not convince in this benchmark, as their false alarm rates (high CFR and FR values) were too high for practical application. The Gabor and statistic class contributed the best performing algorithms within the benchmark.

In detail, the best detection and segmentation results on all databases could be achieved by Kumars Gabor filter bank G1 and Chetverikov's autocorrelation method S5. Unfortunately, the fault rates are too high for practical application and both methods are far too complex for real-time processing of highly resolved images. To get a feeling for the oversensitivity, the CFR of S5 is 6 % on the FIDB-E database. Given a camera frame rate of 15 frames/second, the algorithm spuriously reports 540 defective images during a recording time of 10 minutes. This would not be acceptable in an industrial environment as a human operator would be constantly alerted to ac-

knowledge each false alarm. Post processing techniques could be used to significantly lower the CHR by rejecting small defects below a minimum size, but the problem of oversensitivity cannot be completely solved in this way without compromising the detection accuracy.

Slightly less precise results were observed for the methods S1 and S4. Both algorithms are computationally rather simple in comparison to G1 and S5, but their performance is similar. Especially the good results of S4 were surprising since the method was originally designed to detect defects in patterned fabrics whereas tested images in this benchmark are non-patterned. Much potential is seen for S1 as it is based on Local Binary Patterns. Many version of the original LBP operator were published in recent time [76, 77, 92–94] and given the good detection results of S1, the capability of these new methods to detect fabric defects should be implicitly investigated. In fact, LBP based operators are very popular in the texture classification community, so that an entire fabric defect detection benchmark could be dedicated to these methods only.

Another insight from the benchmark results was the fact, that none of the tested algorithms was able to robustly detect small defects (SDs) within the highly resolved database FIDB-E. As mentioned in Section 4.2.3.2, SDs were defined as defects with less than 0.1 % of the total amount of pixels within an image, i.e. areas of approx. 70×70 pixels or respectively 1.7 mm^2 in FIDB-E images. Even though robust SD-detection could be achieved by several algorithms on FIDB-C, the SD-appearance frequency in FIDB-E is much higher as in FIDB-C (400 compared to 7). The results on the bulk database are hence more representative. The SD-detection capability drops significantly when the image resolution lowers, as it could be seen on the database FIDB-D. Here, small defects have areas of only 12×12 pixels which is too small in most cases to allow for a robust detection as most false detections have similar dimensions. This unreliability of detecting small defects is a major bottleneck of all investigated methods.

From the experiments it can be seen that a priori knowledge about potential defects does not affect the detection results in a positive way. In fact, both supervised methods W2 and F2 give poor to mediocre results compared to alternative non-supervised, respectively semi-supervised methods. Their capability for generalization and detecting unknown and non-trained defects is rather disappointing. Fabric defects are too diverse in their appearance as shape, color, size, and texture vary significantly from sample to sample. Accordingly, off-line databases of known defects can only describe a marginal part of the total set of possible defect characteristics and thus

the major advantage of supervised inspection, i.e. a priori knowledge, is relativized. Moreover, due to the very low appearance probability of fabric defects, any a priori knowledge, given a real-world industrial setting, is rather unlikely. It can be concluded that supervised methods are more or less a theoretical construct and can be classified as unpractical for industrial application.

The choice of block-based versus pixel-based algorithms does not seem to have a decisive impact on the detection performance. In fact, among the three best rated methods, namely G1, S1, and S5, two are block-based and one method detects defects at pixel level. The defect segmentation quality among these methods is comparable as indicated by similar hit and fault rates. The precision and in most cases the computing time of block-based methods depends on the chosen block dimension. As a rule of thumb, blocks with a size of 1-2 % of the image width and height give satisfying results, however the block size must be selected large enough to cover enough information on the underlying texture which is why for specific fabrics, block-based methods have lower segmentation capabilities. By using overlapping blocks, block-based analysis can reach pixel-precision (at the expense of higher computation times) by increasing the overlapping factor accordingly.

Regarding the computational efficiency, more complex methods do not necessarily seem to have significant advantages over computationally saving methods. As an example, the method S4 is considered as one of the most simplistic algorithms implemented in this work, yet its detection performance on all databases ranks constantly within the upper middle field. Also S1 is computationally very effective and competes with the more complex algorithms at a comparable level. However, the methods G1 and S5 gave the best detection results and are simultaneously so demanding that they cannot process highly resolved images in real-time.

4.2.6 Conclusion

Three sources for potential mistakes in this chapter can be identified.

1. It cannot be fully excluded that the author of this work did implementation mistakes or misinterpretation of the algorithmic pipelines that were investigated in this chapter. All algorithms were, however, implemented after thorough analysis

of each paper and were reviewed by at least two people (student assistants and the author).

2. Also the parameter selection for each algorithm might have been erroneous or suboptimal, even though it was conducted by optimizing the output results.
3. Moreover, the results reported by the original authors might have been achieved using algorithmic pipelines that differ from the pipelines presented in the corresponding papers.

Apart from these possible limitations, it can be stated that an important observation made from the experiments in this chapter is, that none of the investigated algorithms was fully able to reach detection accuracies that were at a similar level as the results reported by the original authors in the corresponding papers (see Section 4.2.2). Since the evaluation databases used in this work significantly differed from the databases used by the algorithm authors, it can be concluded that their databases were probably less challenging in terms of real-world requirements. This assumption is supported by the very good performances of most methods on the synthetic image database FIDB-B. Also, it seems that most authors expect defects to have a rather large size with respect to the image dimension. Indeed, when facing these conditions, most algorithms are capable to robustly detect all present defects. In real-world situations, however, severe defects of minor size are frequent and must be detected with certainty.

Hence, the overall results of the benchmark can be considered as insufficient. None of the methods was able to achieve detection results that would qualify it for practical usage in a real-world industrial environment. Solely methods based on texture descriptors such as Local Binary Pattern and procedures based on Gabor filters performed fairly well and have the highest potential for efficient, real-world defect detection. However, more sophisticated processing pipelines must be conceived to make these methods robust. High false positive rates are a major problem for all methods.

The results emphasize that the current state-of-the-art was designed for images with rather low spatial resolution. Given these resolutions, the methods are able to produce acceptable to good results. On higher resolutions, all methods fail to robustly detect (small) defects. It must be clearly stated that all methods were tested as described by their authors, without possible post-processing steps that would further lower the false alarm rates. However, the frequent false detections generated by all algorithms seem to be a problem, that cannot be solved by post-processing procedures only.

It can be concluded that today's approach of using texture analysis methods to detect

defects is perspicuous as low resolved fabric images appear as near regular textures. However, this concept is also linked to a significant amount of uncertainty in terms of the reliability of the results as

1. It is difficult to predict the behavior and the output of most texture analysis algorithms. When operating, they act as black-boxes.
2. Near regular textures are not 100 % regular and generally show high fluctuations in terms of grid and texture appearance (especially for highly resolved images).
3. A trade-off must be found between sensitivity and specificity when tuning the algorithmic parameters. The optimal balance between them might change from image to image.
4. Generally, no methods exist to validate the plausibility of the results.

These general limitations make the design of real-world texture analysis based inspection systems difficult to realize. The question is raised, whether new approaches can be developed to provide more stable and reliable fabric defect detection systems?

Table 4.2: Benchmarking the state-of-the-art in fabric defect detection, results overview table (1/2). Benchmark results of 14 tested algorithms, see Table 4.1, are shown. The algorithms are assessed with respect to the *hit rate* (HR), *fault rate*, *coarse hit rate* (CHR), and *coarse fault rate* (CFR), see Section 4.2.3.2. Values for HR, CHR, and CFR are given in percent (%), and rounded to the nearest integer value. The values for FR are given in permille (‰). Details on the image databases FIDB-A to E can be found in Section 3. The symbols ✓and ✗ represent *yes* and *no* statements, respectively.

		Algorithms													
		Wavelets			Gabor		Statistics					Filtering			
		W1	W2	W3	G1	G2	S1	S2	S3	S4	S5	F1	F2	F3	F4
	Supervised	✗	✓	✗	✗	✗	✗	✗	✗	✗	✗	✗	✓	✗	✗
	Block-based	✗	✓	✓	✗	✗	✓	✓	✓	✗	✓	✗	✗	✗	✗
Database	Metric														
FIDB-A 540 images 450 defective	HR	49	41	39	85	62	86	55	59	75	82	38	32	39	41
	FR	4.72	3.46	2.31	0.61	2.28	0.89	3.22	1.89	1.99	0.65	3.51	4.28	3.63	2.05
	CHR	74	65	61	95	82	91	78	81	86	93	70	81	77	81
	CFR	38	35	32	7	16	4	32	11	9	5	32	22	14	16
	Real-time	✓	✓	✓	✓	✓	✓	✓	✓	✓	✗	✓	✓	✓	✓
	Small defects	✗	✗	✗	✓	✗	✓	✗	✗	✓	✓	✗	✗	✗	✗
FIDB-B 40 images 20 defective	HR	75	72	75	93	79	88	87	88	92	96	60	85	74	76
	FR	1.71	1.92	2.00	0.21	0.98	0.18	1.03	1.13	0.08	0.32	2.09	1.47	0.82	0.67
	CHR	82	85	78	96	91	93	90	91	99	98	79	95	86	72
	CFR	5	10	5	0	0	0	5	5	0	0	10	5	10	5
	Real-time	✓	✓	✓	✓	✓	✓	✓	✓	✓	✗	✓	✓	✓	✓
	Small defects	✓	✗	✗	✓	✓	✓	✓	✓	✓	✓	✗	✓	✗	✗

Table 4.3: Benchmarking the state-of-the-art in fabric defect detection, results overview table (2/2).

Database	Metric	Algorithms														
		Wavelets			Gabor		Statistics					Filtering				
		W1	W2	W3	G1	G2	S1	S2	S3	S4	S5	F1	F2	F3	F4	
FIDB-C 54 images 45 defective	HR	21	17	19	66	47	68	49	53	42	71	32	22	43	56	
	FR	6.28	7.59	6.02	1.98	3.57	1.88	3.97	4.02	4.22	1.71	5.39	4.41	5.66	5.29	
	CHR	45	42	39	91	81	91	74	79	64	89	65	93	76	93	
	CFR	81	81	90	9	26	9	26	33	33	9	72	44	44	36	
	Real-time	✓	✓	✓	✗	✓	✓	✓	✓	✓	✗	✓	✓	✓	✓	
	Small defects	✗	✗	✗	✓	✗	✓	✗	✗	✓	✗	✗	✗	✗	✗	
FIDB-D 54 images 45 defective	HR	32	35	34	77	56	74	62	63	61	76	51	51	48	60	
	FR	4.02	5.71	4.72	1.29	2.17	1.35	2.25	3.33	3.98	1.61	4.07	2.91	3.68	5.02	
	CHR	69	61	59	98	85	95	76	82	84	96	71	80	81	93	
	CFR	44	47	40	9	17	7	18	22	33	4	48	33	27	31	
	Real-time	✓	✓	✓	✓	✓	✓	✓	✓	✓	✗	✓	✓	✓	✓	
	Small defects	✗	✗	✗	✓	✗	✓	✗	✗	✗	✗	✗	✗	✗	✗	
FIDB-E 4000 images 1200 defective	HR	19	15	13	65	29	71	39	74	40	71	26	21	39	49	
	FR	8.02	11.28	8.39	2.21	4.01	2.07	4.71	5.61	4.49	1.99	5.02	3.58	5.82	4.79	
	CHR	25	25	20	90	55	89	81	83	84	91	24	76	85	89	
	CFR	81	90	79	7	32	7	29	36	12	6	64	39	31	28	
	Real-time	✓	✓	✓	✗	✓	✓	✓	✓	✓	✗	✓	✓	✓	✓	
	Small defects	✗	✗	✗	✗	✗	✗	✗	✗	✗	✗	✗	✗	✗	✗	

PART III

ON-LOOM IMAGING

5 On-loom visual inspection

5.1 Introduction

The results of previous sections clearly highlighted that the state-of-the-art in fabric defect detection offers room for improvement. It appears that published approaches cannot meet yet the requirements encountered in real-world industrial environments. As the key problems faced by modern defect detection concepts, i.e. black-box behavior, parameterization trade-off, vulnerability to irregularity etc., do not seem to be solvable in a satisfactory manner, alternative approaches should be conceived. Consequently, the main contribution of this work is the design of a fabric defect detection concept which, except from papers published by the author, was not devised elsewhere. As mentioned in Section 4.1.1, the foundation in this context is the concept and implementation of a novel machine vision framework that relocates the problem of fabric defect detection from the class of surface inspection to the class of dimensional verification. Accordingly, fabrics are measured for the first time with regards to geometry, extent, orientation and shape. This is a significant difference to hitherto approaches that treat fabrics as texture. Although the preconditions for this paradigm change are difficult to meet (the key-words here are image resolution, yarn visibility, real-time), the gathered solutions allow to resolve nearly all key problems faced by current state-of-the-art methods for fabric defect detection (see Section 4.2.6). Dimensional verification systems generally have white-box character and are not affected by parametrization sensitivity problems. Moreover, the resulting measurements can generally be validated, which enhances the overall system robustness and reliability. As new concepts naturally give rise to new problems, Part III of this work now discusses all aspects of the *On-Loom* framework in detail.

The prototype was intended to overcome existing problems of current algorithms by using higher spatial image resolutions of + 415 pixels/cm. In this way, single yarns in woven fabrics can be located, tracked and measured with regards to their location, spacing, shape and appearance. To minimize hardware costs, a traversing camera design was chosen. The new system required the development of innovative image processing algorithms which are expected to meet the imposed requirements. At the same time, efficient solutions statements for the hardware design had to be identified. Accordingly, the main contributions of this chapter are presented in the form of

- a detailed discussion of the mechanical construction of a loom mountable traverse system. This includes details on on-loom back-light illuminations, image acquisition strategies and a concept for machine vibration damping.
- a novel image processing framework for fabric flaw detection. Within this scope, highly resolved images with a spatial resolution of 415 pixels/cm are processed in real-time to locate single yarns and measure them in terms of shape, position and appearance.
- a modular detection concept with stackable algorithmic processing blocks allows for higher precision and robustness.
- an extensive performance evaluation. The results are directly compared to existing state-of-the-art methods.
- a detailed cost analysis for the prototype system which is extended by an economic efficiency calculation for a potential commercial system.

The chapter is structured as follows: Section 5.2 is dedicated towards the mechanics of the On-Loom system. Here, the manufacturing environment is set out on the example of an OMNIPlus-800 [95] loom from Picanol N.V., Ypres (Belgium). Traverse design and lighting techniques are discussed. Moreover, the design of a camera vibration absorber is described on. Section 5.2.3 covers the topic of image acquisition including traverse control, production speed and camera triggering. Section 5.3 presents the image processing pipeline comprising image pre-processing, yarn tracking and defect detection. Before the prototype is discussed in terms of efficiency and costs in Section 5.6, Section 5.5 presents flaw detection results of several on-loom and off-loom test runs. The results are then discussed and compared to other methods in Section 5.7. Finally, a conclusion is given in Section 5.8.

5.1.1 Loom mounted detection systems

Few publications discuss the entire automated visual inspection (AVI) framework, consisting of mechanical construction, controlling, illumination and algorithms. Within this scope, only five papers were published so far. Mak et al. [96] present an AVI system based on Gabor filtering with little details spent on mechanics. In [97], a system based on neural networks is presented, again little detail on mechanics, illumination and controlling is given. Sari-Sarraf [45] addresses the challenge of vibration free image acquisition and processing. Stojanovic et al. describe a complete AVI system [98] and Cho et al. [99] provide an extensive discussion on production speed, optics, and camera resolution for their low price inspection setup. Consequently, examples for commercially available AVI systems are rare, too. Here, the WebSPECTOR [100] (Shelton Machines Ltd, U.K) system such as the IQ-TEX 4 [101] system (Elbit Vision Systems Ltd., Israel) are off-line inspection systems which monitor produced material apart from the loom on a separate cloth inspection table, as a conventional human inspector would do. They are straight forward to set up and benefit from steady operation conditions. On-Loom systems on the other hand are mounted onto the loom and monitor the material on-line during manufacturing. They allow immediate intervention in case of present defects and can hence minimize losses. Two commercially available on-loom systems are the PROCAM 5310 (PROTECHNA Herbst GmbH & Co. KG, Germany) and the ELSIS inspector (Erhardt+Leimer GmbH, Germany). Both systems operate with an array of non-moving, static cameras. BMSVision's (BMS bvba, Belgium) Cyclops system is a traversing system with one camera that is moved across the loom to cover the entire material. The Cyclops system features selective back- and front-illumination.

The Institut für Textilmaschinen (ITA) conducted an evaluation with 12 middle class weaving companies to find out about their experiences with AVI systems for fabric defect detection. Not all companies actually employed an AVI system in their production line, but all of them at least considered the installation of it. The results of the evaluation[1] showed that present fabric quality control systems suffer at least from one of the following problems: low spatial resolution (i.e. small defects could not be found), time and space delay from production (off-line systems), frequent false alarms (lack of robustness), fabric restrictions (only applicable to specific set of fabrics), algorithmic rigidity (too many parameters, only specific defects could be found), low reliability (many defects were not found) and/or high prices. The insights

[1] A reference can not be provided as the evaluation was not published

are congruent with the observations made in Section 4.2.5.

5.2 Mechanical integration

The mechanical part of the inspection system consists of a traversing camera and a synchronously traversing back-light source. The system aims to detect defects quickly so that the time between fabric production and the actual quality control does not exceed five seconds. This would allow for a closed-loop control of the weaving process on similar time scales. Hence, the mounting position close to weft insertion is a fundamental property of the system. Figure 5.19 shows an image of the final prototype system mounted onto the OmniPlus 800 [95] loom. The traverse concept minimizes costs as the vision system is reduced to a single camera which visually covers the complete material but still enables the system to acquire images with high spatial resolution. Nevertheless, several difficulties arise that should not excessively reduce the image quality. The system must for example cope with machine vibrations, motion blur, and limited available space for construction within the loom.

5.2.1 Camera mount

A. Vibration measurement. In order to design a camera mount that is able to damp machine vibrations and hence improve the image quality, the frequencies present at the traverse beam and the camera during production were first measured using four Kistler K-Shear accelerometers from Kistler Instrumente AG, Winterthur, Switzerland. Four different machine speeds were tested in this context, ranging from 250 rpm up to 400 rpm. Spectral analysis of the data was conducted to identify the most dominant frequencies. Table 5.1 lists the three most prominent frequencies identified during each measurement.

The measurements revealed two major peaks in horizontal direction (the direction of production). The analysis showed that the peaks correspond to the actual machine speed and its first harmonic frequency as seen in Figure 5.1a.

B. Design of a vibration absorber. Since the vibrations in the camera mount should be minimal, the system concept provides an absorber block designed to cancel machine

Table 5.1: Measurements of the three most dominant frequencies occurring on the camera mount during loom operation. Shown are the measurements at four different machines speeds.

Speeds [rpm]	Dominant frequencies [Hz]		
250	7.629	8.246	12.51
300	5.188	10.07	14.95
350	5.798	11.60	17.41
400	6.714	13.43	19.84

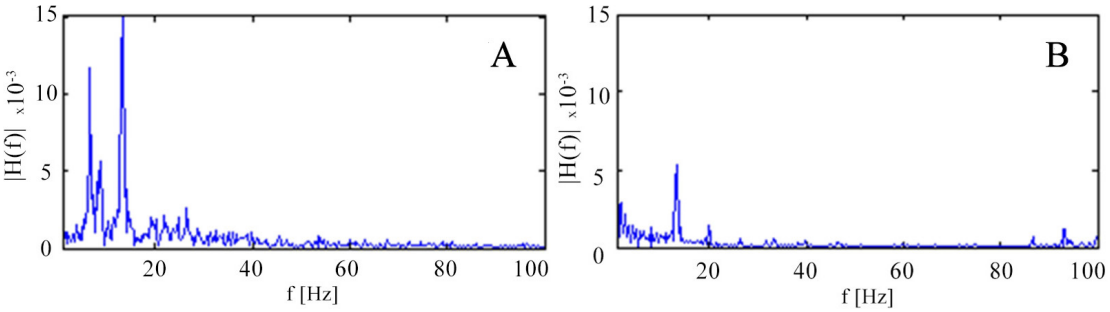

Figure 5.1: Spectra of two machine vibration measurements at 400 machine rotations per minute. A) Normal system, measurements at the camera mount. B) Damped system, measurements at the camera mount

vibrations that are transferred to the mount. A vibration absorber was added to the camera mount in order to decrease the frequency response of the camera during operation at higher machine speeds. The theoretical model and the CAD design of the camera mount with vibration absorber are shown in Figure 5.2.

From the free-body diagram shown in 5.2b, the equations of motion of the spring-mass system were determined. According to Newton's second law, the interaction of forces in a mechanical system can be described by

$$m_i \ddot{x}_i = \sum_j F_{ij}, \tag{5.1}$$

where $\sum_j F_{ij}$ denotes the sum of all forces acting on the mass m_i and $\ddot{x}_i$ is the acceleration of the mass. With respect to Hooke's law, this results in two motion equations for the camera mass (m_c) and the absorber mass (m_a)

$$\begin{aligned} m_c \ddot{x}_c(t) &= -2k_2 x_c(t) - 2k_3 x_c(t) + 2k_2 x_a(t) + 2k_3 x_l(t) \\ m_a \ddot{x}_a(t) &= -2k_2 x_a(t) - 2k_1 x_a(t) + 2k_2 x_c(t) + 2k_3 x_l(t), \end{aligned} \tag{5.2}$$

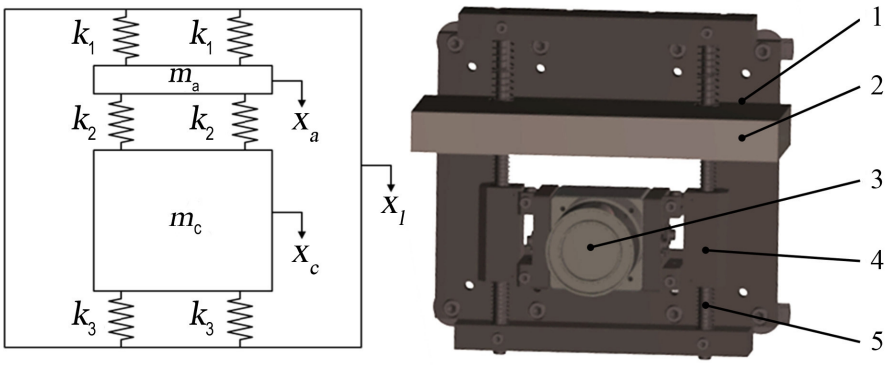

Figure 5.2: Vibration absorber. Left: theoretical model. Right: CAD design with 1) base plate, 2) absorber mass, 3) camera dummy, 4) linear bearings, 5) rod with coil springs.

where $x_l(t)$ represents the displacement of the camera mount caused by the vibrating loom over time t, $x_c(t)$ the displacement of the camera mass, $x_a(t)$ the displacement of the absorber mass, and k_i represents a spring constants. Assuming an harmonic motion, a solution to the differential equation system is given by [102]

$$\begin{aligned} x_i(t) &= A_i\ cos(\omega_i t + \phi_i)\ with \\ \ddot{x}(t) &= -\omega^2 x(t). \end{aligned} \tag{5.3}$$

When the transient effect is neglected and only the steady-state it is analyzed, it can be written that [102]

$$\omega_c = \omega_a = \omega_l\ , \tag{5.4}$$

i.e. all components in the steady-state system oscillate with the excitation frequency. Substituting Equation (5.3) into Equation (5.2) gives

$$\begin{aligned} x_c(t)(-\omega^2 m_c + 2(k_2+k_3)) - 2k_2 x_a(t) &= 2k_3 x_l(t) \\ x_a(t)(-\omega^2 m_c + 2(k_1+k_2)) - 2k_2 x_c(t) &= 2k_1 x_l(t). \end{aligned} \tag{5.5}$$

By solving the equation system (5.5) and rearranging for $x_c(t)$, a relation between $x_c(t)$ and $x_l(t)$ is found

$$x_c(t) = \frac{-2\ x_l(t)(\omega^2 m_a k_3 + 2k_1 k_3 + 2k_2 k_3 + 2k_1 k_2)}{(-\omega^2 m_c + 2k_2 + 2k_3)(-\omega^2 m_a + 2k_1 + 2k_2) - 4k_2^2}. \tag{5.6}$$

Since a value of 0 is desired for $x_c(t)$ (no motion of the camera mass), the numerator in Equation (5.6) is set to zero. This can be achieved for two cases: The straight forward

case $x_l(t) = 0$, i.e. no external force is applied, or when

$$\omega^2 m_a k_3 + 2k_1 k_3 + 2k_2 k_3 + 2k_1 k_2 = 0 \tag{5.7}$$

is full filled. It is emphasized that Equation (5.7) is time independent. Rearranging Equation (5.7) for the frequency ω gives

$$\omega = \sqrt{\frac{2k_1 k_3 + 2k_2 k_3 + 2k_1 k_2}{m_a k_3}}. \tag{5.8}$$

With Equation (5.8) the spring and mass constants k_{1-3}, m_a can be chosen so that a system is defined for which no camera motion occurs at the excitation frequency ω. The value for ω has been fixed to 6.5 Hz according to the measurements in Table 5.1. Various sets of absorber masses and spring constants were tested and applied to the expression for the camera dummy movement $x_c(t)$ to see for which combinations the system response would have a favorable damping characteristic. After several trials, absorber mass and spring constants were empirically selected to be $k_1 = 717\ N/m$, $k_2 = k_3 = 1229\ N/m$, and $m_a = 3.1921\ kg$. The mass of the camera was determined to be $m_c = 1.7547\ kg$. This results in a system response that minimizes frequencies from approximately 5.33 Hz (320 rpm) to 8.3 Hz (500 rpm) and beyond 10.5 Hz (630 rpm). Since the project aims for high-end weaving machines at maximum machine speeds of 800 to 1000 rpm, the designed filter characteristic is acceptable. Figure 5.3 illustrates the normalized camera motion function of the absorber system in dependence of the loom frequency with respect to the function

$$\left| \frac{x_c(t)}{x_l(t)} \right|. \tag{5.9}$$

C. Verification. Verification measurements were carried out on the same weaving machine at the same speeds and with the same accelerometers. With the data collected from the accelerometers, a second frequency analysis was conducted to compare the initial to the improved system. The results are shown in Figure 5.1b where the frequency response of the spring-loaded camera dummy is shown. With comparison to the prior setup, the absorber system significantly lowers the high peaks that correspond to the dominant machine vibrations without amplifying other frequencies too much.

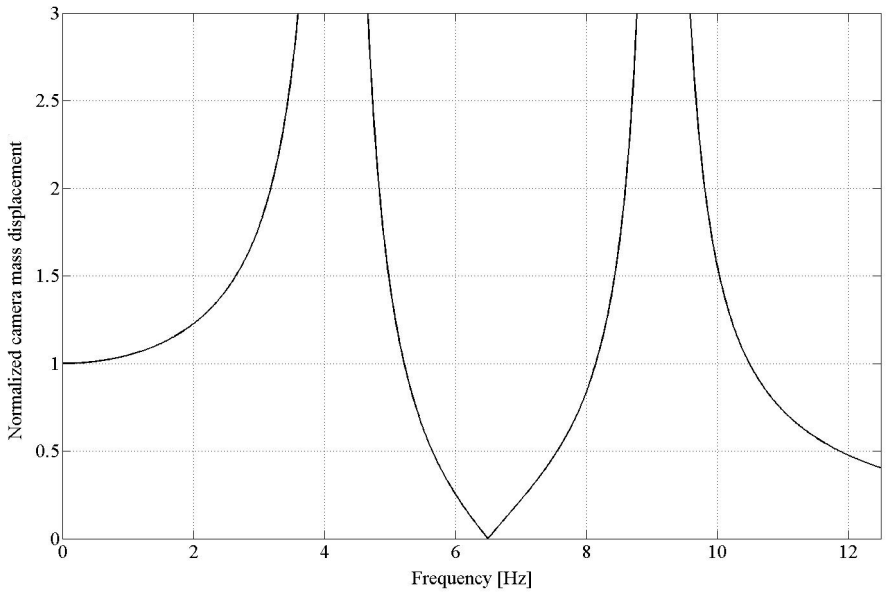

Figure 5.3: Computed camera motion of the absorber system in dependence of the loom frequency with respect to Equation (5.9).

5.2.2 Illumination

Illumination is a decisive factor for the effectiveness of the entire system. Within the project, a trade-off between contrast, durability, and costs is considered. For highest image quality, contrast should be as high as possible in order to keep the camera shutter speed fast and the aperture high. On the other hand, the illumination needs to be economically feasible. LED arrays provide excellent illumination characteristics at continuously decreasing costs. Therefore, a traversing solution on the basis of a LED array is pursued. Several illumination techniques were investigated in a first step in order to evaluate their feasibility for different fabric types. The investigated techniques comprise back- and front-light illumination as well as dark-field illumination.

The considered fabrics are provided by a variety of industrial cooperation partners. The fabrics cover filament and staple fiber fabrics in combination with plain satin and twill weaves. As a conclusion from these samples, back-light illumination turned out to be the most feasible technique since the textile structures are resolved best as it can be seen in Figure 5.5.

Accordingly, the LED array LDL-TP-83x75 (Stemmer Imaging GmbH, Puchheim, Ger-

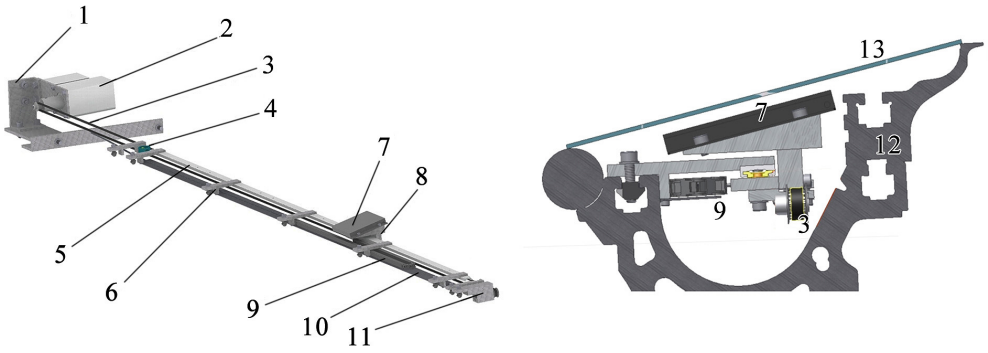

Figure 5.4: CAD model of the traversing illumination system, with an overview (left) and axial view (right). Single components are identified as 1) motor mount, 2) electric motor, 3) timing belt, 4) shock absorbers, 5) linear guide rail, 6) rail support, 7) LED light, 8) adapter for mounting the LED array onto the carriage, 9) energy chain, 10) support for energy chain, 11) bearing of timing belt wheel, 12) machine frame, and 13) the fabric.

many) was chosen as light source. This decision implies that the light source has to be placed on the back side of the first piece of fabric produced. The margin for construction in weaving machines is quite limited and hence the space available below the fabric is restricted by a semicircular cross-section of only 55 mm in diameter, see Figure 5.4. A custom solution had to be developed in order to place the light source. Since a static LED array over the entire machine width does not appear economically feasible, a solution on the basis of a traversing LED array was pursued. A CAD model of the final traversing system is shown in Figure 5.4.

Here, the LED box is mounted onto an adapter structure which is connected to a

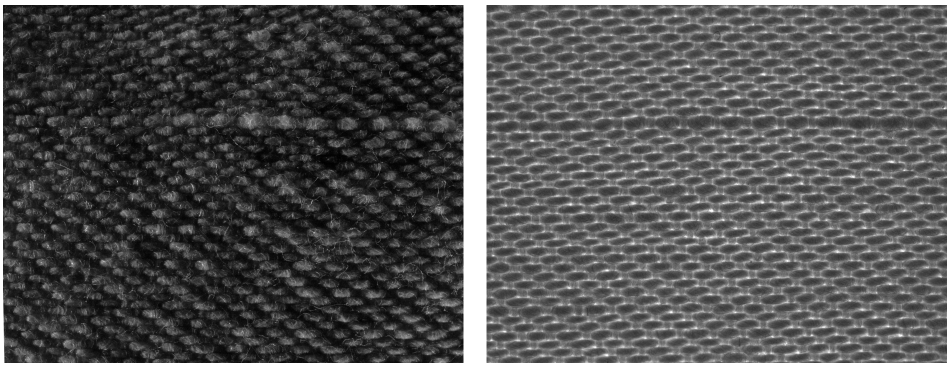

Figure 5.5: Fabric images taken with dark-field illumination (left) and back-light (right) illumination. The defect (thick yarn) is much better perceivable in the back-light illuminated image.

timing belt. The timing belt is connected to an electric motor which enables the LED array to traverse perpendicularly to the direction of production. Signals and power supply are provided through a flexible energy chain. Self-lubricating linear guide rails support the LED carriage in vertical direction and facilitate horizontal movements. The traversing back-light is synchronized to the traversing camera sled so that the LED array always illuminates the region of view of the camera. The traversing light system turned out to be the highest expense factor of the final prototype system.

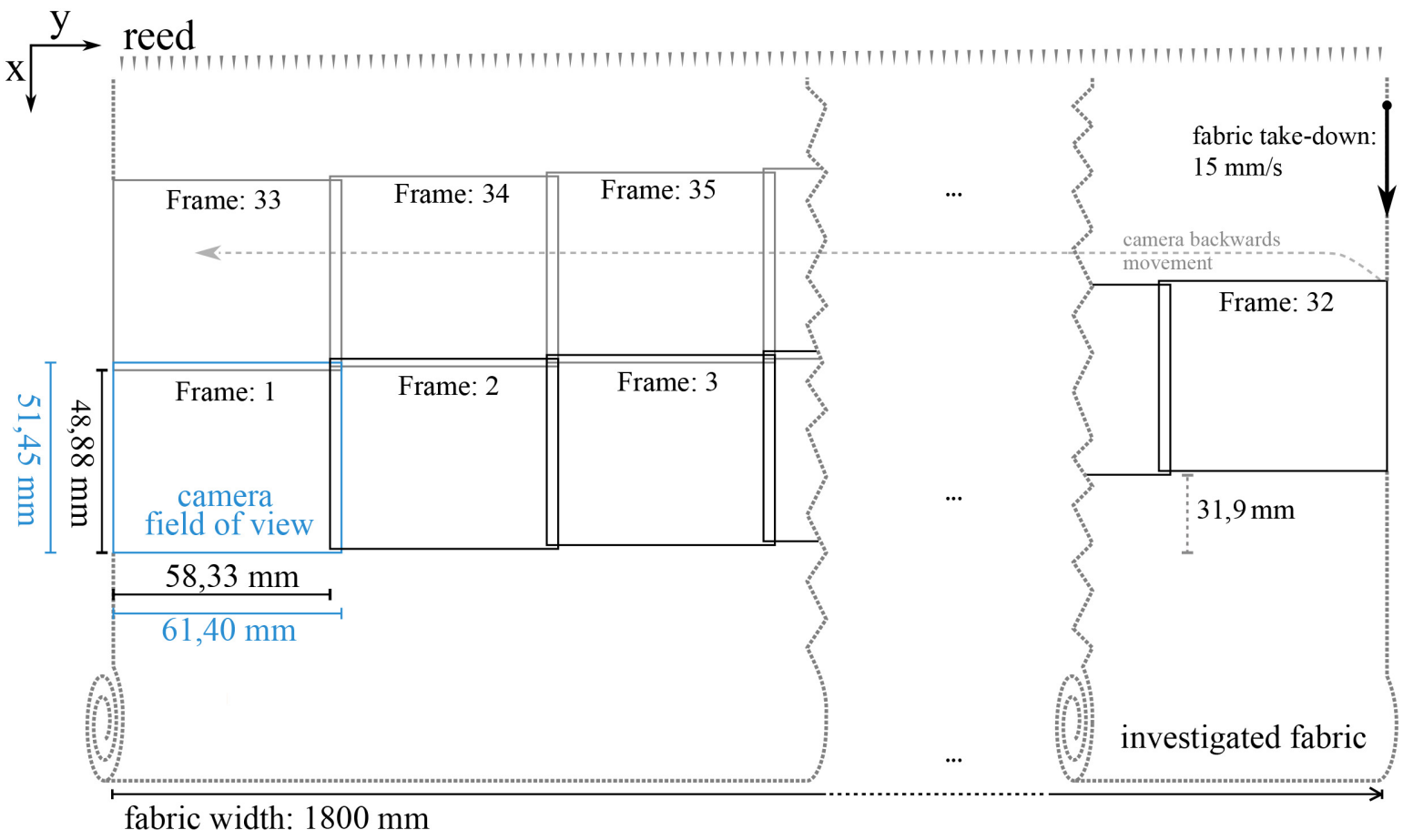

Figure 5.6: Scheme of the image acquisition strategy. The complete fabric width of 1800 mm is covered by the traverse which must cross the loom in approximately 2.5 seconds. In practice, 32 slightly overlapping images are acquired per crossing. The field of view (FOV) of each image covers approx. 49 × 58 mm, the working distance between lens and fabric is fixed to approx. 100 mm resulting in spatial image resolution of +41.5 pixels/mm.

5.2.3 Image acquisition

The image acquisition strategy is based on a single matrix camera which is moved across the loom by the traverse. Even though line scan cameras provide higher resolutions and are generally better suited for surface inspection tasks, within the presented on-loom scenario they cannot be deployed since movements in three directions occur: the camera traverses (y-direction), the fabric is produced and continuously fed forward (x-direction), and the system vibrates due to the reed beat-up (z-direction), see Figure 5.6. For the prototype, the camera model BM-500 GE (JAI, Glostrup, Denmark) was chosen. The camera offers a resolution of five mega-pixels at a frame rate of 15 fps. The camera is combined with a Xenoplan 23 mm / 1.4 lens (Schneider Optische Werke GmbH, Bad Kreuznach, Germany).

The acquisition system has to allow for a full and complete inspection of the entire fabric width of 180 cm at a machine speed of 900 picks per minute. This results in a maximal fabric feed motion of approximately 1 cm/s (given a minimal pickage of 15 wefts/cm). To achieve a spatial image resolution of 415 pixels/cm, the working distance between camera and fabric has been fixed to 10 cm, i.e. the camera's field of view (FOV) covers an area of 6 cm by 5 cm. To guarantee complete material coverage, the traverse must accomplish one cycle of forward and backward movement in less than 5 seconds. Given the FOV's width of 60 mm, at least 30 images must be acquired to visually cover all parts of the material. In practice, more images are acquired to allow an image overlap as depicted in Figure 5.6. Images are acquired during the (slower) forward motion of the traverse and are directly processed in real-time. In case not all calculations can be finished within 66 ms, subsequent images can be buffered in camera memory to be processed during the (faster) traverse backward movement where no images are acquired. Figure 5.6 shows an illustration of the visual coverage of the fabric as implemented in the proposed inspection system.

5.3 Image processing algorithms

The image processing pipeline presented in this work is unique for two reasons. First, a high spatial resolution of 415 pixels/cm makes it possible to treat the image as a netting of single visible yarns instead of as a plain texture. This feature permits

to locate and measure single wefts and warps. To our knowledge, no algorithmic framework operating on similar resolutions has yet been published (except for the papers published by the author of this work). Secondly, the defect detection phase combines three independent analysis blocks, each having particular strengths and weaknesses for segmenting different defect types. The modular algorithmic concept makes the framework robust and versatile for use in manufacturing practice. The block diagram in Figure 5.7 illustrates the separate processing steps employed in the image processing pipeline and their dependences. The key units are identified as image *pre-procssing*, *feature extraction*, *yarn tracking*, and *defect detection*.

5.3.1 Main challenges

Several challenges had to be addresses during the algorithmic system design. As the size of the input stream is 5 megapixels per image, algorithms had to be efficient and economic in terms of data handling and computational needs. Maximum parallelization had to be utilized. This restriction eliminated many standard image processing algorithms right from the very beginning and imposed a compact yet efficient signal processing pipeline. Moreover, the major goal of tracking single yarns turned out to be more difficult as expected, as generally only fractions of a yarn can be seen on the fabric surface. This restriction imposed the need for algorithms to deal with uncertainties and fractional, respectively missing information. Finally, the new system design would have absolutely no advantage over existing concepts (no matter how sophisticated the employed technology is), if it would not be able to reach a new degree in defect detection robustness, i.e. higher detection rates and vastly lower false alarm rates for a broad variety of existing materials and defects. Since defects appear in unpredictable forms, a modular design with different algorithmic specificities for various defect types had to be considered in advance.

5.3.2 Pre-processing

The initial development of the framework started with a investigation of several methods to detect yarn feature points within fabric images as described in Section 5.3.3. It quickly became apparent that the performance of any feature detector considerably depends on the quality of the input images. Inhomogeneous gray-value intensities,

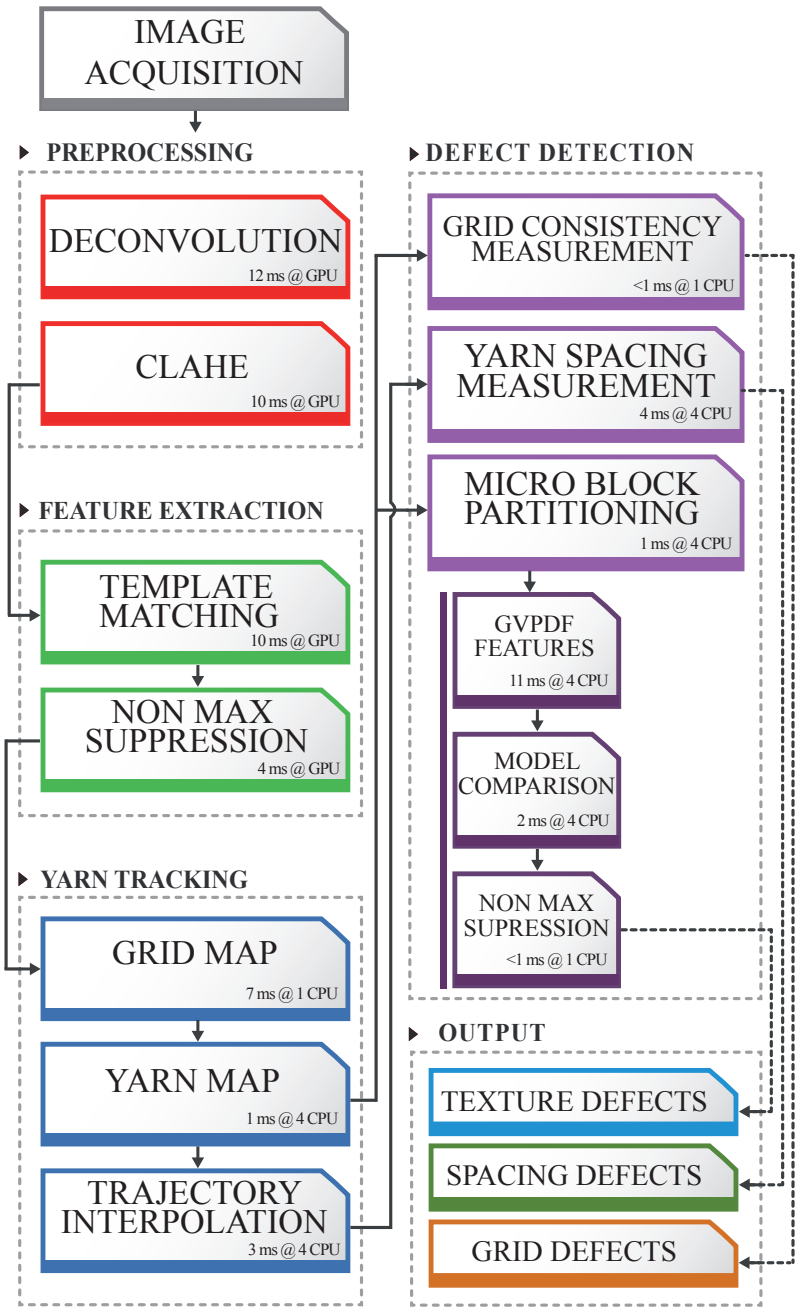

Figure 5.7: Block diagram of the image processing framework. Acquired images are first pre-processed before feature points are found. Found features allow to describe the fabric lattice so that single yarns can be tracked. During defect detection, the consistency of the fabric lattice is controlled and shape, form, and texture of single yarns are analyzed.

blur, noise, low edge contrasts and vignette degradations had a major impact on the feature detection robustness. For most evaluated detection methods, the feature detection performance was generally good/acceptable at the image center but become so bad towards the image borders that feature detection in these regions was not possible. The main sources for degradations were quickly located: image blur was caused by the moving camera and relatively long shutter times. Intensity inhomogeneities were caused by the LED field and strong vignette degradations were generated by the prime lens. These observations made the introduction of image preprocessing modules into the framework necessary in order to normalize the raw image data and hence stabilize the feature extractor. Image de-blurring and contrast normalization are standard procedures in the field of image processing, a multitude of possible algorithms was hence available for application. The following sections discuss the process of selecting and realizing the preprocessing modules for image deconvolution and contrast normalization.

5.3.2.1 Deconvolution

Due to fast traversing motions, the raw input images are degraded by motion blur. Even though the blur effect can be minimized by adjusting the interplay between shutter speed, flash power and camera aperture, it cannot be completely avoided. Since machine movements in industrial settings are generally predictable, the point spread function (PSF) of the imaging system can be modeled, allowing an algorithmic based reduction of motion blur using the concepts of non-blind deconvolution theory. The term *non-blind* refers to algorithms that require the input of a PSF model to sharpen the image. Blind deconvolution algorithms on the other hand estimate the PSF without any prior knowledge. Given the knowledge of a precise PSF model, non-blind deconvolution performs generally better than blind deconvolution.

For uniform motions (as encountered in the On-Loom system), the image blur can be precisely modeled by a point spread function that takes the form of a moving average FIR filter with n coefficients, whereas n corresponds to the number of pixels bypassed by the system during the exposure time T. This is the reason for using non-blind deconvolution in this work. The task of modeling the PSF becomes more challenging when dealing with more complex movements. Other commonly encountered motions in industrial applications are circular motions with constant angular velocity or acceleration. These motions and correspondingly the modeling of a PSF is discussed by Slepian et al. in [103]. Motions with constant acceleration are investigated by Som et

al. [104]. The latter also covers a discussion on modeling motions that are a function of time. Finally, Kopeika et al. [105–107] investigate the behavior of sinusoidal motions as induced by machine vibrations .

To get a feeling for the impact of blur on the On-Loom images, all motions within the system setup that could contribute to degradations were analyzed. In sum, the system consists of a moving matrix camera that slides on a fixed axis across the fabric (y-direction) at a nearly constant velocity of $v_{cam} = 1\,\mathrm{m\,s^{-1}}$. The produced fabric has a constant feed motion (x-direction) of $v_{fabric} = 15 \times 10^{-3}\,\mathrm{m\,s^{-1}}$. In z-direction, motions induced by the reed beat-up and the weft shooting must be considered. Additional periodic machine vibrations may have impact on the image quality in all 3 directions (x,y & z). The camera is set up to have a spatial resolution of $r = 415\,\mathrm{px\,cm^{-1}} = 415 \times 10^{2}\,\mathrm{px\,m^{-1}}$. The exposure time was set to a time interval of $T = 650 \times 10^{-6}\,\mathrm{s}$ which allowed for a relatively high value for the lens aperture of $F \sim 1/11$.

Table 5.2: List of non-blind deconvolution algorithms that were investigated in this work.

	Algorithm	Abrev.	Ref.
1	Wiener Deconvolution	W	[108]
2	Constrained Least Squares Filter	CLSQ	[109]
3	Richardson-Lucy	RL	[110]
4	ForWaRD Method	FWRD	[111]
5	Direct Sparse Deconvolution	DSD	[112]
6	Sparse Deconvolution in frequency domain	SDF	[113]
7	Sparse Deconvolution in time domain	SDT	[113]
	Total Variation based methods		
8	1) mx Total Variation	MXTV	[114]
9	2) irn Total Variation	IRNTV	[115]
10	3) reg Total Variation	REGTV	[116]
11	Local Polynomial Approximation	LPA	[117]
12	Shape Adaptive Discrete Cosine Transform	SADCT	[118]
13	Block matching with 3D-filtering	BM3D	[119]

Using a laser doppler vibrometer, the relative z-direction displacements between camera and fabric during one machine period were measured to find an optimal trigger moment for the camera. This analysis allowed to cancel blur in all directions caused by the reed beat-up and the weft shooting. The measurement was only conducted once

in the laboratory. In a real-world system, this step should be done once during the installation of the system in order to calibrate it. It is, however, expected that weaving machines of the same type have similar vibration characteristics what would eliminate this measurement for other looms. To handle the impact of constant machine vibrations, the vibration absorber discussed in Section 5.2.1 was introduced. To get a feeling of the impact of motion blur in x- and y-direction, the following calculations were considered:

$$\begin{aligned} blur_x &= v_{fabric} \cdot T \cdot r \text{ [px]} \\ &= 15 \times 10^{-3} \frac{\text{m}}{\text{s}} \cdot 650 \times 10^{-6} \text{s} \cdot 415 \times 10^{2} \frac{\text{px}}{\text{m}} \\ &= 0.40 \text{ px} \end{aligned} \tag{5.10}$$

$$\begin{aligned} blur_y &= v_{cam} \cdot T \cdot r \text{ } [px] \\ &= 1 \frac{\text{m}}{\text{s}} \cdot 650 \times 10^{-6} \text{s} \cdot 415 \times 10^{2} \frac{\text{px}}{\text{m}} \\ &= 26.9 \text{ px} \end{aligned} \tag{5.11}$$

As it can be seen, the image degradation in x-direction may be neglected since it is below one pixel. In y-direction, however, the motion blur must be reduced as it covers 27 pixels, which significantly reduces the quality of the image data. Within this context, 13 state-of-the-art algorithms for non-blind image deconvolution were benchmarked by the author in [6]. Table 5.2 lists an overview of the evaluated methods. For all investigated algorithms, Matlab implementations or interfaces are publicly available. Some researchers provide complete source codes, others publish only executable binaries for which Matlab wrappers were written. In order to make a decision about the most suitable algorithm, the four image sharpness metrics 1) Peak Signal-to-noise-ratio, 2) Structural Similarity [120], 3) Edge Stability Binary Difference [121], and 4) Spectral Phase & Magnitude Distortion [121] were evaluated in a first experiment on the image database FIDB-F (see Section 3.6). Consequently, a 1D PSF was modeled by a moving average filter with tap size 27 (see Equation) as input for the deconvolution algorithms. The image blur in the database was created with the same PSF. A quantitative assessment of the precision of the blur model has not been performed. The fitness was evaluated qualitatively by visually comparing artificially blurred images and live images that were acquired by the moving camera. Given the imaging setup discussed in Section 5.2.3, the model is a good fit which is also confirmed by the good live deconvolution results. The experiments showed that all investigated algorithms perform well on reducing motion-blur in the images, even though the general visual impression of the output images varies considerably in between different methods. Figure 5.8 exemplarily shows the visual deconvolution output of 10 selected algorithms for an

artificially blurred fabric in FIDB-F.

Table 5.3: Performance overview of the evaluated deconvolution algorithms as listed in Table 5.2. The test database comprises 48 fabric images divided into 4 fabric classes, 12 images for each class. The used assessment metrics were the Feature Point Distance (FPD) (lower values, better performance) and the running time. For FPD, the highest and lowest FPDs are shown. The results are sorted according to the running time in ascending order. NOOP indicates *no operation*, i.e. no deconvolution was applied.

	FPD [px]	run time [s]
NOOP	0.65 .. 10.49	0.019
W	0.48 .. 2.52	0.039
SDF	0.35 .. 1.68	0.136
CLSQ	0.45 .. 2.97	0.138
RL	0.48 .. 2.56	0.454
SDT	0.39 .. 1.28	0.532
FWRD	0.36 .. 1.65	1.329
REGTV	0.47 .. 2.49	1.779
DSD	0.39 .. 1.22	2.900
MXTV	0.41 .. 2.42	2.977
IRNTV	0.48 .. 2.57	3.979
BM3D	0.42 .. 1.92	4.651
SADCT	0.42 .. 2.00	4.738
LPA	0.33 .. 1.99	10.588

A deeper analysis of the entire image processing pipeline showed that the visual impression of de-blurred images has only little impact on the quality of the overall image processing system. It is by far more important that single yarn features, i.e. warp-floats, are well distinguishable in terms of edge contrast. Since the feature extractor (as discussed in Section 5.3.3) is based on a template matching algorithm, a custom designed metric was introduced to test the performance of the feature extractor in dependence of the chosen deconvolution algorithm output. For this purpose, all sharp reference images in the blurred image database FIDB-F were manually labeled with thousands of ground truth float-points. The Feature Point Distance (FPD) metric then measures the mean Euclidean distances between the feature points detected in a de-blurred test image and the ground truth features in the sharp reference image (only shortest distances were considered). Lower FPD values indicate a better feature extraction performance and hence a more suitable deconvolution algorithm. Table 5.3 lists the benchmark results of all tested algorithms with respect to the FPD metric and the Matlab computation times. For all images within a fabric class, the FPD

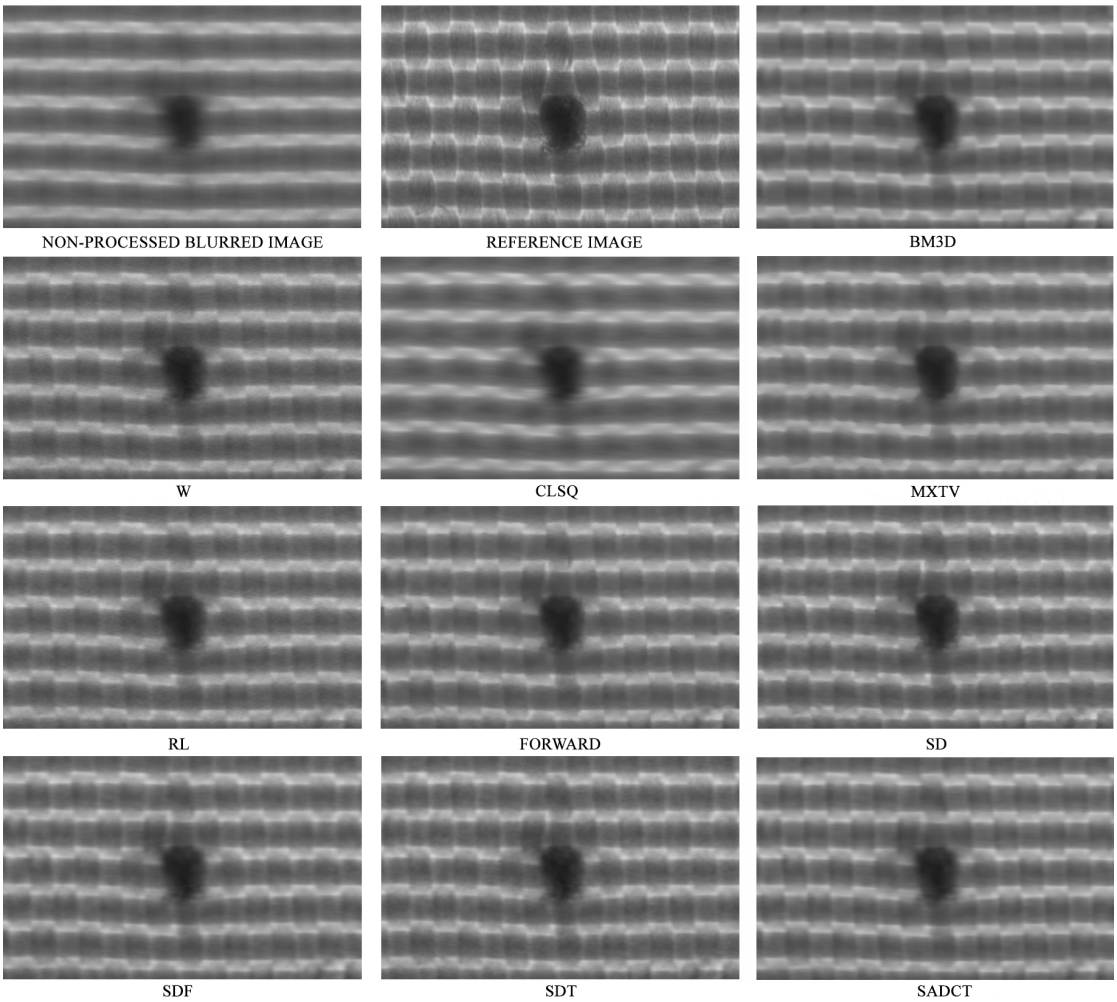

Figure 5.8: Overview of the deconvolution performance of 10 selected algorithms and corresponding, artificially blurred fabric image. All abbreviations relate to the listings in Table 5.2.

performance values were averaged. The maximum and minimum performance values of all four classes are shown in the table. The values for computation times were averaged among all 48 images in the database and each algorithm. The operator NOOP represents the *no filter operator*, i.e. the blurred input image without any pre-processing. It was included as reference for a better assessment of the other filters. For all experiments, the feature extractor of the final On-Loom system was used. Experiments showed that FPD values above 6.0 significantly lowered the yarn tracking performance as described in later Sections (see Section 5.3.4). Values below 3.0 are sufficient for robust yarn tracking.

From Table 5.3 it can be seen, that all methods improve the image quality with respect to the NOOP operator. The best performance in terms of the FPD was obtained for

the SDT, SD and LPA methods. In terms of computational efficiency, Wiener Deconvolution turned out to be the least demanding method. As all algorithms achieved FPD values below the critical threshold of 3.0, Wiener deconvolution was identified as the most suitable method for implementation in the On-Loom project. Correspondingly, it was implemented and adapted for the given GPU hardware. Deconvolution computation times of 2.4 ms per megabyte could be achieved in this context. Algorithmic details about the software implementation and possible optimizations for the real-time deconvolution module are given in [6].

5.3.2.2 Histogram Equalization

The illumination setup of the proposed vision system is not optimized in terms of homogeneity. Accordingly, the acquired raw input images don't show a uniform illumination level – some areas are brighter, others are darker due to imperfections of the illumination source and characteristics of the optical path. The contrast in the images is quite low and towards the border regions, a considerable drop-off in intensity can be observed. The observed vignette effect was caused by the characteristics of the lens and could not be handled on a mechanical/hardware level since cost restrictions didn't allow for the acquisition of higher quality imaging hardware. Corresponding lenses would significantly increase the costs of the system. Figure 5.11a shows a typical, unprocessed raw input image with non-uniform gray-level intensities and low contrast. Within the context of on-line deconvolution, the first test series made with possible feature extraction methods showed that the performance of any method could be considerably improved by applying histogram normalization [122] to the images prior to the feature extraction step. Histogram normalization is a transformation that aims to flatten out the image histogram in order to improve the images contrast. Normalized images have better contrast, show more distinct edges and minor illumination inconstancies can be corrected. These improvements make the detection of possible features easier to accomplish. As a plus, standard histogram equalization is computationally very saving. However, it works globally and is not adaptive, i.e. the same transformation is applied the entire image. This is why larger contrast and illumination inconstancies, as observed in the On-Loom raw images, cannot be compensated. The observed effect is that the feature extraction performance is improved within the central part of the image. The image center forms the majority of the image content and hence dominates the characteristics of the normalizing transformation. At the smaller border regions, however, the feature extraction results worsen considerably since a transformation rule is applied which is computed based

on intensity statistics from the central part. These observations motivated the need for a normalizing algorithm that operates locally adaptive. All methods for adaptive histogram equalization discussed in [123] were hence implemented and tested in this work . The experiments showed that Clip Limited Adaptive Histogram Equalization [124] (CLAHE) is the most suitable method for usage in the On-Loom project due to its strong capabilities to even out vignette degradations and local intensity inequalities, its scalability, straight forward parameterizability, its ability to be parallelized on GPU hardware which makes the method computationally very efficient, and most importantly, its build-in feature to limit noise amplification that allows to control the degree of contrast enhancement.

In CLAHE, the image is divided into a grid of $N \times M$ non-overlapping blocks of the same size. For each block, a local histogram, i.e. a probability density function for the pixel intensities $pdf_{m,n}(x)$ ($\forall n, m \in \mathbb{N}, 0 \leq m \leq M-1, 0 \leq n \leq N-1$) is computed. The cumulative distribution function for each histogram is then given by

$$cdf_{m,n}(x) = \sum_{j=0}^{x} pdf_{m,n}(j), \tag{5.12}$$

where x is the total number of pixels in a block and j is a linear index that iterates trough all pixels in the vectorized block $pdf()$. Equation 5.12 forms the basis for the general histogram equalization transformation function given by

$$hetf_{m,n}(x) = round\left(\frac{cdf_{m,n}(x) - min(cdf_{m,n})}{(N \times M) - min(cdf_{m,n})}\right) \cdot (B-1), \tag{5.13}$$

where B denotes the number of bins in the histogram and is generally fixed to 256. To control the effect of noise amplification in homogeneous blocks, CLAHE limits the slope (and hence the contrast enhancement strength) of the histogram equalization transformation function by clipping the histogram values in the corresponding local histograms $pdf_{m,n}(x)$ at a certain limit. The clipped parts of each histogram are cumulated and evenly redistributed among all bins after clipping. The clipping value is an adjustable parameter expressed as percentage to the average bin value of the local histogram. Once $cdf_{m,n}(x)$ is determined for each block, the intensity values of every pixel in a block are transformed according to Equation (5.13). The block-wise normalization causes strong contrast gaps between adjacent blocks which manifest themselves as clearly visible lines along the block borders. To diminish the effect, CLAHE combines the normalization transformation with an interpolation scheme that considers the contrast information of adjacent blocks. In detail, the image is divided into three regions, i.e. a corner region, a border region and the central region. Blocks within each region are normalized differently: bilinear interpolation with four

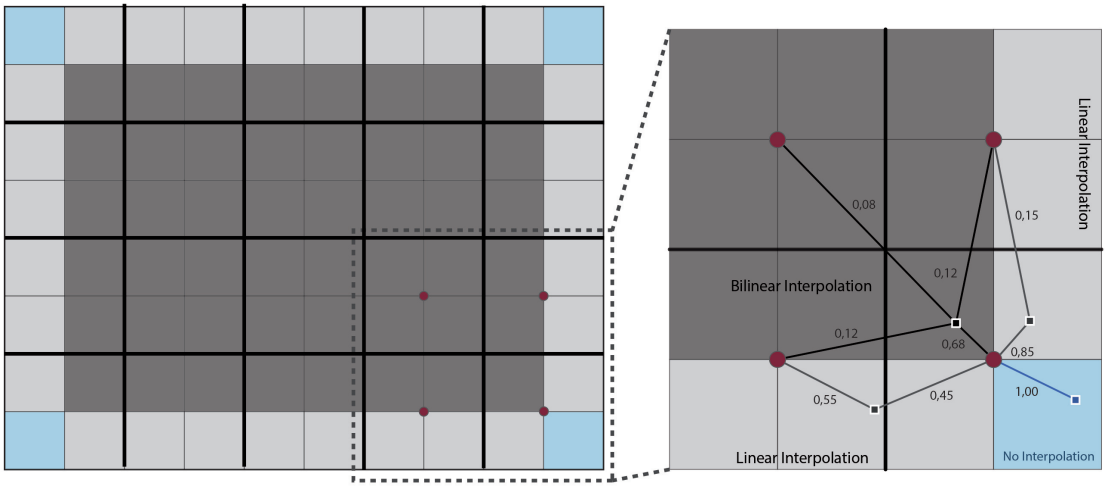

Figure 5.9: Illustration of the CLAHE interpolation concept using a 4 × 5 grid. The image is partitioned into three regions: the center regions (dark gray), the border regions (light gray) and the corner region (blue). Pixels residing in the center region are contrast enhanced using bilinear interpolation among the four histogram equalization functions of the four adjacent blocks. A new contrast value for a given pixel is computed by evaluating Equation 5.13 for each of the four blocks. The four values are weighted with respect to the Euclidean distance between the block centers and the pixel position (weights are exemplarily shown in the figure). The weighted sum is computed among all four values to give the final pixel value. Correspondingly, pixels in the border region are transformed using linear interpolation based on two histogram equalization functions of two adjacent blocks and pixels in the corner region are transformed directly without interpolation.

transformation functions is used to transform the intensity values of pixels located in central region of the image. Linear interpolation using two transformation functions is used for pixels in the border region and no interpolation is used for pixels residing in the corner region. Figure 5.9 illustrates the distinct image regions and details how the normalization for blocks in each region is conducted using inter-block interpolation.

The CLAHE algorithm was implemented and parallelized in this work for the given GPU hardware. Within this context, data throughputs of 2.8 ms per megabyte could be achieved. Details on the efficient real-time implementation were published by the author in [5]. Figure 5.11b illustrates the effect of CLAHE when applied to an input fabric image.

5.3.3 Feature extraction

Due to the high spatial resolution of the imaging system, single yarns can clearly be distinguished within the acquired fabric images. However, depending on the weave and weft density, large yarn parts may not be visible on the material surface since they are covered by several other overlapping yarns. One of the main difficulties in detecting the trajectory of single yarns is hence caused by limited yarn visibility. A possible solution to the problem would be to first algorithmically identify the visible parts of each yarn. As the mechanical properties of a loom always impose a more or less straight course for a yarn over short distances, it would then be possible to estimate the trajectory of non-visible yarn segments by linearly interpolating between visible segments. This idea motivated the research for yarn features that allow to identify the visible segments of a given yarn. As a precondition, the features must be robust, i.e. their detection must be trustworthy and repeatable, and their distribution must be dense along the run length of a yarn, so that possible trajectory estimations are only done for relatively short distances.

First, suitable features had to be defined. It turned out that the only characteristic all woven fabrics share in common is the fact, that warps and wefts are interlaced according to some predefined weave. The intersecting cross-points between wefts and warps take a different shape for each material and weave. They are, however, very distinctive, dense and their visual appearance is constant for a given material. These first observations suggested to use weft/warp cross-points as feature points as algorithmic foundation to locate single yarns within fabric images. Figure 5.10 illustrates a scheme of a plain weave with highlighted wefts and warps, the intersections are denoted as *float-points*. It is distinguished between warp-floats (a warp resides on top) and weft-floats (a weft is on top). Several image processing methods were tested to detect float-points in the On-loom fabric images. First experiments with edge and corner features extracted by Harris corner detection [125] and Canny edge detection [126] in combination with neural networks as classifier gave no utilizable results. The features were not stable enough and the computational complexity was too high as multiple convolution operations over the complete image were necessary in order to extract the features. Further experiments with correlation based matching quickly gave promising results. Here, a warp-float template was first cropped from a reference image. On a different test image, the template was matched to all pixels of the test image using the sum of absolute difference (SAD) metric which is popular the video processing community for stereo matching. Warp-points in most fabric images could be detected at low computational costs. However, the metric turned out

to be unstable in inhomogeneous fabric regions and is very sensitive to illumination changes. As a conclusion, template matching seemed to be an efficient method for detecting warp-float features in real-time, but a suitable comparison metric had to be identified. For this reason, 9 common correlation metrics [127] used in the fields of robot and computer vision were evaluated:

1. Sum of absolute difference (SAD)
2. Zero-mean Sum of Absolute Differences (ZSAD)
3. Locally scaled Sum of Absolute Differences (LSAD)
4. Sum of Squared Differences (SSD)
5. Zero-mean Sum of Squared Differences (ZSSD)
6. Locally scaled Sum of Squared Differences (LSSD)
7. Normalized Cross Correlation (NCC)
8. Zero-mean Normalized Cross Correlation (ZNCC),
9. Sum of Hamming Distances (SHD).

To evaluate the performance of the proposed metrics, a similar procedure was applied as for the selection of the deconvolution algorithm discussed in Section 5.3.2.1. Again, the evaluation was done with the image database FIDB-F (see Section 3.6) since it contains an extensive set of grounsd truth float-point labels. Also the feature point distance (FPD) was used to assess the float-point detection capability of each metric. The number of non detected float-points and falsely detected float-points was additionally evaluated and considered for the selection of a suitable metric. It is noted that the experiments were conducted on normalized and sharp input images, i.e. CLAHE was applied but no Wiener deconvolution.

For the evaluation, from each of the four fabric classes in FIDB-F, one of the twelve fabric images was removed and used to extract a float-point template from it. This resulted in four templates, one for each fabric class. For each of the 11 remaining fabric images of each class, template matching was conducted with the nine correlation metrics mentioned above. Feature points were extracted from the resulting correlation images (the detailed methodology for feature detection is discussed a little later in the text). Around each ground truth float-point, a rectangular region of interest was automatically defined. The size of the ROIs was the same for every float-point within the same fabric class and was defined so that adjacent ROIs do not overlap. The following four cases were distinguished during the evaluation:

- Within the ROI of a given ground truth float-point, one single float-point was detected. Here, the Euclidean distance between ground truth and detection was computed.

- Within the ROI of a given ground truth float-point, no float-point was detected. The missing float-point was registered.
- Within the ROI of a given ground truth float-point, several float-point were detected. The Euclidian distance between ground truth float-point and the closest detection was computed, the number of excessive float points was registered.
- detected float points that didn't reside in any region of interest were counted as excessive.

Computed feature point distances were averaged and the number of missing and excessive float-points were accumulated for all images in the database. In total, 44 images (four images were used for template extraction) with 72,818 labeled ground truth float-points were tested. Table 5.4 summarizes the results of the experiment.

Table 5.4: Correlation metric evaluation results. Values for FPD are averaged over all images in database FIDB-F and are given in pixels. Values for missed (f_m) and excessive (f_e) float-points are given in percent, relative to the total number of ground truth float-points (n = 72,818).

	ø FPD	f_m [%]	f_e [%]
SAD	3.17	11.17	2.03
ZSAD	2.92	8.12	1.37
LSAD	2.92	8.12	1.03
SSD	2.37	7.24	1.57
ZSSD	2.29	7.02	1.18
LSSD	2.87	6.23	1.91
NCC	0.91	1.39	0.43
ZNCC	0.37	0.32	0.28
SHD	3.23	9.26	1.03

The results emphasize that false positive detections are not really relevant for the selection of the correlation metric. All metrics gave relatively low false positives rates. Also all FPD values are in a range that is acceptable for subsequent tracking algorithms (FPD values of 3.0 and below were identified as unproblematic). On the other hand, the false negative rates vary significantly among the different metrics. As it can be seen from Table 5.4, some correlation metrics do not detect up to 11 % of the total amount of float-points. Among all methods, the zero-mean-normalized-cross-correlation (ZNCC) performed best. In particular, only 276 float-points were not detected using ZNCC and detected float-points deviated from the ground truth by only 0.37 pixels in average. The reason for this superior performance is the denominator in ZNCC (see.

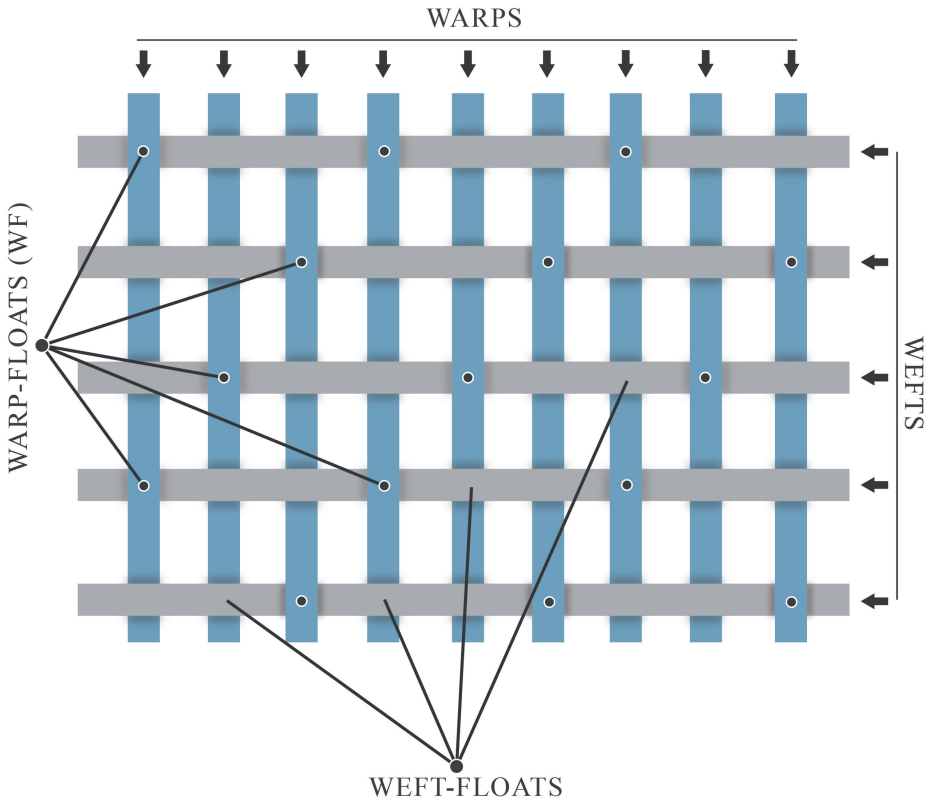

Figure 5.10: Illustration of a 3 × 3 twill weave with intersecting wefts (gray) and warps (blue). Float-point features denote weft/warp crossings. More specifically, warp-floats denote crossing where a warp is on top (black dots) and correspondingly, weft-floats denote crossings were a weft is on top.

Equation (5.14)) which normalizes all computations locally with respect to the images' standard deviation and mean. As a result, the metric becomes very robust against local intensity changes. Nevertheless, numerous local computations of standard deviations and means are computationally very demanding and make the method unsuitable for real-time applications. Fortunately, the standard expression of ZNCC can be transformed into a computationally more friendly form which allows to accelerate the correlation significantly.

The ZNCC function [128] is defined as

$$corr(u,v) = \frac{n(u,v)}{d(h,v)} = \frac{\sum_{x,y}\left[f(x,y) - \bar{f}_{u,v}\right]\left[t(x-u,y-v) - \bar{t}\right]}{\sqrt{\sum_{x,y}\left[f(x,y) - \bar{f}_{u,v}\right]^2 \sum_{x,y}\left[t(x-u,y-v) - \bar{t}\right]^2}}, \quad (5.14)$$

where $t(x,y)$ is the warp-float template, $\bar{t}$ is the template mean, $f(x,y)$ is the pre-processed input image, $\bar{f}_{u,v}$ is the mean of the input image region under the template

and $corr(u,v)$ is the correlation result. Equation (5.14) can be reformulated into a more compact and computationally optimized form according to the derivation presented in Appendix B. The final, compact formula is given by

$$corr(\mathbf{I},\mathbf{t}) := \frac{\mathscr{F}^{-1}\left[\mathscr{F}(\mathbf{I})\cdot\mathscr{F}^{*}(\mathbf{t})\right]}{\sqrt{\sum\mathbf{I}^{2}-\frac{1}{A}\left[\sum\mathbf{I}\right]^{2}}\cdot\sqrt{A}\cdot\sigma_{t}}. \tag{5.15}$$

Here, $\mathscr{F},\mathscr{F}^{-1},\mathscr{F}^{*}$ denote the Fourier transform, its inverse and complex conjugate respectively, $\mathbf{I}$ is the input image, $\mathbf{t}$ is a mean subtracted template, A the area of the template, and σ_T the standard deviation of the template. The operator $(\cdot)$ denotes a point-wise multiplication. Equation (5.15) allows for a very fast computation of the ZNCC based on GPU hardware. In fact, the sum terms in the denominator can be very efficiently computed using summed area tables [129]. In [5], the author discusses an efficient algorithm that allows to compute Equation (5.15) in real-time on GPU hardware. Experiments showed that the float-point detection still works with sufficient precision when the fabric images are scaled to as low as 60% of the original image size. The scaling in this work is done with down sampling and nearest neighbor interpolation. This characteristic has been employed in the system design. Source code for the GPU implementation is available on the project website [13]. Due to the optimizations, the computation time of the correlation matching could be reduced to 3.3 ms per megabyte.

The resulting correlation image $\mathbf{I}_{xcor} = g(\mathbf{I},\mathbf{T})$ shows strong local maxima at locations where the fabric image resembles the template, i.e. at float-point locations. In order to quickly retrieve the xy-coordinates of these local maxima, the correlation image is further processed by a maximum filter which sets pixels values within a defined neighborhood to the local maximum. The process is also known as morphological dilation [90].

$$\mathbf{I}_{dilated}(u,v) = \mathbf{I}_{xcorr}(u,v) \oplus str_{rect}. \tag{5.16}$$

The operator $\oplus$ denotes a gray value dilation and str_{rect} is a circular structure element with fixed radius. The radius is a crucial parameter of the system design. It controls the area in which adjacent maxima are suppressed. Too large values cause false negative detections, too low values cause false positive detections. At this point, the radius is empirically fine-tuned. Section 6.2.3, however, discusses an automatic selection of the parameter.

In the next step, the dilated image is compared pixel-wisely to the correlation image:

$$\mathbf{I}_{nodes}(u,v) = \begin{cases} 1 & \text{if } \mathbf{I}_{dilated}(u,v) = \mathbf{I}_{xcorr}(u,v) \\ 0 & \text{otherwise.} \end{cases} \tag{5.17}$$

Pixel locations where the gray values of both images are equal ($\mathbf{I}_{nodes}(u,v) = 1$), correspond to local maxima and are considered as float-point coordinates in the image. Accordingly, a float-point is a pixel with an x- and a y-coordinate. The term float-point feature subsequently describes a structure with the xy-coordinates of a single float-point and its corresponding correlation coefficient. All found float-point features of a given fabric image are saved in a list **L**. Also the feature extraction part was entirely implemented on GPU hardware achieving computation times of 1.3 ms/MB

The selected size of the template doesn't influence the computation time (since the Fourier Transformation of the template is computed off-line) and has only a minor effect on the feature detection performance. Good results could be achieved in all experiments by a template that covers the area between two adjacent float-points in y- and x-direction. Figures 5.13a-c illustrate three fabric samples of different materials and weaves and their corresponding template selections.

In Figure 5.11, the single steps of the total feature extraction pipeline, namely normalization, correlation and extraction, are shown on the example of a plain fabric.

5.3.4 Yarn tracking

In order to identify the location of single yarns, stand-alone spatial locations of warp-float-features have no expressiveness about the constitutive pattern of the investigated fabric sample. They must be structured and linked according to their relative positions such that a grid structure may be derived from that information. The concept of a grid matrix is hence introduced. The grid matrix is a container in which features are organized in rows and columns such that adjacent matrix entries correspond to feature point proximities in the fabric image. Figure 5.12 illustrates the concept of the grid matrix. Here, four grid vectors $\{\pm\mathbf{g}_a, \pm\mathbf{g}_b\}$ define expected feature proximities within the fabric lattice. Within the grid matrix, features are placed in adjacent rows (columns) when they are proximate in the image with respect to the grid vector $\pm\mathbf{g}_a$ ($\pm\mathbf{g}_b$).

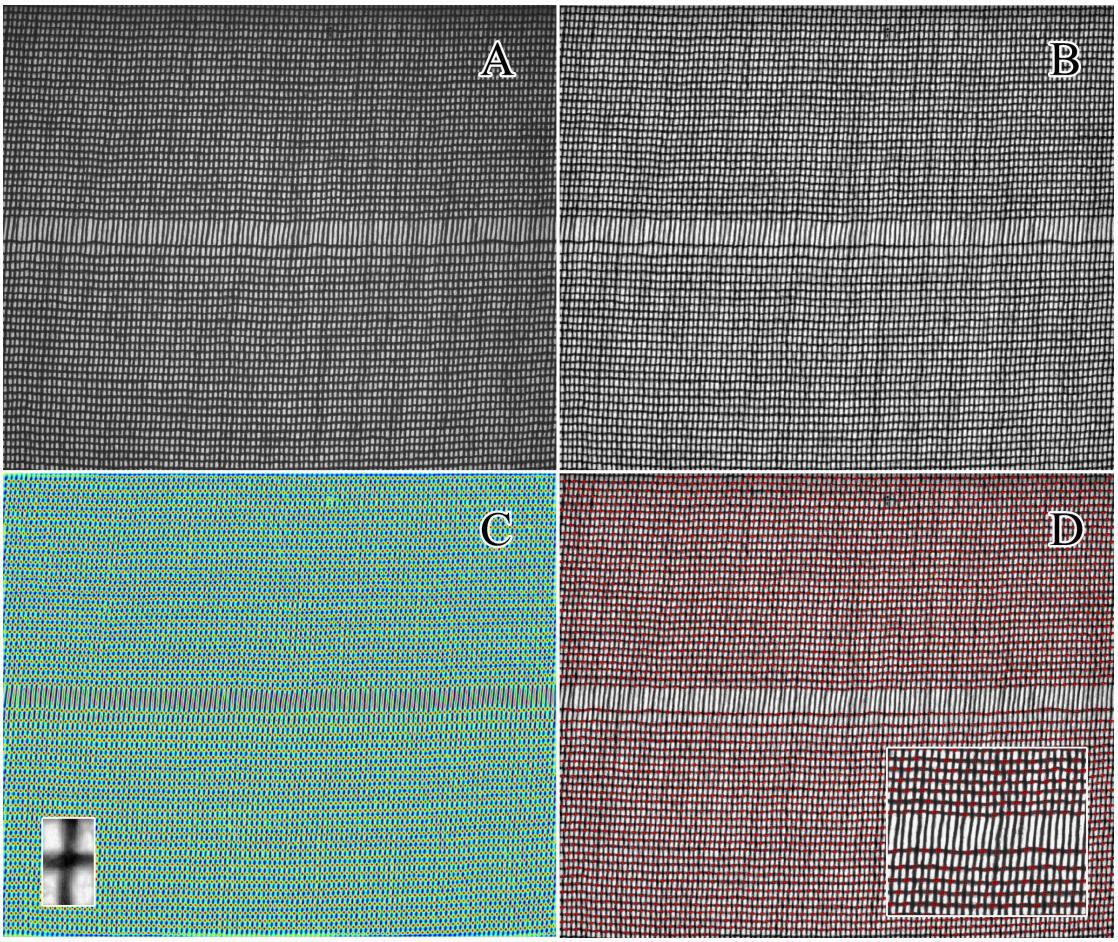

Figure 5.11: Illustration of the feature extraction pipeline. A) Input image after deconvolution. B) CALHE enhanced input image, C) correlation image according to Equation (5.15) (the template is shown additionally), D) detected float-point features plotted on top of the CLAHE image.

A grid vector defines the direction between a given float-point to one of its closest, adjacent float-points within the fabric image. The selection of the two vectors is arbitrary and the precision of the xy-coordinates must not be pixel-exact, it can be approximate. Real-world fabric images are near regular textures, i.e. they are slightly irregular on a local scale which is why a perfect grid vector pair for the entire image cannot be selected. Subsequent algorithms are designed to handle this characteristic. The basic orientation of the vectors must, however, roughly fit to the real alignment of adjacent float-points and they must be distinct. The tolerance for the selection of the grid vectors $\mathbf{g}_a$ and $\mathbf{g}_b$ is controlled by a regularization term κ and the minimal distance (in pixel) between two adjacent float-points. If the minimal distance d_{min} is

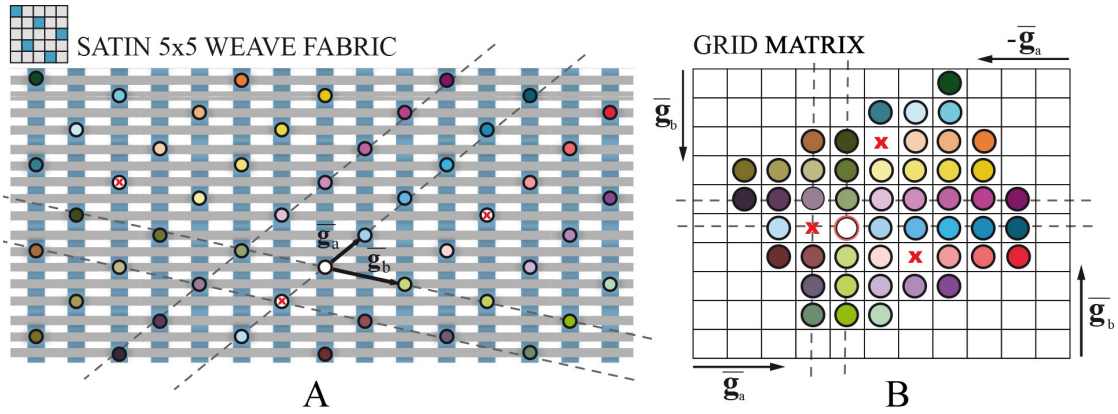

Figure 5.12: Illustration of a 5×5 satin weave fabric with corresponding grid matrix. A) Scheme a of a satin weave with warp-float features marked as color coded dots. Two grid vectors $\mathbf{g}_a, \mathbf{g}_b$ are shown. B) Corresponding grid matrix in which warp-float features are sorted relatively to the grid vectors. The dotted lines indicate the directions along which features were sorted.

for example 50 pixels, the tolerance ψ_{xy} for the grid vectors is computed by

$$\psi_x = \psi_y = d_{min} \cdot \kappa, \tag{5.18}$$

i.e. it is a circle of radius 20 in the above example with $\kappa = 0.4$. Figure 5.13d depicts a possible selection for a grid vector pair $(\mathbf{g}_a, \mathbf{g}_b)$ on the example of a plain weave. Subsequent sections discuss the selection of the term κ. All parameters can be retrieved in a straight-forward manner from one single fabric reference image using an image processing tool that allows to display the coordinates of individual pixels. As a convenient alternative, Section 6.1 discusses a method that uses Fourier analysis and Fuzzy C-mean clustering to calculate the grid and yarn vectors automatically within the context of blind weave detection in woven fabrics.

5.3.4.1 The grid matrix

The main challenges in building the grid matrix are given by:

- Warp-floats are not regularly spread within the image, thus ruling out the possibility of a simple coordinate transformation.
- Some warp-floats may be missing or redundant, making it more difficult to link adjacent floats.

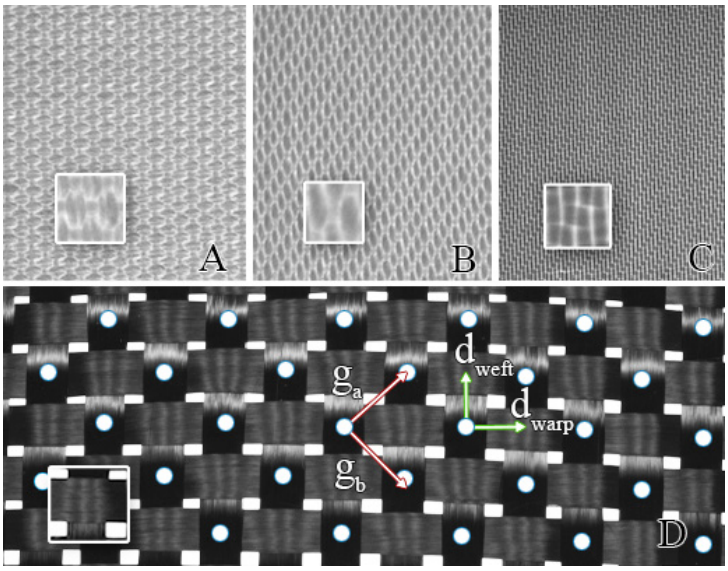

Figure 5.13: Four fabric samples of plain (a,d), satin (b) and twill (c) weave [11]. Possible selections for corresponding float-point templates are shown (magnified). On the example of the plain weave fabric image d, its float-points are marked with white dots, a possible selection for the grid vector are highlighted with red arrows and the weft and warp distance vectors are shown by green colored arrows.

- For most fabric weaves, warps barely reside on the surface of the material and are hence not visible.
- Defects of any size and shape must be anticipated within the signal, what may further disturb the grid structure in a random way by causing large gaps within it.

To face these difficulties, a locally operating, iterative algorithm has been designed that processes each float-point in a lawn-mower fashion by moving from one float to another. To begin with, a temporary search matrix **S**, a queue **Q** and the grid matrix **G** are initialized with zeros. By starting at an arbitrary warp-float (generally chosen to be the closest warp-float to the image center), the structuring algorithm proceeds according to the Matlab pseudo-code presented in Listing 1. Each element in the query queue is represented by a structure defined by a field for its estimated image coordinates and a field for its grid matrix coordinates. During each iteration, a float-point q is removed from the query queue, and its closest warp-float (in terms of Euclidian distance) is found (Listing 1, line 11-13). If the closest float-point exceeds a certain distance to q, the search matrix is marked as *not found* at the position indicated by the matrix coordinates of q and a new iteration starts (line 16). Otherwise, a *found* flag is registered in **S**, and the image coordinates of the closest float-point are saved in the grid matrix at the matrix coordinates given by q (line 19-20). Now,

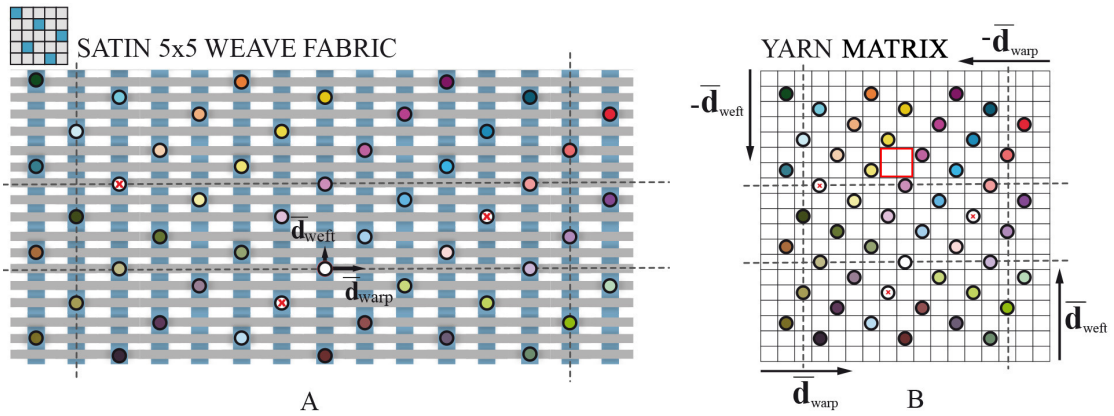

Figure 5.14: Illustration of a 5 × 5 satin weave fabric with corresponding yarn matrix. A) Scheme a of a satin weave with warp-float features marked as color coded dots. Two possible yarn vectors $\mathbf{d}_{weft}$ and $\mathbf{d}_{warp}$ are shown. B) The final yarn matrix in which warp-float features are arranged according to the yarn vectors. Now, warp-floats in a row (column) correspond to features of the same weft (warp) in the fabric. Dotted lines indicate the directions along which features were sorted.

since q could be matched to a node point, four new *potential* float-points positions p_{1-4} are derived from that position. The new matrix coordinates of the four points are calculated by $\{\{x_m+1, y_m\}, \{x_m-1, y_m\}, \{x_m, y_m+1\}, \{x_m, y_m-1\}\}$, where x_m and y_m are the individual matrix coordinates of q (line 19). The search matrix is labeled as *listed* at the four new matrix coordinates. Additionally, four new image coordinates are estimated for the new positions p_{1-4} by adding the four grid vectors $\{\pm\mathbf{g}_1, \pm\mathbf{g}_2\}$ to the image coordinates of of the matched warp-float (line 23). The four new points are attached to the query queue and a new iteration starts (line 25). Only matrix positions that are neither labeled as *found, not found* nor *listed* are processed. In this way, the algorithm will converge and **Q** will be empty at some point, i.e. when the process terminates.

5.3.4.2 The yarn matrix

The grid matrix **G** is a compact and sparse representation of the fabric grid, yet no information about yarn locations is provided. If the approximate distance between adjacent warps and wefts in the image is known, the grid matrix can be transformed into a yarn matrix representation that allows to allocate specific warp-float features to individual wefts and warps, respectively. Let $\mathbf{d}_{warp}$ and $\mathbf{d}_{weft}$ denote two yarn vectors representing the expected distance in pixels between neighbored wefts and

warps in the fabric image as shown in Figure 5.12. This information contained in the yarn vectors directly corresponds to the density of the fabric. Figure 5.13d illustrates a possible selection for a yarn vector pair. The selection of the yarn vectors must not be pixel-precise, yet some limitations apply in order for the overall algorithm to succeed. The implied accuracy for the selection directly depends on the fabric weave and the spatial arrangement of float-points within the fabric. The minimal precision for the yarn vectors $\mathbf{d}_{weft}$ and $\mathbf{d}_{warp}$ in x- and y-direction in pixels is computed by

$$\rho_x = \frac{W_x[pixel]}{l_x} \tag{5.19}$$

$$\rho_y = \frac{W_y[pixel]}{l_y}, \tag{5.20}$$

where W_x, W_y represent the spatial extent (in x- and y-direction, respectively) of a normal weave within a fabric image in pixels and l_x, l_y represent the number of elements in the fabrics basic weave pattern in x- and y-direction. As an example, Figure 5.15 illustrates a 3-1 twill fabric. The spatial extent of a normal weave in this fabric image is 84 × 135 pixels (as indicated by the red square in Figure 5.15c). The basic weave pattern has a dimension of 4 × 4 (see Figure 5.15b) and correspondingly, the tolerance for the selection of the yarn vectors is 21 × 33 pixels.

Once a yarn vector pair is determined, the grid matrix **G** is can be transformed into a yarn matrix **Y** by means of a transformation matrix **T** according to

$$\forall x \in \{1,...,O\}, \forall y \in \{1,...,P\}:$$

$$\mathbf{Y}(x', y') = \mathbf{G}(x, y), \text{ with} \tag{5.21}$$

$$\begin{bmatrix} x' \\ y' \end{bmatrix} = round(\mathbf{T} \cdot \begin{bmatrix} x \\ y \end{bmatrix}), \text{ and} \tag{5.22}$$

$$\mathbf{T} = \begin{bmatrix} \mathbf{d}_{weft} & \mathbf{d}_{warp} \end{bmatrix}^{-1} \cdot \begin{bmatrix} \mathbf{g}_a & \mathbf{g}_b \end{bmatrix}. \tag{5.23}$$

Since both the grid and yarn matrix are sparse, i.e. not all positions are filled, the transformation is only conducted for non-empty matrix positions. Values O and P in the above equations are the height and width of the matrices **G** and **Y**, the function $round(\mathbf{x})$ rounds each double precision entry in a matrix to its nearest integer value. The mathematical derivation of the transformation matrix **T** can be derived as follows. First, the coordinates **a, b, c** of a given float point with respect to the coordinate system of the image plane, the coordinate system spanned by the grid vectors and the

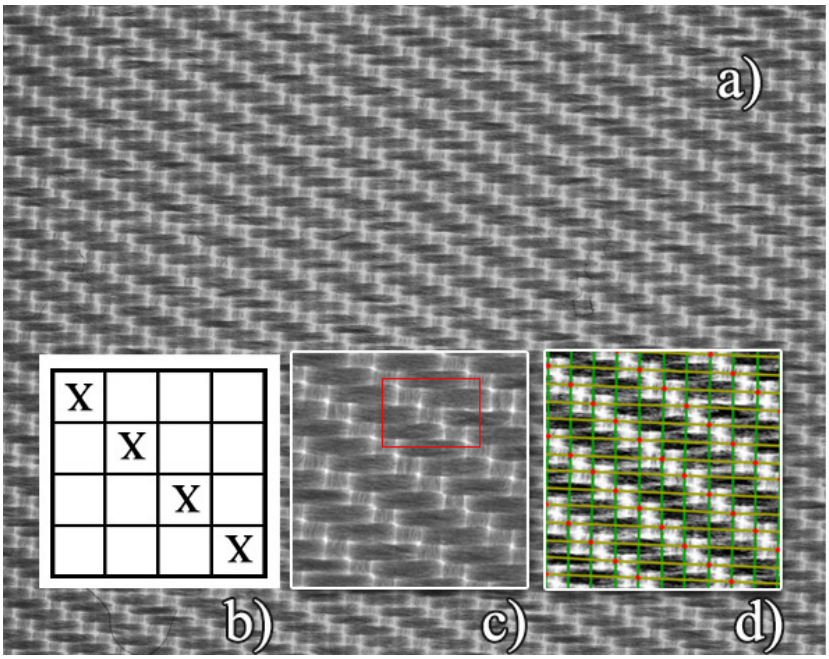

Figure 5.15: Sample of the 3-1 polyester twill fabric used in this work for the evaluation of the proposed machine vision based measurement system. The bottom images show b) the basic weave pattern (the letter *x* marks warp-floats, c) a magnified view of the material and the spatial extend of a weave (red square), and d) tracked yarns and detected float-points.

coordinate system spanned by the yarn vectors are denoted as

$$\mathbf{a} = \begin{bmatrix} x \\ y \end{bmatrix}, \mathbf{b} = \begin{bmatrix} x_b \\ y_b \end{bmatrix}, \mathbf{c} = \begin{bmatrix} x_c \\ y_c \end{bmatrix}, \tag{5.24}$$

respectively. It can now be written

$$\mathbf{a} = \begin{bmatrix} \mathbf{g}_a & \mathbf{g}_b \end{bmatrix} \cdot \mathbf{b} = \begin{bmatrix} \mathbf{d}_{weft} & \mathbf{d}_{warp} \end{bmatrix} \cdot \mathbf{c} \tag{5.25}$$

Rearranging Equation (5.25) allows to define the transformation matrix $\mathbf{T}$, that maps coordinates expressed with respect to the coordinate system spanned by the grid vectors into the coordinate system spanned by the yarn vectors

$$\mathbf{c} = \mathbf{T} \cdot \mathbf{b}, \text{ with} \tag{5.26}$$

$$\mathbf{T} = \begin{bmatrix} \mathbf{d}_{weft} & \mathbf{d}_{warp} \end{bmatrix}^{-1} \cdot \begin{bmatrix} \mathbf{g}_a & \mathbf{g}_b \end{bmatrix}. \tag{5.27}$$

As depicted in Figure 5.12b, the yarn matrix $\mathbf{Y}$ structures all warp-float features that reside on the same warp (weft) in a column (row). The yarn matrix representation

allows to assign single features to specific yarns and hence forms the basis for yarn tracking.

5.3.4.3 Trajectory interpolation

To visualize yarn trajectories (i.e. the coordinates of center pixels of a yarn), the pathway of a yarn between two adjacent column/row warp-floats a and b in $\mathbf{Y}$ is modeled by a straight line. The slope of that line is used to interpolate the coordinates of all pixels between a and b. Figure 5.16a illustrates the concept. By connecting all lines for a specific column or row, yarn trajectories can be visualized efficiently as shown in Figure 5.16b-d. The procedure is based on the idea that the trajectory of a yarn may not change abruptly within the short distance that separates two adjacent warp-floats. Conditioned by mechanical restrictions of the weaving process, the assumption holds also for defective material as validated in all on-loom tests. Further examples for the quality of the proposed tracking method are shown in Appendix D.

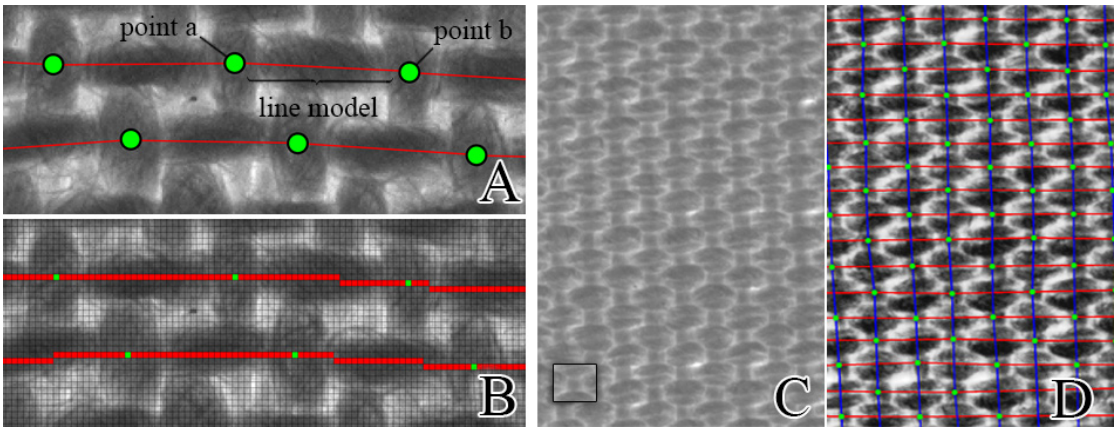

Figure 5.16: Illustration of the concept of yarn tracking using interpolation between warp-floats. A) Due to the mechanically defined, short distance between adjacent warp-floats (green), the trajectory of single yarns can be modeled by a direct line between them (red). B) Discrete pixel coordinates. C) Plain weave fabric with D) yarn tracking results plotted on top.

5.3.5 Defect detection

The implementation of the yarn tracking procedure provides a precise and compact description of the fabric yarn structure. This information is now further exploited to spot potential anomalies within the fabric. Robust defect detection is challenging due to variety of defect characteristics, shapes, and sizes which makes it difficult to cover all flaw classes with only one analysis strategy. Moreover, normal fabric irregularities (i.e. yarn thickness, texture and trajectory variations that are not defective) in real-world images may spuriously be taken as defects and often cause AVI-systems to report false alarms. To face these problems, we introduce three independent defect detection modules to cover

1. defects altering the near-regular pattern of the fabric,
2. too tight or loose yarn spacings and yarn windings, and
3. defects that impact the surface texture of single yarns.

It is shown that a combination of all three strategies allows robust, precise, and yet versatile defect detection – in real-time.

5.3.5.1 Grid control

The yarn matrix **Y** derived in Section 5.3.4.2 is analyzed to control the regularity of the fabric structure. Each of its entries is an index, linking to a warp-float feature with given xy-coordinates and a normalized correlation coefficient. By filtering entries for which the correlation coefficient falls below a threshold, the matrix **Y** is thinned out and coherent blanks in it can be found using connected component analysis [130]. The term *blanks* is used to describe entries in **Y** which are empty (i.e. filled with zeros). The matrix **Y** is binarized and subsequently processed by a morphological dilation operator using a rectangular or cross shaped structure element. The width, height and shape of the structure element are chosen to cover blanks in a normal defect-free **Y** matrix. Figure 5.14b illustrates a suitable structure element for the given fabric (red square). A defect-free yarn matrix will not show any blanks after dilation. Contrary, the yarn matrix of a defective sample will show blank areas (blobs) within the yarn matrix. Using connected component analysis, it is straightforward to classify potential blobs according to their area. Larger blobs are considered as defects. In order to match

the position of blobs found in **Y** to a defect position in the fabric image, the image coordinates of non-blank **Y** matrix entries around each blob are interpolated to define a convex hull in the image. Figures 5.21b and 5.21 illustrate grid defect detection results for a given fabric sample. Due to the small size of matrix **Y** (typically about 150×150 entries), grid control can be executed in fractions of a millisecond.

5.3.5.2 Yarn spacing and curvature measurement

The density of a fabric is a crucial factor for the quality of the material, especially for fabrics used in technical makes like air bags or water-repellent products. It is of vital interest for any quality inspection system to ensure density consistency with high precision. Within the On-Loom fabric inspection setup, images are acquired by a minimal spatial resolution of 415 pixels/cm, corresponding to 25 μm per pixel which is the theoretical lower bound for the density measurement of the system. To determine inter-weft spacings, weft trajectories (as found in Section 5.3.4.3) are stored in a $L \times N$ matrix **M**, where L is the number of wefts in the image and N is the fabric image width. Only the y-coordinate of each trajectory pixel is stored within the matrix, positions where no trajectory exists are kept blank (marked with zeros). This compact representation allows for a straight forward pixel-wise weft spacing measurement for every point on a trajectory by following the formula

$$d(x,l) = \mathbf{M}(l-1,x) - \mathbf{M}(l,x), \tag{5.28}$$

$d(x,l)$ being the distance in pixels of the lth weft to its upper neighbor at column position x. The measurement for inter-warp distances is performed analogously. The calculations can be parallelized efficiently. The spacing measurement works robustly as validated in several on-loom test runs in which the density of different materials has been varied within a range of 8 wefts/cm up to 30 wefts/cm. It must be stated, that when larger changes of the density are applied, the grid and yarn vectors introduced in Section 5.3.4 must be manually re-calibrated to match the new material structure. Section 7 introduces methods to automate this process. For stand-alone defect detection applications, the selection of an upper and lower spacing threshold for relative pixel distances is sufficient to precisely detect abnormalities within the image. When absolute density values (in millimeters) for measurement and control tasks are aspired, the system must be calibrated first. Calibration was not necessary for the On-Loom system.

For weft curvature measurement, the yarn coordinate matrix **M** is processed once

again. Yarns within fabric images should be straight without any curvature – wefts should run orthogonal to warps. It is an indicator for potential defects when these basic rules are violated. For the measurement, the slope of the line connecting the weft trajectory point $M(l,x)$ to its δth right neighbor $M(l,x+\delta)$ is determined and should be smaller than a predefined threshold. Curvature is hence controlled using a sliding slope operator. Again, the measurement for warp curvature is performed analogously. The value for δ is selected to have the width/height of the basic fabric weave. This is considered as the smallest range in which curvature abnormalities can be detected robustly. Figures 5.21d and 5.21f depict defect detection results for spacing and curvature defects.

5.3.5.3 Block partitioning

Experiments showed that the defect detection modules for *grid control* and *yarn spacing measurement* are already able to reliably detect 70 % of the defects occurring during fabric production. However, defects altering the visual appearance of single yarns (dirt/oil defilements, thick or thin yarns) cannot be detected. The third defect detection module is hence designed to overcome this shortcoming by controlling the texture consistency for single yarns. Each yarn is partitioned into a set of small blocks: Using the information provided by the yarn matrix, a rectangular region of interest is first placed around each warp-float feature. Subsequently, the yarn segment between two adjacent features is further partitioned into several smaller blocks of different sizes. Each block along such a segment belongs to a specific class, up to 6 different block types are supported by the current system design. The optimal amount of blocks and their size depends on the material and weave and must be selected empirically during calibration. The basic concept behind the block partitioning idea is to break down the texture analysis task into sub-regions of minimal size and with known and hardly changing textural characteristics. This will reduce the texture complexity of individual blocks and makes simple yet fast texture descriptors applicable for the quality control task. Figure 5.18 exemplarily illustrates the block partitioning concept.

Since fabric defects have a very low occurrence probability, a labeled training set for new materials are generally not available. Thus, classification techniques that are based on supervised learning are not applicable. Instead, it is proposed to deploy an elementary texture descriptor that can be calibrated with defect-free samples only and which proved to be very efficient when combined with the yarn block partitioning concept. For each block individually, a gray value histogram is determined and its

number of bins is compressed from 256 to 32. Several bin sizes have been tested in this work, the selected size of 32 proved to be the best trade-off in terms of speed and accuracy. The condensed histogram is normalized to unit area to give a probability density function (PDF). Zero-mean and unit-variance normalization are not applied to keep the descriptor sensitive for homogeneous intensity changes. Figure 5.17 illustrates the process.

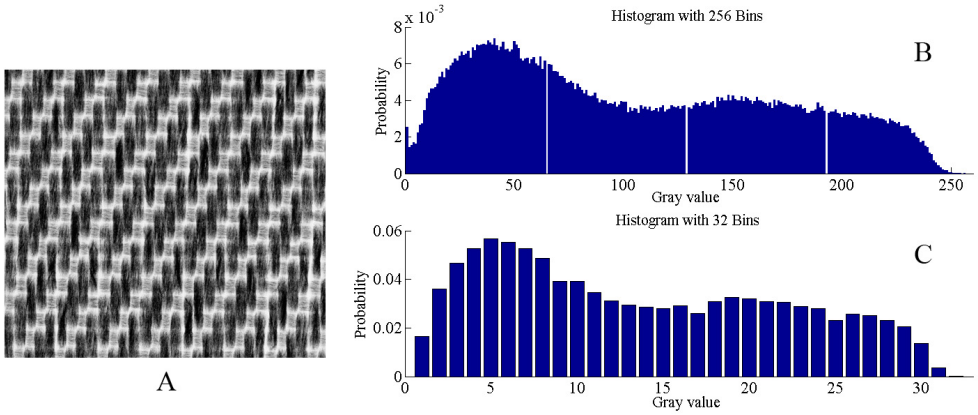

Figure 5.17: Illustration of bin compressing process. A) gray-value fabric image. B) Its normalized histogram, i.e. PDF, with 256 bins. C) the compressed PDF with only 32 bins.

A set of 45 PDF similarity/distance measures [84] has been tested to conclude which measure is most suitable to compare a condensed gray value PDF (gvPDF) of a given block to a reference gvPDF. The *Kumar-Johnson* (KJ) measure

$$d_{KJ} = \sum_{i=1}^{32} \left(\frac{(P_i^2 - Q_i^2)^2}{2(P_i Q_i)^{\frac{3}{2}}} \right) \tag{5.29}$$

performed best with regards to the *F2-score* [131] with a result of 0.90 on a manually labeled ground truth data set. Here, P_i denotes the *gvPDF* of a given block at bin i and Q_i represents a reference *gvPDF* learned from defect-free blocks. A block is classified as defective if its KJ-measure exceeds a predefined threshold. All thresholds are set to low values to ensure a high detection sensitivity at the expense of a higher false alarm rate. A non-maximum-suppression mechanism is subsequently applied to cancel out false positive blocks which retroactively lowers the false alarm rate. For this purpose, the position of each block is mapped to one (or several) entries in the yarn matrix $\mathbf{Y}$. The corresponding entries are marked as defective in $\mathbf{Y}$ and for each entry, the amount of marked positions within a predefined neighborhood is counted. If the number of conjoint blocks is too low, the corresponding block is unmarked as defect-free. The shape of the neighborhood can be arbitrary, a rectangular shape is used in our system

design.

The reference gvPDFs (one for every block type) must be calculated in a calibration step from defect-free fabric images. The images are hereby partitioned into blocks of n types according to the predefined block grid layout. A total number of n gray value histograms (256 bins) is accumulated from all reference blocks – one for each block-type. Histograms are subsequently condensed and normalized to give n reference gvPDFs used for on-line processing.

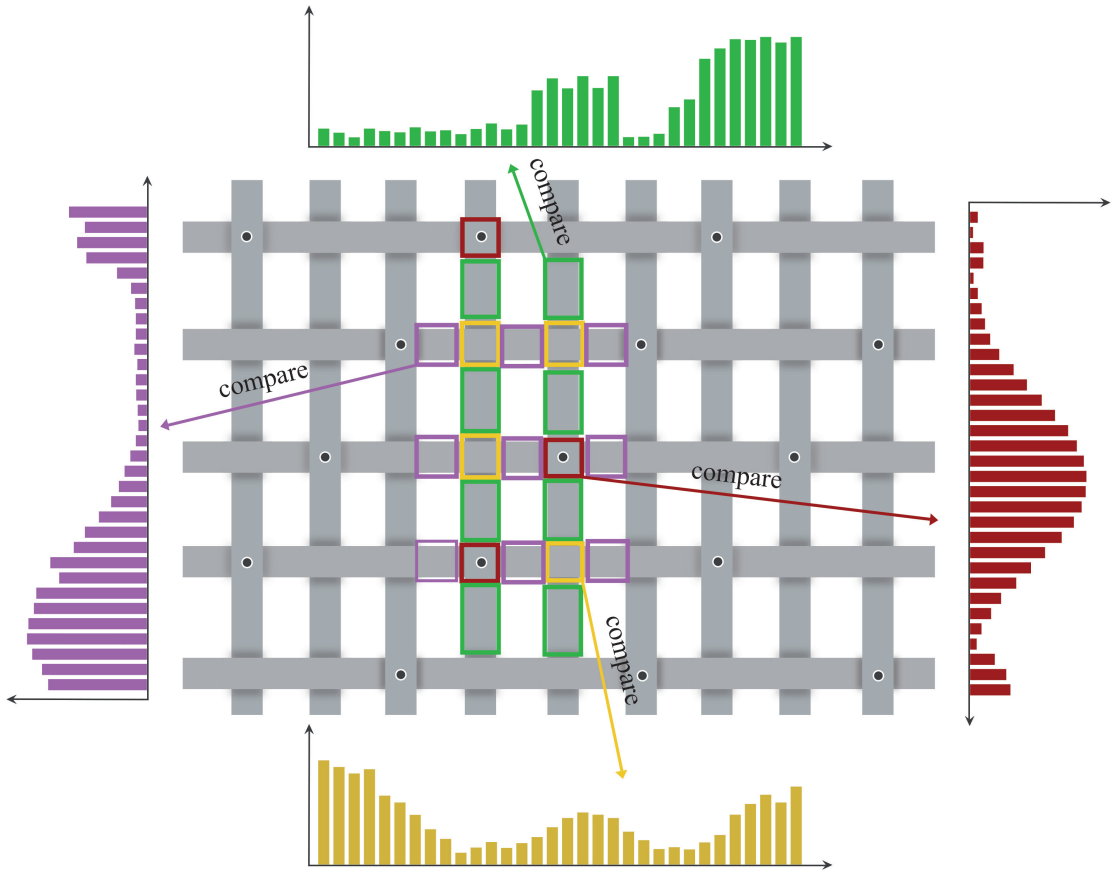

Figure 5.18: Illustration of the block partitioning concept for yarn based texture analysis. The example shows a possible partitioning of a fabric into four block types (yellow, green, purple, red). Four each block, a 32 bin gray-value PDF is computed and is compared to a reference PDF corresponding to its block type. The Kumar-Johnson similarity metric is used to decide if a tested PDF is similar enough to a given reference.

The proposed block analysis framework is efficient for three reasons:

1. The training phase is straight forward. Several defect-free reference images are enough to automatically learn all models and thresholds.

2. It overcomes the problem of over-sensitivity due to normal but frequent fabric irregularities by applying an elementary yet effective filtering of false positives.
3. It can be implemented in real-time for a large amount of data.

Once a block has been classified as defective, all pixels within that block are marked as defective. Figures 5.21b and 5.21f illustrate defect detection results for the block-analysis module.

5.4 Evaluation

Figure 5.19: Image of the On-Loom imaging prototype system for fabric defect detection mounted onto a OMNIPlus-800 loom from Picanol.

The proposed framework for on-loom fabric defect detection has been realized as a prototype system mounted to a OMNIPlus-800 [95] loom. Mechanics and image acquisition strategies are detailed in Section 5.2. Figure 5.19 shows the final prototype including the back-light set up on the loom. The following sections discuss the evaluation environment and finally present on-line defect detection results.

5.4.1 Datasets

In order to make the results comparable to the findings of Chapter 4, the image databases FIDB-C, FIDB-E were used to off-line evaluate the proposed software framework. The deconvolution module was disabled for these databases. In addition, database FIDB-G was included in the evaluation. Accordingly, it represents the main dataset in this evaluation as it contains only images that were directly acquired by the On-Loom prototype system. The databases FIDB-A, FIDB-B, and FIDB-D could not be considered as their spatial resolution is too low so that single yarns cannot be distinguished.

5.4.2 Assessment criteria

As assessment criteria, the same evaluation metrics were used as in Section 4.2.3.2. Correspondingly, the hit rate (HR), the fault rate (FR), the coarse hit rate (CHR) and the coarse fault rate (CFR) were used to assess the defect detection capabilities of the proposed framework.

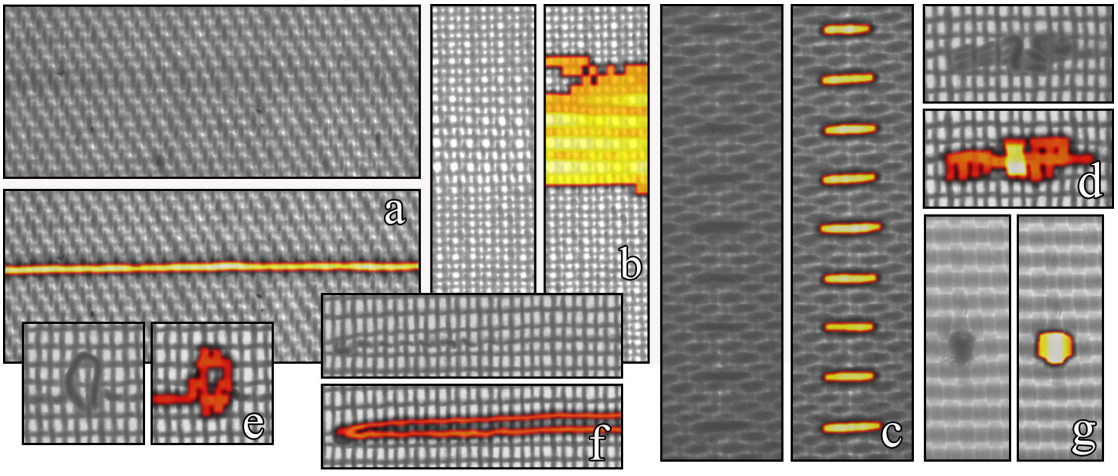

Figure 5.20: Defect detection results for the off-line database FIDB-C. a) Cotton, twill weave, thick yarn b) Cotton, plain weave, large knitting c) Polyester, satin weave, wrong warp d) Cotton, plain weave, wound up yarn e) Cotton, plain weave, loop f) Cotton, plain weave, broken yarn g) Polyester, plain weave, blob defect

5.5 Results

For a fair comparison with the benchmark conducted in Section 4.2.4, the border regions of each image were not analyzed either, as vignette degradations would spuriously worsen the results. A frame of 100 pixels distance to the borders was drawn onto each image and the evaluation was performed within it. Figure 5.21b illustrates an example of false alarms caused by vignette degradations (marked by white circles). Table 5.5 summarizes the defect detection results of the evaluation. Here, the values for HR, CHR and CFR are given in percent (%) and the values for FR are given in per mill (‰). On database FIDB-C, the system achieved optimal detection results in terms of practical applicability. In fact, the values for CHR and CFR are 100 % and 0 %, respectively. This means that the system identified all defective images in the database and no defect-free image was labeled as defective. The defect segmentation capabilities are not perfect but still very precise, especially the low fault rate of 0.36 ‰is worth mentioning. The results slightly worsen on the on-loom databases FIDB-E and FIDB-G. Optimal coarse hit rates could still be achieved but at the same time the coarse fault rates rise to 0.5 % and 0.4 %, respectively. This is still an improvement by a factor of 14 compared to the best result achieved by state-of-the-art algorithms evaluated in Section 4.2.2. Another surprising insight was the fact, that the system actually performs better on database FIDB-G than on database FIDB-E, even though motion blur degraded the images and was reduced by deconvolution. This observation is explained by the loss of high frequency information during the blurring and deconvolution, as edges were smoothed what might have a positive impact on the feature extraction part and the gray value histogram analysis. Small defects were reliably detected on all databases by the proposed framework. Figures 5.21a-f and 5.20a-g show defect detection results achieved for database FIDB-G and FIDB-C, respectively.

5.5.1 Computing time

All machine-vision algorithms run on dedicated hardware consisting of a i7950 CPU, 8GB RAM and an NVIDIA GTX 580 GPU. An overview of computation times in milliseconds for all processing modules is given in Figure 5.7. All times were averaged and relate to the processing of fabric images within the databases FIDB-C,E and F. The total

Table 5.5: Evaluation results of the On-Loom imaging framework. The method was assessed with respect to the *Hit Rate* (HR), *Fault Rate*, and *Coarse Hit Rate* (CHR), and *Coarse Fault Rate* (CFR), see Section 4.2.3.2. Values for HR, CHR, and CFR are given in percent (%), and are rounded to the nearest integer value. The values for FR are given in per mill (‰). Details on the image databases FIDB-C, .E and .G can be found in Section 3.

	FIDB-C	FIDB-E	FIDB-G
	54 images, off-line, no camera motion, diff. materials	4000 images, on-loom, no camera motion, one material	4000 images, on-loom, camera motion, motion blur, one material
Hit Rate	94.2	89.4	92.1
Fault Rate	0.36	0.77	0.62
Coarse Hit Rate	100	100	100
Coarse Fault Rate	0.00	0.53	0.47

computation time sums up to 65 ms per image which enables the system to monitor the production process in real-time for a given frame rate of 15 fps. In detail, Wiener deconvolution can be executed in less than 2.4 milliseconds/Megabyte (ms/MB) using GPU hardware, less than 2.0 ms/MB are spent to enhance image contrast and equalize illumination inhomogeneities (CLAHE), less than 2.8 ms/MB are spent to detect NP-features in all investigated fabric types (with 60 % image down-scale). The process of building the grid matrix, transforming it to a yarn matrix and interpolating trajectory coordinates takes 2.2 ms/MB in average on the given hardware. The computational time rises linearly with the amount of NP-features in the image and hence depends on the yarn density of the material. The number of feature points of the fabric images analyzed in this work ranges from 2000-8000 features per image, real-time requirements could be meet in all cases without difficulty. The computation time for spacing and curvature measurement rises with higher densities. Within the scope of this work, fabric densities have been varied within a range of 8-30 wefts/cm, resulting in computation times of 3-6 ms. Finally, the computational needs of the block analysis module amount to 3 ms/MB on average, whereas the *gvPDF* calculation takes about 80% of the time.

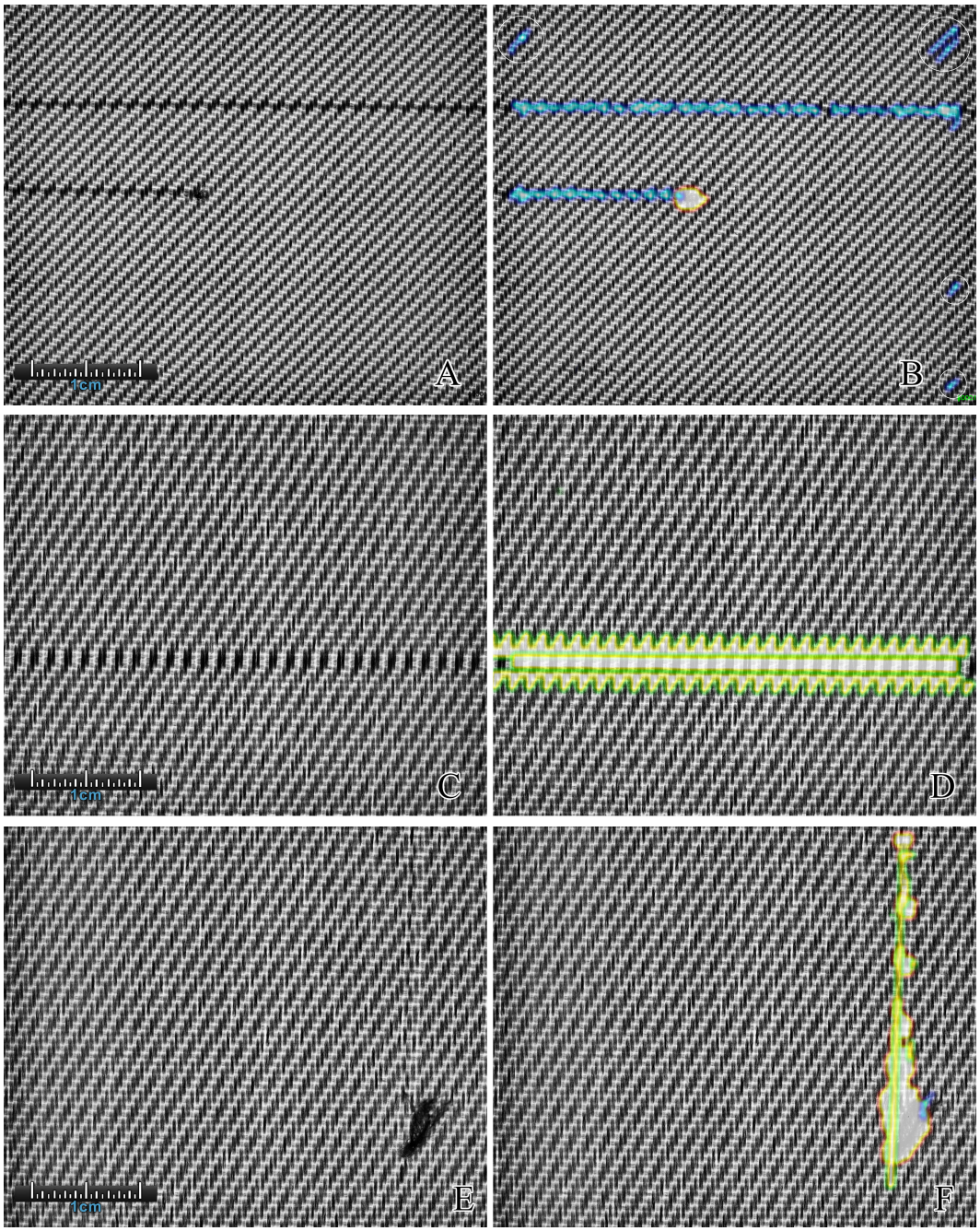

Figure 5.21: On-Loom fabric defect detection results for three samples of the database FIDB-G. Left column: defective, de-blurred and contrast enhanced live image. Right column: Defect detection results. Blue areas were detected by the micro block yarn texture analysis module, orange areas by the grid control module and green areas by the spacing measurement module. Four false alarms were detected in sample A near the border regions of the image (highlighted with white circles for illustration purposes).

5.6 Economic feasibility

Table 5.6 gives a detailed cost overview of the current prototype system as it has been implemented in the laboratory. The production costs for an optimized commercial solution are estimated to be 4600 € in 2013 and a price drop of 20% is expected in the next four years. The relevant measures for the cost effectiveness of the system are

1. the systems purchase price,
2. the reduction of material rejects δ,
3. the service life λ of the system,
4. the amount of annually produced fabric κ, and
5. the costs of the produced fabric.

It is distinguished here between the worst case and best case scenario in which the annual fabric production varies between 150×10^3 m^2/a and 300×10^3 m^2/a, respectively. These values are realistic for common air jet, rapier and projectile weaving machines. The system performance is described by the reduction of rejects (ROR) rate, which indicates by how many percentage points (pp) the relative amount of rejects can be reduced (e.g. if 2.00 % of the produced makes are currently rejected, an AVI system with a ROR of 0.10 pp would reduce this value to 1.90 %). It is conservatively assumed that the ROR is 0.03 pp and 0.10 pp for the worst and best case scenarios, respectively. The service life has been assumed to be 5 years in both cases. Table 5.7 summarizes all basic conditions assumed for the worst and best case. As assessment criterion, the net present value of difference investments (ΔNPV)

$$\Delta NPV = -\Delta I + \sum_{t=1}^{\lambda} \frac{1}{(1+z)^t} \Delta R \tag{5.30}$$

$$\Delta R = \delta \cdot \kappa \cdot \Delta C, \tag{5.31}$$

is used, whereas ΔI denotes the initial investment, ΔC the material costs, and z the interest rate (which has been neglected due to the small period of time λ). The ΔNPV indicates if a given investment is profitable. Negative values indicate losses and positive values gains, a ΔNPV of zero marks the break-even point of an investment, i.e. the point where the investment becomes profitable. Assuming a ΔNPV of zero and neglecting the interest rate, Equation (5.30) can be reformulated to

$$\Delta C = \frac{\Delta I}{\lambda \cdot \delta \cdot \kappa}. \tag{5.32}$$

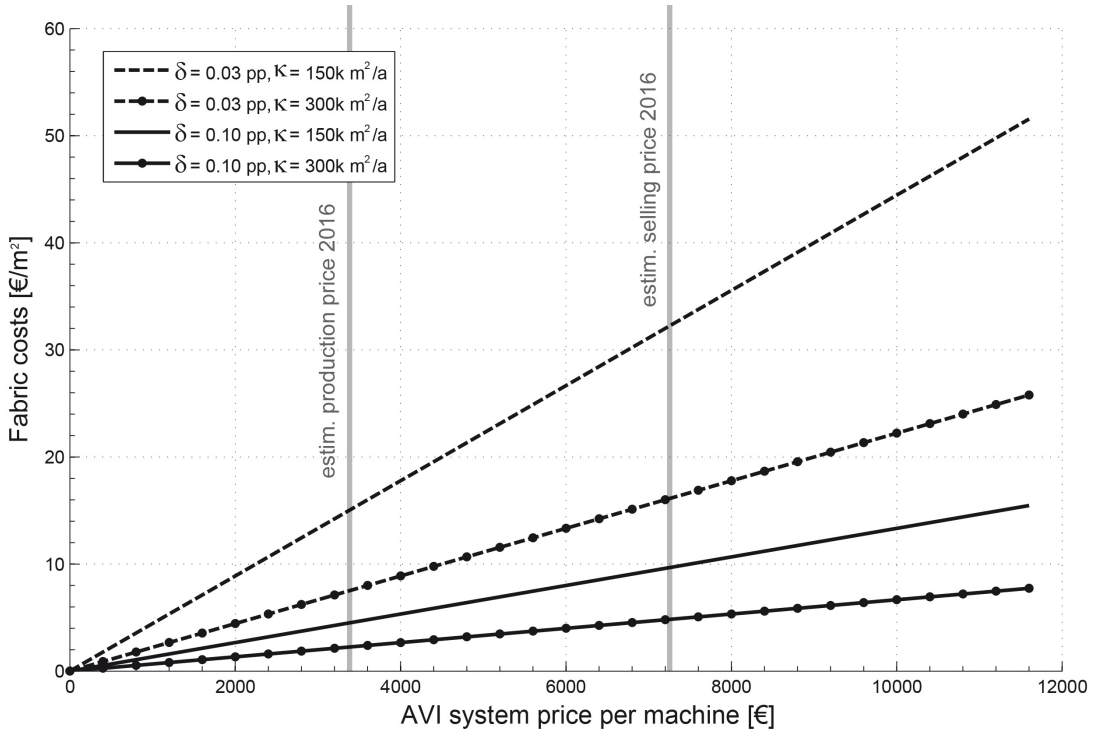

Figure 5.22: Cost forecast for the proposed On-Loom defect detection system. Shown are the curves that define the net present value of difference investments that is zero, i.e. the point where the investment in an defect detection system becomes profitable. Four curves for best and worst case scenarios are shown.

By assuming that the system is sold at 100% of its production costs, Figure 5.22 plots the four price curves for best and worst case scenarios according to Equation (5.32) and Table 5.7. It can be concluded that the system application becomes profitable in the best case scenario for fabric materials within a price range of 5 €/m^2 and above. This would make it attractive also for mass market application. In worse scenarios, the system turns profitable for higher material costs of 10 €/m^2 and above, as generally paid for technical fabrics. As an example, carbon fabric with a mass per unit area of 400 g/m^2 and a roving price of 30 €/kg is already sold by a price of 12 €/m^2.

5.7 Discussion

The evaluation results clearly demonstrated the robustness and reliability of the proposed algorithmic framework for fabric defect detection. Coarse hit rates of 100 % on all databases could not be achieved by any other evaluated algorithm (see Tables

Table 5.6: Costs overview of the current prototype (PT) system and estimated price evaluation for a commercial system (CS) based on estimated yearly costs decays on single construction parts.

	Costs PT in 2013	**Costs CS** in 2013	**Costs CS** in 2016	**Decay** by year
Camera	2900 €	800 €	525 €	10%
Lens	742 €	700 €	700 €	0%
LED field	583 €	500 €	261 €	15%
Strobe Control	556 €	500 €	408 €	5%
Linear axle	5000 €	1000 €	1000 €	0%
Computer	2916 €	1000 €	656 €	10%
Misc.	263 €	100 €	100 €	0%
∑	**12,960** €	**4600** €	**3650** €	

4.2 and 4.3). More importantly, the false alarm indicators, i.e. the coarse fault rate and the fault rate, could be lowered by a factor of 14 compared to the best performing algorithm evaluated in earlier sections. This is the major contribution of this work as too frequent false alarms will prevent any system from being used in practice. Moreover, about 20 different fabric samples with plain, twill, and satin weaves have been analyzed successfully in database FIDB-C – a good indicator for the universal validity of the framework which is a must-have feature for a potential commercial distribution. Also small defects could be detected reliably in all databases which is a major improvement compared to the state-of-the-art. In fact, the high resolution of the acquired fabric images allows for the first time to detect and measure defects that are smaller than 1 mm. The concept of shifting the task of fabric defect detection from a surface inspection problem to a dimensional verification task, i.e. from filtering to a measuring task, proved to be a seminal strategy to build highly reliable and robust defect detection systems.

Even though the achieved results are convincing, several issues of the current design need to be addressed. First, the results illustrate that the image acquisition setup is not optimal in terms of the obtained image quality, as significant vignette degradations cause higher false alarms than necessary. Even though the image border regions were not considered in this work, the overall results would improve once the quality of the images is enhanced. The problem will be covered in future work as it is intended to improve the back-light illumination, optimize camera and lens interplay and build in

Table 5.7: Basic conditions for the economic efficiency calculation. It is distinguish between a worse case and best case scenario.

Parameter	**Worst Case**	**Best Case**
Service life λ	5 [a]	5 [a]
Reduction of rejects δ	0.03 [pp]	0.10 [pp]
Annual production κ	150×10^3 [m^2/a]	300×10^3 [m^2/a]

a software-based lens correction module. Moreover, the worst achieved false coarse rate of 0.53 % means that within 10 minutes of recording, about 20 false alarms will be triggered by the current system (while keeping the sensitivity high enough to detect all defects). Even though this represents a significant improvement compared to current systems, this rate is still too high for commercial usage. The two main reasons for false alarms within the current system design are the gvPDF texture descriptor which shows (as expected) fluctuations and already discussed vignette degradations (that also impact the gvPDF descriptor). In fact, most false alarms were reported close to the border frame by the gvPDF descriptor (see. Figure 5.21b). Possible solutions to this problem would include a better imaging hardware but also a more robust texture descriptor. In this work, gvPDF was mainly developed and used because of its computational frugality. It is likely, that are a more sophisticated method, as for example a modified and adapted LBP descriptor, would further lower false alarms and hence empower the On-Loom system to approach a zero false alarm quota. However, to achieve this goal several algorithmic modules must first be simplified and accelerated in order for the system to keep its real-time processing capability. Additionally, a more sophisticated post-processing scheme could be implemented that better filters false pixel classifications before defects are reported.

The current On-Loom system must be calibrated off-line using defect free reference images to define grid and yarn vectors, such as the float-point template. Even though the process is not time consuming, it requires a skilled person to do the calibration and should hence be automated. In Part III of this work the problem will be addressed as a byproduct of the automatic weave detection algorithm.

Another drawback of the proposed framework is its current restriction to non-patterned fabrics with mono-colored wefts and warps. Wefts and warps must be of uniform color each, otherwise the correlation will fail to robustly detect the correct

location of repetitive features. This limit relates to the current strategy for feature point extraction as described in Section 5.3.3, since a single template can only be used to detect float-points that look alike. Once yarns with different colors are worked into the material, the current method will fail. Future work may investigate methods for replacing the template matching module so that multi-colored materials can be investigated. The usage of statistical operators to characterize float-points seems to be a promising instrument in this context as for example proposed by Wang et al. and Lin et al. [132, 133] who did research on automated fabric density measurement. Another way to handle this limitation could be by altering the imaging method. Color might have no visible effect in fabric images acquired with near infrared, infrared or ultra-violet light. The confirmation of this hypothesis will be subject to future work.

Moving mechanical parts may be an additional disadvantage for practical usage of the system. In fact, the sliding camera mount is prone to abrasion and might cause maintenance work when operated over a longer period of time. On the contrary, the traverse concept allows very high image resolution and complete material coverage at a low price. A corresponding system with no moving parts would require an array of 36 fixed cameras mounted to the loom, which would be rather expensive. Discussions with representatives of leading weaving mills showed that a price of 5000 € per machine is a critical limit for potential investments in quality control. Thus, the production price should be further lowered by 1150 € with regards to the estimated price in 2016 (cf. Table 5.6). The highest and fastest price reduction potential is seen for alternative camera and lens hardware, the complexity reduction of machine vision algorithms, and a simplified illumination strategy which uses top-light instead of back-light. Current work evaluates if the back-light illumination can be replaced by light sources mounted to the camera sled without loss of defect detection accuracy. This alteration would greatly simplify the mechanics and also reduce the costs of the entire system.

5.8 Conclusion

The results of Part I of this work, i.e. benchmarking the state-of-the-art, revealed weaknesses of modern algorithms for fabric defect detection and hence motivated a development of novel algorithmic design concept. Accordingly, a new prototype system for on-loom fabric defect has been developed and was mounted to a real-word

loom. Several off-line and on-line evaluation test runs proved high defect detection accuracy and robustness for a variety of fabric materials and defect classes. By measuring single yarns in terms of their shape, position and appearance, new standards in defect detection accuracy could be set by the proposed framework. Also the false alarm rates of the system are significantly lower than for other methods. Nevertheless, some improvements should be implemented as the current false alarm rates are still too high for practical usage. Also, fabric inspection with the proposed framework is yet limited to mono-colored materials. A detailed cost analysis illustrated that the price for a final, commercial product could theoretically be reduced to a level that allows the system to be applied profitably for quality control of low price mass-market materials. To resume the discussion on problems of current state-of-the-art systems for automatic fabric defect detection, it is believed that this work provided promising solution statements to overcome the difficulties of low spatial resolution, time and space delay from production, frequent false alarms and algorithmic rigidity. The system production price must be further lowered in order to achieve industrial acceptance and the framework should be extended to support patterned materials. Future work will face these problems and will focus on optimizing the image acquisition process, as lens blur and border obscuration yet degrade acquired images which results in occasional false alarms. The concept of the yarn matrix allows to retrieve detailed information about the binding of the investigated fabric. Additionally, the concept of measuring single yarns in terms of their distances to each other allows to measure the yarn density. Both concepts were consequently adopted in Part III of this work to develop efficient algorithms for blind weave detection and adaptive density measurement in woven fabrics.

PART IV

EXTENSIONS

6 Blind weave detection

The algorithms developed in Part II of this work allow to measure single yarns for fabric defect detection. The presented core ideas are extended in this part to provide solutions for two related problems, namely the detection of weave patterns without prior knowledge about the material, and the measuring of changing weft densities during production. Both problems relate to the subject of fabric quality control although the specific field of application differs from the On-Loom system. In fact, the detection of a fabric binding is of interest for characterizing unknown material samples off-line or to control correct machine settings on a first machine start. The measurement of densities on the other hand is of great interest for controlling the fabric grammage over time or to monitor non-uniform fabrics. Accordingly, Section 6.1 now discusses an algorithmic framework for blind weave detection in woven fabrics. Within this context, a method is presented that allows to automatically determine the grid and yarn vectors introduced in Section 5.3.4. Subsequently, Section 7 introduces a methodology to precisely measure changing weft densities on-line. The results are extensively evaluated and also compared to existing methods.

6.1 Introduction

The topic of fabric defect detection has been extensively discussed in Part I and Part II of this work. However, in case of some quality control applications, details about the four fabric composition parameters are required. The four main characteristics of woven fabric are determined by

1. its yarn material and composition,

2. the yarn density, and
3. the fabric weave.

Highly topical papers discuss the problem of vision based yarn quality control [134–138] and several companies such as *Uster Technologies AG* (Swizerland) and *Textechno GmbH & Co. KG* (Germany) (to name only two) provide sensors and machines to test properties and the condition of single yarns before they are fed as raw material into the weaving process. This section focuses on the problem of automatic visual weave detection for woven fabrics. The weave defines the pattern according to which warps and wefts are interlaced among each other to form a cloth. Details on the characteristics of the basic fabric weaves were given in Section 2.3. The automated detection of weave pattern is helpful for machine operators who want to check if their settings are correct or for identifying and characterizing unknown fabric samples. To this date, no commercial system is available that is able to analyze fabric weaves and only few publications treat the topic.

Within this scope, the weave detection framework of Kang et al. [139] acquires a reflecting and a transmitting light image. Morphological operators and basic image processing techniques are applied to these images to derive yarn trajectories and the underlying weave. A very similar approach is presented in [140] where images are processed by morphological image operators to locate float-points. The information is combined with pixel intensity analysis to differentiate between weft- and warp-floats which finally allows to derive the weave pattern. Huang et al. [141] propose a method based on gray value scan-line integrals along image rows and columns. Local minima and maxima in the scan plots are located and the information is fed into a decision tree classifier to conclude for weft/warp floats and the weave pattern. Several other authors adopt the principle of integral scans [140, 142, 143] but replace the decision tree by fuzzy clustering to classify the output of texture descriptors applied to detected float-points. In [144], the authors model fabric images in frequency and space domain by a convolution and an additive model. Sophisticated frequency space analysis is applied to extract the basic weave tile. The binary weave code and detailed evaluation results are not provided though. A filtering based algorithm is introduced by Lachkar et al. [145, 146], who process the power spectrum of the fabric image to segment single warps and wefts and to derive float-points, but only plain weaves have been investigated in their work. In [147], Wavelet sub-band decomposition is used to extract texture features of different weave patterns. A classifier is trained off-line with those features and is used on-line to assign a weave class to an unknown fabric. A very promising and versatile approach is discussed in [148]. Here, Fourier spectra of known weaves are normalized and learned from an off-line fabric database. The spectrum of an unknown fabric image is analogously normalized and matched to all

off-line template spectra using a distance metric. The reference fabric with the most resembling spectrum determines the unknown weave.

Direct implementations of the proposed methods showed that the discussed approaches suffer from either tight weft/warp alignment restrictions or are vulnerable to natural yarn irregularities. Other algorithms are not afflicted by these limitations but require considerable a priori knowledge of potential fabric weaves in order to perform well. Those are not blind (fully automatic) and require an off-line learning phase. To overcome the above mentioned shortcomings, this section presents a robust algorithmic framework for blind, i.e. fully automatic, weave detection in woven fabrics. The core idea of the method is based on the yarn matrix concept introduced in Section 5.3. In fact, a readily build yarn matrix allows to directly read the weave pattern from it. The major problem here is, that the On-Loom system requires a priori knowledge of the material, i.e. the expected densities for warps and wefts (yarn vectors), expected local proximities and orientations (grid vectors), and texture information (template). All three parameters must be calibrated by a human operator in order for the system to work. This section discusses an algorithmic framework to automatically retrieve these parameters so that the fabric weave can be found without prior knowledge.

6.2 Methodology

The reader is first given an overview of the rather complex algorithmic framework for blind weave detection. Figure 6.1 illustrates the process chain.

1. The process starts with a spectral analysis of the input fabric image. The purpose here is twofold as the alignment/rotation of the image is corrected and a list of prominent frequency pairs is extracted that might correspond to the period (spacing) between adjacent wefts and warps in the image. These frequencies directly correspond to the yarn vectors.
2. The next processing block corresponds to the feature extraction module discussed in Section 5.3.3. Here, a random template is extracted for the correlation step.
3. Subsequently, feature points are accumulated with respect to their relative proximities and are subject to clustering. From the cluster centers, the grid vectors can be derived.
4. According to Section 5.3.4, the grid and yarn matrices are computed. Single

yarns are tracked.

5. The trajectories of single wefts and warps are subsequently approximated by polynomials, allowing to calculate the angles between wefts and warps in a straight-forward way. If the results do not meet a weft/warp orthogonality criterion, the current weft/warp spacing pair as well as the corresponding yarn matrix are considered as incorrect and become subject to rejection. A new iteration with a different yarn vector pair is initiated and restarts at 2).
6. When all weft/warp spacing pairs have been analyzed, the best result is selected and the weave pattern is extracted from the winning yarn matrix. Knowing the spatial resolution of the image acquisition system, weft and warp densities can directly be derived from the final weft/warp spacings.

It should be noted that the proposed framework works iteratively to find an optimal result. All discussions for subsequent algorithmic blocks refer to one iteration.

6.2.1 Rotation detection and correction

In an off-line scenario where the aim is to characterize an unknown fabric sample, the fabric image can be acquired with an arbitrary rotation and alignment. Correspondingly, its orientation should be detected first and subsequently corrected if necessary, so that wefts and warps run parallel to the borders of the image. This adaptation will facilitate later processing steps as the yarn tracking core algorithm discussed in Section 5.3.4 is employed. It assumes that yarns run parallel to the image borders.

A typical characteristic of fabric images is a spectrum with very prominent spectral peaks that are structured in a grid around the direct component (DC) of the spectrum. Here, a line (i.e. orientation) with significantly higher spectral energy can generally be distinguished. Figure 6.2a-c illustrates the correspondence between fabric image orientation and the orientation of the dominant spectral direction. In this work, the detected line is always associated with the alignment of wefts. This assumption does not hold when warps are more prominent in the image than wefts. An automatic distinction, however, is not feasible without meta information of the fabric. If the orientation assignment is wrong, the detection results for weft and warp densities will be swapped (but correct) and the detected weave pattern will be rotated by 90°.

Let $\mathbf{I}$ denote the discrete fabric image and $\tilde{\mathbf{I}}$ its *Fourier* transformation represented as a logarithmized magnitude spectrum with the DC located at the image center $\mathbf{O}$.

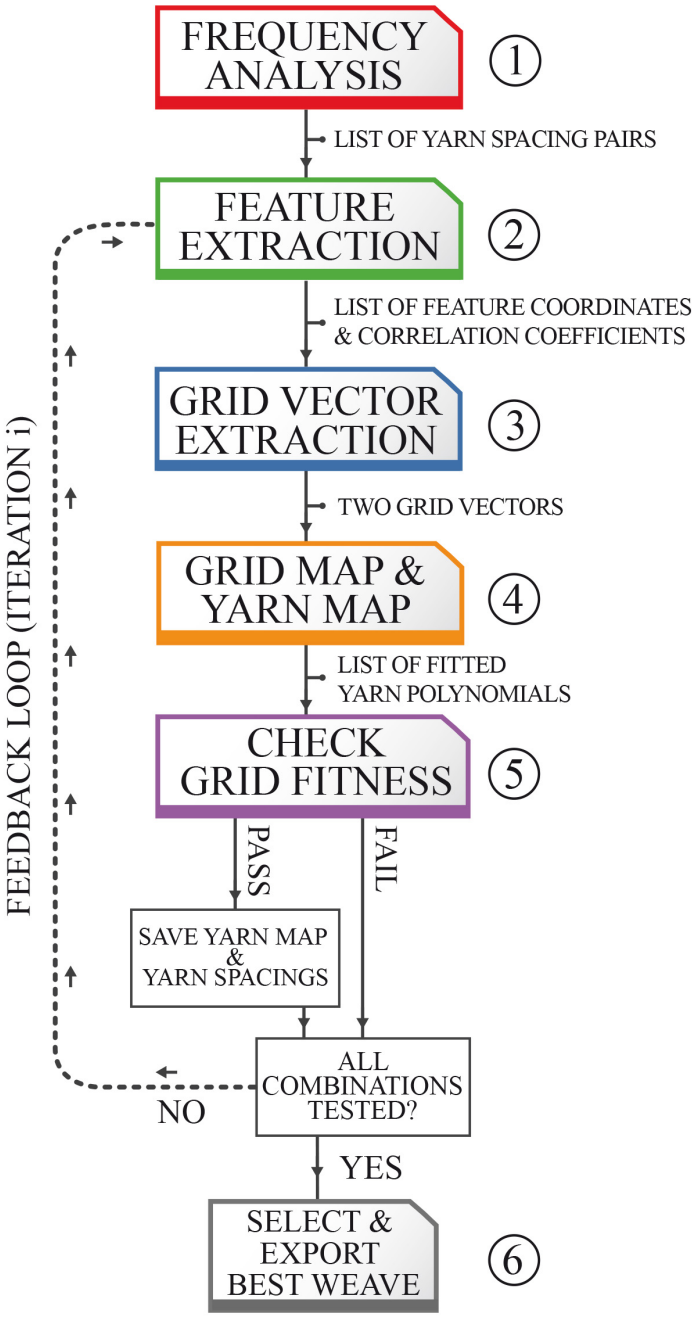

Figure 6.1: Block diagram of the proposed framework for blind weave detection in woven fabrics. Numbers on the process blocks refer to enumerations in Section 6.2.

Let **C** denote the set of all border pixels on the right half of the spectrum along the north, east and south borders of the image. A line is spanned from **O** to each of the **C** pixels and the intensity values at discrete positions along each line are extracted. Bilinear interpolation is used to approximate intensity values at non-integer positions. For each line, the mean of its intensity values is calculated. If H and W are the height

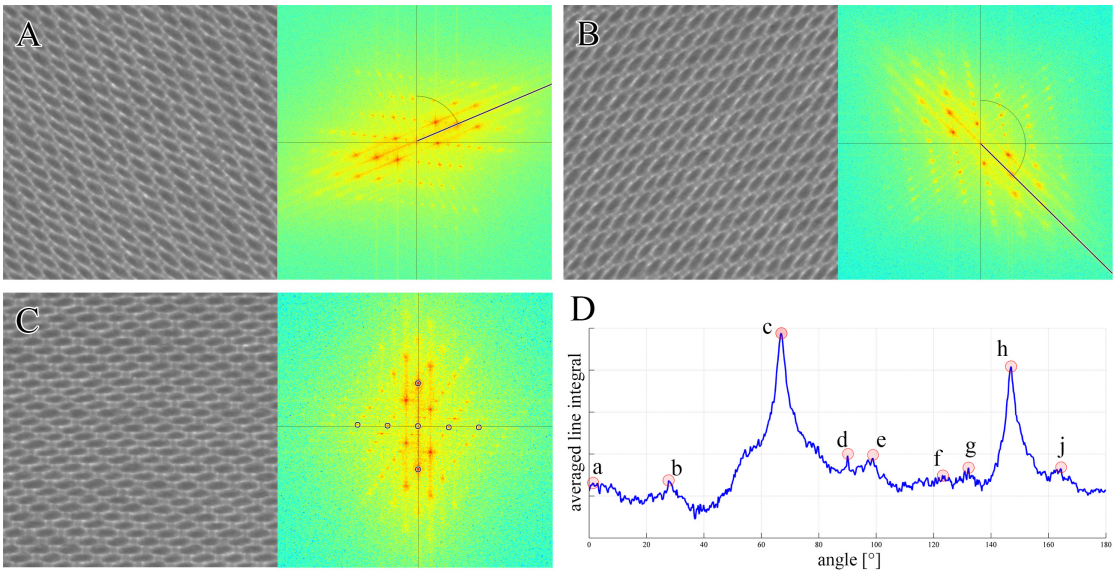

Figure 6.2: Rotated fabric images and corresponding *Fourier* spectra. A) Fabric images are rotated by 60° and B) by 140°. Black lines mark detected orientations of highest spectral energy. The angle between the line and the y-axis of the spectrum corresponds to the fabric's rotation. C) Illustration of the same with corrected rotation. Detected peaks close the x- and y-axis are marked by circles. D) Averaged radial line integrals of A) plotted against the angle between integral lines and the y-axis of the same fabric spectrum. Detected local maxima are highlighted with circles. A peak is only selected when a corresponding peak at ±90° exists, e.g. peak *c* can be matched to peak *h* in the above example.

and width of $\tilde{\mathbf{I}}$, a total amount of $H \cdot W$ mean values will be calculated. Figure 6.2d plots averaged line integrals against the angle between each line and the y-axis for a fabric image that has been rotated by 60°. Detected local maxima are highlighted with red marks. Since wefts and warps should run orthogonally to each other, for each local maximum a corresponding local maximum at an angle of approximately ±90° should be found. From all peaks that meet this requirement, the peak with the highest value is selected and its corresponding angle determines the weft rotation. The image is rotated accordingly using bilinear interpolation and is subsequently cropped to remove border artifacts caused by the rotation process. Figures 6.2a-c illustrate the effect of rotation correction for a fabric image and its corresponding magnitude spectrum.

6.2.2 Yarn density estimation

The correctly rotated fabric image $\mathbf{I}_R$ is transformed into a logarithmized magnitude spectrum $\tilde{\mathbf{I}}_R$ once again. Within the spectrum, prominent image frequencies appear as strong and clearly distinguishable peaks. To locate frequency peaks efficiently, $\tilde{\mathbf{I}}_R$ becomes subject to the same peak detection as described in Section 5.3.3 by Equation (5.17). Within the resulting image $\tilde{\mathbf{I}}_{R,P}$, all pixels unequal to zero mark positions of detected peaks. Peak coordinates and corresponding spectral intensities are saved in a peak list $\mathbf{P}$. The final matrix $\mathbf{P}$ has N rows and 3 columns. Each row corresponds to a peak, defined by its x- and y- coordinates stored in columns 1 and 2 and the spectral intensity of the peak stored in column 3.

Due to the rotation correction applied earlier, spectral peaks corresponding to weft and warp spacings are expected to reside close to the y- (weft spacing) and x-axis (warp spacing). A peak is rejected when the length of the normalized projection of its x- and y-components onto the main axes is higher than a given threshold λ:

$$\frac{min(\mathbf{P}(i,1),\mathbf{P}(i,2))}{|\mathbf{P}(i,1{:}2)|} > \lambda. \tag{6.1}$$

The term $|\mathbf{P}(i,1{:}2)|$ denotes the l^2-norm of a peak stored in the ith row of matrix $\mathbf{P}$. Figure 6.2c illustrates a fabric image spectrum with all detected peaks. The yarn spacing corresponding to each peak location is calculated by dividing the fabric image width and height by the x- and y-component of the peak, respectively. The resulting values are potential measurements for the approximate distance between adjacent wefts and warps within the fabric image and hence relate directly to potential yarn vectors. It is unclear which measurement really corresponds to the inter-weft/warp distances in the image, since frequencies corresponding to arbitrary patterns in the fabric image may cause spurious spectral peaks with higher intensities than real yarn spacing frequencies. For this reason, all peaks need to be considered and Section 6.2.5 introduces an assessment criterion to rate the goodness of fit of calculated spacing measurements. To this end, all possible yarn vectors are stored in a spacing matrix $\mathbf{S}$. All subsequent process blocks are executed iteratively, whereas a different yarn vector pair from $\mathbf{S}$ is used as input parameter in each iteration. Figure 6.1 illustrates the iterative concept of the algorithmic framework.

6.2.3 Blind feature point extraction

Given the rotation corrected fabric image and a set of potential yarn vector pairs, periodic features are now extracted from the corrected fabric image. The method here follows directly the procedure described in Section 5.3.3. The image is first normalized using CLAHE and subsequently feature points are extracted using the ZNCC metric and a given template. Since no float-point template is given, an arbitrary template $\mathbf{T}$ is created by cropping a sub-image of $a \cdot \mathbf{d}_{weft,i}$ by $b \cdot \mathbf{d}_{warp,i}$ pixels right from the center of the fabric image $\mathbf{I}_R$. Factors a and b are empirically set to $a = b = 2$. This method obviously doesn't allow to locate float-point features, but only to detect repetitive parts within the fabric. However, this knowledge is sufficient to determine a grid matrix and later yarn matrix, from which a fabric weave can be extracted. Once a correlation image is computed, peak detection according to Equation (5.17) is applied once again. Given the yarn vector pair $\{\mathbf{d}_{weft,i}, \mathbf{d}_{warp_i}\}$ at iteration i, the size of the dilating structure element is determined to have a radius d of

$$d = \lfloor max(\mathbf{d}_{weft,i}, \mathbf{d}_{warp,i}) \cdot \delta \rfloor, \tag{6.2}$$

where δ is an important fine tuning parameter. Each feature consists of a x- and y-coordinate and its correlation coefficient. Weak features, i.e. maxima with correlation coefficients below a given threshold γ, are rejected. The coordinates of all found periodicity features are stored in a feature matrix $\mathbf{L}$ for further processing.

6.2.4 Grid vector pair estimation

In the On-Loom system, the grid vector pair $\{\mathbf{g}_a, \mathbf{g}_b\}$ had to be configured manually. It is here discussed how these vectors can be retrieved automatically by analyzing the local feature point proximities in the feature matrix $\mathbf{L}$. Accordingly, for each feature point in $\mathbf{L}$, its nearest adjacent features within a given distance are found and their relative coordinates are accumulated in a neighborhood map. By clustering and filtering the map, information of grid vectors can be derived in a straight-forward way.

To begin with, the radius r defines a search area for adjacent features according to

$$r = \sqrt{\frac{A}{N \cdot \pi}} \cdot \beta, \tag{6.3}$$

where β is again a fine-tuning parameter to control the extension of the search area, A is the total number of pixels in $\mathbf{I}_R$ and N is the number of detected feature points. A *k-d search tree* [149] is build from the feature matrix $\mathbf{L}$ to accelerate subsequent nearest neighbor searches. For each feature point $\mathbf{f}$ in $\mathbf{L}$, the following steps are repeated:

1. Adjacent feature points to $\mathbf{f}$ within the distance r are found.
2. Their coordinates are normalized by subtraction of the coordinates of $\mathbf{f}$.
3. The normalized 2D coordinates of all found neighbors are stored a cluster matrix $\mathbf{C}$
4. The number of found neighbors is accumulated in a histogram $\mathbf{h}$.

Figure 6.3 plots a cluster matrix $\mathbf{C}$ and its corresponding histogram $\mathbf{h}$ for a given fabric sample. The strongest bin in the histogram allows to conclude for the amount of clusters in $\mathbf{C}$ which is a required parameter for most clustering algorithms. Fuzzy C-Mean clustering [150] is hence applied to partition points in $\mathbf{C}$ into distinct sets and locate their corresponding centers. For each found cluster, the mean distance μ from each point to its cluster center and the corresponding standard deviation σ are calculated. Clusters are consolidated by removing outliers for which the Euclidean distance to a cluster center exceeds the range $\mu + \sigma$. The clustering is repeated one more time.

Given a total amount of c detected cluster centers, the coordinates of each center define a unique lattice vector, giving a total of $\binom{c}{2}$ grid vector tuples $\{\mathbf{g}_i, \mathbf{g}_j, \forall\, i, j \in [1..c]\}$ that can be formed by combining two vectors. For each tuple, the cost function

$$\delta(\mathbf{g}_i, \mathbf{g}_j) := \frac{1}{N} \sum_{k=1}^{N} \sqrt{\mathbf{d}_{k1}^2 + \mathbf{d}_{k2}^2} \tag{6.4}$$

$$\mathbf{d} = |\,\mathbf{w} - \lfloor \mathbf{w} \rceil\,|^T \tag{6.5}$$

$$\mathbf{w} = \left[\mathbf{g}_i, \mathbf{g}_j\right]^{-1} \cdot \mathbf{L}^T \tag{6.6}$$

is evaluated. The term $\mathbf{L}$ denotes the $N \times 2$ feature matrix, the function $\lfloor \cdot \rceil$ rounds floating point values to the nearest integer value, the operators + and − apply point-wise plus and minus operations, and the operator $(\cdot)$ here symbolizes a matrix multiplication. The function first transforms the feature point coordinates into the vector basis

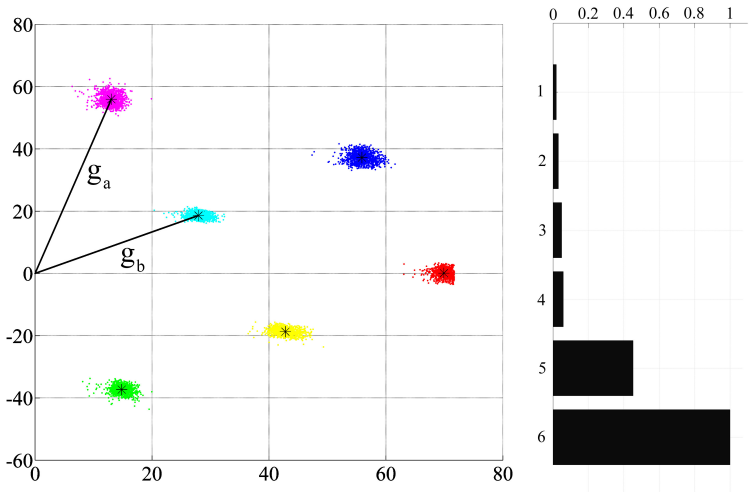

Figure 6.3: Cluster map (left) and neighbor count histogram (right, normalized to its maximum) for a given fabric sample. The amount of expected clusters (6) can be read from the histogram. Distinct clusters have been colored individually and corresponding centers are marked by black stars. The determined grid vector pair $\{\mathbf{g}_a, \mathbf{g}_b\}$ is plotted additionally.

spanned by the two grid vectors, Eq. (6.6). It then computes the absolute distance between each feature point and its nearest point on the grid that is defined by $\mathbf{g}_i$ and $\mathbf{g}_j$. The grid vector pair with the lowest average distance with respect to Equation (6.4) is then selected as a grid vector pair for subsequent processing blocks. Figure 6.3 illustrates the resulting grid vector pair for a given fabric sample.

6.2.5 Feedback loop for candidate selection

At this point at the current iteration i, a yarn vector pair $\{\mathbf{d}_{weft,i}, \mathbf{d}_{warp,i}\}$, a grid vector pair $\{\mathbf{g}_{a,i}, \mathbf{g}_{b,i}\}$ and a list $\mathbf{L}_i$ with feature points are available. The grid and yarn matrix $\mathbf{Y}_i$ are built according to the algorithmic pipeline discussed in Section 5.3.4. As mentioned in Section 6.2.2, the detected yarn vector pairs are ambiguous and must be assessed in order to select the pair that suits the real density of the fabric image. The measurement of orthogonality between wefts and warps is used here as exclusion criterion for non-valid vector pairs. The remaining valid pairs are subsequently ranked according to an assessment criterion and the best pair is chosen accordingly. It is then shown that the yarn matrix corresponding to the finally determined yarn vector pair provides direct information about the weave pattern of the fabric image.

Wefts and warps within fabric images should run orthogonally to each other. When the trajectories of wefts and warps contained in the yarn matrix do not meet this orthogonality criterion, the yarn vector pair that has been used to construct the transformation matrix $\mathbf{T}_i$, Equation (5.23), cannot correspond to the image.

To measure the orthogonality of wefts and warps, the unique structure of the yarn matrix is analyzed. For the current iteration i, single yarns of the fabric are represented by periodicity features structured in rows and columns in the yarn matrix $\mathbf{Y}_i$. A line is fitted to the feature xy-coordinates of each row and column in $\mathbf{Y}_i$ in order to model the trajectory of single wefts/warps. Figure 6.4 plots fitted yarn polynomials onto corresponding input images. Given N fitted weft polynomials $p_n(x)$ and M fitted warp polynomials $p_m(x)$, an orthogonality assessment criterion Ω_i is calculated according to

$$\begin{aligned} &p_m(x) = \alpha_m x + c_1, \;\; p_n(x) = \beta_n x + c_2, \\ &\Omega_i = \frac{1}{NM} \sum_{n=1}^{N} \sum_{m=1}^{M} \frac{\pi}{2} - \arctan\left(\left| \frac{\alpha_m - \beta_n}{1 + \alpha_m \beta_n} \right| \right). \end{aligned} \tag{6.7}$$

Equation 6.7 basically calculates the average angle between approximated weft and warp trajectories in the image. If the value Ω_i exceeds a given threshold κ, the current yarn spacing pair $\{d_{weft,i}, d_{warp,i}\}$ and its corresponding yarn matrix $\mathbf{Y}_i$ are considered as non-fitting and are discarded. From all pairs that pass the orthogonality test, the best pair is selected by evaluating

$$\underset{i}{\operatorname{argmax}} \{ g(d_{weft,i}) \cdot g(d_{warp,i}) \}, \tag{6.8}$$

where the function $g(x)$ returns the *Fourier* coefficients of the spectral peak corresponding to the frequency x. Therefore, the final yarn spacing pair is selected according to the maximum product of spectral intensities.

6.2.6 Weave detection

The yarn matrix $\mathbf{Y}_i$ corresponding to the selected yarn vector pair $\{d_{weft,i}, d_{warp,i}\}$ is further analyzed to extract the weave pattern of the fabric image. In Figure 5.14 it can be seen that the final yarn matrix clearly displays the underlying fabric weave pattern. To extract the weave, the yarn matrix is first binarized to transform all non-zero entries to ones. For each non-zero entry in the binarized matrix, a sub-matrix is extracted

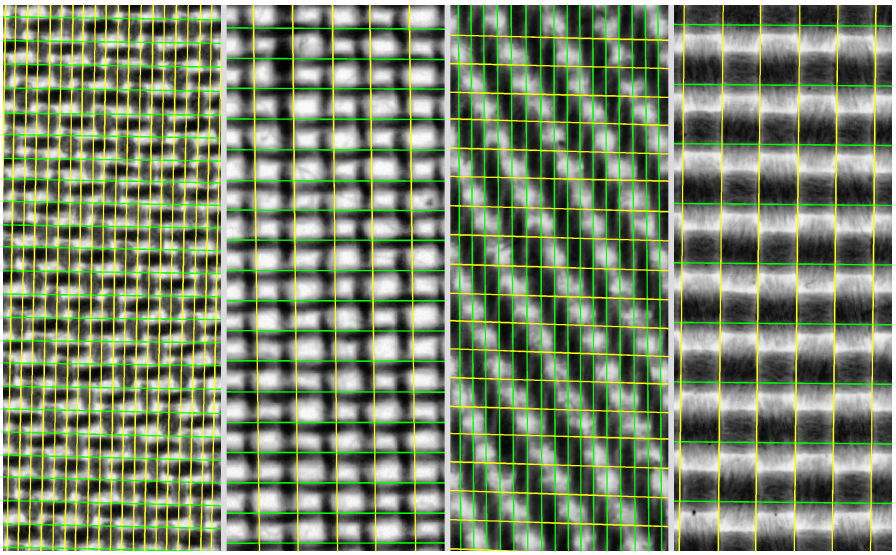

Figure 6.4: Approximated weft and warp trajectories for various fabric samples. The orthogonality between wefts and warps is good indicator for the fitness of calculated grid and yarn vectors.

so that each column and row in the matrix contains only one non-zero element. The extracted sub-matrix is point-wise added to an accumulator matrix $\mathbf{A}$. Once a sub-matrix has been extracted and accumulated for each non-zero entry in $\mathbf{Y}_i$, the final accumulator matrix is normalized to the total amount of extracted sub-matrices. A threshold ρ is applied to the accumulator to map all entries below ρ to zero. Rows and columns in $\mathbf{A}$ without entries are removed. The final accumulator matrix contains only rows and columns with a single entry and directly corresponds to the weave pattern of the fabric image. The proposed procedure for weave extraction successfully overcomes the problem of missing or redundant entries in the yarn matrix.

6.3 Evaluation

The presented algorithmic framework for blind weave and yarn density detection was evaluated on database FIDB-H (see Section 3). The entire evaluation image set is provided on the project website [13].

A cross-validating scheme would be the standard approach to assess the universality of the proposed method and to evaluate the fitness of the selected parameter set for unknown samples. However, since the current implementation of the framework is

far to time consuming to perform e.g. a 10-fold cross-validation on the given dataset, two additional experiments were conducted to assess the influence of the parameter fine tuning. In a first test, each of the seven free parameters was altered in a range of ±25 % in steps of 5 % around its default value as shown in Table 6.1, while all other parameters were kept unchanged (parameter ρ has been altered in a limited interval of -25 % to +5 %). The dataset was evaluated with each of the 77 generated parameter vectors to see which influence individual parameters have on the system's performance. The results are shown in Figure 6.5.

For the second experiment, random sampling was used by generating a set of all possible parameter combinations (same parameter ranges as for experiment 1), from which 300 random samples where selected according to a uniform distribution. The entire database has been evaluated with each of the 300 parameter vectors. The results of Experiment 2 are shown in the last column of Table 6.2.

6.4 Results

In a first experiment, suitable values for all free parameters were selected empirically as each step in the process chain was carefully analyzed and suitable settings were derived. Selected parameters were subsequently fixed and kept unchanged during the evaluation to ensure the fabric analysis to be blind and conducted without any prior knowledge. Table 6.1 lists the manually selected parameters which were introduced in previous sections. Table 6.2 lists the condensed analysis results for test images within the database. All ground truth values for yarn densities have been determined manually and are assumed to have a measurement error of up to $\pm 1\ yarn/cm$. A more detailed results table is provided in Appendix E, where also exact measurement errors for each sample are listed.

With reference to the evaluation results presented in Table 6.2, the averaged absolute measurement errors for weft and warp densities differ by a minimum of 0.11 yarns/cm and a maximum of 0.82 yarns/cm from the ground truth data. All values are below the assumed ground truth measurement error of ±1 yarn/cm. The overall accuracy for weave detection in this experiment is 97 %, i.e. 136 of 140 fabric images in the dataset were correctly classified, 3 of the misclassified images belong to sample K.

Table 6.1: Fixed settings for all crucial parameters used during the evaluation of the proposed algorithmic framework for blind weave detection.

Parameter	Discussed in	Type	Value
λ	Section 6.2.2	threshold	0.13
γ	Section 5.3.3	threshold	0.50
δ	Section 5.3.3	tuner	0.80
β	Section 6.2.4	tuner	2.80
ζ	Section 6.2.4	tuner	0.40
κ	Section 6.2.5	threshold	0.13
ρ	Section 6.2.6	threshold	0.90

6.5 Discussion

The achieved precision for density measurements are comparable to results reported in [133, 143, 151, 152]. Furthermore, the evaluation results proved that the proposed method for blind weave detection is reliable and robust for the selected parameter settings. Twill and satin weaves are much harder to detect and impose a proper selection of the parameters. For plain weaves, the parameter selection is far less significant. The evaluation showed that the parameter δ is the major bottleneck of the system. It is directly linked the to the feature extraction part of the framework, which lies within the focus of future work as discussed in Section 6.5.2. Given a reasonable parameter set, only little improvements can be achieved on the discussed dataset since weave classification is already 97 % accurate. A limitation can be seen in the experiments conducted on images of sample K, where the averaged ground truth deviation for wefts raises to 28.6 yarns/cm. This inaccurate result is caused by the high weft density of 62 yarns/cm for images of sample K. Single wefts in class K are resolved by only 7 pixels per yarn which causes the measurement system to struggle. A higher spatial resolution (by shortening the distance between camera lens and fabric sample for example) of the image acquisition system would overcome this problem. Although the analysis was conducted completely blind, the results outperform prior knowledge based methods as discussed in [148]. Wang et al. [143] report perfect weave classification results in their work. It must be emphasized that the offered real-world dataset is far more comprehensive and challenging than datasets used by other authors. For example, several proposed algorithms for weave detection are

Table 6.2: Evaluation results for the blind weave detection framework. For each of the 14 fabric samples A-N, 10 rotated images have been evaluated – in total 140 images. The block *Ground Truth* lists manually measured reference values for weft/warp densities and the correct weave pattern. Densities are given in $yarns/cm$. The *Error Rates* block summarizes the evaluation results. Mean and standard deviation of the differences between measurements and ground truth values are listed for each fabric class. The column *Weave Classification* lists the total amount of wrong classifications for each fabric sample. The column *Random Sampling* lists the correct classification rates in percent of the random sampling experiment (Section 6.5.1) that was conducted to assess the parameter sensitivity.

		SAMPLE													
		A	B	C	D	E	F	G	H	I	J	K	L	M	N
Ground Truth	Weft Density	20	20	26	2	21	20	45	24	15	7	30	41	35	2
	Warp Density	13	16	13	328	16	40	21	24	14	12	62	35	20	2
	Weave	P1	P1	P1	S41	T31	S41	T31	P1	P1	P1	T31	T31	T21	P1
Error Rates	$\frac{\mu}{\sigma}$ Weft Density	$\frac{0.17}{0.04}$	$\frac{0.25}{0.11}$	$\frac{0.62}{0.16}$	$\frac{0.66}{0.22}$	$\frac{0.47}{0.13}$	$\frac{0.21}{0.10}$	$\frac{0.18}{0.11}$	$\frac{0.16}{0.17}$	$\frac{0.61}{0.10}$	$\frac{0.66}{0.08}$	$\frac{7.33}{3.35}$	$\frac{0.12}{0.12}$	$\frac{0.19}{0.08}$	$\frac{0.82}{0.64}$
	$\frac{\mu}{\sigma}$ Warp Density	$\frac{0.26}{0.13}$	$\frac{0.23}{0.14}$	$\frac{0.18}{0.10}$	$\frac{0.47}{0.22}$	$\frac{0.51}{0.26}$	$\frac{0.23}{0.16}$	$\frac{0.31}{0.16}$	$\frac{0.32}{0.18}$	$\frac{0.11}{0.12}$	$\frac{0.11}{0.07}$	$\frac{28.6}{19.2}$	$\frac{0.56}{0.13}$	$\frac{0.36}{0.27}$	$\frac{0.28}{0.10}$
	Weave Class.	0	0	0	0	0	0	1	0	0	0	3	0	0	0
	Rand. Sampling	100	100	100	100	63	81	71	100	100	100	55	71	100	100

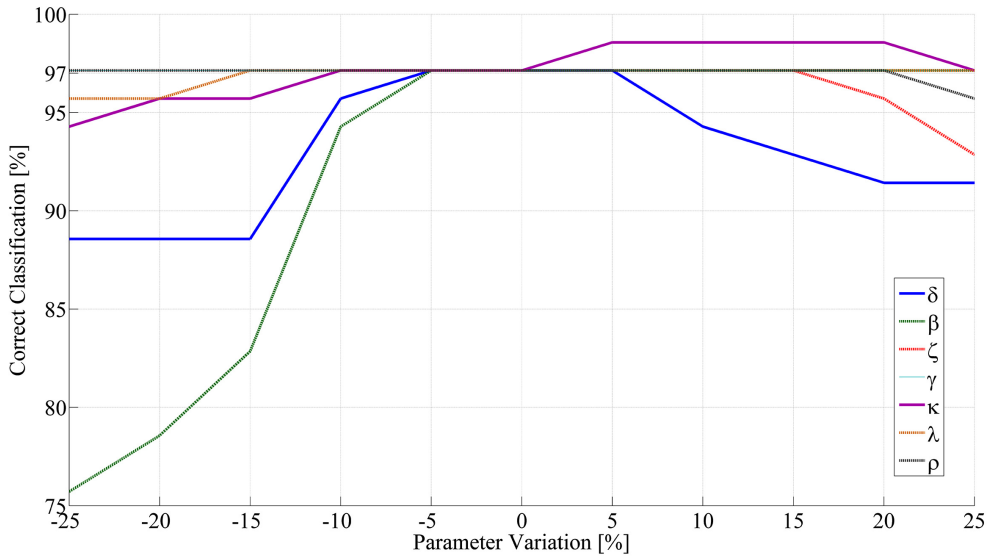

Figure 6.5: Evaluation results of the individual parameter variation experiment. Each of the 7 parameters has been varied within a range of ±25% around its standard value (see Table 6.1) while all other parameters were kept unchanged. The database has been evaluated with all 77 parameter combinations. The graph plots the correct classifications rates for each parameter against its relative change to the standard value.

based on gray value scan-line profiles of fabric images [139–143]. These approaches do, however, not work on the majority of real-world fabric images included in our database. Complex weave structures, natural yarn shape irregularities and misaligned images will detain scan-line profile based methods to work reliably. Similarly, methods based on pure spectral filtering (as proposed in [146]) to locate float-points will fail on many database samples, too. As mentioned earlier in Section 6.2.2, the choice of correct values for warp and weft spacings can not only be based on spectral peak intensities. Random patterns in the fabric may be more dominant than the frequencies of interest. An example for this behavior can be seen in all images of sample F, where dominant and sought frequencies differ significantly.

6.5.1 Parameter sensitivity

From Figure 6.5 it can bee seen that all thresholds $\kappa, \lambda, \gamma, \rho$ and the tuner ζ have very little influence on the system performance within the given range of variation. In fact, a less strict selection of the parameter κ results in an even better result, as the

correct classification rate raises to 98.5 %. On the other hand, the system performance is sensitive to larger changes of the tuners δ and β. While larger values for β do not seem to affect the overall result in a negative way, smaller values cause the correct classification rate to drop down to as low as 75 %. The parameter δ has a variation window of ± 10 % for which the weave detection result doesn't vary much. Smaller and larger values, however, cause the system performance to drop to 88 %. Because of its small tolerance window, the tuner δ is considered as the main limiting factor for the system's generalizability.

As shown in Table 6.2, the total correct classification rate for the random sampling experiment exceeded 88 %. It can be stated that the detection accuracy of plain weaves is very little affected by any variation of the parameters, as it is close to 100 % for each of the plain weave samples in the database. For twill and satin weaves, however, a poor parameter selection affects the classification result in a negative way as the detection rate drops down to 63 % (sample E, 55 % for sample K, respectively).

6.5.2 Limitations

Most of the limitations mentioned in the discussion Section 5.7 of Part II of this work apply for the blind weave detector, too. Good illumination of the fabric is a key factor. For most samples, back-light proved to be the best method to achieve robust weave detection results. Very dark, thick or highly dense materials, however, require top-light (e.g. sample M) or a mix of top- and back-light (e.g. samples and K and N), respectively. The illumination method should be chosen such that float-points within the fabric image have good contrast and visibility.

The 23 mm prime lens used in the image acquisition system limits the working distance between sample and camera to approximately 10 cm. A different lens would allow reducing that distance and hence raise the spatial resolution. Fabrics with densities of +60 yarns/cm could then be robustly measured.

Again, (see Section 5.7 for comparison) the major bottleneck of the current system design is the extraction of periodicity features using normalized cross-correlation. The arbitrary selection of the template may cause the detection of misleading feature points for some uncommon fabric patterns. Even more important, the template matching limits the framework to non-patterned materials. Wefts and warps must be of uniform color each, otherwise the correlation will fail to robustly detect the

correct location of repetitive features. Yu et al. [148] propose to overcome this problem by considering edges only when analyzing patterned fabrics. Edge filtered images derived from our database have edges that are far too noisy and inadequate for robust pattern analysis. It is likely that the best way to handle the problem of patterned fabric analysis is by altering the imaging method. Color might have no visible effect in fabric images acquired with near infra-red, infra-red or ultra-violet light. The confirmation of this hypothesis could be subject to future work. Another strategy to handle patterned fabrics would be based on models of weft/warp floats in terms of probability density functions of gray value intensities. More advanced techniques could model distributions based on the output of texture descriptors or combinations of different descriptors. Several authors proposed similar strategies [139, 141, 143] which have been tested successfully. However, further research and considerable modifications would be required to guarantee stable and robust float-point detection results when applying these techniques to real-world fabric images.

7 Adaptive density measurement

Among the three main composition parameters of woven fabrics (yarn material properties, weave, density), only the measurement of weaves has been addressed in this work so far. Other groups have been working on methods to characterize yarn material properties such as yarn texture [153], roughness [132], surface resistance [154], and hairiness [135]. The yarn density of a woven material is the third important quality characteristic and is defined by the number of wefts per unit length. Common fabric densities for industrial products are commonly in a range of 7-100 wefts/cm. Its exact measurement is of importance for quality assurance and control tasks, as for example the automatic control of the material grammage. The material grammage and fabric density have a linear relation so that one can be derived from the other. This final section addresses the problem of measuring the yarn density of fabrics that are produced with changing loom weft insertion rates, i.e. when the fabric density is varying over time.

7.1 Introduction

Several authors published possible methodologies to quantify yarn densities using digital fabric images. Lin [133] proposes to use co-occurrence statistics as introduced by Haralick [155] to calculate the period of repetitive fabric patterns and derive the weft density from it. Good results are reported for plain weaves whereas the algorithm tumbles when applied to satin and twill weaves. Jeong et al. [152] employ a method based on gray-value scan-line intensity profiles along single rows and columns of a fabric image. The period of the resulting sinusoidal curves allows to derive the fabric density. The proposed method is straight-forward and computational inexpensive.

A similar concept is proposed by Pan et al. [151] which combines scan-line profiles with the Hough-Transformation and image binarization to measure yarn densities. The presented results seem to be robust and precise, but the computational time of the proposed framework is expected to exceed real-time limitations. A combination of scan-line profiles for float-point detection and co-occurrence statistics for float-point classification is also proposed by Wang et al. [132, 143]. The authors report excellent results for fabric weave detection and density measurement as evaluated on a database of 8 woven fabric images with twill and plain weaves. Our experiments, however, clearly showed that VBM methods based on scan-line profiles are not applicable to measure the yarn density of many real-world fabric types since very tight yarn alignment and regularity restrictions apply in order for these methods to succeed. Natural fabric images, especially satin and twill fabrics, do not meet these requirements. Corresponding sample fabrics can be found in the database published in [10]. Techniques for fabric density measurement based on the analysis of the fabric's *Fourier* spectrum are discussed by Xu et al. [156], Tunák et al. [157], Ravandi et al. [158] and Sari-Sarraf [159]. The authors design straight-forward band-pass filters in the frequency domain and apply these to the signal to extenuate frequencies that do not relate the repetitive pattern of wefts and warps. After filtering and inverse transformation into the spatial domain, basic image processing techniques are used to the measure the periodicity of the filtered image and hence derive the distance between adjacent yarns. Reported measurements are stable and precise for either plain, twill or satin weaves. In fact, spectral analysis can generally be considered as a good approach to achieve high precision measurements at moderate computation times. It can, however, only provide a global density measurement in contrast to a local measurements, which would allow measuring the density at different locations in the image. Moreover, the stability of these methods can not be guaranteed for twill or satin weaves as we found out in our experiments. Pan et al. [160] address the difficult problem of density measurements in colored fabric materials. Within this scope, the authors propose to use a combination of color-gradients, gray-level scan-line profiles and band-pass filtering to measure the density of yarns in double-system colored fabrics. In addition, they recently proposed a method to measure the density of single-system colored materials [161] by color clustering different blocks of the fabric image and then applying the gray-value scan-line method to each block individually. Finally, Techniková et al. [162] conducted a competitive benchmark comprising the majority of the aforementioned methods which revealed, that all proposed algorithms work well for plain weaves and selected fabric classes, but there is no method yet that works reliably on a wider range of fabric types.

To overcome the aforementioned problems, this section re-uses the key algorithms proposed in Section 5.3 for tracking singles yarns and introduces extensions that allow

the system to automatically adapt to continuously changing yarn densities in fabrics during manufacturing. The main advantages of the proposed method are

1. applicability to a variety of woven fabric types,
2. its real-time capability,
3. robust measurement of local densities,
4. a space-saving design, and
5. easy integration into the existing On-Loom defect detection framework.

Several measurement series on a real-world industrial air-jet loom are finally conducted to evaluate the fitness and robustness of the proposed framework. To our best knowledge, this is the first on-line measurement experiment for yarn density quantification reported in literature. For comparative reasons, three parallel density measurements were recorded by using two alternative *Fourier*-space based algorithms and an additionally installed X-ray sensor.

7.2 Methodology

The core algorithm for tracking yarns as proposed in Section 5.3 is kept unchanged. By knowing the spatial resolution of the imaging system, measured pixel distances can be directly transformed into millimeter and by knowing the spatial dimensions of the image, the amount of yarns per centimeter can be derived. An image with a ruler lied on top of the fabric was acquired to calibrate the system and to determine the correct of spatial resolution manually. The template for feature point extraction (see Section 5.3.3) must also be selected manually, the grid and yarn vectors can, however, be determined automatically using the procedure discussed in Section 6.2.

The main problem when facing changing yarn densities are the gird and yarn vectors that do no fit to the fabric structure any more once the density changed too much. The distances between adjacent wefts raise or shrink so that the core algorithm that sorts float-features into the grid matrix does not work properly any more, as the correct grid vectors also change with the varying density. Accordingly, the calculation of the transformation matrix is wrong since the correct yarn vector that describes the inter-weft distances changed. In summary, the core yarn tracking algorithm of the On-Loom system is suitable to control if the current yarn density corresponds to a predefined value but fails once the density is allowed to change over time.

7.2.1 Adaptions to the yarn tracking algorithm

Several straight-forward changes and updates to the described procedure for tracking yarns will allow the algorithm to measure varying densities in real-time. The basic concept here is to continuously adapt the grid and yarn vectors with respect to the measurements made in preceding camera images. It is expected that the fabric's density may change only little between two subsequent images (images are acquired with a framerate of 15 fps, i.e. 66 ms between two images). As the existing algorithm has a tolerance regarding the precision of the grid and yarn vectors (see Sections 5.3.3 and 5.3.4.1), contentious small adaptations after each frame will allow to handle large changes that happen over a longer time period. Accordingly, the x- and y-coordinates of the yarn vectors are updated after each acquired fabric image according to the average weft and warp density measured in it. New update values for the x- and y-coordinates of the grid vector can be precisely estimated from the new yarn vector values. The detailed procedure is described as follows.

1. To begin with, the active measuring area within the fabric is restricted by defining a region of interest (ROI) around the central part of the image. The ROI covers about 70% of the original image area. The intention here is to avoid measurement errors at border regions of the image which may be caused by lens induced distortions and vignetting. A convenient side effect is the higher computational efficiency due to the reduced data volume.
2. Within the ROI, the distance between adjacent wefts and warps is calculated at pixel level. For each yarn trajectory, the number of pixels to the next left (warp) or lower (weft) yarn trajectory is calculated. The distances are first averaged for all pixels of a given yarn and then averaged again for all wefts and warps within the fabric's ROI. This results in two precise measurements α' (weft) and β' (warp) of the averaged spacing between adjacent wefts and warps, respectively.
3. The new values for yarn vectors are compared to existing measurements α and β which were calculated from the preceding image (or were defined off-line by the operator). For comparison, the absolute difference between existing and new measurements is calculated: $\Delta\alpha = \alpha - \alpha'$, $\Delta\beta = \beta - \beta'$.
4. When the yarn density varies from one image to another, changes in yarn vectors can be captured as described above. Changing grid vectors are, however, more difficult to determine. Fortunately, yarn vector variations and grid vector changes are linearly proportional. In this way, the alteration of grid vectors can be estimated by calculating the component-wise ratio between yarn vectors

and grid vectors

$$\lambda_1 = \frac{g_1(1)}{\alpha}, \lambda_2 = \frac{g_1(2)}{\beta}$$
$$\gamma_1 = \frac{g_2(1)}{\alpha}, \gamma_2 = \frac{g_2(2)}{\beta}.$$

The operator $(\cdot)$ denotes an element-wise access to single elements within a vector.

5. The proportional factors $\lambda_1, \lambda_2, \gamma_1$, and γ_2 are used to estimate the change of the grid vectors depending on the yarn vector change by updating according to

$$g_1(1) = g_1(1) - \lambda_1 \cdot \Delta\alpha,\ g_1(2) = g_1(2) - \lambda_2 \cdot \Delta\beta$$
$$g_2(1) = g_2(1) - \gamma_1 \cdot \Delta\alpha,\ g_2(2) = g_2(2) - \gamma_2 \cdot \Delta\beta.$$

6. The search radius from Listing 1 is updated

$$searchArea = \kappa \cdot min(|\mathbf{g}_1|, |\mathbf{g}_2|).$$

7. The current yarn vectors are updated for future processing:

$$\alpha := \alpha',\ \beta := \beta'.$$

8. The yarn matrix in Equation (5.21) is recalculated and updated.
9. The float-point template image is updated. A new template is cropped from the current fabric image at a position which is centered around the float-point which is closest to the center of the image.

For the grid vectors, only the y-components are expected to vary during the weaving process since a variation in weft densities is not expected to affect the density of warps. Hence, the x-components of the grid vectors are updated for consistency only. The above listed adjustments allow the system to reliably measure the fabric density, even if it is quickly changing over time. The fabric material is in consistent motion during production and continuously rolls down into the field of view of the camera. In case of abrupt changes, the upper and lower portion of the image generally show different densities which, however, are averaged during the measurement process. This property of the image acquisition system corresponds to a low pass characteristic, smooths abrupt changes in yarn density and hence allows the system to work in a robust and reliable way.

7.3 Evaluation

As in previous sections, the proposed framework for adaptive yarn density measurement has been evaluated again on an Omni Plus 800 loom from Picanol [95]. Image acquisition and computation hardware have been set up as described in Section 5.2. The measurement series were taken on the operating loom (without moving the camera) during the production of a polyester 3-1 twill fabric corresponding to the fabrics of the image databases FIDB-E and FIDB-F in Section 5.4.1, however, no images were recorded in this experiment. During the measurements, the fabric densities were varied in a range of 8 wefts/cm up to 36 wefts/cm in different time intervals. The overall time for each measurement varied between one and ten minutes for each measurement. In addition to the proposed method, three alternative measurement methods were evaluated in order to provide a medium for comparison and benchmarking. Within this context, an X-ray sensor was installed at the loom's take up (see Section 7.3.2) and additionally, two custom algorithms that are based on the analysis of the fabrics Fourier spectrum (see Section 7.3.1) were implemented and tested. Both analog signals, i.e. the operator machine target values and the X-ray signal, were sampled with a sampling rate of 100 Hz. Images were recorded with a frame rate of 15 frames per second. To synchronize all signals, the lower resolved density signals retrieved by the digital image processing algorithms were interpolated to match the sampling rate of the analog signals. The spatial resolution of the fabric images has been fixed to 415 pixels/cm. Two additional experiments were conducted to quantitatively assess the measurement precision of the proposed system and its applicability to different materials and weaves.

7.3.1 Fourier analysis

The analysis of the fabric's Fourier spectrum is considered to be the most robust option for density measurements as opposed to methods that deploy gray-level scanline profiles or various pattern analysis tools. Thus, two customized Fourier analysis algorithms are introduced here to evaluate their performance on the given image data set.

For both algorithms, the following steps apply. The fabric image is first transformed

into the Fourier domain using a 2D Fast-Fourier transformation. The spectrum is then shifted so that the direct component is located at the image center. Subsequently, the spectrum is logarithmized to align its power distribution. A peak detection procedure, similar to the method discussed in Section 5.3.3, is conducted. The spectral image is hereby processed by a dilating maximum filter and the result is compared to the input image pixel by pixel. Locations where the intensity values do not change are considered as local maxima (i.e. peaks). Localized peaks are further filtered by using an empirically selected threshold for their spectral intensity values.

- In the first method, the system is calibrated off-line by manually selecting the spectral peak that corresponds to the density of the first (calibration) image of the density measurement series. The *xy*-coordinates of that peak are saved in a variable and its adjacencies serve as region of interest (ROI). For every new fabric image, a spectral peak is found that is closest to the current ROI (in terms of Euclidean distance). This peak is considered as the target peak. The method follows the assumption that the density between two subsequent fabric images varies within the precision limitations discussed in Section 5.3.3. The matched peak then becomes the new ROI, which allows the system to adapt itself to varying densities. The algorithm is denoted here as *Fourier ROI tracking*.
- The second method doesn't require a calibration. Localized peaks are filtered again by discarding all points that are located too far from the central *y*-axis of the spectral image (again, an empirically selected threshold is used). Among the remaining peaks, the peak with the highest spectral intensity is found and is considered as the target peak. This method assumes that a) the repetitive pattern of wefts within the fabric image appears as the most prominent frequency along the *y*-axis in the spectral domain (next to the direct component), and b) that wefts run completely horizontal within the fabric image. The algorithm is denoted here as *Fourier maximum tracking*.

Once a target peak has been identified, the weft density for the current image can be calculated as follows:

$$d_{weft} = \frac{R \cdot \left| p_y - c_y \right|}{H}, \tag{7.1}$$

where H is the image height, p_y is the y-coordinate of the current target peak, c_y is the y-coordinate of the direct component and R is the spatial resolution of the image.

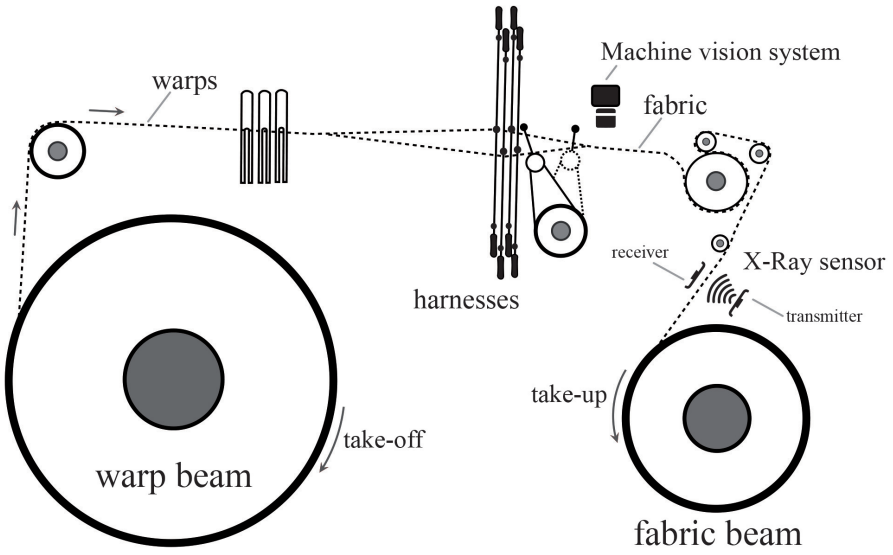

Figure 7.1: Scheme of a weaving machine, lateral view. The machine vision system is installed right behind the recoil of the fell at beat-up, whereas the X-ray sensor is installed next to the fabric beam because of its larger dimension.

7.3.2 X-ray measurement

In addition to the camera sensor, an X-ray sensor has been installed on the loom. The permeability of the fabric material for X-ray radiation varies anti-proportionally with its weft density. This characteristic is used in the measurement setup to capture the change in weft densities during production. Due to their rather large dimension, the X-ray transmitter and receiver must be installed next to the fabric beam where the finished produced fabric is taken-up, see Figure 7.1. This causes a measurement delay of up to 7 minutes (depending on the machine production speed and the density) with respect to the measurement of the machine vision system, which is installed right behind the fell at beat-up. The dynamic range of the X-ray sensor for fabric densities between 20 and 36 yarns/cm is between 3.3 and 3.6 V. In this way, the signal must be amplified and transformed according to the scaling function

$$d_{weft}(x) = \frac{a}{x} - b, \tag{7.2}$$

to provide meaningful information about the weft density. Here, the variable x represents the X-ray signal in Volt, and the scaling constants $a = 860$ and $b = 225$ were found empirically by comparison with the ground truth data. Since the X-ray signal

is very noisy, a large 1000-tap sliding average low-pass filter has been applied to the signal after recording. The number of taps for the filter has been selected according to the sampling frequency of 100 Hz.

7.3.3 Generalization capabilities

To evaluate the capability of measuring the density of fabrics with arbitrary weaves, i.e. plain, twill and satin, database FIDB-I (see Section 3) was used to test the proposed framework. One image from each fabric class in FIDB-I was used for the calibration of the parameters (grid vectors, yarn vectors and the template) and four images were kept for the evaluation. A ground truth error of maximum ± 1 yarns/cm is assumed due to the manual measurement. As the algorithmic key components did not change significantly with regards to the experiments made in Section 6.4, the results were expected to be comparable to the results in Table 6.2. Table 7.1 summarizes the achieved performance by showing the averaged weft densities for all four images of each class and the corresponding standard deviation.

7.3.4 Precision and measurement uncertainty

In order to get a quantitative statement of the measurement precision and uncertainty, additional on-loom measurements were performed using the polyester 3-1 twill fabric introduced earlier. Densities from 5 yarns/cm to 40 yarns/cm in steps of 5 yarn/cm were produced. For each density, 30 seconds of image material were recorded and analyzed without varying the density during the analysis. The density in the fabric images was controlled by picking images at random and by manually counting the number wefts per centimeter using a photo processing software. This way, the machine production precision could be validated. Again, a ground truth error of ± 1 yarns/cm is assumed. The results are presented in Table 7.2.

7.4 Results

The curves in Figure 7.2 and 7.3 show the results of two conducted experiments that evaluate the proposed algorithmic framework for visual yarn density measurement. Here, only the density measurements of the proposed method and the ground truth machine target density have been recorded over time periods of 6 and 1 minutes, respectively. In a third experiment, the proposed method and two Fourier based algorithms (see Section 7.3) have been tested in parallel. The X-ray sensor has been additionally added to the measurement setup. The results of the *all-in* experiment are shown in Figure 7.5. For all conducted experiments, the machine vision system and all hardware related components were kept unchanged and have been set up on the operating loom as detailed in Section 5.2.

In Figure 7.2, the blue dashed curve shows the operator's input for targeted machine density values plotted against time. The red curve depicts all measurements recorded by our proposed image processing framework during the same time period. The resulting signal is shown without any further post-processing. It can be seen that measurements are very precise, as the deviation from the targeted machine values seldomly exceeds 0.2 yarns/cm as soon as the sensor's field of view matches the produced fabric corresponding to the machine target value (see black circle). By comparing the two curves in Figure 7.2, it can be seen that there is a time delay between operator input and the actual measurement, which depends on the fabric's density. For lower densities of 8 yarns/cm, the delay is approximately 10 seconds and increases to up to 28 seconds for densities of 22 yarns/cm.

In Figure 7.5, the green curve depicts the measurements of the X-ray sensor. The signal was low-pass filtered and scaled as described in Section 7.3.2. Furthermore, due to the rearwards location of the X-ray sensor, the original signal was shifted to the left by 270 seconds by post-processing for illustration reasons and to allow a facilitated comparison with the other signals. Apart from its noisiness, the shifted X-ray signal corresponds well to the ground truth curve. Higher deviations from the set density can be observed at approximately 3.30 min. The X-ray sensor is not affected by abrupt changes in density.

The curves for the Fourier maximum tracking (dashed black), Fourier ROI tracking (gray) and the proposed method (red) were not post-processed. The curves are based on the analysis of more than 9000 images of the earlier discussed 3-1 twill fabric. It can be seen that the Fourier based algorithms correspond very well to the ground

truth machine target values with very little noise. The ROI tracker gives the best measurement results until approximately 6.50 min, where a abrupt density change from 20 to 25 yarns/cm occurs. The algorithm hence loses the correct target peak and is not able to recover afterwards as the measurement curve significantly differs from the ground truth. The Fourier maximum tracker on the other hand loses the correct signal at an abrupt density change from 36 to 30 yarns/min that occurs at approximately 3.5 min. The algorithm is, however, able to recover afterwards as it guides itself back to the correct measurement curve and keeps track of it until to the end of the experiment. During the stable measurement phases, both algorithms return exactly the same result which is expected, since discrete spectral peak detection forms the basis for both measurements.

Finally, the measurement curve of the proposed method is only slightly more noisy than the Fourier based methods, but handles all abrupt density changes without problems. As a qualitative statement, the measurement corresponds well to the programmed density of the produced fabric – it is very precise as soon as the sensor measurement and machine target values are in sync.

The programmed curves (blue) in Figures 7.2-7.5 obviously do not correspond to the real produced fabric because of the production delay that is a function of the density. Accordingly, experiments 1-3 only give qualitative insights into the system performance with regards to stability and robustness. A quantitative assessment of the system's precision can be concluded from Table 7.2 which summarizes the results of the constant density experiment (see Section 7.3.4).

7.5 Discussion

The presented experiments show that the proposed method outperforms existing algorithms for fabric density measurement. Gray-level scan-line based methods (as proposed by [132]) are limited to materials with rather simple weave pattern and were not applicable to several of the highly resolved images which have been investigated in this work. Figure 7.4 illustrates scan-line profiles computed from one of the fabrics introduced in Section 7.3.3. Here, it can be seen that weft locations cannot be detected reliably. The Fourier-based algorithms have the best measurement accuracy but show severe stability problems when facing abrupt changes in density. The X-ray sensor does not face these problems, but is susceptible to noise, shows higher measurement deviations and must be installed at a distant location from the actual fabric production

Table 7.1: Evaluation results of the proposed method for fabric density measurement on a database of 50 fabric images in 10 fabric classes A-J with plain (P), satin (S) and twill (T) weaves. For each class, five images were acquired: one for the calibration of the system parameters and four for the evaluation. Shown are the ground truth values (GT) and the measurement values (MM) of the mean density $\bar{x}$ and the corresponding standard deviations s.

		Sample									
		A	B	C	D	E	F	G	H	I	J
GT	Weft density	20	26	15	24	45	20	41	24	30	35
	Weave	P	P	P	S	T	S	T	P	T	T
MM	$\bar{x}$	19.68	26.23	15.41	23.85	45.05	19.93	39.83	24.28	29.92	35.34
	s	0.07	0.15	0.09	0.18	0.21	0.12	0.25	0.19	0.23	0.28

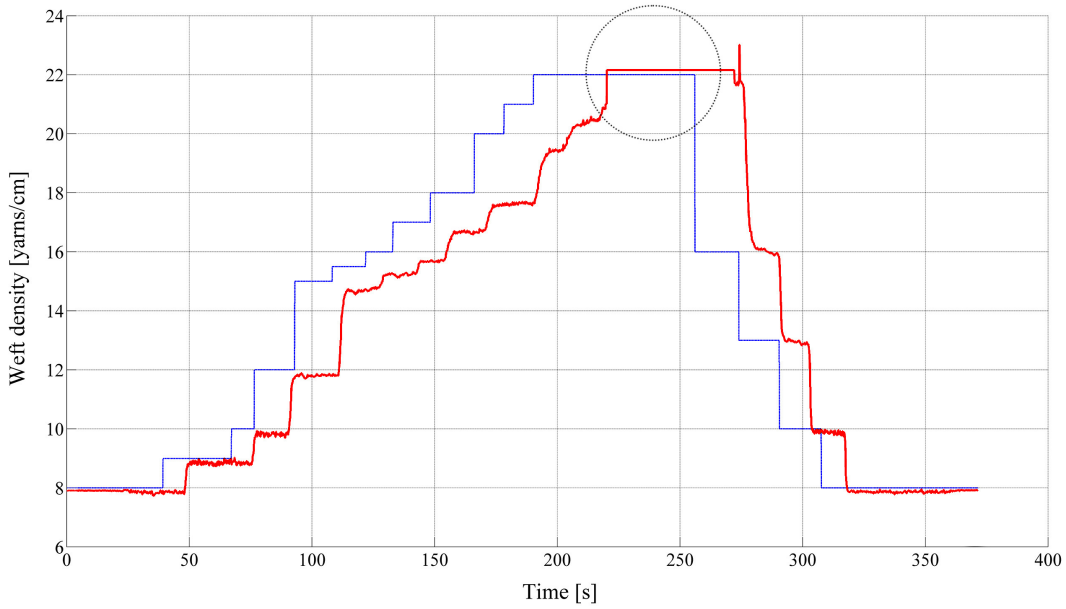

Figure 7.2: On-loom density measurement (red) for an time interval of 360 seconds and corresponding ground truth densities (dashed blue) [11]. A very precise measurement can be achieved when the system is in sync as indicated by the dashed circle. The density depending time delay between targeted machine values and actual measurement can clearly be seen.

due to its dimension, which makes time critical control and quality assurance tasks difficult to implement because of the large dead-time.

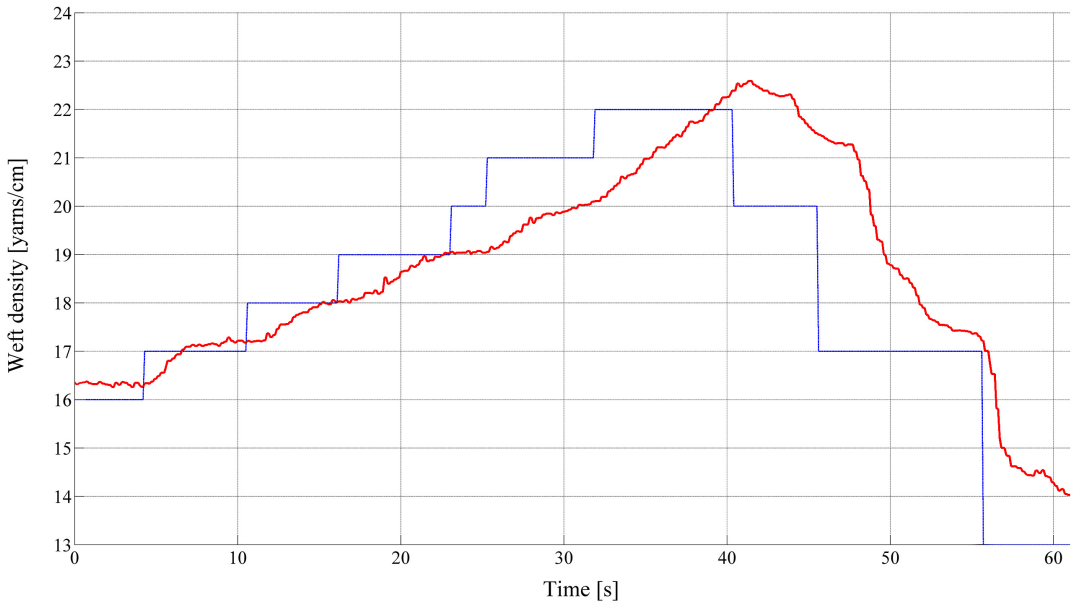

Figure 7.3: On-loom density measurement (red) for a time interval of 60 seconds and corresponding ground truth densities (dashed blue) [11]. For too abrupt changes, the system shows a blur-out on quick density variations.

The proposed algorithmic framework overcomes the mentioned shortcomings as it shows a robust and reliable measurement characteristic with little deviation as it can be seen in Table 7.2. Abrupt changes in density do not affect the system. The time delay between operator input and the actual measurement is directly linked to the constant machine pick rate of 900 picks per minute which causes the production rate to decrease with higher densities. Hence, the measurement curve will always have a bias compared to the target machine curve. There is one outlier at about 274 seconds in Figure 7.2 when the density abruptly changes from 22 yarns/cm to 16 yarns/cm. As anticipated in Section 7.2.1, the large jump from 22 to 16 yarns/cm could be handled, i.e. the system quickly re-calibrated itself. Similarly, Figure 7.3 shows a measurement over a shorter time period of 60 seconds. Here, the described low-pass characteristic of the proposed system can be observed, as sharp changes in density over a short time interval ($\leq$ 10 s) cause a wash-out of the measurement curve. The measurement precision is similar to the results reported by Wang et al. [132], however, the authors based their findings on the evaluation of only eight fabric images, whereas this work was bulk evaluated in 5 experiments covering several thousand images of fabrics with different materials and weaves. The results are hence expected to be more meaningful. With regards to Table 7.2, it can be seen that the density measurement of the proposed framework is precise over the entire density range as the averaged measurement results correspond well to the ground truth. A maximal difference of

0.33 yarns/cm can be observed on a density of 25 yarns/cm. Higher deviations can be observed for higher fabric densities. In consideration of the assumed ground truth error of ± 1 yarn/cm, it can be stated that the system measurements are precise. Also, from Table 7.1 it can be seen, that the system performance is not affected by the fabric material or weave. Precise measurements with little deviation can be reported for either plain, twill or satin weaves. The measurement precision appears to be precise enough for potential control tasks. An important add-on is that the proposed method allows the measurement of local densities among different areas of the fabric image, which has high value for defect detection tasks.

Table 7.2: Evaluation results of the proposed method on eight measurement series with constant weft densities. For each experiment, 30 seconds of image material (450 images each) were recording without altering the density of the 3-1 polyester twill fabric. Shown are the mean density measurement $\bar{x}$ and the corresponding standard deviation s for each measurement series.

GT density	5	10	15	20	25	30	35	40
$\bar{x}$	5.32	10.13	14.75	21.02	25.33	30.03	34.78	40.32
s	0.25	0.27	0.25	0.31	0.28	0.31	0.35	0.36

Besides the grid vectors and yarn vectors, the method requires the template and the regularization term κ to be selected manually. As different (within limitations discussed in Section 5.3.3) selections for the grid vectors, yarn vectors, and the regularization term will have no impact on the overall measurement, the selection of varying float-point templates will alter the results. For instance, the yarn trajectories will differ by some pixels for each selected template; but, since all yarn trajectories shift the same way, the overall density measurement (which is based on relative distances between adjacent yarns) is not affected.

Nevertheless, several drawbacks could be addressed in future work:

- The framework is rather complex when compared to other image processing based methods, which rises the need for more powerful and hence more expensive computing hardware.
- The method requires off-line parametrization and expert knowledge in order to set up and calibrate the system.
- As discussed in Section 5.7, the method is yet limited to non patterned fabric materials due to the chosen template matching approach for float-point detection.

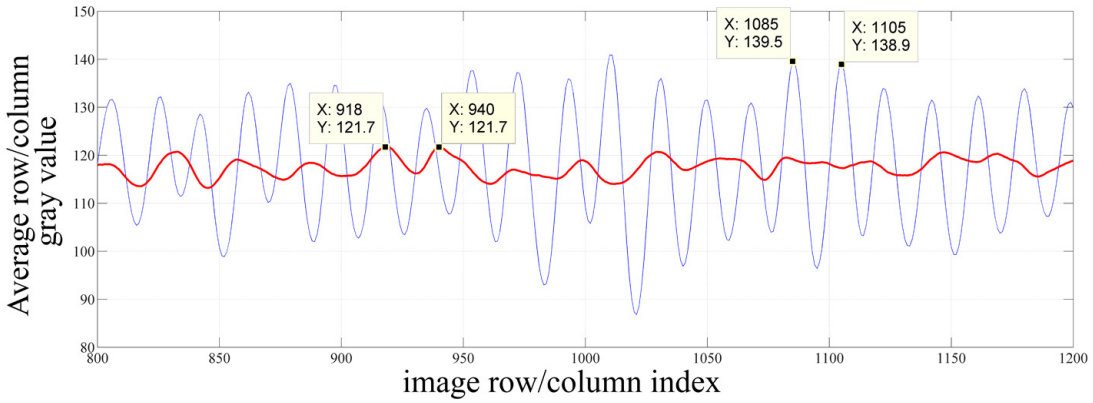

Figure 7.4: Row and column scan-line profiles (averaged gray values for single image rows and columns) for an image of sample D (see Table 7.1). Whereas the scan results in warp direction (blue, scanned columns) are harmonic as well as periodic and could be used to locate single warps within the image, the low pass filtered curve in weft direction (red, scanned rows) is too inaccurate for robust weft detection. The correct spacing between adjacent warps and wefts for sample D is approx. 20 pixels and 11 pixels, respectively.

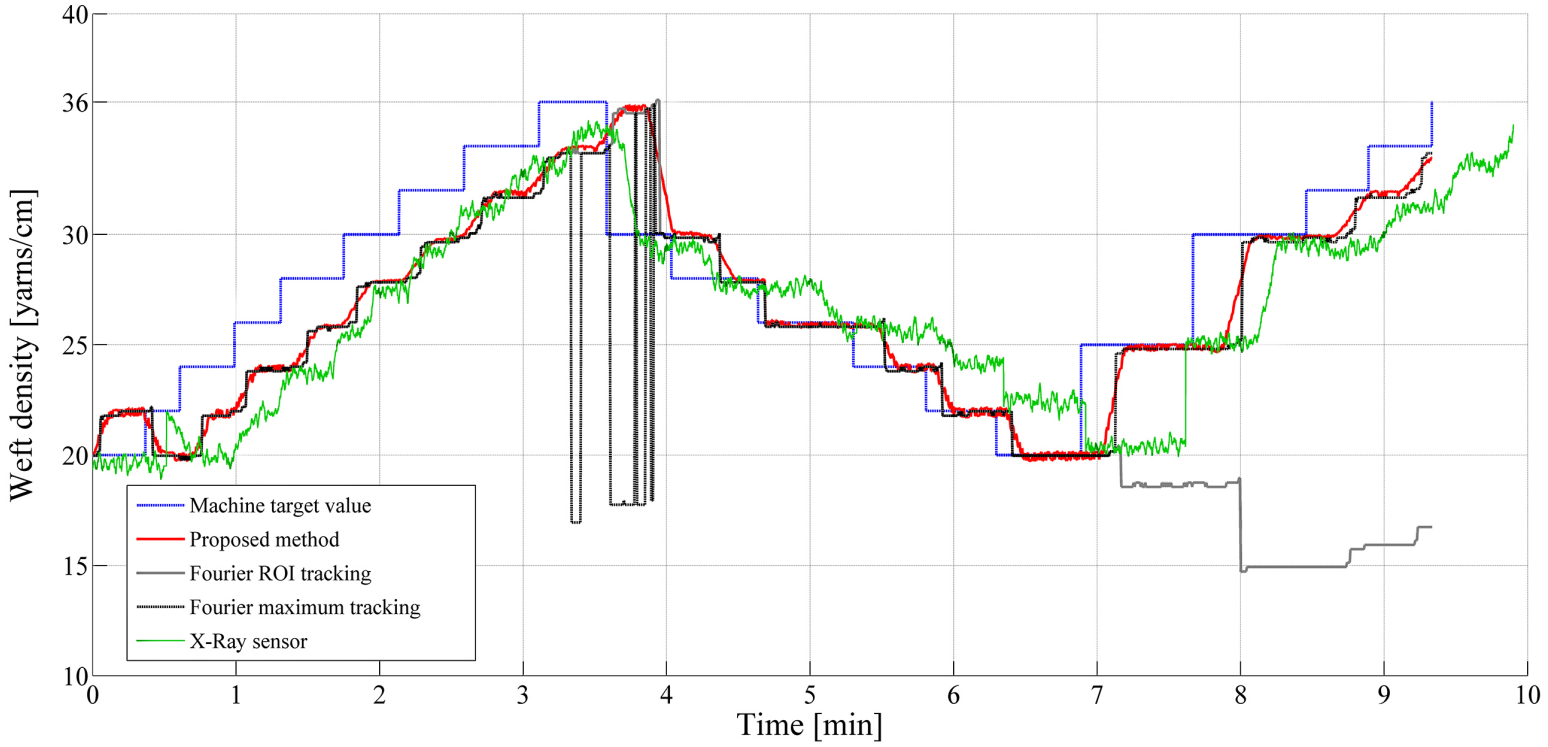

Figure 7.5: On-line measurement results with additional sensors and alternative algorithmic evaluation. Machine target values (blue) for fabric densities and measurements recorded by the proposed image processing framework (red) are shown. The measurement of the X-ray sensor (green) is shown. Due to the delay of X-ray measurement, the signal has been shifted here to the left by 4.5 minutes to allow for comparison with the other measurements (Section 7.3.2). The results of two Fourier analysis based methods for density measurement (Section 7.3.1) are additionally plotted (gray & dashed black).

PART V

CONCLUSION

8 Summary

This work presented comprehensive analyses, designs and discussions of current and future methods for process integrated visual fabric quality control. For this purpose, an extensive benchmark of modern algorithms for vision based fabric defect detection was first conducted to evaluate and identify potential strength and weaknesses of the state-of-the-art. The main contributions within this context were

- the large coverage of 14 evaluated algorithms representing the most important algorithmic classes within the area of texture analysis. A benchmark of this kind and extend has not been conducted before.
- The uniformity of the benchmark. All algorithms were self-implemented in Matlab, and were tested with the same assessment criteria and the same databases. All metrics and databases were clearly defined and described.
- The extent and the quality of the employed databases. Five databases with varying fabric types, defect characteristics, and image resolutions were used to test all selected algorithms. Some of the database contain more than 4000 images, all manually labeled to obtain a meaningful ground truth for the evaluation.
- the extensive literature overview that also covered topical algorithms for automated visual inspection in general.

Hundreds of published papers discuss the problem of fabric defect detection in great detail, but a meaningful comparison was not possible to this point as the reported results exhibit a lack of standardization. The evaluation revealed weaknesses of current state-of-the-art methods for fabric defect detection. Most algorithms performed well on synthetic image data, but gave rather poor results when applied to real-world fabric images. Some algorithmic classes turned out to be completely unpractical, other algorithms could detect defects robustly among most databases but were computationally too expensive for real-time implementation. Very small defects could not

be detected by any of the investigated methods in a robust way. Moreover, all methods exhibited a considerable over-sensitivity which resulted in high false alarm rates that disqualify each method from being used in an industrial context.

These insights motivated the design of a novel system that was intended to overcome the problems faced by conventional algorithms. Instead of treating fabric defect detection as a surface inspection problem, i.e. texture analysis, the novel design frames the problem within the context of visual dimensional verification, i. e. a measuring and inspection task. For this purpose, highly resolved fabric images were acquired that allow to identify single yarns within the fabric. Accordingly, new machine vision algorithms were developed that allow the system to track single yarns and subsequently measure them in terms of their position, shape and appearance. The algorithmic framework was embedded into a traversing imaging system that moves a camera quickly over the entire length of an operating loom during production. The main contributions of the developed On-Loom system are

- the innovative concept of identifying and measuring single yarns.
- The degree of detail that could be achieved using the new technology. Here, small defects of less than 1 mm size can be detected reliably.
- Lower false alarm rates by orders of magnitude.
- Higher defect detection precision by orders of magnitude, achieved by three independent algorithmic modules to detect location, regularity and texture of singles yarns. This feature also enables the system to easily classify defects into defect classes.
- A price reducing realization using a one-camera traverse design.
- The design of a camera vibration damper.
- Real-time processing of highly resolved images.

The On-Loom system was evaluated on-line and off-line. It proved to outperform current algorithms, with respect to the conducted benchmark, by magnitudes. Moreover, financial aspects were discussed as the system was analyzed with respect to its production costs and a potential commercial distribution.

Two additional extensions to the framework were introduced that allow the detection of fabric weave patterns without any prior knowledge and the adaptive measurement of changing yarn densities. The main contributions here were

- the totally blind detection of woven fabric weaves.
- The robust analysis of plain, satin, and twill weaves.

- The applicability to real-world fabric images.
- On overall weave detection rate of 97 % among all basic weave types.
- A precise and relatively noise-free measurement of changing yarn densities.
- A robust densities measurement, also for quickly changing densities.
- A local density measurement, that allows to characterize sub-regions of an image.

Built on top of the On-Loom framework, the two algorithmic extension for blind weave detection and adaptive density measurement proved to be practical and robust. Both methods outperform existing algorithms in terms of accuracy and noise robustness as it could be shown in the evaluation sections. As for the On-Loom system, specific problems need to be addresses in future work to make both methods applicable for daily industrial use. It is emphasized again, that both extensions are directly integrated into the existing defect detection system, without any need for alternate imaging hardware or changes among the loom mechanics. A simple change in the system's configuration file allows to enable/disable both features. This characteristic creates a very versatile and complete vision system for woven fabric quality control. In combination with the two extensions, the On-Loom system represents an comprehensive framework that covers all major parts within the scope of woven fabric quality control. In fact, material defects, weaves, and material densities (and accordingly the grammage) can be monitored with the same system – with yet unrivaled precision and robustness and in real-time.

9 Outlook

Even though the presented results are convincing and outperform the state-of-the-art, it is believed that the current prototype is not yet technically mature enough for usage within industrial environments. Several issues need to be addressed first. Thereupon, answers to the most prevalent questions regarding further developments, drawbacks and weaknesses are now given.

Q1: "*Where is the highest potential for algorithmic improvement seen?*"

Most false alarms were caused by image degradations created by the imaging system, i.e. by vignette obscuration along the border regions of an image. These should be corrected on a software basis are better with alternative imaging hardware. Likewise, the major bottleneck of the algorithmic pipeline was determined to be the feature extraction module for float-point detection. The template based correlation approach limits the framework to the analysis of non-patterned, mono-colored materials. It is believed that the development of an robust and universal feature extractor is not trivial but feasible. For instance, the usage of statistical information about the orientation dependent pixel intensities that define a fabric float-point seems to be a promising starting point for further developments in this context.

Q2: "*Is the traverse design an advantage or disadvantage when compared to a fixed-camera solution?*"

Both cases apply. With regards to the minimization of costs, the choice of a traversing camera seems to be the best choice for a on-line fabric defect detection system.

Especially when detecting single yarns, a fixed-camera solution is not realizable if the entire length of the loom must be monitored. An camera array, which will be needed to guarantee the same spatial image resolution as the traversing system, will exceed any financial limits. Conversely, moving parts and complex mechanics of the traverse will alienate any potential purchaser, as they are prone for malfunctions, breakdowns and need regular maintenance. These are factors for additional costs that need to be considered carefully.

Q3: "*What is the best strategy to lower system costs?*"

Clearly, the traversing back-light should be replaced by a top-light illumination. This change will dramatically reduce the costs of the overall system by 30 % as the complete traverse unit that is installed below the fabric can be dispensed. When using top-light, the proposed machine vision algorithms must be adapted and further extended. Nevertheless, at this point it cannot be foreseen if the defect detection accuracy under top-light can ever be as precise and as robust as the reported results in this work. For instance, some defects are simply not visible under these light conditions, other defects become more visible. A system that works reliably with top-light would allow to control very dark and/or thick materials, that do not let the back-light illumination pass trough.

Q4: "*Will the On-Loom prototype be commercialized at some point?*"

The achievements of this work define new standards within the research area of fabric defect detection. It is, however, very unlikely that the proposed system will reach a commercial stage of maturation with regards to the apparel mass market. First, the project funding expired so that no further developments will be supplied. Further, without a strong and disposed industrial partner, the prototype will not leave its academic environment. Moving mechanical parts, large investments (a system must be installed on every loom), low product prices and a need for infrastructural extensions in each weaving mill will discourage potential investors from the apparel industry from engaging them-self in the system development. On the contrary, it is conceivable that the system may enforce itself on the market for technical textiles. Here, its application is very likely because higher standards for quality exist, a modern infrastructure is available in most cases and the system price is relativized by much higher fabric costs. Especially in the area of Carbon-fiber-reinforced polymer materials, a very high potential for application is seen for the On-Loom system. Here, the

algorithmic pipeline could be combined with a measurement of fiber orientations to provide a complete system for fabric quality control. After all, the project should be further advertised and potential industrial partners should be contacted. For instance, the project website [13] shows videos with on-line demonstrations of the yarn tracker, and defect detector. Image databases, source codes and publications related to this work are provided and hopefully help and engage other researchers around the world to further improve the state-o-the-art of on-loom fabric defect detection.

APPENDICES

A Surface inspection literature by domain

To continue the discussion on literature related to the field of automated visual inspection, this appendix highlights selected publications that are related to the field of surface inspection (other than textile inspection). Cited papers are not listed in any of the survey papers mentioned in Section 4.1.2. The field of automated surface inspection is here broken down to its main fields of application, namely the inspection of metal, wood, nutrition, leather, and stone materials.

- *Metal inspection.* Metallic bands are usually 0.3 to 2.0 m wide and serve as raw material for (upon others) the automotive, electronic and electrical industry. During production, the strips become repetitively subject to automatic forming by pressing, punching and finishing which requires definable properties of the metal's surface. Common defect types are cracks, scratches, stains and abrasions. Even though the topic is highly relevant to the industry, no related survey paper has yet been published. Also topical publications discussing specific applications (for example a specific production process or material type) are relatively rare. A conference report by Normanton et al. [163] gives a general overview of the problem statement and discusses the question if automated inspection systems of that time could meet the erstwhile requirements of the industry. A practical application of image processing techniques for metal inspection is given by Piironen et al. [164]. The authors propose a prototype system for on-line inspection of steel bands. The work has been published in 1990 and mainly focuses on the design of the image acquisition system. Basic image processing techniques are employed such as adaptive thresholding, morphological filtering and connected component analysis. In 2002, Zheng et al. [165] propose to use a top-hat filter and two subsequent threshold operations to detect defects in bumpy (as opposed to completely flat) metal surfaces. They use a genetic algorithm for automatic parameter selection. Wu et al. [166] employ a modified version of the co-occurrence matrix method to inspect metal surfaces of any kind. A similar method will also be tested in Section 4.2.2.3 within the context of fabric inspection. A very different field of application for metal surface inspection is introduced by Mandriota et al. [167]. Here, the authors present a methodology based on a Gabor Wavelet filter bank to inspect rail tracks for corrugations. This is a good example of surface inspection applied as a post-production quality control tool. Similarly, Wiltschi et al. [168] use Gabor filter banks in combination with shape features to assess the quality of

carbide distributions. Wavelets are also used by Ghorai et al. [169] who propose a real-time prototype system for the inspection of hot-rolled steel bands. As for many other approaches, images here are (Wavelet) filtered, divided into non-overlapping sub-windows, features are extracted and finally fed into a classifier to make a decision about potential defects. This processing pipeline is very common and will also be tested with respect to fabric inspection in later sections. Other examples of the application of wavelet transforms for metal inspection are given by [170] and [171]. An interesting approach based on the combination of linear Curvelet filtering, non-linear morphological filtering and statistical learning for optimal feature selection is successfully tested by Card et al. [172]. Other authors use common techniques like Local Binary Pattern [173, 174], shape features like invariant moments [175] such as image histogram analysis [176] to detect defects in flat metal surfaces.

- *Leather inspection.* As for the inspection of metal surfaces, no survey paper yet bundles publications related to the topic of leather surface inspection. Published papers in the area relatively often employ wavelet based filtering for defect segmentation. Within this context, Branca et al. [177, 178] employ a multi-resolution approach using wavelet decomposition and edge detection to discriminate defects that are characterized by sharp intensity variations with high directionality. Sobral [179] designed a wavelet filter bank in combination with an optimized smoothing filter bank to emphasize defects in leather materials. He et al. [180] add an automatic selection of the best wavelet decomposition channels to further improve the procedure. Tsa et al. [181] on the other hand use Gabor filters to locate irregularities in leather textures, whereas Kwak et al. [182] employ a simple thresholding scheme combined with basic filtering techniques and an artificial neural network to detect and classify defects in leather materials. Other than filtering, Krastev et al. [183] propose to use a fuzzy logic decider combined with connected components analysis to separate defective leather parts from non-defective ones. Finally, motivated by research for leather inspection, Wen et al. [184] describe a methodology for consolidating edges (and hence simplify the segmentation) of meaningful objects (defects) which are surrounded by a textured background.

- *Wood inspection.* An out-dated but still informative overview of publications related to the area of automated visual wood inspection is given by the Ph.D. thesis of Erik Åstrand from 1996 [185]. A more specific application of wood defect detection is described by Lampinen [186] who uses generic feature vectors constituted by RGB color features, Gabor features and gray value histogram features to train a feed-forward artificial neural network. Martin et al. [187] use diffuse laser light as special illumination technique to facilitate the wood

defect segmentation which is accomplished by an iterative active contour algorithm. Patricio and Maravall [188] introduce a special statistics measurement denoted as the "frequency histogram of connected elements", to investigate wooden pallets. They employ Bayesian statistics and sophisticated threshold optimization to detect and measure cracks smaller than a millimeter. Silven et al. [189–191] divide their input images into non-overlapping cells and for each cell, employ accumulated color histograms and Local Binary Pattern as input features for a self-organizing map classifier. Wyckhuyse and Maldague present in a comprehensive two volume publication different methodologies for the inspection of wood poles and wood defects using infrared thermography [192, 193]. A multistage region-growing type of algorithm in combination with a kNN-classifier are deployed by Alapuranen and Westman [194], whereas Hall and Ström [195] focus on the design of parallel computation hardware for real-time inspection of wooden materials. Finally, more recent publications are provided by Li et al. [196, 197] which cover the inspection of wooden veneer. The publication also covers the topic of optimized features selection for improved training of a neural network classifier.

- *Nutrition inspection.* Next to fabric inspection, the inspection of food is the second most common area of application for AVI systems if measured with respect to the amount and the topicality of published papers. In fact, several recent survey papers and trend overviews can be found, and with the *Journal of Food Measurement and Characterization*[1], such as the Journal for *Food Control*[2] an entire research area is created around the task of nutrition inspection. The begin with, the most recent and complete overview of published papers is given by Patel et al. [198] in 2012, who reviewed 186 papers related to the topic of Machine Vision algorithms for automated food quality control. Additionally, Da-Wen Sun edited an entire book in 2012 discussing the topic of *Computer Vision Technology in the Food and Beverage Industries* [199]. The book is divided into three parts comprising an general overview, general operations and specialized applications. Here, general topics like common computer vision techniques for sorting, foreign body detection, cutting, and the analysis of food microstructures are addressed and discussed in great extent. More details are later given for the specific production areas of meat, poultry, fish, fruits, vegetables, grains, and bakery goods. With respect to the specific area of fruit and vegetable inspection, Zhang et al. [200] published a comprehensive overview in which they not only survey the state-of-the-art, but also cover basic theories and analytical methods such as recent developments and applications of vision

[1] Springer, ISSN 2193-4126
[2] Elsevier, ISSN 0956-7135

systems for the analysis of fruits and vegetables. Moreover, two recent but rudimentary trend overviews are given by Methew and Janardhana [201, 202] in 2013 which evaluate the topic by focusing on common image processing pipelines and techniques. In 2004, Brosnan et al. [203] published a detailed overview of computer vision aided control of food products. The authors here investigate necessary hardware components, methodological procedures and a literature survey of the erstwhile state-of-the-art. Concrete applications are reported among others by Ginesu [204] who detect foreign bodies in food using thermal imaging, by Mateo et al. [205] who control tuna meat for impurities and Han et al. [206] who demonstrate how terahertz imaging can be used for food quality purposes on the example of cracker and nut inspection.

- *Stone & ceramic inspection.* Compared to previously examined products for visual surface inspection, the application of machine vision for stone and ceramic inspection is with respect to the amount of available publications a niche area. To begin with, a complex image processing work-flow for automatic crack detection in concrete structures has recently been published by Adhikari et al. [207]. The authors deploy sophisticated image stitching algorithms, Neural Networks and 3D visualization techniques to measure and assess potential cracks in concrete bridges. Similarly, Choudhary et al. [208] propose a framework for crack detection in concrete surfaces that is also based on artificial neural networks and combines it with fuzzy logic algorithms. Also Tong et al. [209] address the problem of crack detection in concrete bridges. Their real-time system is based on standard image pre-processing techniques and straight-forward shape criteria for noise removal and crack segmentation. In 2012, Ershad proposes a methodology for classifying stone textures by combining Local Binary Pattern with edge features and co-occurrence statistics [210]. Surface damages in ceramic ground pieces are found by Chen et al. [211] by using spectral filtering and the design of customized surface features in combination with a decision tree classifier. Smith and Stamp [212] introduce an automated inspection system for complex surfaces of ceramic tiles which is based on the analysis of topographic and chromatic material properties. Lin proposes to inspect ceramic capacitor chips using Wavelet decomposition [213]. The inspection of marble slabs is addressed separately by Doğan and Selver [214, 215]. Selver discusses a novel hierarchical clustering approach and customized morphological features to send control commands to an electro-mechanical system that sorts out misclassified marble slabs. Doğan et al. on the other hand use an Adaboost classifier to assess the quality of marble slabs based on features that are derived from image color histograms. Two more general approaches for the classification of colored, random (stone) textures are proposed by Xie [216] and Kittler et al. [217]. Xie

proposes to use a promising method based on clustered image patches (Texems) in combination with Gaussian Mixture Models, whereas Kittler discusses the use of the pseudo-Wigner spectrum, color clustering, and structural blob analysis.

B Derivation of the optimized form of the ZNCC

The Zero-Mean-Normalized-Cross-Correlation function [128] is defined as

$$g(u,v) = \frac{n(u,v)}{d(h,v)} = \frac{\sum_{x,y}\left[f(x,y) - \bar{f}_{u,v}\right]\left[t(x-u,y-v) - \bar{t}\right]}{\sqrt{\sum_{x,y}\left[f(x,y) - \bar{f}_{u,v}\right]^2 \sum_{x,y}\left[t(x-u,y-v) - \bar{t}\right]^2}}, \tag{1}$$

where $t(x,y)$ is the warp-float template, $\bar{t}$ is the template mean, $f(x,y)$ is the pre-processed input image, $\bar{f}_{u,v}$ is the mean of the input image region under the template and $g(u,v)$ is the correlation result with the same size as the input image. By defining $t'(x-u,y-v) = \left[t(x-u,y-v) - \bar{t}\right]$, the numerator can be reformulated according to Lewis [218] as

$$\begin{aligned} n(u,v) &= \sum_{x,y}\left[f(x,y) - \bar{f}_{u,v}\right] t'(x-u,y-v) \\ &= \sum_{x,y} f(x,y)\, t'(x-u,y-v) - \sum_{x,y} \bar{f}_{u,v}\, t'(x-u,y-v) \\ &= \sum_{x,y} f(x,y)\, t'(x-u,y-v) - \bar{f}_{u,v} \sum_{x,y} t'(x-u,y-v) \end{aligned}$$

and since t' has no mean, $\sum_{x,y} t'(x-u,y-v) = 0$, leaving

$$\begin{aligned} n(u,v) &= \sum_{x,y} f(x,y)\, t'(x-u,y-v) \\ &= \mathscr{F}^{-1}\left[\mathscr{F}(f(x,y)) \cdot \mathscr{F}^*(t'(x,y))\right]. \end{aligned} \tag{2}$$

The denominator was also rearranged according to

$$\begin{aligned} d(u,v) &= \sqrt{\sum_{x,y}\left[f(x,y) - \bar{f}_{u,v}\right]^2 \sum_{x,y}\left[t(x-u,y-v) - \bar{t}\right]^2} \\ \sum_{x,y}\left[f(x,y) - \bar{f}_{u,v}\right]^2 &= \sum_{x,y}\left[f^2(x,y) - 2\bar{f}_{u,v} f(x,y) + \bar{f}_{u,v}^2\right] \\ &=^* \sum_{x,y} f^2(x,y) - 2A\bar{f}_{u,v}^2 + \sum_{x,y} \bar{f}_{u,v}^2 \\ &\quad {}^*(\text{since } \sum_{x,y} 2\bar{f}_{u,v} f(x,y) = 2\bar{f}_{u,v} \sum_{x,y} f(x,y) = 2A\bar{f}_{u,v}^2) \\ &= \sum_{x,y} f^2(x,y) - 2A\bar{f}_{u,v}^2 + A \cdot \bar{f}_{u,v}^2 = \sum_{x,y} f^2(x,y) - A \cdot \bar{f}_{u,v}^2 \\ &= \sum_{x,y} f^2(x,y) - \frac{1}{A}\left[\sum_{x,y} f(x,y)\right]^2 \end{aligned}$$

$$\Rightarrow d(u,v) = \sqrt{\left[\sum_{x,y} f^2(x,y) - \frac{1}{A}\left[\sum_{x,y} f(x,y)\right]^2\right]\sum_{x,y} t'^2}$$

$$= \sqrt{\sum_{x,y} f^2(x,y) - \frac{1}{A}\left[\sum_{x,y} f(x,y)\right]^2} \cdot \sqrt{A} \cdot \sigma_t, \tag{3}$$

where σ_t is the standard deviation of the template and $A = (X \cdot Y)$, the number of pixels in the template. The numerator (2) and denominator (3) are combined to give the final, compact correlation function

$$g(\mathbf{I},\mathbf{T}) := \frac{\mathscr{F}^{-1}\left[\mathscr{F}(\mathbf{I}) \cdot \mathscr{F}^*(\mathbf{T})\right]}{\sqrt{\sum \mathbf{I}^2 - \frac{1}{A}\left[\sum \mathbf{I}\right]^2} \cdot \sqrt{A} \cdot \sigma_T}, \tag{4}$$

where $\mathscr{F}, \mathscr{F}^{-1}, \mathscr{F}^*$ denote the Fourier transform, its inverse and complex conjugate respectively, $\mathbf{I}$ is the input image, $\mathbf{T}$ is a mean subtracted template, A the area of the template, and σ_T the standard deviation of the template. The operator $(\cdot)$ denotes a point-wise multiplication.

C Matlab pseudo code for the grid map build algorithm

Listing 1: Matlab pseudo-code for the grid matrix algorithm.

```
%Q -> Float-Point queue
%S -> Search Matrix
%G -> Grid Matrix
%L -> Float-point list

Q = initializeQueryQueue();
S = initializeSearchMatrix();
G = initializeGridMatrix();

while hasMoreElements(Q)
  q = popFromQueue(Q)

  seekPt = nearestNeighbor(L, q.imageCoord, searchArea)

  if isEmtpy(seekPt)
    S(q.matrixCoord) = NOT_FOUND
    continue;
  else
    S(q.matrixCoord) = FOUND
    G(q.matrixCoord) = seekPt.imgCoord

    [p14,S] = updateNeighbors(S, q.matrixCoord)
    p14     = estimXY(g_a, g_b, seekPt, p14)

    Q(end+1) = p14)
  end
```

```
27  end
28
29  function [p14, S] = updateNeighbors(S, mc)
30   x = mc.x
31   y = mc.y
32
33   p14 = [];
34
35   if S(y+1, x) == NOT_PROCESSED
36    S(y+1, x) = LISTED;
37    tmpSeed.matrixCoord.x = x;
38    tmpSeed.matrixCoord.y = y+1;
39    p14(end+1) = tmpSeed;
40   end
41
42   if S(y-1, x) == NOT_PROCESSED
43    S(y+1, x) = LISTED;
44    tmpSeed.matrixCoord.x = x;
45    tmpSeed.matrixCoord.y = y-1;
46    p14(end+1) = tmpSeed;
47   end
48
49   % ...
50   % repeat this for the positions
51   %{y,x+1} and {y, x-1} >
52  end % end updateNeighbors
53
54  function ns = estimXY(g_a, g_b, sp, ns)
55   ns(1).imgCoord = sp.imgCoord + g_a
56   ns(2).imgCoord = sp.imgCoord - g_a
57   ns(3).imgCoord = sp.imgCoord + g_b
58   ns(4).imgCoord = sp.imgCoord - g_b
59  end
```

D Examples of the yarn tracker output

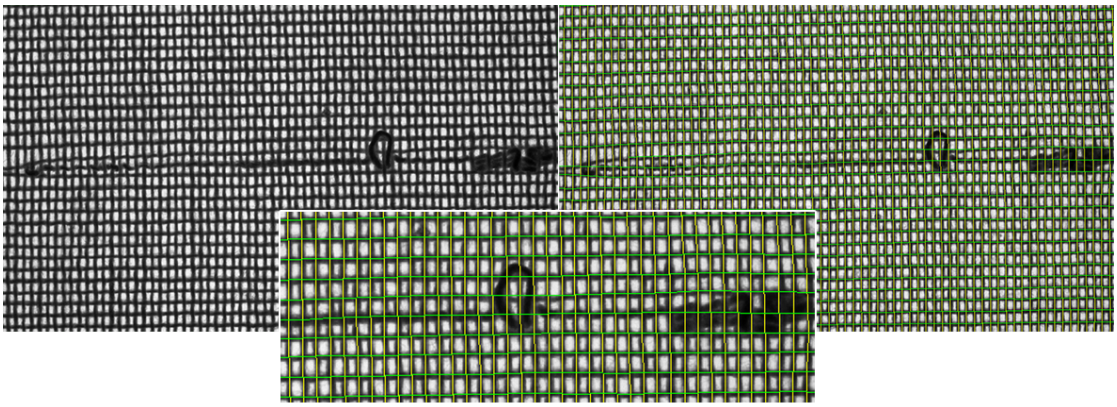

Figure 1: Different fabric samples with super-imposed trajectories of the interpolated yarn positions, 1/4.

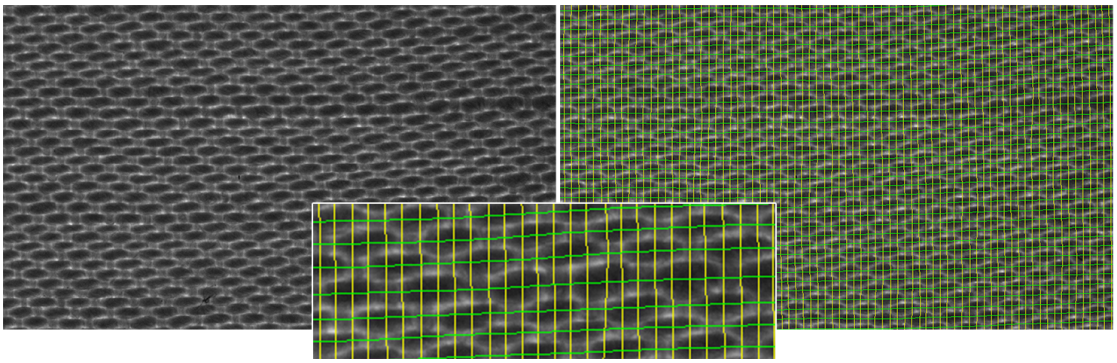

Figure 2: Different fabric samples with super-imposed trajectories of the interpolated yarn positions, 2/4.

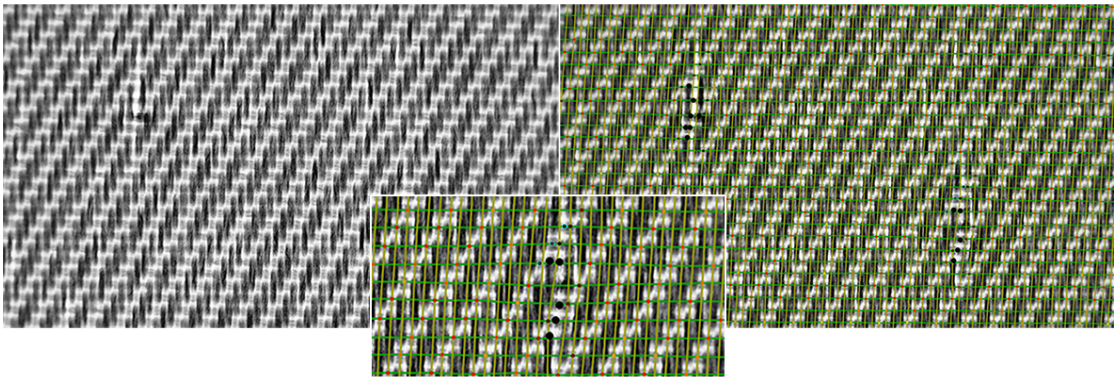

Figure 3: Different fabric samples with super-imposed trajectories of the interpolated yarn positions, 3/4.

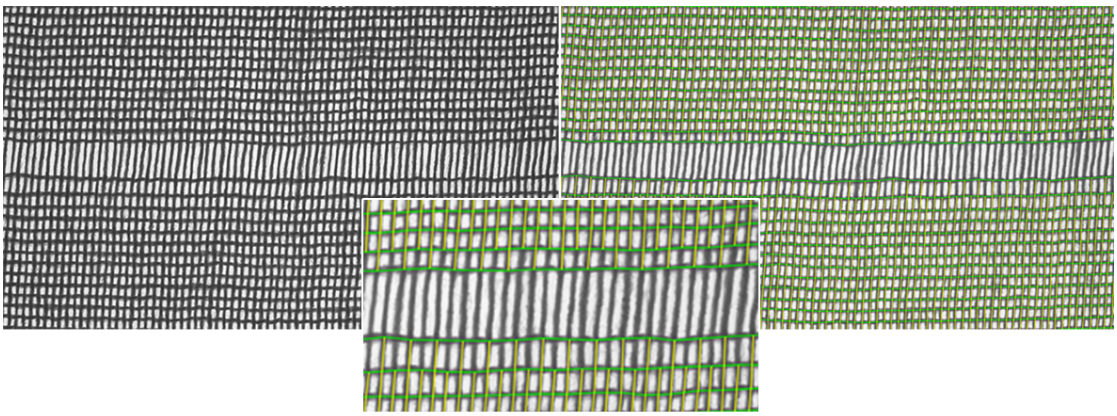

Figure 4: Different fabric samples with super-imposed trajectories of the interpolated yarn positions, 4/4.

E Detailed blind weave detection results

Table 1: Detailed evaluation results for the blind weave detection framework (1/2). For each of the 14 fabric samples A-N, 10 rotated images were evaluated – in total 140 images. The column *Ground Truth* list manually measured reference values, automatically measured yarn densities and weave pattern are listed in the *Measurements* field. Densities are given in yarns/cm. The *Error* column lists the averaged absolute measurement difference from the ground truth and the misclassification rate for each fabric sample. Values that are marked by (*) distinguish measurements where the correct assignment of weft and warp directions had been interchanged, i.e. the image has been rotated by 90° so that wefts were taken as warps and vice versa.

		Ground truth	Measurements										
			0°	20°	40°	60°	80°	100°	120°	140°	160°	180°	Error
Sample A	Weft Dens.	20	20.07	19.84	19.84	19.84	19.79	19.79	20.18	19.84	19.84	19.79	0.17
	Warp Dens.	13	12.82	12.88	12.88	12.53	12.82	12.82	12.88	12.88	12.53	12.82	0.22
	Weave	P1	P1	P1	P1	P1	P1	P1	P1	P1	P1	P1	0/10
Sample B	Weft Dens.	20	20.18	20.18	20.18	20.18	20.34	20.34	20.18	20.53	20.18	20.18	0.25
	Warp Dens.	16	15.66	15.66	15.66	15.66	15.89	15.89	15.66	16.01	15.66	16.01	0.23
	Weave	P1	P1	P1	P1	P1	P1	P1	P1	P1	P1	P1	0/10
Sample C	Weft Dens.	26	26.75	26.45	26.80	26.45	26.75*	26.80	26.80	26.45	26.45	26.48	0.62
	Warp Dens.	13	12.82	12.88	12.88	12.53	12.82*	12.88	12.88	12.88	12.88	12.82	0.18
	Weave	P1	P1	P1	P1	P1	P1	P1	P1	P1	P1	P1	0/10
Sample D	Weft Dens.	24	24.76	24.71	24.36	24.36	24.80	25.08	24.36	24.71	24.71	24.76	0.66
	Warp Dens.	32	32.52	32.36	32.36	32.71	32.89	32.61	32.02	32.36	32.36	32.52	0.47
	Weave	S42	S42	S42	S42	S42	S42	S42	S42	S42	S42	S42	0/10
Sample E	Weft Dens.	21	21.41	21.58	21.58	21.23	21.23	21.46	21.58	21.58	21.58	21.46	0.47
	Warp Dens.	16	17.01	16.70	16.36	16.01	16.36	16.44	16.36	16.70	16.70	16.44	0.51
	Weave	T31	T31	T31	T31	T31	T31	T31	T31	T31	T31	T31	0/10
Sample F	Weft Dens.	20	19.85	19.84	19.84	19.84	19.79	19.79	19.84	19.49	19.84	19.79	0.21
	Warp Dens.	40	40.18	40.37	40.37	40.02	40.41	40.41	40.02	40.37	40.02	40.13	0.23
	Weave	S41	S41	S41	S41	S41	S41	S41	S41	S41	S41	S41	0/10
Sample G	Weft Dens.	45	45.43	45.15	45.24	44.89	45.15	45.15	0.00	45.24	45.24	45.15	0.20
	Warp Dens.	21	20.90	20.62	20.53	20.53	20.62	20.62	0.00	20.88	20.53	20.62	0.35
	Weave	T31	T31	T31	T31	T31	T31	T31	-	T31	T31	T31	1/10

Table 3: Detailed evaluation results for the blind weave detection framework, 2/2

		Ground truth	Measurements 0°	20°	40°	60°	80°	100°	120°	140°	160°	180°	Error
Sample H	Weft Dens.	24	24.25	24.52	24.01	24.01	24.25	24.25	24.01	24.01	24.01	24.25	0.16
	Warp Dens.	24	23.97	23.97	24.36	24.36	24.52	24.52	24.36	24.36	24.36	24.25	0.32
	Weave	P1	P1	P1	P1	P1	P1	P1	P1	P1	P1	P1	0/10
Sample I	Weft Dens.	15	15.61	15.61*	15.66	15.66	15.66	15.31	15.66	15.66	15.66	15.61	0.61
	Warp Dens.	14	13.93	13.93*	13.92	13.92	13.92	13.92	13.92	13.92	14.27	14.21	0.11
	Weave	P1	P1	P1	P1	P1	P1	P1	P1	P1	P1	P1	0/10
Sample J	Weft Dens.	7	7.52	7.66	7.66	7.66	7.80	7.80	7.66	7.66	7.66	7.52	0.66
	Warp Dens.	12	11.98	11.83	11.83	11.83	11.98	11.98	11.83	11.83	11.83	11.98	0.11
	Weave	P1	P1	P1	P1	P1	P1	P1	P1	P1	P1	P1	0/10
Sample K	Weft Dens.	30	20.74*	20.88*	21.23*	30.62	30.66	21.18*	21.23*	20.88*	20.88*	20.93*	7.33
	Warp Dens.	62	29.89*	30.62*	30.62*	77.95	79.15	30.38*	30.62*	30.62*	30.28*	30.33*	28.57
	Weave	T31	S41	T31	T31	S41	S41	T31	T31	T31	T31	T31	3/10
Sample L	Weft Dens.	41	41.04	40.82	40.71	41.06	40.97	40.97	41.41	41.06	40.97	40.97	0.12
	Warp Dens.	35	35.51	35.61	35.50	35.50	35.67	35.67	35.84	35.50	35.39	35.39	0.56
	Weave	T31	T31	T31	T31	T31	T31	T31	T31	T31	T31	T31	0/10
Sample M	Weft Dens.	35	35.24	35.15	35.15	35.15	35.15	34.84	35.15	35.15	34.80	34.57	0.19
	Warp Dens.	20	20.56	20.18	20.18	20.18	20.53	20.34	20.53	20.53	20.18	19.62	0.36
	Weave	T21	T21	T21	T21	T21	T21	T21	T21	T21	T21	T21	0/10
Sample N	Weft Dens.	2	2.47	2.47	4.45	2.40	2.20	2.47	2.40	4.45	2.47	2.42	0.82
	Warp Dens.	2	2.20	2.20	2.40	2.40	2.20	2.20	2.40	2.40	2.20	2.21	0.28
	Weave	P1	P1	P1	P1	P1	P1	P1	P1	P1	P1	P1	0/10

Bibliography

[1] J. Denton, *Society and the Official World: A Reintroduction to Sociology*. Reynolds series in sociology, Rowman & Littlefield Publishers, Incorporated, 1990.

[2] C. Riethmueller, "Thoughts on fabric inspection on the weaving machine," *Melliand Textilberichte English*, vol. 81, pp. 196–E197, 2000.

[3] S. Adanur, *Handbook of Industrial Textiles*. Taylor & Francis, 1995.

[4] D. Schneider, T. Holtermann, F. Neumann, A. Hehl, T. Aach, and T. Gries, "A vision based system for high precision online fabric defect detection," in *Industrial Electronics and Applications (ICIEA), 2012 7th IEEE Conference on*, pp. 1494–1499, 2012.

[5] D. Schneider, "Tracking yarns in high resolution fabric images: a real-time approach for online fabric flaw detection," *Proc. SPIE*, vol. 8656, pp. 865603–865603–12, 2013.

[6] D. Schneider, T. van Ekeris, J. zur Jacobsmuehlen, and S. Groß, "On benchmarking non-blind deconvolution algorithms: A sample driven comparison of image de-blurring methods for automated visual inspection systems," in *Instrumentation and Measurement Technology Conference (I2MTC), 2013 IEEE International*, pp. 1646–1651, 2013.

[7] D. Schneider and T. Aach, "Vision-based in-line fabric defect detection using yarn-specific shape features," *Proc. SPIE*, vol. 8300, pp. 83000G–83000G–10, 2012.

[8] F. Neumann, T. Holtermann, D. Schneider, A. Kulczycki, T. Gries, and T. Aach, "In-process fault detection for textile fabric production: onloom imaging," *Proc. SPIE*, vol. 8082, pp. 808240–808240–12, 2011.

[9] D. Schneider, T. Holtermann, and D. Merhof, "A traverse inspection system for high precision visual on-loom fabric defect detection," *Machine Vision and Applications*, pp. 1–15, 2014.

[10] D. Schneider and D. Merhof, "Blind weave detection for woven fabrics," *Pattern Analysis and Applications*, pp. 1–13, 2014.

[11] D. Schneider and D. Merhof, "High precision on-loom yarn density measurement in woven fabrics," in *Instrumentation and Measurement Technology Conference (I2MTC), IEEE International*, 2014.

[12] D. Schneider, Y.-S. Gloy, and D. Merhof, "Vision-based on-loom measurement of yarn densities in woven fabrics," *Instrumentation and Measurement, IEEE Transactions on*, vol. PP, no. 99, pp. 1–1, 2014.

[13] D. Schneider, "On-loom imaging project webpage." http://onloom.lfb.rwth-aachen.de, July 2014.

[14] E. Kvavadze, O. Bar-Yosef, A. Belfer-Cohen, E. Boaretto, N. Jakeli, Z. Matskevich, and T. Meshveliani, "30,000-year-old wild flax fibers," *Science*, vol. 11, p. 1359, 2009.

[15] S. Adanur, *Handbook of Weaving*. Taylor & Francis, 2000.

[16] United States. Congress. Office of Technology Assessment, *The U.S. textile and apparel industry : a revolution in progress : special report.* DIANE Publishing, 1987.

[17] V. T. Machinery, "German textile machinery industry - key figures," tech. rep., VDMA, June 2013.

[18] Gesamtverband Textil + Mode, "Zahlen zur Textil und Bekleidungsindustrie," tech. rep., Gesamtverband der deutschen Textil + Mode Industrie e.V., July 2013.

[19] F. Neumann, "IGF-Projekt Onloom Imaging, Datenerhebung Relevante Gewebetypen und Gewebefehler," tech. rep., Institut für Textiltechnik der RWTH Aachen, 2010.

[20] Arbeitskreis Gesamttextil, "Webereitechnik gewebefehler," tech. rep., Arbeitskreis Gesamttextil - Frankfurt am Main, 1989.

[21] H. Schulz-Mirbach, "Ein Referenzdatensatz zur Evaluierung von Sichtprüfverfahren für Textiloberflächen," internal report, Technische Universität Hamburg-Harburg, 1996.

[22] E. N. Malamas, E. G. Petrakis, M. Zervakis, L. Petit, and J.-D. Legat, "A survey on industrial vision systems, applications and tools," *Image and Vision Computing*, vol. 21, no. 2, pp. 171 – 188, 2003.

[23] T. S. Newman and A. K. Jain, "A survey of automated visual inspection," *Computer Vision and Image Understanding*, vol. 61, no. 2, pp. 231 – 262, 1995.

[24] A. Thomas, M. Rodd, J. Holt, and C. Neill, "Real-time industrial visual inspection: A review," *Real-Time Imaging*, vol. 1, no. 2, pp. 139 – 158, 1995.

[25] E. Bayro-Corrochano, "Review of automated visual inspection 1983-1993, part i: conventional approaches," *Proc. SPIE*, vol. 2055, pp. 128–158, 1993.

[26] E. Bayro-Corrochano, "Review of automated visual inspection 1983-1993, part ii: approaches to intelligent systems," *Proc. SPIE*, vol. 2055, pp. 159–172, 1993.

[27] R. T. Chin, "Automated visual inspection: 1981 to 1987," *Computer Vision, Graphics, and Image Processing*, vol. 41, no. 3, pp. 346 – 381, 1988.

[28] R. T. Chin, "Automated visual inspection techniques and applications: A bibliography," *Pattern Recognition*, vol. 15, no. 4, pp. 343 – 357, 1982.

[29] R. T. Chin and C. A. Harlow, "Automated visual inspection: A survey," *Pattern Analysis and Machine Intelligence, IEEE Transactions on*, vol. PAMI-4, pp. 557–573, Nov 1982.

[30] X. Xie, "A review of recent advances in surface defect detection using texture analysis techniques," *Electronic Letters on Computer Vision and Image Analysis*, vol. 7, no. 3, pp. 1–22, 2008.

[31] A. Kumar, "Computer-vision-based fabric defect detection: A survey," *Industrial Electronics, IEEE Transactions on*, vol. 55, pp. 348–363, Jan. 2008.

[32] P. Mahajan, Kolhe, "A review of automatic fabric defect detection techniques," *Advances in Computational Research*, vol. 1, no. 2, pp. 18–29, 2009.

[33] H. Y. Ngan, G. K. Pang, and N. H. Yung, "Automated fabric defect detection–a review," *Image and Vision Computing*, vol. 29, no. 7, pp. 442–458, 2011.

[34] J. Hu, ed., *Computer Technology for Textiles and Apparel*. Woodhead Publishing Limited, 2011.

[35] A. Kumar, "3 - computer vision-based fabric defect analysis and measurement," in *Computer Technology for Textiles and Apparel* (J. Hu, ed.), Woodhead Publishing Series in Textiles, pp. 45 – 65, Woodhead Publishing, 2011.

[36] A. Bodmarova, M. Bennamoun, and K. Kubik, "Suitability analysis of techniques for flaw detection in textiles using texture analysis," *Pattern Analysis & Applications*, vol. 3, no. 3, pp. 254–266, 2000.

[37] T. Randen and J. Husoy, "Filtering for texture classification: a comparative study," *Pattern Analysis and Machine Intelligence, IEEE Transactions on*, vol. 21, pp. 291 –310, apr 1999.

[38] F. Cohen, Z. Fan, and S. Attali, "Automated inspection of textile fabrics using textural models," *Pattern Analysis and Machine Intelligence, IEEE Transactions on*, vol. 13, pp. 803 –808, aug 1991.

[39] S. Ozdemir and A. Ercil, "Markov random fields and karhunen-loeve transforms for defect inspection of textile products," in *Emerging Technologies and Factory Automation, 1996. EFTA '96. Proceedings., 1996 IEEE Conference on*, vol. 2, pp. 697–703 vol.2, Nov 1996.

[40] A. Limas Serafim, "Segmentation of natural images based on multiresolution pyramids linking of the parameters of an autoregressive rotation invariant model. application to leather defects detection," in *Pattern Recognition, 1992. Vol.III. Conference C: Image, Speech and Signal Analysis, Proceedings., 11th IAPR International Conference on*, pp. 41–44, Aug 1992.

[41] D. Brzakovic, P. Bakic, N. Vujovic, and H. Sari-Sarraf, "A generalized development environment for inspection of web materials," in *Robotics and Automation, 1997. Proceedings., 1997 IEEE International Conference on*, vol. 1, pp. 1–8 vol.1, Apr 1997.

[42] D. P. Brzakovic and N. S. V. A. Liakopoulos, "Approach to quality control of texture web materials," in *Proc. SPIE 2597, Machine Vision Applications, Architectures, and Systems Integration IV*, 1995.

[43] S. C. Kim and T. J. Kang, "Texture classification and segmentation using wavelet packet frame and Gaussian Mixture Model," *Pattern Recognition*, vol. 40, no. 4, pp. 1207 – 1221, 2007.

[44] X. Z. Yang, G. K. H. Pang, and N. H. C. Yung, "Discriminative fabric defect detection using adaptive wavelets," *Optical Engineering*, vol. 41, no. 12, pp. 3116–3126, 2002.

[45] H. Sari-Sarraf and J. Goddard, J.S., "Vision system for on-loom fabric inspection," *Industry Applications, IEEE Transactions on*, vol. 35, pp. 1252–1259, nov/dec 1999.

[46] A. Kumar and G. Pang, "Fabric defect segmentation using multichannel blob detectors," *Optical Engineering*, vol. 39, no. 12, pp. 3176–3190, 2000.

[47] F. Tajeripour, E. Kabir, and A. Sheikhi, "Fabric defect detection using modified local binary patterns," *EURASIP J. Adv. Signal Process*, vol. 2008, pp. 60:1–60:12, January 2008.

[48] J. L. Raheja, B. Ajay, and A. Chaudhary, "Real time fabric defect detection system on an embedded {DSP} platform," *Optik - International Journal for Light and Electron Optics*, vol. 124, no. 21, pp. 5280 – 5284, 2013.

[49] A. Latif-Amet, A. Ertüzün, and A. Erçil, "An efficient method for texture defect detection: sub-band domain co-occurrence matrices," *Image and Vision Computing*, vol. 18, no. 6–7, pp. 543 – 553, 2000.

[50] H. Ngan and G. Pang, "Regularity analysis for patterned texture inspection," *Automation Science and Engineering, IEEE Transactions on*, vol. 6, pp. 131 –144, jan. 2009.

[51] D. Chetverikov and A. Hanbury, "Finding defects in texture using regularity and local orientation," *Pattern Recognition*, vol. 35, no. 10, pp. 2165 – 2180, 2002.

[52] K. Mak, P. Peng, and K. Yiu, "Fabric defect detection using morpholfilters filters," *Image and Vision Computing*, vol. 27, no. 10, pp. 1585–1592, 2009.

[53] A. Kumar and G. Pang, "Defect detection in textured materials using optimized filters," *Systems, Man, and Cybernetics, Part B: Cybernetics, IEEE Transactions on*, vol. 32, pp. 553 – 570, oct 2002.

[54] A. Abouelela, H. M. Abbas, H. Eldeeb, A. A. Wahdan, and S. M. Nassar, "Automated vision system for localizing structural defects in textile fabrics," *Pattern Recognition Letters*, vol. 26, no. 10, pp. 1435 – 1443, 2005.

[55] S. Mallat, *A Wavelet Tour of Signal Processing*. Electronics & Electrical, Academic Press, 1999.

[56] D. L. Fugal, *Conceptual Wavelets in Digital Signal Processing*. Space and Signal Technical Publishing, 2009.

[57] S. Kim, H. Bae, S.-P. Cheon, and K.-B. Kim, "On-line fabric-defects detection based on wavelet analysis," in *Computational Science and Its Applications – ICCSA 2005* (O. Gervasi, M. Gavrilova, V. Kumar, A. Laganá, H. Lee, Y. Mun, D. Taniar, and C. Tan, eds.), vol. 3483 of *Lecture Notes in Computer Science*, pp. 1075–1084, Springer Berlin Heidelberg, 2005.

[58] H. Y. Ngan, G. K. Pang, S. Yung, and M. K. Ng, "Wavelet based methods on patterned fabric defect detection," *Pattern Recognition*, vol. 38, no. 4, pp. 559 – 576, 2005.

[59] A. Serdaroglu, A. Ertuzun, and A. Ercil, "Defect detection in textile fabric images using subband domain subspace analysis," *Pattern Recognition and Image Analysis*, vol. 17, pp. 663–674, 2007.

[60] A. Serdaroglu, A. Ertuzun, and A. Ercil, "Defect detection in textile fabric images using wavelet transforms and independent component analysis," *Pattern Recognition and Image Analysis*, vol. 16, pp. 61–64, 2006.

[61] X. Yang, G. Pang, and N. Yung, "Robust fabric defect detection and classification using multiple adaptive wavelets," *Vision, Image and Signal Processing, IEE Proceedings -*, vol. 152, pp. 715 – 723, dec. 2005.

[62] M. Unser, "Texture classification and segmentation using wavelet frames," *Image Processing, IEEE Transactions on*, vol. 4, pp. 1549–1560, Nov 1995.

[63] D. Reynolds, "Gaussian mixture models," in *Encyclopedia of Biometrics* (S. Li and A. Jain, eds.), pp. 659–663, Springer US, 2009.

[64] M. Abdulghafour and M. A. Abidi, "Data fusion through nondeterministic approaches: a comparison," in *Proc. SPIE Sensor Fusion VI*, vol. 2059, pp. 37–53, 1993.

[65] N. Otsu, "A threshold selection method from gray-level histograms," *Systems, Man and Cybernetics, IEEE Transactions on*, vol. 9, pp. 62–66, Jan 1979.

[66] Y. Zhang, Z. Lu, and J. Li, "Fabric defect detection and classification using Gabor filters and Gaussian Mixture Model," in *Computer Vision – ACCV 2009* (H. Zha, R.-i. Taniguchi, and S. Maybank, eds.), vol. 5995 of *Lecture Notes in Computer Science*, pp. 635–644, Springer Berlin Heidelberg, 2010.

[67] A. Srikaew, K. Attakitmongcol, P. Kumsawat, and W. Kidsang, "Detection of defect in textile fabrics using optimal Gabor Wavelet Network and two-dimensional PCA," in *Advances in Visual Computing* (G. Bebis, R. Boyle, B. Parvin, D. Koracin, S. Wang, K. Kyung-

nam, B. Benes, K. Moreland, C. Borst, S. DiVerdi, C. Yi-Jen, and J. Ming, eds.), vol. 6939 of *Lecture Notes in Computer Science*, pp. 436–445, Springer Berlin Heidelberg, 2011.

[68] A. Kumar and G. Pang, "Defect detection in textured materials using gabor filters," *Industry Applications, IEEE Transactions on*, vol. 38, pp. 425 –440, mar/apr 2002.

[69] S. Arivazhagan, L. Ganesan, and S. Bama, "Fault segmentation in fabric images using Gabor wavelet transform," *Machine Vision and Applications*, vol. 16, no. 6, pp. 356–363, 2006.

[70] A. Jain and F. Farrokhnia, "Unsupervised texture segmentation using gabor filters," in *Systems, Man and Cybernetics, 1990. Conference Proceedings., IEEE International Conference on*, pp. 14 –19, Nov. 1990.

[71] J. L. Raheja, S. Kumar, and A. Chaudhary, "Fabric defect detection based on {GLCM} and gabor filter: A comparison," *Optik - International Journal for Light and Electron Optics*, vol. 124, no. 23, pp. 6469 – 6474, 2013.

[72] S. Grigorescu, N. Petkov, and P. Kruizinga, "Comparison of texture features based on gabor filters," *Image Processing, IEEE Transactions on*, vol. 11, pp. 1160 – 1167, oct 2002.

[73] A. Bodnarova, M. Bennamoun, and S. Latham, "Optimal gabor filters for textile flaw detection," *Pattern Recognition*, vol. 35, no. 12, pp. 2973 – 2991, 2002. Pattern Recognition in Information Systems.

[74] P. Vautrot, N. Bonnet, and M. Herbin, "Comparative study of different spatial/spatial-frequency methods (gabor filters, wavelets, wavelets packets) for texture segmentation/-classification," in *Image Processing, 1996. Proceedings., International Conference on*, vol. 3, pp. 145–148 vol.3, Sep 1996.

[75] T. Ojala, M. Pietikainen, and T. Maenpaa, "Multiresolution gray-scale and rotation invariant texture classification with local binary patterns," *Pattern Analysis and Machine Intelligence, IEEE Transactions on*, vol. 24, pp. 971–987, Jul 2002.

[76] S. Brahnam, L. Jain, L. Nanni, and A. Lumini, eds., *Local Binary Patterns: New Variants and Applications*. Springer Berlin / Heidelberg, 2014.

[77] J. Chen, S. Shan, C. He, G. Zhao, M. Pietikäinen, X. Chen, and W. Gao, "Wld: A robust local image descriptor," *Pattern Analysis and Machine Intelligence, IEEE Transactions on*, vol. 32, pp. 1705 –1720, sept. 2010.

[78] H. Tamura, S. Mori, and T. Yamawaki, "Textural features corresponding to visual perception," *Systems, Man and Cybernetics, IEEE Transactions on*, vol. 8, pp. 460 –473, june 1978.

[79] R. M. Haralick, "Statistical and structural approaches to texture," *Proceedings of the IEEE*, vol. 67, pp. 786 – 804, may 1979.

[80] T. Mäenpää, J. Viertola, and M. Pietikäinen, "Optimising colour and texture features for real-time visual inspection," *Pattern Analysis & Applications*, vol. 6, pp. 169–175, 2003.

[81] T. Mäenpää, M. Turtinen, and M. Pietikäinen, "Real-time surface inspection by texture," *Real-Time Imaging*, vol. 9, no. 5, pp. 289 – 296, 2003.

[82] J. Livarinen, "Surface defect detection with histogram-based texture features," in *Proceedings of SPIE 4197*, pp. 140–145, 2000.

[83] B. Mingde, S. Zhigang, Z. Cao, and L. Yesong, "Real-time textural defect detection based on label run length co-occurrence matrix," in *Transportation, Mechanical, and Electrical Engineering (TMEE), 2011 International Conference on*, pp. 271 –274, dec. 2011.

[84] S.-h. Cha, "Comprehensive survey on distance / similarity measures between probability density functions," *International Journal of Mathematical Models and Methods in Applied Sciences*, vol. 1, no. 4, pp. 300–307, 2007.

[85] D. Chetverikov, "Pattern regularity as a visual key," *Image and Vision Computing*, vol. 18, p. 2000, 1998.

[86] M. Shi, R. Fu, S. Huang, Y. Guo, and B. Xu, "A method of fabric defect detection using local contrast deviation," in *Image and Signal Processing, 2009. CISP '09. 2nd International Congress on*, pp. 1 –5, oct. 2009.

[87] K. Mak and X. Tian, "Textile fabric flaw detection using singular value decomposition," in *Green Circuits and Systems (ICGCS), 2010 International Conference on*, pp. 381 –386, june 2010.

[88] A. Kumar, "Neural network based detection of local textile defects," *Pattern Recognition*, vol. 36, no. 7, pp. 1645 – 1659, 2003.

[89] H. Castilho, J. Pinto, and A. Serafim, "Nn automated defect detection based on optimized thresholding," in *Image Analysis and Recognition* (A. Campilho and M. Kamel, eds.), vol. 4142 of *Lecture Notes in Computer Science*, pp. 790–801, Springer Berlin / Heidelberg, 2006.

[90] E. Dougherty and J. Astola, *An Introduction to Nonlinear Image Processing*. Books in the SPIE Tutorial Texts Series, SPIE Optical Engineering Press, 1994.

[91] C. J. V. Rijsbergen, *Information Retrieval*. Newton, MA, USA: Butterworth-Heinemann, 2nd ed., 1979.

[92] L. Nanni, A. Lumini, and S. Brahnam, "Local binary patterns variants as texture descriptors for medical image analysis," *Artificial Intelligence in Medicine*, vol. 49, no. 2, pp. 117 – 125, 2010.

[93] F. Khellah, "Texture classification using dominant neighborhood structure," *Image Processing, IEEE Transactions on*, vol. 20, pp. 3270–3279, Nov 2011.

[94] S. Liao, M. Law, and A. Chung, "Dominant local binary patterns for texture classification," *Image Processing, IEEE Transactions on*, vol. 18, pp. 1107–1118, May 2009.

[95] P. NV, "Picanol omni plus 800 technical brochure." Web, Dec. 2006.

[96] K. Mak, P. Peng, and H. Lau, "A real-time computer vision system for detecting defects in textile fabrics," in *Industrial Technology, 2005. ICIT 2005. IEEE International Conference on*, pp. 469–474, dec. 2005.

[97] H. Castilho, P. Goncalves, J. Pinto, and A. Serafim, "Intelligent real-time fabric defect detection," in *Image Analysis and Recognition* (M. Kamel and A. Campilho, eds.), vol. 4633 of *Lecture Notes in Computer Science*, pp. 1297–1307, Springer Berlin / Heidelberg, 2007.

[98] R. Stojanovic, P. Mitropulos, C. Koulamas, Y. Karayiannis, S. Koubias, and G. Papadopoulos, "Real-time vision-based system for textile fabric inspection," *Real-Time Imaging*, vol. 7, no. 6, pp. 507–518, 2001.

[99] C.-S. Cho, B.-M. Chung, and M.-J. Park, "Development of real-time vision-based fabric inspection system," *Industrial Electronics, IEEE Transactions on*, vol. 52, pp. 1073–1079, aug. 2005.

[100] Shelton Vision, "The shelton webspector," *Computing Control Engineering Journal*, vol. 15, p. 19, aug.-sept. 2004.

[101] Elbit Vision Systems Ltd., "IQ-TEX 4 - Vision Empowered Process Monitoring." Product Brochure, published online (accessed Feb. 2013).

[102] S. Rao, *Mechanical Vibrations*. Pearson/Prentice Hall, 2004.

[103] D. Slepian, "Restoration of photographs blurred by image motion," *The Bell System Technical Journal*, vol. 46, pp. 2353–2362, December 1967.

[104] S. C. Som, "Analysis of the effect of linear smear on photographic images," *Journal of the Optical Society of America*, vol. 61, pp. 859–864, July 1971.

[105] S. Rudoler, O. Hadar, M. Fisher, and N. S. Kopeika, "Image resolution limits resulting from mechanical vibrations. Part 2: Experiment," *Optical Engineering*, vol. 30, pp. 577–589, May 1991.

[106] O. Hadar, M. Fisher, and N. S. Kopeika, "Image resolution limits resulting from mechanical vibrations. Part III: numerical calculation of modulation transfer function," *Optical Engineering*, vol. 31, pp. 581–589, March 1992.

[107] O. Hadar, I. Dror, and N. S. Kopeika, "Image resolution limits resulting from mechanical vibrations. Part IV: real-time numerical calculation of optical transfer functions and experimental verification," *Optical Engineering*, vol. 33, pp. 566–578, February 1994.

[108] T. F. Chan and J. Shen, *Image processing and analysis: variational, PDE, wavelet, and stochastic methods*. Society for Industrial and Applied Mathematics, 2005. ISBN 978-0-89871-589-7.

[109] R. C. Gonzalez and R. E. Woods, *Digital Image Processing*. Pearson Prentice Hall, third ed., 2008. ISBN 978-0-13168-728-8.

[110] W. H. Richardson, "Bayesian-based iterative method of image restoration," *Journal of the Optical Society of America*, vol. 62, pp. 55–59, January 1972.

[111] R. Neelamani, H. Choi, and R. Baraniuk, "ForWaRD: Fourier-wavelet regularized deconvolution for ill-conditioned systems," *IEEE Transactions on Signal Processing*, vol. 52, pp. 418–433, February 2004.

[112] A. Levin, R. Fergus, F. Durand, and W. T. Freeman, "Image and depth from a conventional camera with a coded aperture," in *ACM SIGGRAPH 2007 Papers*, SIGGRAPH '07, (New York, NY, USA), ACM, 2007.

[113] A. Levin, R. Fergus, F. Durand, and W. T. Freeman, "Deconvolution using natural image priors." -, 2007.

[114] J. Dahl, P. C. Hansen, S. H. Jensen, and T. L. Jensen, "Algorithms and software for total variation image reconstruction via first-order methods," *Numerical Algorithms*, vol. 53, pp. 67–92, January 2010.

[115] P. Rodriguez and B. Wohlberg, "Efficient minimization method for a generalized total variation functional," *IEEE Transactions on Image Processing*, vol. 18, pp. 322–332, February 2009.

[116] T. Goldstein and S. Osher, "The split bregman method for L1-regularized problems," *SIAM Journal on Imaging Sciences*, vol. 2, pp. 323–343, April 2009.

[117] V. Katkovnik, K. Egiazarian, and J. Astola, "A spatially adaptive nonparametric regression image deblurring," *IEEE Transactions on Image Processing*, vol. 14, pp. 1469–1478, October 2005.

[118] A. Foi, K. Dabov, V. Katkovnik, and K. Egiazarian, "Shape-adaptive DCT for denoising and image reconstruction," in *Proceedings of SPIE Electronic Imaging*, vol. 6064 of *Image Processing: Algorithms and Systems, Neural Networks, and Machine Learning*, (San Jose, California, USA), pp. 60640N–1–60640N–12, February 2006.

[119] K. Dabov, A. Foi, V. K., and K. Egiazarian, "Image restoration by sparse 3D transform-domain collaborative filtering," in *Proceedings of SPIE Electronic Imaging*, vol. 6812 of *Image Processing: Algorithms and Systems VI*, (San Jose, California, USA), March 2008.

[120] Z. Wang and A. C. Bovik, "Mean squared error: Love it or leave it? A new look at signal fidelity measures," *IEEE Signal Processing Magazine*, vol. 26, pp. 98–117, January 2009.

[121] I. Avcibas, B. Sankur, and K. Sayood, "Statistical evaluation of image quality measures," *Journal of Electronic Imaging*, vol. 11, pp. 206–223, April 2002.

[122] J. C. Russ, *Image Processing Handbook, Fourth Edition.* Boca Raton, FL, USA: CRC Press, Inc., 4th ed., 2002.

[123] S. M. Pizer, E. P. Amburn, J. D. Austin, R. Cromartie, A. Geselowitz, T. Greer, B. ter Haar Romeny, J. B. Zimmerman, and K. Zuiderveld, "Adaptive histogram equalization and its variations," *Computer Vision, Graphics, and Image Processing*, vol. 39, no. 3, pp. 355 – 368, 1987.

[124] P. Heckbert, ed., *Graphic Gems IV.* San Diego: Academic Press Professional, 1994.

[125] C. Harris and M. Stephens, "A combined corner and edge detector," in *In Proc. of Fourth Alvey Vision Conference*, pp. 147–151, 1988.

[126] J. Canny, "A computational approach to edge detection," *IEEE Transactions on Pattern Analysis and Machine Intelligence*, vol. 8, pp. 679–698, November 1986.

[127] H. Christensen and J. Phillips, eds., *Empirical Evaluation Methods in Computer Vision.* Machine Perception and Artificial Intelligence, Singapore: World Scientific Press, July 2002.

[128] H. Christensen and J. Phillips, eds., *Empirical Evaluation Methods in Computer Vision.* Machine Perception and Artificial Intelligence, Singapore: World Scientific Press, July 2002.

[129] E. Tapia, "A note on the computation of high-dimensional integral images," *Pattern Recognition Letters*, vol. 32, no. 2, pp. 197 – 201, 2011.

[130] G. Stockman and L. G. Shapiro, *Computer Vision.* Upper Saddle River, NJ, USA: Prentice Hall PTR, 1st ed., 2001.

[131] N. Chinchor, "Muc-4 evaluation metrics," in *Proceedings of the 4th conference on Message understanding*, MUC4 '92, (Stroudsburg, PA, USA), pp. 22–29, Association for Computational Linguistics, 1992.

[132] X. Wang, N. D. Georganas, and E. Petriu, "Fabric texture analysis using computer vision techniques," *Instrumentation and Measurement, IEEE Transactions on*, vol. 60, pp. 44–56, Jan 2011.

[133] J.-J. Lin, "Applying a co-occurrence matrix to automatic inspection of weaving density for woven fabrics," *Textile Research Journal*, vol. 72, pp. 486–490, June 2002.

[134] D. Yuvaraj and R. C. Nayar, "A simple yarn hairiness measurement setup using image processing techniques," *Indian Journal of Fibre & Textile Research*, vol. 37, pp. 331–336, 2012.

[135] A. Fabijańska and L. Jackowska-Strumiłło, "Image processing and analysis algorithms for yarn hairiness determination," *Machine Vision and Applications*, vol. 23, no. 3, pp. 527–540, 2012.

[136] A. Guha, C. Amarnath, S. Pateria, and R. Mittal, "Measurement of yarn hairiness by digital image processing," *Journal of the Textile Institute*, vol. 101, no. 3, pp. 214–222, 2010.

[137] X.-H. Wang, J.-Y. Wang, J.-L. Zhang, H.-W. Liang, and P.-M. Kou, "Study on the detection of yarn hairiness morphology based on image processing technique," in *Machine Learning and Cybernetics (ICMLC), 2010 International Conference on*, vol. 5, pp. 2332–2336, 2010.

[138] V. Carvalho, F. Soares, R. Vasconcelos, M. Belsley, and N. Goncalves, "Yarn hairiness determination using image processing techniques," in *Emerging Technologies Factory Automation (ETFA), 2011 IEEE 16th Conference on*, pp. 1–4, 2011.

[139] T. J. Kang, C. H. Kim, and K. W. Oh, "Automatic recognition of fabric weave patterns by digital image analysis," *Textile Research Journal*, vol. 69, no. 2, pp. 77–83, 1999.

[140] Kuo, C.-Y. Shih, and J.-Y. Lee, "Automatic recognition of fabric weave patterns by a fuzzy c-means clustering method," *Textile Research Journal*, vol. 74, no. 2, pp. 107–111, 2004.

[141] C.-C. Huang, S.-C. Liu, and W.-H. Yu, "Woven fabric analysis by image processing: Part i: Identification of weave patterns," *Textile Research Journal*, vol. 70, no. 6, pp. 481–485, 2000.

[142] C.-F. J. Kuo, C.-Y. Shih, C.-E. Ho, and K.-C. Peng, "Application of computer vision in the automatic identification and classification of woven fabric weave patterns," *Textile Research Journal*, vol. 80, no. 20, pp. 2144–2157, 2010.

[143] X. Wang, N. D. Georganas, and E. Petriu, "Automatic woven fabric structure identification by using principal component analysis and fuzzy clustering," in *Instrumentation and Measurement Technology Conference (I2MTC), 2010 IEEE*, pp. 590–595, 2010.

[144] M. Ralló, J. Escofet, and M. S. Millán, "Weave-repeat identification by structural analysis of fabric images," *Appl. Opt.*, vol. 42, pp. 3361–3372, Jun 2003.

[145] A. Lachkar, T. Gadi, R. Benslimane, L. D'Orazio, and E. Martuscelli, "Textile woven-fabric recognition by using fourier image-analysis techniques: Part i: A fully automatic approach for crossed-points detection," *Journal of the Textile Institute*, vol. 94, no. 3-4, pp. 194–201, 2003.

[146] A. Lachkar, R. Benslimane, L. D'Orazio, and E. Martuscelli, "Textile woven fabric recognition using fourier image analysis techniques: Part ii – texture analysis for crossed-states detection," *Journal of the Textile Institute*, vol. 96, no. 3, pp. 179–183, 2005.

[147] J. Shen, X. Zou, F. Xu, and Z. Xian, "Intelligent recognition of fabric weave patterns using texture orientation features," in *Information Computing and Applications* (R. Zhu, Y. Zhang, B. Liu, and C. Liu, eds.), vol. 106 of *Communications in Computer and Information Science*, pp. 8–15, Springer Berlin Heidelberg, 2010.

[148] X. Yu, *Micro structure information analysis of woven fabrics.* PhD Thesis, Hong Kong Polytechnic University department of computing, 2007.

[149] M. Muja and D. G. Lowe, "Fast approximate nearest neighbors with automatic algorithm configuration," in *International Conference on Computer Vision Theory and Application VISSAPP'09*, pp. 331–340, INSTICC Press, 2009.

[150] J. C. Bezdek, *Pattern Recognition with Fuzzy Objective Function Algorithms.* Advanced Applications in Pattern Recognition, Springer US, 1981.

[151] R. Pan, F. Gao, J. Liu, and H. Wang, "Automatic inspection of woven fabric density of solid colour fabric density by the hough transform," *Fibres & Textiles in Eastern Europe*, vol. 18, no. 4 (81), pp. 46–51, 2010.

[152] Y. J. Jeong and J. Jang, "Applying image analysis to automatic inspection of fabric density for woven fabrics," *Fibers and Polymers*, vol. 6, no. 2, pp. 156–161, 2005.

[153] A. Song, Y. Han, H. Hu, and J. Li, "A novel texture sensor for fabric texture measurement and classification," *Instrumentation and Measurement, IEEE Transactions on*, vol. 63, pp. 1739–1747, July 2014.

[154] M. Tokarska, "Evaluation of measurement uncertainty of fabric surface resistance implied by the van der pauw equation," *Instrumentation and Measurement, IEEE Transactions on*, vol. 63, pp. 1593–1599, June 2014.

[155] R. M. Haralick, "Statistical and structural approaches to texture," *Proceedings of the IEEE*, vol. 67, no. 5, pp. 786–804, 1979.

[156] B. Xu, "Identifying fabric structures with Fast Fourier Transform techniques," *Textile Research Journal*, vol. 66, pp. 496–506, 1996.

[157] M. Tunák, A. Linka, and P. Volf, "Automatic assessing and monitoring of weaving density," *Fibers and Polymers*, vol. 10, no. 6, pp. 830–836, 2009.

[158] S. H. Ravandi, "Fourier transform analysis of plain weave fabric appearance," *Textile Research Journal*, vol. 65, no. 11, pp. 676–683, 1995.

[159] H. Sari-Sarraf and J. S. Goddard, Jr., "Online optical measurement and monitoring of yarn density in woven fabrics," in *SPIE Automated Optical Inspection for Industry*, pp. 444–452, 1996.

[160] R. Pan, W. Gao, J. Liu, H. Wang, and X. Qian, "Automatic inspection of double-system-mélange yarn-dyed fabric density with color-gradient image," *Fibers and Polymers*, vol. 12, no. 1, pp. 127–131, 2011.

[161] R. Pan, J. Liu, and W. Gao, "Measuring linear density of threads in single-system-mélange color fabrics with fcm algorithm," *Color Research & Application*, vol. 38, no. 6, pp. 456–462, 2013.

[162] L. Techniková and M. Tunák, "Weaving density evaluation with the aid of image analysis," *Fibres & Textiles in Eastern Europe*, vol. 2 (98), pp. 74–79, 2013.

[163] A. S. Normanton, A. Chown, I. Baillie, S. Higson, and G. Stephens, "Online measurements for quality in the metals industries: does automated inspection meet the need?," *Ironmaking and Steelmaking Journal*, vol. 31, no. 1, pp. 2–7, 2003.

[164] T. Piironen, O. Silven, M. Pietikainen, T. Laitinen, and E. Strommer, "Automated visual inspection of rolled metal surfaces," *Machine Vision and Applications*, vol. 3, no. 4, pp. 247–254, 1990.

[165] H. Zheng, L. Kong, and S. Nahavandi, "Automatic inspection of metallic surface defects using genetic algorithms," *Journal of Materials Processing Technology*, vol. 125–126, no. 0, pp. 427 – 433, 2002.

[166] W. Wu, C. Hou, *et al.*, "Automated metal surface inspection through machine vision," *Imaging science journal*, vol. 51, no. 2, pp. 79–88, 2003.

[167] C. Mandriota, E. Stella, M. Nitti, N. Ancona, and A. Distante, "Rail corrugation detection by gabor filtering," in *Image Processing, 2001. Proceedings. 2001 International Conference on*, vol. 2, pp. 626–628, Oct 2001.

[168] K. Wiltschi, A. Pinz, and T. Lindenberg, "An automated assessment scheme for steel quality inspection." online, November 1998.

[169] S. Ghorai, A. Mukherjee, M. Gangadaran, and P. Dutta, "Automatic defect detection on hot-rolled flat steel products," *Instrumentation and Measurement, IEEE Transactions on*, vol. 62, pp. 612–621, March 2013.

[170] X.-W. Zhang, L.-Z. Xu, Y.-Q. Ding, X.-N. Fan, L.-P. Gu, and H. Sun, "Inspection of surface defects in copper strip based on machine vision," in *Life System Modeling and Intelligent Computing* (K. Li, M. Fei, L. Jia, and G. Irwin, eds.), vol. 6328 of *Lecture Notes in Computer Science*, pp. 304–312, Springer Berlin Heidelberg, 2010.

[171] S. Ren, Z. Zhang, M. Tetsuo, H. Fujiwara, and T. Imamura, "Inspection of smooth metallic surface using complex discrete wavelet transform," in *Innovative Computing Information and Control, 2008. ICICIC '08. 3rd International Conference on*, pp. 63–63, June 2008.

[172] A. Cord, F.Bach, and D. Jeulin, "Texture classification by statistical learning from morphological image processing: application to metallic surfaces," *Journal of Microscopy*, vol. 239, pp. 159–166, 2010.

[173] M. Mansano, L. Pavesi, L. Oliveira, A. Britto, and A. Koerich, "Inspection of metallic surfaces using local binary patterns," in *IECON 2011 - 37th Annual Conference on IEEE Industrial Electronics Society*, pp. 2227–2231, Nov 2011.

[174] S. Aghdam, E. Amid, and M. Imani, "A fast method of steel surface defect detection using decision trees applied to lbp based features," in *Industrial Electronics and Applications (ICIEA), 2012 7th IEEE Conference on*, pp. 1447–1452, July 2012.

[175] F. Gao, Z. Li, G. Xiao, X. Yuan, and Z. Han, "An online inspection system of surface defects for copper strip based on computer vision," in *Image and Signal Processing (CISP), 2012 5th International Congress on*, pp. 1200–1204, Oct 2012.

[176] N. Bonnot, R. Seulin, and F. Merienne, "Machine vision system for surface inspection on brushed industrial parts," in *Machine Vision Applications in Industrial Inspection XII, Proceedings of the SPIE* (J. R. and F. Meriaudeau, eds.), vol. 5303, pp. 64–72, 2004.

[177] A. Branca, M. Abbate, F. Lovergine, G. Attolico, and A. Distante, "Leather inspection through singularities detection using wavelet transforms," in *Image Analysis and Processing* (A. Bimbo, ed.), vol. 1311 of *Lecture Notes in Computer Science*, pp. 584–591, Springer Berlin Heidelberg, 1997.

[178] A. Branca, F. Lovergine, G. Attolico, and A. Distante, "Defect detection on leather by oriented singularities," in *Computer Analysis of Images and Patterns* (G. Sommer, K. Daniilidis, and J. Pauli, eds.), vol. 1296 of *Lecture Notes in Computer Science*, pp. 223–230, Springer Berlin Heidelberg, 1997.

[179] J. Sobral, "Leather inspection based on wavelets," in *Pattern Recognition and Image Analysis* (J. Marques, N. Pérez de la Blanca, and P. Pina, eds.), vol. 3523 of *Lecture Notes in Computer Science*, pp. 682–688, Springer Berlin Heidelberg, 2005.

[180] Z. C. C. Fu Qiang He, Wen Wang, "Automatic visual inspection for leather manufacture," *Key Engineering Materials*, vol. 326 - 328, pp. 469–472, 2006.

[181] D.-M. Tsa and S.-K. Wu, "Automated surface inspection using gabor filters," *The International Journal of Advanced Manufacturing Technology*, vol. 16, no. 7, pp. 474–482, 2000.

[182] C. Kwak, J. A. Ventura, and K. Tofang-Sazi, "A neural network approach for defect identification and classification on leather fabric," *Journal of Intelligent Manufacturing*, vol. 11, no. 5, pp. 485–499, 2000.

[183] K. Krastev and L. Georgieva, "Identification of leather surface defects using fuzzy logic," in *International Conference on Computer Systems and Technologies*, 2005.

[184] W. Wen and A. Xia, "Verifying edges for visual inspection purposes," *Pattern Recognition Letters*, vol. 20, no. 3, pp. 315 – 328, 1999.

[185] E. Åstrand, *Automatic Inspection of Sawn Wood*. S-581 83 linköping, sweden, Linköping University, Department of Electrical Engineering, 1996.

[186] J. Lampinen, S. Smolander, and M. Korhonen, "Wood surface inspection system based on generic visual features," in *Industrial Applications of Neural Networks, pages 3542. World Scientic Pub Co*, 1995.

[187] D. Martin, M. C. Garcia-Alegre, and D. Guinea, "Laser diffuse lighting in a visual inspection system for defect detection in wood laminates," in *Modern Approaches To Quality Control* (A. B. Eldin, ed.), Intect Open Science, November 2011.

[188] M. n. Patricio and D. Maravall, "Automatic visual inspection of wooden pallets," in *Developments in Applied Artificial Intelligence* (P. Chung, C. Hinde, and M. Ali, eds.), vol. 2718 of *Lecture Notes in Computer Science*, pp. 277–286, Springer Berlin Heidelberg, 2003.

[189] O. Silvén, M. Niskanen, and H. Kauppinen, "Wood inspection with non-supervised clustering," *Machine Vision and Applications*, vol. 13, no. 5-6, pp. 275–285, 2003.

[190] M. Niskanen, O. Silvén, and H. Kauppinen, "Color and texture based wood inspection with non-supervised clustering.," in *Proc. 12th Scandinavian Conference on Image Analysis*, pp. 336–342, June 2001.

[191] H. Kaupinnen, "Development of a color machine vision method for wood surface inspection," Master's thesis, Department of Electrical Engineering and Infotech Oulu, University of Oulu, 1999.

[192] A. Wyckhuyse and X. Maldague, "A study of wood inspection by infrared thermography, part i: Wood pole inspection by infrared thermography," *Research in Nondestructive Evaluation*, vol. 13, no. 1, pp. 1–12, 2001.

[193] A. Wyckhuyse and X. Maldague, "A study of wood inspection by infrared thermography, part ii: Thermography for wood defects detection," *Research in Nondestructive Evaluation*, vol. 13, no. 1, pp. 13–21, 2001.

[194] P. Alapuranen and T. Westman, "Automatic visual inspection of wood surfaces," in *Pattern Recognition, 1992. Vol.I. Conference A: Computer Vision and Applications, Proceedings., 11th IAPR International Conference on*, pp. 371–374, Aug 1992.

[195] M. Hall and A. Ström, "High speed wood inspection using a parallel VLSI architecture," in *Algorithms and Parallel VLSI Architectures III* (M. Moonen and F. Catthoor, eds.), pp. 215 – 226, Amsterdam: Elsevier Science B.V., 1995.

[196] M.-X. Li and C. dong Wu, "A vprs and nn method for wood veneer surface inspection," in *Intelligent Systems and Applications, 2009. ISA 2009. International Workshop on*, pp. 1–4, May 2009.

[197] M.-X. Li and C.-D. Wu, "A vision based inspection method for wood veneer classification," in *Robotics, Automation and Mechatronics, 2008 IEEE Conference on*, pp. 494–498, Sept 2008.

[198] K. Patel, A. Kar, S. Jha, and M. Khan, "Machine vision system: a tool for quality inspection of food and agricultural products," *Journal of Food Science and Technology*, vol. 49, no. 2, pp. 123–141, 2012.

[199] D.-W. Sun, ed., *Computer Vision Technology in the Food and Beverage Industries*. Woodhead Publishing Limited, 2012.

[200] B. Zhang, W. Huang, J. Li, C. Zhao, S. Fan, J. Wu, and C. Liu, "Principles, developments and applications of computer vision for external quality inspection of fruits and vegetables: A review," *Food Research International*, vol. 62, no. 0, pp. 326 – 343, 2014.

[201] G. Mathew, J. George, J. Jaya, S. Janardhana, and K. Sabareesaan, "Quality analysis of food products through computer aided visual inspection: A review," in *Current Trends in Engineering and Technology (ICCTET), 2013 International Conference on*, pp. 105–109, July 2013.

[202] S. Janardhana, J. Jaya, K. Sabareesaan, and J. George, "Computer aided inspection system for food products using machine vision - a review," in *Current Trends in Engineering and Technology (ICCTET), 2013 International Conference on*, pp. 29–33, July 2013.

[203] T. Brosnan and D.-W. Sun, "Improving quality inspection of food products by computer vision—a review," *Journal of Food Engineering*, vol. 61, no. 1, pp. 3 – 16, 2004. Applications of computer vision in the food industry.

[204] G. Ginesu, D. Giusto, V. Margner, and P. Meinlschmidt, "Detection of foreign bodies in food by thermal image processing," *Industrial Electronics, IEEE Transactions on*, vol. 51, pp. 480–490, April 2004.

[205] A. Mateo, F. Soto, J. Villarejo, J. Roca-Dorda, F. D. la Gandara, and A. García, "Quality analysis of tuna meat using an automated color inspection system," *Aquacultural Engineering*, vol. 35, no. 1, pp. 1 – 13, 2006.

[206] S.-T. Han, W. K. Park, Y.-H. Ahn, W.-J. Lee, and H. S. Chun, "Development of a compact sub-terahertz gyrotron and its application to t-ray real-time imaging for food inspection," in *Infrared, Millimeter, and Terahertz Waves (IRMMW-THz), 2012 37th International Conference on*, pp. 1–2, Sept 2012.

[207] R. Adhikari, O. Moselhi, and A. Bagchi, "Image-based retrieval of concrete crack properties for bridge inspection," *Automation in Construction*, vol. 39, no. 0, pp. 180 – 194, 2014.

[208] G. Choudhary and S. Dey, "Crack detection in concrete surfaces using image processing, fuzzy logic, and neural networks," in *Advanced Computational Intelligence (ICACI), 2012 IEEE Fifth International Conference on*, pp. 404–411, Oct 2012.

[209] X. Tong, J. Guo, Y. Ling, and Z. Yin, "A new image-based method for concrete bridge bottom crack detection," in *Image Analysis and Signal Processing (IASP), 2011 International Conference on*, pp. 568–571, Oct 2011.

[210] S. F. Ershad, "Texture classification approach based on combination of edge & co-occurrence and local binary pattern," in *The 2014 International Conference on Image Processing, Computer Vision, and Pattern Recognition*, vol. abs/1203.4855, 2012.

[211] S. Chen, B. Lin, X. Han, and X. Liang, "Automated inspection of engineering ceramic grinding surface damage based on image recognition," *The International Journal of Advanced Manufacturing Technology*, vol. 66, no. 1-4, pp. 431–443, 2013.

[212] M. L. Smith and R. J. Stamp, "Automated inspection of textured ceramic tiles," *Computers in Industry*, vol. 43, no. 1, pp. 73 – 82, 2000.

[213] H.-D. Lin, "Computer-aided visual inspection of surface defects in ceramic capacitor chips," *Journal of Materials Processing Technology*, vol. 189, no. 1–3, pp. 19 – 25, 2007.

[214] H. Doğan and O. Akay, "Using adaboost classifiers in a hierarchical framework for classifying surface images of marble slabs," *Expert Systems with Applications*, vol. 37, no. 12, pp. 8814 – 8821, 2010.

[215] M. A. Selver, O. Akay, F. Alim, S. Bardakçı, and M. Ölmez, "An automated industrial conveyor belt system using image processing and hierarchical clustering for classifying marble slabs," *Robotics and Computer-Integrated Manufacturing*, vol. 27, no. 1, pp. 164 – 176, 2011.

[216] X. Xie and M. Mirmehdi, "Texems: Texture exemplars for defect detection on random textured surfaces," *Pattern Analysis and Machine Intelligence, IEEE Transactions on*, vol. 29, pp. 1454–1464, Aug 2007.

[217] J. Kittler, R. Marik, M. Mirmedi, M. Petrou, and J. Song, "Detection of defects in coulour texture surfaces," in *IAPR Workshop on Machine Vision Application*, 1994.

[218] J. Lewis, "Fast normalized cross-correlation," *Vision Interface*, vol. 10, pp. 120–123, 1995.

About the author

Dorian Schneider was born in Berlin, Germany in 1984. He received the diploma degree in electrical engineering from the Berlin University of Technology in 2009 and its master degree in digital signal processing from the Shanghai Jiao Tong University in 2008. From 2009 to 2010 he worked as a development engineer in the area of industrial automation for a Berlin based solar company. In 2010 he became a Ph.D. candidate at the Institute of Imaging and Computer Vision, RWTH Aachen University and graduated with highest honors in 2015. His research interests are in signal processing, pattern recognition, and computer vision within the context of industrial control and quality assurance.